UiT The Arctic University of Norway

GHENT UNIVERSITY

Department of Building, Energy and Material Technology

Analysis of early-age properties of geopolymers with various waste materials

Dario De Muynck

UiT & UGent student number: 579260 & 01607520

Marie-Laure Heyndrickx

UiT & UGent student number: 579223 & 01408146

Supervisors: Iveta Nováková, PhD (UiT), Prof. dr. ir. Veerle Boel (UGent)

Counsellors: Boy-Arne Buyle (UiT), ing. Leo Van Cauter (UGent)

Master's dissertation submitted in order to obtain the academic degree of

Master of Science in de industriële wetenschappen: bouwkunde at Ghent University

Academic year: 2022-2023

UiT The Arctic University of Norway

GHENT UNIVERSITY

Department of Building, Energy and Material Technology

Analysis of early-age properties of geopolymers with various waste materials

Dario De Muynck

UiT & UGent student number: 579260 & 01607520

Marie-Laure Heyndrickx

UiT & UGent student number: 579223 & 01408146

Supervisors: Iveta Nováková, PhD (UiT), Prof. dr. ir. Veerle Boel (UGent)

Counsellors: Boy-Arne Buyle (UiT), ing. Leo Van Cauter (UGent)

Master's dissertation submitted in order to obtain the academic degree of

Master of Science in de industriële wetenschappen: bouwkunde at Ghent University

Academic year: 2022-2023

Preface

As we pursued on our journey of completing our master's thesis, we are filled with gratitude for the many people who assisted us along the way and for the invaluable lessons we have learned. This challenging topic has opened our eyes to different branches of engineering and has forced us to think differently about sustainability. The topic gave us an interesting view on the future of construction, geopolymer concrete and different ways of utilizing waste. We also gained valuable knowledge on research methodology, data analysis and technical writing. We are grateful for the opportunity to apply these skills to a real-world problem while contributing to the field of geopolymer concrete and research that follows.

First and foremost, we would like to express our gratitude to our thesis advisors. We thank prof. dr. ir. Veerle Boel (UGent) for her guidance, feedback and expertise in providing us with materials and mix designs needed for our research. We also would like to thank ing. Leo Van Cauter (UGent) for his help during the early stages of exploring the geopolymer world, teaching us the mix procedure and the interesting conversations in the Magnel-Vandepitte laboratory. In addition we would like to thank Iveta Nováková, PhD (UiT) for her professional guidance, feedback and pleasant cooperation. We also want to thank her for introducing us to GEOSUMAT. This allowed us to connect with experts in our research topic. We would also like to express our sincere appreciation to Boy-Arne Buyle (UiT) for assisting and navigating us in Narvik and the lab environment. We cherish his valuable advice.

We also would also like express our thanks to Eirik Gjerløw for providing general information about the XRF and XRD machines, as well as Ashfaque Ahmed Jhatial for his knowledge and help with the particle size analyzer and XRD machine. Furthermore we would like to thank Aritro Banerjee for his assistance with chemistry, calculations and the valuable, critical questions. His devotion and input towards our research is also much appreciated. We would also like to extend our thanks to Klevis Xhura, Martin-André S. Husby, and Richard-Mathias Klausen for their help, insights, talks and willingness to respond to our questions.

We would like to express our gratitude to our families and close friends for their love and encouragement, as well as for being a constant source of advice and feedback throughout this journey. Each one of them provided us with the resources and courage to tackle this adventure. We could not have done it without your constant encouragement and assistance.

Finally, we would like to express our gratitude to one another for the countless hours spent brainstorming, mixing geopolymer concrete, analysing data and writing. Through the extremely though and challenging times we could motivate each other. Working together has been an honour and we are proud of what we have accomplished and contributed to the world of geopolymer concrete.

Dario De Muynck,
Marie-Laure Heyndrickx *Narvik, Norway - May 2023*

Acknowledgement

15/05/2023

Remark on the master's dissertation and the oral presentation

This dissertation was initially titled: "Evolution of mineralogy and microstructure during the curing stage of geopolymers". Several reasons led to the modification of the dissertation's title. "Analysis of early-age properties of geopolymers with various waste materials" was selected as an alternative because the early development of the parameters is not limited to the mineralogy and microstructure. Including the mechanical properties allows to explain and correlate the chemical and mechanical properties and their evolution. In addition, it was interesting for the research to include and use other waste materials to explore the potential and effect on early-age properties.

This master's dissertation is part of an exam. Any comments formulated by the assessment committee during the oral presentation of the master's dissertation are not included in this text.

Analysis of early-age properties of geopolymers with various waste materials

Dario De Muynck & Marie-Laure Heyndrickx

Supervisors: Iveta Nováková, PhD (UiT) & Prof. dr. ir. Veerle Boel (UGent)
Counsellors: Boy-Arne Buyle (UiT) & ing. Leo Van Cauter (UGent)

Master's dissertation submitted in order to obtain the academic degree of
Master of Science in de industriële wetenschappen bouwkunde at Ghent University

Academic year 2022-2023

Abstract

As the demand for concrete increases to meet the expanding need, the environmental impact of its production cannot be ignored. The use of ordinary Portland cement (OPC) is known to deplete natural resources and release large amounts of CO_2 into the atmosphere. Geopolymer concrete (GPC), made from waste and industrial by-products, has shown the potential to overcome the environmental issues associated with OPC-based concrete. In addition to being a sustainable alternative, GPC has properties comparable to or superior to those of OPC-based concrete. This research aims to investigate the early-age properties of GPC and the influence of incorporating alternative waste materials on these properties. Samples of GPC were examined for their mechanical properties and mineralogy in the early stages of curing. By partially integrating alternative waste sources (such as waste wood ash, recycled aggregates and seawater), the influence on these early-age properties were analysed. The results of this research indicate that the majority of strength gain is developed within the first few hours of elevated curing, with the final strength being achieved after approximately ten hours. The strength development during these first ten hours can be approached by a logarithmic function and beyond this point no significant increase in strength is observed. Additionally, the observed changes in mineralogy and microstructure indicate an initial correlation with the development of mechanical properties. An effect on early-age properties was observed by integrating various alternative waste sources. Each different waste source indicated at least some effect on the fresh or hardened properties, the rate at which they developed, and the mineralogy. Some mechanical properties were improved by the use of these alternative waste sources in combination with significant changes in mineralogy. Initial observations encourage further research and show the potential benefits of using alternative waste materials in geopolymers, not only in terms of performance but also for a more sustainable future in construction.

Keywords

Geopolymer concrete•Early-age•Properties•Microstructure•Mineralogy•Recycled aggregates•Sustainable materials•Waste

Analysis of early-age properties of geopolymers

Dario De Muynck[1,2], Marie-Laure Heyndrickx[1,2], Veerle Boel[1] and Iveta Nováková[2]

[1] *Ghent University, Department of Structural Engineering and Building Materials, Ghent, Belgium*
[2] *UiT The Arctic University of Norway, Department of Building, Energy and Material Technology, Narvik, Norway*

Abstract— As the demand for concrete continues to increase to meet the growing needs of the world's ever growing population and urbanisation, it is crucial not to ignore the environmental impact of its production. The use of ordinary Portland cement (OPC) is known to deplete natural resources and release large amounts of CO_2 into the atmosphere. Geopolymer concrete (GPC) is primarily made from waste and industrial by-products and has shown the potential to tackle the environmental issues associated with OPC-based concrete. As well as being a sustainable alternative, GPC has properties that are comparable or superior to those of OPC-based concrete. The aim of the research was to investigate the early-age properties of GPC. Samples of GPC were analysed to determine their mechanical properties and mineralogy during the early stages of elevated temperature curing. The results of this research indicate that the majority of strength gain is developed within the first few hours of elevated curing, with the final strength being achieved after approximately 10 hours. The strength development during these first 10 hours can be estimated by a logarithmic function and beyond this point no significant increase in strength is observed. In addition, the changes observed in the mineralogy and microstructure indicate an initial correlation with the development of the mechanical properties. These observations encourage further research into the mineralogy and microstructure of geopolymers during the curing stage in order to confirm a correlation with the development of mechanical properties.

Keywords— Geopolymer concrete, Early-age, Elevated temperature, Blast-furnace slag, Metakaolin, Properties, Sustainable materials, XRF, XRD

1. Introduction

Geopolymer concrete, an eco-friendly alternative to traditional cement-based concrete, is gaining more attention due to its high strength and lightweight properties. Unlike conventional concrete, which utilizes ordinary Portland cement, GPC uses industrial by-products and waste as a binding agent, making it a more environmentally sustainable option. As global population growth and urbanization increasing the demand for construction materials, it is crucial for the building industry to adopt more sustainable options [1, 2].

The building industry is a major contributor to the global carbon dioxide (CO_2) emissions, it is responsible for around 40% of all emissions [3]. Cement production, which constitutes about 8% of total emissions, is a significant contributor to this problem. The production of ordinary Portland cement (OPC) is particularly problematic due to its chemical composition and production process. Cement production involves calcination of limestone ($CaCO_3$) with silico-aluminous minerals, resulting in the chemical reaction [4]:

$$5CaCO_3 + 2SiO_2 \Longrightarrow (3CaO.SiO_2)(2CaO.SiO_2) + 5CO_2$$

For each ton of cement produced, the reaction produces 0,55 tons of CO_2. Additionally, burning carbon-based fuels releases an extra 0,4 tons of CO_2. This implies that the production of one ton of cement generates roughly one ton of CO_2 [4]. The sizable amount of CO_2 emissions linked with the production of OPC presents a notable obstacle in achieving sustainability goals and avoiding additional harm to the environment [5].

By eliminating the use of OPC as a binding agent and utilizing an alkali or acidic medium to activate alumino-silicate precursors through a process called geopolymerization, GPC resolves this issue, leading to a reduction of 22-72% in CO_2 emissions. The Paris Agreement, signed in December 2015, identified the environmental impact of cement production and the need for more sustainable alternatives as a top priority. GPC not only reduces CO_2 emissions but also offers an effective waste management system, which could positively impact global health and the environment [5, 6].

Research has shown that GPC has comparable mechanical properties to conventional concrete, while also having the ability to decrease CO_2 emissions. Additionally, GPC has exceptional features such as adaptable thermal expansion, resistance to high temperatures, and acid resistance, making it a material that is suitable for diverse construction applications, particularly in environments characterized by elevated levels of heat and acidity [6].

In general, GPC shows great promise as a substitute for conventional concrete, having the capability to decrease CO_2 emissions and enhance the sustainability of the construction industry. GPC has the potential to significantly contribute to a more eco-friendly future, thanks to its impressive strength and lightweight properties, along with its capacity to reduce emissions and handle waste [1].

1.1. History of geopolymer concrete

The geopolymer research began in the 1930s as a significant improvement in alumino-silicate chemistry. During this and the following two decades, the focus was on the development of zeolites and alkali-activated materials (AAM) by reacting alumino-silicates with alkali hydrates. Geopolymer chemistry was first mentioned in the 1970s in the work of the French professor Davidovits on kaolinite. Where in 1975 the first patent for a fire-resistant resin composed of MK and soluble alkali silicates was filed. It wasn't until 1978 that the term "geopolymer" was introduced. Davidovits and Sawyer filed the first geopolymer cement patent, titled "Early-Strength Mineral Polymer," in the United States in 1984 [7, 8, 9].

1.2. Compared to traditional cement-based concrete

GPC has many advantages, it is a very stable and reliable building material that outperforms traditional OPC in many ways. It is more resistant to chemicals, corrosion, temperature changes, cold and high temperatures in general and is therefore more fire resistant than OPC. In addition, GPC is environmentally friendly because it uses primarily waste materials and industrial by-products. GPC is still in its early stages of development, while traditional concrete has already dominated the building industry. Considering all of the benefits, geopolymer concrete has a high potential to become very popular very soon [1, 8].

1.3. Potential applications

The advantages of using GPC are numerous and varied, with its strength and durability it becomes particularly well-suited for construction applications such as roads, bridges, tunnels, marine developents, etc. [2, 10]. One of the benefits of GPC is its high resistance to chlorides, which means that it can withstand exposure to calcium chlorides found in road salts typically used during the winter season [1]. Therefore, GPC is a desirable option for footpaths and bike paths, as demonstrated by projects completed in Australia, such as on Brady Street, Kings Road, and the route around Taylers Lake [11, 12]. Additionally, GPC is suitable for pavements, as demonstrated by the construction of pavements in Wyndham Street, located in the heart of Sydney [13]. Bridges are also well-suited to GPC, as evidenced by the Salmon Street Bridge constructed in Port Melbourne, Australia, as well as two landscape retaining walls built in-situ as part of the Yarra River bridge construction [11, 14]. In addition, a GPC-based pedestrian bridge was constructed in the Russian city of Skolkovo, highlighting the international appeal of this modern and innovative construction material [8].

GPC can also be used to construct buildings. In 1989, a residential building in Lieptsk, Russia, was constructed using an alkali-activated concrete that did not contain OPC [10]. In 2012, the University of Queensland used precast GPC floor beams in the construction of its building [15, 16]. The Brisbane West Well-camp Airport in Australia is a significant engineering accomplishment, using the largest amount of GPC, in a single project, in the world and took almost 50 years to complete [17]. The first 3D printed GPC house was built in Siberia in 2018, representing the most recent innovation in the use of GPC in residential construction [8].

1.4. Mechanism of geopolymerization

Geopolymerization is a complex chemical reaction that integrates minerals. The strength of the GPC is developed by the reaction between alumino-silicate source materials and either acidic or alkaline activators. Various amounts of different source materials have been used in the production of GPC and a proper selection will benefit the desired properties. An example geopolymer product is used to illustrate the process and kinetics of the geopolymerisation reaction. It is the result of the reaction between metakaolin 750 (MK-750) and sodium silicate (Na_2SiO_3), an alkaline activator [8, 18, 19, 20, 21].

The geopolymerization mechanism is initiated by the alkalination of metakaolin particles. The chemistry of alkalination is determined by the nature of both the alumino-silicate sources and the used activators. However, the reaction relies on the same mechanisms regardless of the initial materials. Due to alkalination, the Al atom has a valency of 4 and becomes tetravalent in the side group sialate Si-O-Al-$(OH)_3Na^+$, as illustrated in Figure 1 [8, 20, 21].

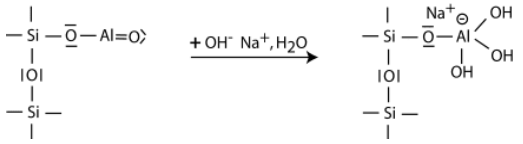

Figure 1: Alkalination of sialate group [21]

The aluminium atom either acts as an acid or a base, depending on the substance it's reacting with. This implies that the Al atom can either be trivalent or tetravalent by respectively giving up or accepting protons from other atoms. In the following stage, shown in Figure 2, the pentavalent silicon atom is formed by interaction with the OH^- cation. This initiates the alkali dissolution on the particle edges [8, 21].

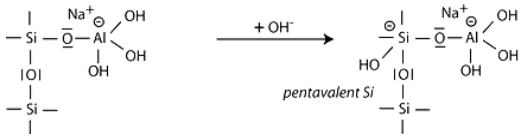

Figure 2: Initiation of superficial alkali dissolution [21]

The next step in the reaction is the separation of the siloxane oxygen (Si-O-Si) by the transfer of the electron from Si to O. This causes the silicon atom to return to a tetravalent state. This leads to the formation of the intermediate silanol (Si-OH) and basic siloxo ($Si-O^-$) as shown in Figure 3 [8, 21].

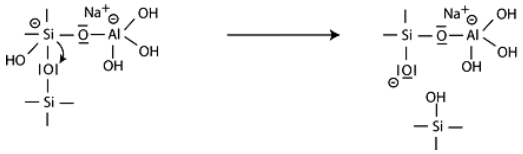

Figure 3: Formation of intermediate silanol (Si-OH) and basic siloxo ($Si-O^-$) [21]

The reaction continues with the formation of silanol groups (Si-OH) and isolation of the ortho-sialate molecule, shown in Figure 4, which is the primary unit in geopolymerization [8, 21].

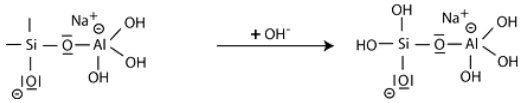

Figure 4: Formation of primary unit of geopolymerization [21]

A reaction between the basic siloxo ($Si-O^-$) and the sodium cation Na^+, causes the formation of the Si-O-Na terminal bond. The terminal atom Na^+ is bonded to the central oxygen atom, visible in Figure 5 [8, 21].

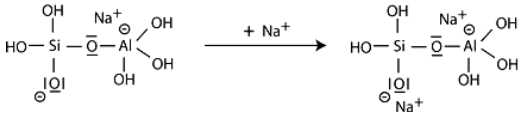

Figure 5: Formation of orthosialate molecule [21]

A cyclo-tri-sialate structure is formed by condensation between the ortho-sialate molecules, the reactive groups (Si-O-Na) and the aluminum hydroxyl molecules (OH-Al). This condensation produces the alkaline substance NaOH. As the cyclic structure is formed, the alkali is released and is again available for reaction, responsible for further polycondensation into the Na-poly(sialate) nepheline backbone as can be seen in Figure 6 [8, 21].

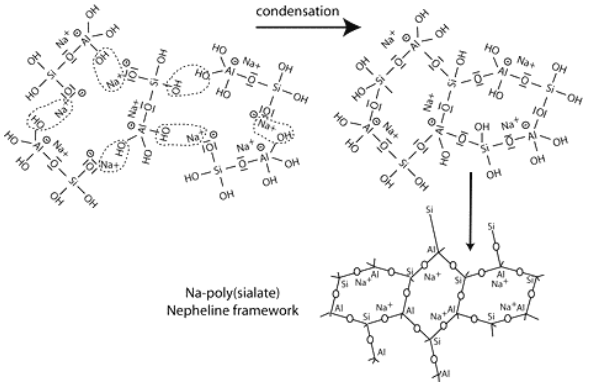

Figure 6: Condensation of the ortho-sialates [21]

Condensation also takes place between di-siloxinate and ortho-sialate molecules, due to the presence of waterglass. As shown in Figure 7, the reactive groups Si-O-Na, Si-OH and OH-Al˙ form the cyclic ortho-sialate-disiloxo structure through which the alkali NaOH is released and reacts a second time [8, 21].

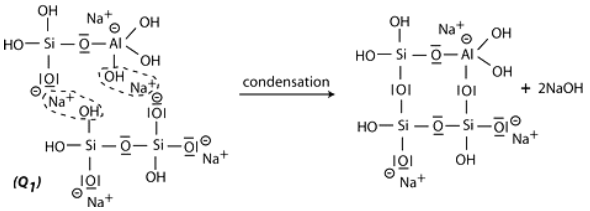

Figure 7: Condensation into cyclic ortho-sialate-disiloxo [21]

During further polycondensation, the chains formed interact through hydrogen bonding to form the three-dimensional geopolymer network. The free NaOH is completely consumed during the formation of the network and a Na-poly (sialate-disiloxo) albite framework with a typical feldspar crankshaft chain structure is formed, as shown in Figure 8. The hydrogen bonds lead to in dehydroxylation, causing water to evaporate and form the final stable network through solidification [8, 21].

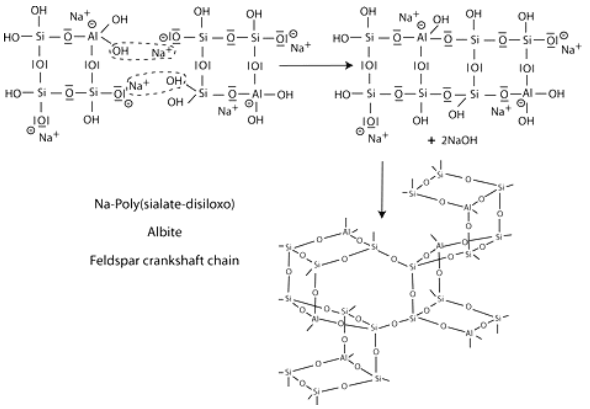

Figure 8: Formation of 3D geopolymeric network [21]

1.5. Mineralogy of geopolymers

The phases detected in geopolymer concrete are either amorphous or semi-crystalline. The primary phase is a geopolymer gel which is formed by the chemical reaction between the alkaline activator and the precursor. Depending on the used alkaline activator, the geopolymer gel can either be sodium or potassium-based. The gel has a three-dimensional polymer network structure formed by tetrahedral and octahedral units of Si, Al and O.

The gel also has a high specific surface area, which means it can absorb water and other chemicals, contributing to the strength and durability of the concrete. In addition to the geopolymer gel, geopolymer concrete can contain secondary crystalline phases, such as zeolites and alumino-silicate hydrates, similar to those found in OPC-based concrete. Geopolymers typically contain alumino-silicate hydrates, the type of which depends on the used alkaline activator and precursors. [22, 23, 24, 25, 26].

1.6. Microstructure of geopolymers

Geopolymers have a microstructure that differs from traditional cement-based concrete due to the mechanisms of geopolymerization. It results in a denser, more homogeneous material with a lower porosity and a more uniformly distributed binder phase.

The microstructure is mainly composed of three types of features: the geopolymer gel, the aggregates and the interfacial transition zone (ITZ), which are shown in Figure 9 through an image obtained by a scanning electron microscope. The gel forms a continuous matrix around the aggregates and fills the voids between them, while the aggregates provide most of the mechanical strength. The ITZ is the region where the gel and aggregates meet and it plays an important role in the final mechanical properties of the geopolymer [9, 27, 28, 29].

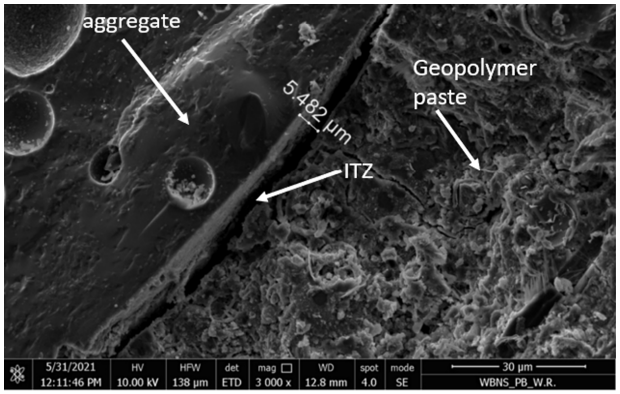

Figure 9: Interfacial transition zone between coarse aggregate and geopolymer paste [27]

1.7. Influencing factors

Various factors such as curing temperature and time, curing conditions and the chemical composition of the raw materials play a unique role in the development of the final product. A small change can have a large effect on the mineralogy and development of the geopolymer concrete, affecting its microstructure and physical properties such as strength. Therefore, careful selection of precursors and mix design is critical in the design of GPC [19].

2. Materials and Methods

2.1. Materials

2.1.1. Metakaolin

Metakaolin (MK) is obtained by calcination and dehydroxylation of kaolinitic clay at temperatures in the range of 500°C to 900°C. In addition to being an amorphous alumino-silicate source material, MK is also a highly reactive natural pozzolan. MK has porous, angular-shaped, platy particles with an average size that can range from 1 to 20 µm and a specific gravity of 2,20 to 2,60 [8, 30, 31].

The physical properties and chemical composition of the used MK are given in Table 1, it should be noted that the density is slightly higher than reported in the literature [4]. The MK mainly consists of SiO_2 and Al_2O_3, the sum of which is about 80% of the total weight percentage. The amount of SiO_2 is almost 1,80 times higher than that of Al_2O_3. These results are based on handheld X-ray fluorescence (XRF) data. Since this is a handheld spectrometer, no elements lighter than magnesium are detected and the elemental composition had to be converted to oxide composition. Several major crystal phases were identified in the X-ray diffraction (XRD) pattern shown in Figure 10. The major phases detected in the MK pattern are kaolinite ($Al_2Si_2O_5(OH)_4$) and quartz (SiO_2). Small traces of anatase (TiO_2) are also identified. The XRD pattern also shows a slightly higher background in the range 17.5-30° 2θ, indicating the presence of an amorphous phase. This broad amorphous area is typical for MK and is caused by the thermal calcination process [32].

2.1.2. Ground granulated blast-furnace slag

Ground granulated blast-furnace slag (GGBFS) is the main by-product of the iron and steel production. A carefully controlled combination of limestone, iron ore and coke are melted together in a blast furnace. This produces iron and slag in a molten state. This molten slag is rapidly cooled by powerful water jets, transforming it into GGBFS. Only highly amorphous slag can be used as a precursor for geopolymers, but it lacks certain molecular structures to be used as the only precursor in the GPC process. The small particle size, ranging from 5 to 25 µm, increases the specific surface area and its reactivity. The particles are angular and irregular, resembling broken glass particles, with a specific gravity ranging from 2,50 to 2,90 [8, 33].

The chemical composition of GGBFS, obtained by a handheld XRF spectrometer, used in this research is given in Table 1. It is mainly composed of CaO, SiO_2, Fe_2O_3 and Al_2O_3, the sum of which is close to 85% of the total weight. The XRD pattern of the examined GGBFS sample (Figure 10) shows that its structure is almost entirely amorphous. This makes it difficult to identify peaks in the pattern. It is suggested in the literature that the angular band in the range of 25 - 35° 2θ could be attributed to a significant proportion of the amorphous structure, such as glass. It is highly likely that some of the slag partially crystallized during the cooling process [34]. Small peaks of calcite ($CaCO_3$), quartz (SiO_2) and anorthite ($CaAl_2Si_2O_8$) were identified through the amorphous content.

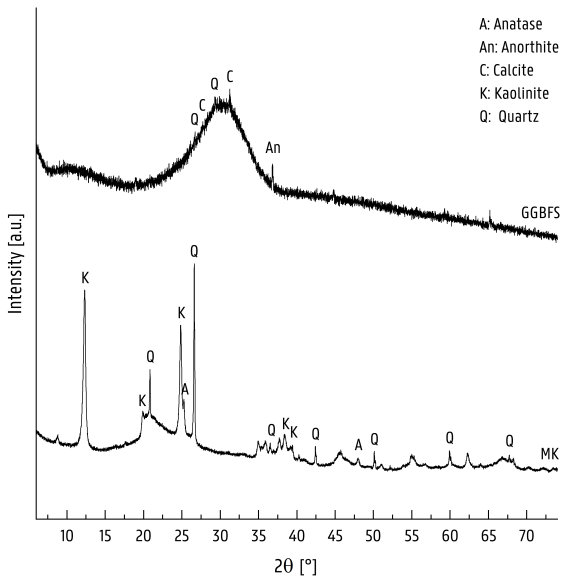

Figure 10: XRD pattern of MK and GGBFS

Table 1: Physical and chemical properties of MK and GGBFS

Properties	MK	GGBFS
Specific surface area [cm²/g][1]	21 710	4 380
Density [g²/cm³]	2,68 ± 0,03	2,89 ± 0,06
pH [-]	5,10 ± 0,04	11,67 ± 0,03
SiO_2 [wt.-%]	53,09 ± 0,20	24,97 ± 0,04
Al_2O_3 [wt.-%]	29,75 ± 0,28	6,65 ± 0,06
Fe_2O_3 [wt.-%]	4,80 ± 0,22	0,74 ± 0,02
CaO [wt.-%]	0,83 ± 0,01	48,02 ± 0,10
MgO [wt.-%]	-	6,14 ± 0,15
K_2O [wt.-%]	0,75 ± 0,07	1,13 ± 0,01

[1] Measured by the Blaine method

2.1.3. Sodium silicate solution

The sodium silicate solution (SSS) used to activate the geopolymerization reaction in this research is based on a commercially available solution. However, the ready-to-use SSS did not have a suitable SiO_2/Na_2O molar ratio (MR). The purchased SSS has a MR of approximately 3,4 while the it is recommended to use a SiO_2/Na_2O MR in the range of MR=1,7 to 1,9 [21]. The used SSS has an adjusted MR by dissolving additional sodium hydroxide (NaOH). An MR $\simeq$ 1,7 is obtained by adding 7,5 wt.-% of NaOH to the original solution and keeping it for 24 hours before use.

2.1.4. Geopolymer preparation

The MK, GGBFS based geopolymer mix used in this research was prepared according to the mix design shown in Table 2. The geopolymer was prepared using the following mixing procedure. First, the aggregates and GGBFS were mixed at low speed for three minutes and then kept in a separate bowl. The MK and SSS were then mixed at high speed for 10 minutes to initiate alkalination of the sialate groups. The mixed aggregates and GGBFS were added to the MK & SSS-mixture and mixed at low speed for five minutes together with the additional water. The resulting mixture was poured into standardised prism moulds (160x40x40 mm^3) and vibrated with a vibrating table for one minute.

Table 2: Mix design used geopolymer [kg/m³]

	MK	GGBFS	SSS	Sand EN 196-1	Water
DM8	163,33	381,11	263,33	1 324,44	110,00

The filled moulds were kept sealed with plastic foil to prevent premature condensation and cured at an elevated temperature of 70°C. All samples underwent curing at 70°C for a maximum of 24 hours. The samples to be tested at 28 days were removed from the moulds after 24 hours of elevated temperature and kept sealed at ambient temperature.

2.2. Methods

2.2.1. Fresh density and workability

The fresh properties of the concrete mix were analysed. The density of the fresh concrete was determined by using the EN 12350-6 standard. The concrete mix was layered into a container and compacted with a compacting rod. The filled container was weighed after full compaction, and the density of the fresh concrete was calculated by dividing the difference in mass [kg] by the known volume [m^3]. Furthermore, the flowtable test was used to assess the workability of fresh concrete, which uses the Haegermann cone and follows the standard EN 1015-3:1999.

2.2.2. Flexural and compressive strength

The flexural and compressive strength of the prisms were evaluated at different curing times using a consistent curing process for all samples. The flexural strength tests were performed on solid prisms with dimensions of 160x40x40 mm^3, while the compressive strength tests were performed on the broken half-prisms. The process for both tests followed the EN 196-1:2016 standard.

2.2.3. Mineralogy and microstructure

The development of mineralogy and microstructure during the curing phase of geopolymers was evaluated by XRD analysis. The analysis is based on powder samples that were obtained by grinding the samples which were crushed after the strength related tests. Using a bowl grinder to minimise the generated heat in the powder, reducing the risk of phase change during powder preparation. After each of the mechanical property tests, a sample is taken for XRD analysis. This allows the development of the mechanical properties to be linked to the mineralogy and microstructure.

3. Results and Discussion

3.1. Evolution of mechanical properties

The average density and workability of the fresh concrete are shown in Table 3. The obtained results are an average of 17 batches.

Table 3: Fresh properties DM8

Mix	Density of mix		Workability[1]	
	ρ [kg/m³]	S.G. [-]	D_{avg} [cm]	F_{avg} [-]
DM8	2 170	2,17	23,35	133,53

[1] Tested with Hägermann flow table according to EN 1015-3

The measured mechanical properties at different curing times are shown in Table 4. The outliers are treated according to EN 196-1 and ISO 5725-2 (Grubb's test for outliers), for the compressive and flexural strengths, respectively. In Figure 11 the development of compressive strength as a function of the age is shown. Whereas development of the flexural strength in function of the age is shown in Figure 12.

Within the margin of error, there is no further strength development. So it can be concluded that the strength of this mix is fully developed after one day of curing at an elevated temperature of 70°C. For GPC it is not uncommon to exhibit a rapid increase in strength at high temperatures [19, 35]. Within the first 6 hours of elevated curing, most rapid curing occurs in both compressive and flexural strength. The strength development continues slowly until 10 hours of curing are reached, after which roughly full strength is achieved. The increases in strength that follow after this first 10 hours of curing are minimal, because the measured strengths lie within the margin of error of the 24 hour cured samples. At 7 and 9 hours of curing, something unusual happens to the measured flexural strength. Because of the sudden drop in strength, more samples were taken to ensure that these values are representative.

The margins of error are generally small. Because compressive strength is based on twice as many samples as flexural strength, they are almost always smaller. Since the measured values for flexural strength are much lower compared to compressive strength, the impact of a small error is proportionally greater.

The flexural and compressive strengths after 6 hours of curing have already reached nearly 60 and 70% of their total strength, respectively. The relative compressive and flexural strengths continue to increase until they reach almost full strength after 10 hours of curing. After this, the strength is more or less the same than at 28 days curing. This observation suggests that the mix behaves similarly in terms of compressive and flexural strength development over time. However, the flexural strength lags slightly behind the compressive strength. There is no significant deviation in the trend between the two strength properties.

Table 4: Early-age mechanical properties of DM8 mixtures

Age	Absolute values		
	$\sigma_{c,avg}$ [MPa]	$\sigma_{f,avg}$ [MPa]	S.G. [-]
0 h	-	-	2,17 ± 0,02
1 h	6,6 ± 0,2	0,6 ± 0,1	2,18 ± 0,01
2 h	14,3 ± 0,5	1,3 ± 0,1	2,14± 0,02
3 h	36,6 ± 1,3	2,1 ± 0,4	2,18 ± 0,02
4 h	41,9 ± 1,7	2,6 ± 0,1	2,15 ± 0,01
5 h	49,1 ± 0,6	2,9 ± 0,1	2,16 ± 0,01
6 h	49,3 ± 1,3	3,5 ± 0,3	2,16 ± 0,03
7 h	57,1 ± 1,6	2,5 ± 1,3	2,16 ± 0,02
8 h	60,7 ± 2,7	3,6 ± 0,2	2,17 ± 0,03
9 h	61,9 ± 3,6	3,4 ± 0,6	2,17 ± 0,04
10 h	69,8 ± 2,5	5,2 ± 0,4	2,20 ± 0,01
12 h	67,9 ± 2,0	5,7 ± 1,0	2,15 ± 0,02
14 h	63,4 ± 2,8	5,0 ± 0,5	2,16 ± 0,04
16 h	72,6 ± 1,6	5,4 ± 1,0	2,16 ± 0,02
18 h	65,1 ± 4,4	5,1 ± 1,0	2,14 ± 0,03
20 h	65,0 ± 3,6	4,3 ± 0,4	2,12 ± 0,01
22 h	73,7 ± 3,2	4,9 ± 0,9	2,15 ± 0,02
24 h	72,4 ± 3,9	4,7 ± 1,1	2,17 ± 0,01
28 d	71,6 ± 1,7	5,8 ± 0,1	2,17 ± 0,01

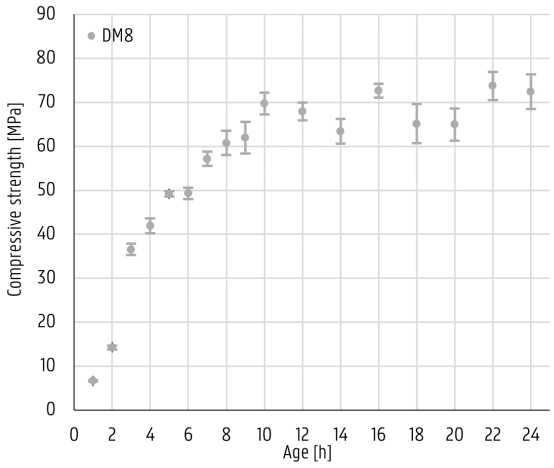

Figure 11: Development compressive strength DM8

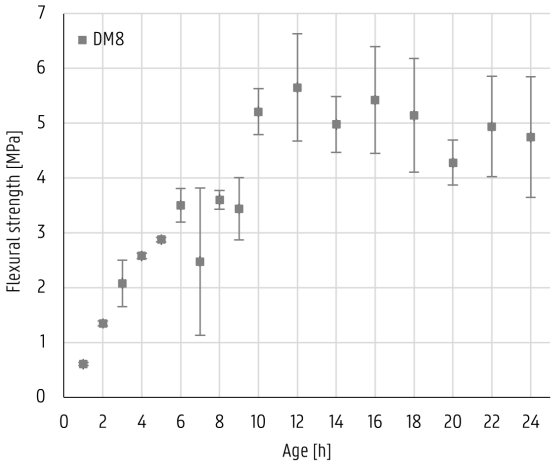

Figure 12: Development flexural strength DM8

Figure 13 summarises the first 10 hours of curing and shows the curing time on a logarithmic scale. This illustrates that strength development can be interpreted as a logarithmic correlation until maximum strength is achieved. Several parameters influence the angle at which the curves are plotted, in addition to the time required for the line to become horizontal. One of these parameters is the elevated temperature at which the samples are cured.

Temperatures have been found to have a considerable impact on the curing time of the material. For example, a higher temperature may accelerate the curing process, resulting in a shorter overall curing time. A lower temperature, on the other hand, may cause the curing process to take longer.

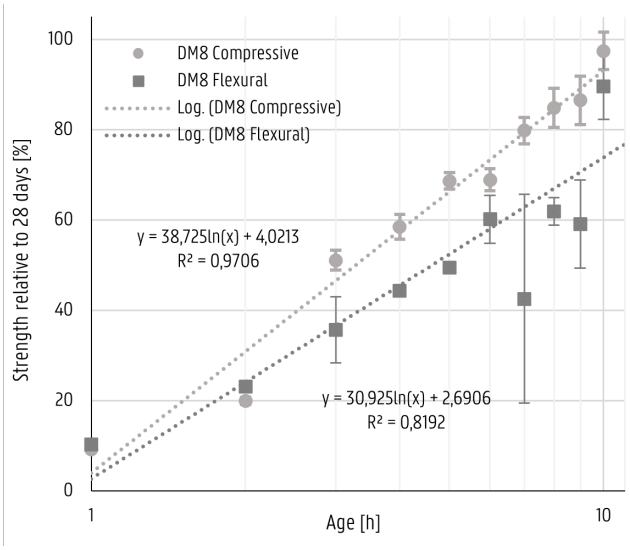

Figure 13: Relative strength development DM8 (log. scale)

3.2. Evolution of mineralogy and microstructure

The observed changes in mineralogy and microstructure are summarized and the most significant changes are shown in Figure 14. The majority of phases detected by XRD in the sample after 1 hour of elevated curing is quartz and some additional traces of kaolinite were identified. This is most likely to be originated from metakaolin, as it is one of its main phases.

After 6 hours of elevated curing, the presence and increasing amorphous content in the range of 27,5 - 32,5° 2θ indicates the formation of sodium alumino silicate hydrate gel, amorphous in nature and structured as a three-dimensional network [36]. At this point in time, approximately 70% of the final compressive strength has already been developed. The increase in amorphous content could be responsible for this initial strength development. Some small traces of microcline can also be observed from 6 hours onwards.

In the XRD patterns observed from six hours onwards, other phases are occasionally identified, while there is a slight increase in the amorphous phase. The additional phases detected, mainly the clay mineral illite and feldspar microcline, tend to be identified at angles 20 and 25° 2θ where kaolinite was previously detected.

The patterns from 10 hours up to 28 days of curing do not show any significant changes after 10 hours of elevated curing. They are mainly composed of quartz with some additional traces of kaolinite, illite and microcline identified by XRD. The presence of illite or microcline at 30° 2θ is observed in most of the samples from the nine hours of elevated curing samples. Typically, but depending on the sample, the original peaks of kaolinite at 20 and 25° 2θ are replaced by either illite or microcline.

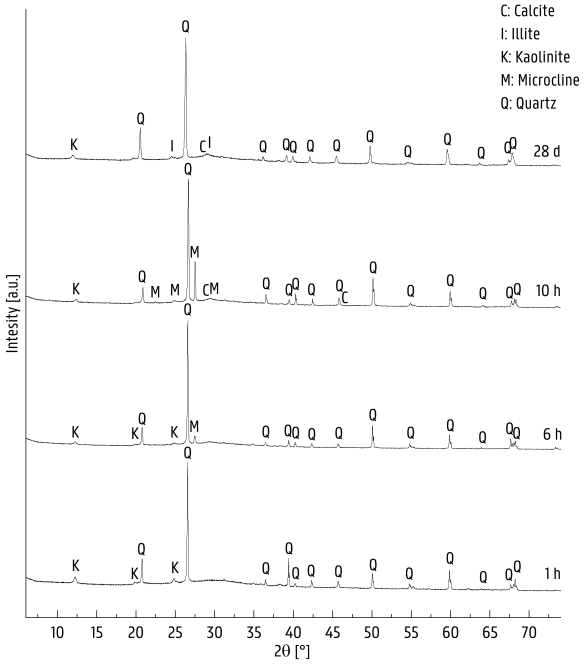

Figure 14: Highlights XRD patterns DM8

4. Conclusions

In this research, a GPC mix was made by using MK and GGBFS as precursors and a sodium silicate solution as the geopolymerization initiator. The batches were cured for the first 24 hours at 70°C before being stored at room temperature. To prevent premature condensation, the samples were always sealed with plastic foil. In the early stages of curing, GPC samples were examined for mechanical properties and mineralogy. The results show that 60% and 70% of the flexural and compressive strength is developed within the first 6 hours of elevated curing, respectively. After about 10 hours, more than 90% of the final strength is achieved in comparison to strength measured at 28 days. A logarithmic function can be used to approximate the strength development during the first 10 hours, no significant increase in strength is observed beyond this point. Both flexural and compressive strengths are expressed relative to the values measured after 28 days of curing, indicating that they may follow the same curing pattern.

XRD spectroscopy is used to get a first idea of the evolution of mineralogy in order to correlate it with the evolution of strength. According to the literature, the increasing presence of an amorphous phase in the range of 27,5 - 32,5° 2θ indicates that a sodium alumino silicate hydrate gel is mainly being formed in the first 6 hours. Later on, more clay and feldspar minerals, illite and microcline, are detected in the XRD patterns as the amorphous content continues to increase. After 10 hours of elevated curing, more than 90% of the full strength is achieved and no significant changes are visible in the patterns. These observed changes in mineralogy and microstructure indicate an initial correlation with the development of mechanical properties.

5. Further research

The results of this research are heavily influenced by the resources used to produce the GPC, as well as the quantification methods and curing conditions. Further research is needed to make more a more general conclusion about the development of the early-age properties of geopolymers. This could also include different curing temperatures and durations to achieve an ideal curing method.

The obtained results regarding mineralogy and microstructure are based on the specific samples and sample preparation methods used in this study. Further research is required to confirm these results with a sufficient amount of data to support them. A more accurate understanding of the amorphous content can be obtained by using additional techniques such as NMR and FTIR. XRD does not easily detect amorphous phases. These methods could provide researchers with a more complete picture of the mechanisms of geopolymerization, the resulting microstructure and how this relates to the development of the mechanical properties.

Author Contributions

Conceptualization, D.D.M., M.L.H., V.B. and I.N.; Data curation, D.D.M. and M.L.H.; Investigation, D.D.M, M.L.H., I.N. and V.B.; Writing - original draft, D.D.M. and M.L.H.; Supervision, V.B. and I.N.

Declaration of Conflict of Interests

The authors declare that they have no known competing financial interests or personal relationships that could have appeared to influence the work reported in this paper.

Acknowledgements

This research is included in the master's dissertation submitted in order to obtain the academic degree of Master of Science in de industrieële wetenschappen: bouwkunde. It is part of the GEOSUMAT project, an international research project funded by M-ERA.NET.

References

[1] K. K. Poloju, *Advanced materials and sustainability in civil engineering*, 1st ed. Singapore, Singapore: Springer, 2021.

[2] N. Shehata, O. A. Mohamed, E. T. Sayed, M. A. Abdelkareem, and A. G. Olabi, "Geopolymer concrete as green building materials: Recent applications, sustainable development and circular economy potentials," *SCIENCE OF THE TOTAL ENVIRONMENT*, vol. 836, AUG 25 2022.

[3] A. 2030, "Why the built environment?" 2022. [Online]. Available: https://architecture2030.org/why-the-building-sector/The%20built%20environment%20generates%2040,for%20an%20additional%2013%25%20annually

[4] Z. G. Ralli and S. J. Pantazopoulou, "State of the art on geopolymer concrete," *INTERNATIONAL JOURNAL OF STRUCTURAL INTEGRITY*, vol. 12, no. 4, pp. 511–533, AUG 9 2021.

[5] S. Qaidi, H. Najm, S. Abed, H. Ahmed, H. Al Dughaishi, J. Al Lawati, M. Sabri, F. Alkhatib, and A. Milad, "Fly ash-based geopolymer composites: A review of the compressive strength and microstructure analysis," *Materials*, vol. 15, p. 7098, 10 2022.

[6] L. Rodgers, "Climate change: The massive co2 emitter you may not know about," Dec 2018. [Online]. Available: https://www.bbc.com/news/science-environment-46455844?fbclid=IwAR3UdWPQ3F2jBqMHiARsbG4AWWaYCwFJgDQzRhi4NKCFeF3E5piJp8hgobY

[7] S. Luhar, D. Nicolaides, and I. Luhar, "Fire resistance behaviour of geopolymer concrete: An overview," *BUILDINGS*, vol. 11, no. 3, MAR 2021.

[8] Z. G. Ralli and S. J. Pantazopoulou, "State of the art on geopolymer concrete," *INTERNATIONAL JOURNAL OF STRUCTURAL INTEGRITY*, vol. 12, no. 4, pp. 511–533, AUG 9 2021.

[9] "Alkali activated materials : State-of-the-art report, rilem tc 224-aam," Dordrecht, 2014.

[10] A. L. Almutairi, B. A. Tayeh, A. Adesina, H. F. Isleem, and A. M. Zeyad, "Potential applications of geopolymer concrete in construction: A review," *CASE STUDIES IN CONSTRUCTION MATERIALS*, vol. 15, DEC 2021.

[11] F. Andrews-Phaedonos, "Specification and use of geopolymer concrete," 2014. [Online]. Available: https://austroads.com.au/publications/bridges/abc-sas203-14

[12] Z. P. L. a. D. o. C. a. B. E. J S J van Deventer, "Geopolymer concrete - a commercial reality," Feb 2011. [Online]. Available: https://www.globalcement.com/magazine/articles/316-geopolymer-concrete-a-commercial-reality?fbclid=IwAR1lRO4oqWYZOoOaRqpi5wgHho4liOSEyTi6dntdGp2RGCRx_z3qHHC_YzU

[13] A. H. Mahmood, X. Shen, A. Parvez, J. Aldred, and S. Foster, "Performance of geopolymer concrete pavement at wyndham street for city of sydney: Update november 2020," in *Performance of Geopolymer Concrete Pavement at Wyndham Street for City of Sydney: Update November 2020*, 06 2021.

[14] F. Andrews-Phaedonos, "Geopolymer "green" concrete – reducing the carbon footprint – the vicroads experience," 2011.

[15] R. Bligh and T. Glasby, "Development of geopolymer precast floor panels for the global change institute at university of queensland."

[16] K. H. Mo, U. J. Alengaram, and M. Z. Jumaat, "Structural performance of reinforced geopolymer concrete members: A review," *Construction and Building Materials*, vol. 120, pp. 251–264, 2016. [Online]. Available: https://www.sciencedirect.com/science/article/pii/S0950061816308121

[17] T. Glasby, J. Day, R. Genrich, and J. Aldred, "Efc geopolymer concrete aircraft pavements at brisbane west wellcamp airport," 2015.

[18] A. Gholampour and T. Ozbakkaloglu, "8 - oven-cured alkali-activated concrete," in *Handbook of Advances in Alkali-Activated Concrete*, ser. Woodhead Publishing Series in Civil and Structural Engineering, F. Pacheco-Torgal, P. Chindaprasirt, and T. Ozbakkaloglu, Eds. Woodhead Publishing, 2022, pp. 157–186. [Online]. Available: https://www.sciencedirect.com/science/article/pii/B9780323854696000192

[19] D. Khale and R. Chaudhary, "Mechanism of geopolymerization and factors influencing its development: a review," *JOURNAL OF MATERIALS SCIENCE*, vol. 42, no. 3, pp. 729–746, FEB 2007.

[20] L. Yun-Ming, H. Cheng-Yong, M. M. Al Bakri, and K. Hussin, "Structure and properties of clay-based geopolymer cements: A review," *PROGRESS IN MATERIALS SCIENCE*, vol. 83, pp. 595–629, OCT 2016.

[21] J. Davidovits, "About geopolymerization," Apr 2006. [Online]. Available: https://www.geopolymer.org/science/about-geopolymerization/

[22] ——, *Geopolymer Chemistry and Applications*. Geopolymer Institute, 2008. [Online]. Available: https://books.google.be/books?id=dliw_KTYq4oC

[23] K. Komnitsas and D. Zaharaki, "Geopolymerisation: A review and prospects for the minerals industry," *Minerals Engineering*, vol. 20, no. 14, pp. 1261–1277, 2007. [Online]. Available: https://www.sciencedirect.com/science/article/pii/S089268750700204X

[24] B. Walkley, R. San Nicolas, M.-A. Sani, G. J. Rees, J. V. Hanna, J. S. van Deventer, and J. L. Provis, "Phase evolution of c-(n)-a-s-h/n-a-s-h gel blends investigated via alkali-activation of synthetic calcium aluminosilicate precursors," *Cement and Concrete Research*, vol. 89, pp. 120–135, 2016. [Online]. Available: https://www.sciencedirect.com/science/article/pii/S0008884616302381

[25] P. Duxson, A. Fernández-Jiménez, J. Provis, G. Lukey, A. Palomo, and J. Van Deventer, "Geopolymer technology: The current state of the art," *Journal of Materials Science*, vol. 42, pp. 2917–2933, 05 2007.

[26] J. Provis and S. Bernal, "Geopolymers and related alkali-activated materials," *Annual Review of Materials Research*, vol. 44, 07 2014.

[27] A. Zbiciak and T. Markiewicz, "A new extraordinary means of appeal in the polish criminal procedure: the basic principles of a fair trial and a complaint against a cassatory judgment," *Access to Justice in Eastern Europe*, vol. 6, no. 2, pp. 1–18, Mar. 2023.

[28] H. Alanazi, "Study of the interfacial transition zone characteristics of geopolymer and conventional concretes," *Gels*, vol. 8, no. 2, p. 105, Feb. 2022. [Online]. Available: https://doi.org/10.3390/gels8020105

[29] Z. Luo, W. Li, K. Wang, A. Castel, and S. P. Shah, "Comparison on the properties of itzs in fly ash-based geopolymer and portland cement concretes with equivalent flowability," *Cement and Concrete Research*, vol. 143, p. 106392, 2021. [Online]. Available: https://www.sciencedirect.com/science/article/pii/S0008884621000417

[30] D. K. Panesar, "3 - supplementary cementing materials," in *Developments in the Formulation and Reinforcement of Concrete*, 2nd ed., ser. Woodhead Publishing Series in Civil and Structural Engineering, S. Mindess, Ed. Woodhead Publishing, 2019, pp. 55–85. [Online]. Available: https://www.sciencedirect.com/science/article/pii/B9780081026168000034

[31] J. M. Khatib, O. Baalbaki, and A. A. ElKordi, "15 - metakaolin," in *Waste and Supplementary Cementitious Materials in Concrete*, ser. Woodhead Publishing Series in Civil and Structural Engineering, R. Siddique and P. Cachim, Eds. Woodhead Publishing, 2018, pp. 493–511. [Online]. Available: https://www.sciencedirect.com/science/article/pii/B9780081021569000158

[32] D. Moro, R. Fabbri, J. Romano, G. Ulian, A. Calafato, A. Solouki, C. Sangiorgi, and G. Valdrè, "Thermal, x-ray diffraction and oedometric analyses of silt-waste/naoh-activated metakaolin geopolymer composite," 2021. [Online]. Available: https://www.mdpi.com/2504-477X/5/10/269

[33] J. Ahmad, K. J. Kontoleon, A. Majdi, M. T. Naqash, A. F. Deifalla, N. Ben Kahla, H. F. Isleem, and S. M. A. Qaidi, "A comprehensive review on the ground granulated blast furnace slag (ggbs) in concrete production," *Sustainability*, vol. 14, no. 14, 2022. [Online]. Available: https://www.mdpi.com/2071-1050/14/14/8783

[34] A. Nourredine and R. Jauberthie, "Calcium silicate materials: Substitution of hydrated lime by ground granulated blast furnace slag in autoclaving conditions," *Journal of Materials in Civil Engineering*, vol. 24, pp. 1230–1236, 09 2012.

[35] M. Nurruddin, S. Haruna, B. Mohammed, and I. Shaaban, "Methods of curing geopolymer concrete: A review," *International Journal of ADVANCED AND APPLIED SCIENCES*, vol. 5, pp. 31–36, 01 2018.

[36] M. Criado, W. Aperador, and I. Sobrados, "Microstructural and mechanical properties of alkali activated colombian raw materials," *Materials*, vol. 9, no. 3, p. 158, Mar. 2016. [Online]. Available: https://doi.org/10.3390/ma9030158

Influence of various waste materials on early-age properties of geopolymers

Dario De Muynck[1,2], Marie-Laure Heyndrickx[1,2], Veerle Boel[1] and Iveta Nováková[2]

[1] *Ghent University, Department of Structural Engineering and Building Materials, Ghent, Belgium*
[2] *UiT The Arctic University of Norway, Department of Building, Energy and Material Technology, Narvik, Norway*

Abstract— As the demand for concrete grows, so does the environmental impact associated with its production. The use of ordinary Portland cement (OPC) is known to deplete natural resources and release large amounts of CO_2 into the atmosphere. Geopolymer concrete (GPC), made from waste and industrial by-products, has shown the potential to overcome the environmental issues associated with OPC-based concrete. GPC has comparable or superior properties to OPC-based concrete, in addition to being a sustainable alternative. This research aims to investigate the influence of incorporating alternative waste materials on the early-age properties of GPC. Samples of GPC with partially integrated alternative waste sources were examined for their mechanical properties and mineralogy in the early stages of curing. An effect on early-age properties was observed by integrating various alternative waste sources. Each different waste source indicated at least some effect on the fresh or hardened properties, the rate at which they developed, and the mineralogy. Some mechanical properties were improved by the use of these alternative waste sources in combination with significant changes in mineralogy. Initial observations show the potential benefits of using alternative waste materials in geopolymers, not only in terms of performance but also for a more sustainable future in construction.

Keywords— Geopolymer concrete, Early-age, Properties, Recycled aggregates, Seawater, Sustainable materials, Waste materials

1. Introduction

Geopolymer concrete is a high-strength, lightweight material that is gaining ground as a more environmentally friendly alternative to traditional cement-based concrete. Unlike traditional concrete, which contains ordinary Portland cement, GPC contains waste and industrial by-products as a binding agent, making it a more environmentally friendly option. With an expected increase in demand for construction materials due to global population growth and urbanisation, it is critical that the building industry considers more sustainable options [1, 2].

The building industry contributes significantly to global carbon dioxide (CO_2) emissions in our atmosphere, accounting for approximately 40% of global emissions (Figure 1) [3]. Cement production is responsible for a substantial portion of the world's CO_2 emissions, accounting for approximately 8% of the total [4]. The chemistry of OPC production has a significant contribution to global warming. Cement is made by calcination of limestone ($CaCO_3$) with silico-aluminous minerals, which results in the following chemical reaction [5]:

$$5CaCO_3 + 2SiO_2 \Longrightarrow (3CaO.SiO_2)(2CaO.SiO_2) + 5CO_2$$

This reaction generates 0,55 tons of CO_2 for every ton of cement produced. Furthermore, the combustion of carbon-fuel emits an additional 0,4 tons of CO_2. This means that for every ton of cement produced results in the generation of approximately one ton of CO_2 [5]. The substantial CO_2 emissions associated with the production of OPC poses a significant challenge to meeting sustainability targets and to avoid further contribution to negative environmental impacts [6].

GPC solves this problem by eliminating the use of OPC as a binding agent. Instead, it uses an alkali or acidic medium to activate aluminosilicate precursors through a process known as geopolymerization, resulting in a 22-72% reduction in CO_2 emissions. The environmental impact of cement production and the need for more sustainable alternatives has been marked as a priority in the Paris Agreement that has been signed in December 2015. GPC does not only reduces CO_2 emissions but also provides an efficient waste management system, which may benefit global health and the environment [4, 6].

Studies have shown that GPC has similar mechanical characteristics as traditional concrete, while being able to reduce CO_2 emissions. GPC also has superior properties such as adjustable thermal expansion, high-temperature resistance and acid resistance. This makes it a versatile material that can be used in various construction applications, particularly in environments with high levels of heat and acidity [4].

Overall, GPC is a promising alternative to traditional concrete, with the potential to reduce CO_2 emissions and improve building industry sustainability. GPC has the potential to play a significant role in building a greener future due to its high strength and lightweight characteristics, as well as its ability to reduce emissions and manage waste [1].

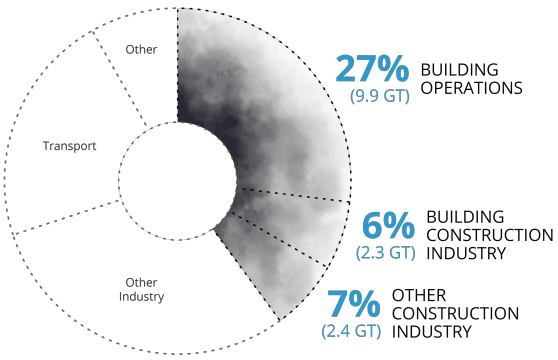

Figure 1: Annual global CO_2 emissions [3]

Geopolymerization is a complex reaction that chemically integrates minerals. The strength of the geopolymer concrete is developed through the reaction between alumino-silicate source materials and acidic or alkaline activators. It involves the dissolution of the resource materials in the activator solution, followed by the formation of a three-dimensional geopolymer network of covalent bonds between the Al and Si atoms through polymerization and cross-linking. Resulting in the formation of a final stable network with a typical feldspar crankshaft chain structure, shown in Figure 2 [7, 8, 9, 10].

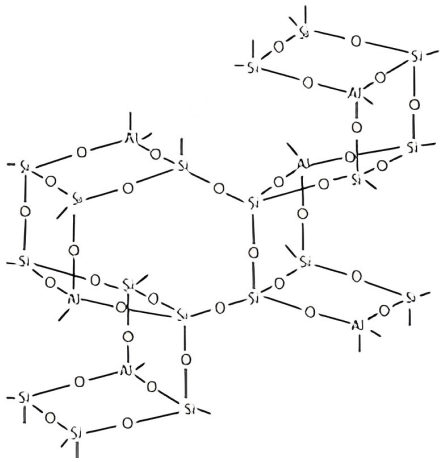

Figure 2: 3D geopolymeric network with typical feldspar crankshaft chain structure [11]

Various amounts of different source materials were used in the production of geopolymer concrete. In addition, different types of activators are used to activate these alumino-silicate materials. A proper selection of the alumino-silicate materials and activators will benefit the desired properties of the geopolymer concrete. However, many factors such as curing time, temperature, conditions, silicate to aluminium ratio, aluminium source, age of concrete, etc. play a unique role in the development of the final product. This means that even a small change in the overall process can result in a completely different product [7, 8, 9, 10].

2. Materials and Methods

2.1. Materials

2.1.1. Metakaolin

Metakaolin (MK) is an amorphous alumino-silicate source material that is a highly reactive natural pozzolan. MK is the result of calcination and dehydroxylation of kaolinitic clay at temperatures between 500°C and 900°C. Metakaolin 750 (MK-750) is the most common type of MK used in geopolymer concrete and is the product of kaolinite calcination at 750°C. MK is a porous, angular-shaped, platy particle with a mean size that can range from 1 to 20 µm and a specific gravity from 2,20 to 2,60 [9, 12, 13].

The MK used in this research has a slightly higher density than reported in the literature and its chemical composition is given in Table 1 [5]. Based on the results from the conversion of the handheld X-ray fluorescence (XRF) data from elements to oxides, the MK mainly consists of SiO_2 and Al_2O_3 with their sum accounting for approximately 80% of the total weight percentage. The amount of SiO_2 is almost 1,80 times higher than Al_2O_3. The X-ray diffraction (XRD) pattern, shown in Figure 3, confirms the presence of several major crystal phases. The major phases identified in the MK pattern are kaolinite ($Al_2Si_2O_5(OH)_4$) and quartz (SiO_2). In addition small traces of anatase (TiO_2) are also detected. The presence of an amorphous phase is detected by a slightly higher background on the pattern in the range of 17,5-30° 2θ. This broad amorphous hump is a typical feature of metakaolin and is caused by the thermal calcination process [14]. Due to its high content of SiO_2 and Al_2O_3 , MK is used in this research as precursor for the geopolymers at a rate of 30% in the precursor raw material.

Table 1: Physical and chemical properties of MK and GGBFS

Properties	MK	GGBFS
Specific surface area [cm²/g][1]	21 710	4 380
Density [g²/cm³]	2,68 ± 0,03	2,89 ± 0,06
pH [-]	5,10 ± 0,04	11,67 ± 0,03
SiO_2 [wt.-%]	53,09 ± 0,20	24,97 ± 0,04
Al_2O_3 [wt.-%]	29,75 ± 0,28	6,65 ± 0,06
Fe_2O_3 [wt.-%]	4,80 ± 0,22	0,74 ± 0,02
CaO [wt.-%]	0,83 ± 0,01	48,02 ± 0,10
MgO [wt.-%]	-	6,14 ± 0,15
K_2O [wt.-%]	0,75 ± 0,07	1,13 ± 0,01

[1] Measured by the Blaine method

2.1.2. Ground granulated blast-furnace slag

Ground granulated blast-furnace slag (GGBFS) is a major by-product of the iron and steel production. A carefully controlled combination of limestone, iron ore and coke are melted together in a blast furnace. This produces iron and slag in a molten state. This molten slag is rapidly cooled with powerful water jets. Converting it to GGBFS, a finer, granular and glass-like material. Only highly amorphous slags can be used as a geopolymer precursor, but it lacks certain molecular structures to be used as the only precursor in GPC. The small particle size, ranging from 5–25 µm, increases the specific surface area and its reactivity. The grains are angular and irregular resembling fractured glass particles. Its specific gravity ranges from 2,50 to 2,90 [9, 15].

The chemical composition of GGBFS as determined by handheld XRF spectrometry is shown in Table 1. The GGBFS used in this research mainly consists of CaO, SiO_2, Fe_2O_3 and Al_2O_3, the sum of which is close to 85% of the total weight. Figure 3 shows the XRD pattern of the examined GGBFS sample. Its structure is almost entirely amorphous, which makes it difficult to identify peaks in the pattern. Literature suggests that the angular band in the range of 25-35° 2θ could be attributed to a significant proportion of amorphous structure, such as glass. According to Arabi and Jauberthie, it is likely that some of the slag agglomerates partially crystallized during the cooling process [16]. Some minor traces of calcite ($CaCO_3$), quartz (SiO_2) and anorthite ($CaAl_2Si_2O_8$) have been detected. GGBFS is used in this research in combination with MK as a precursor, at a rate of 70% in the precursor raw material.

2.1.3. Seawater

As seawater (SW) is an abundant and sustainable resource, it could reduce the strain on freshwater resources. Researchers are proposing the use of SW as a substitute for fresh water in concrete production to address this issue. Water is only required during the polymerization process. Hydrogen bonds create the three-dimensional geopolymer network. When the process is complete, the water evaporates. Due to the function of water in geopolymers, SW is expected to be less harmful to geopolymers than OPC-based concrete [9, 17, 18, 19]. The seawater used in this research was collected from Ornesvik beach in Narvik, Norway, before the snow and ice had melted. It has a measured density of 1,02 ± 0,01 g/cm³ and a slightly alkaline pH of 8,30 ± 0,02. In this research it will only be used to replace the additional water in the mix design.

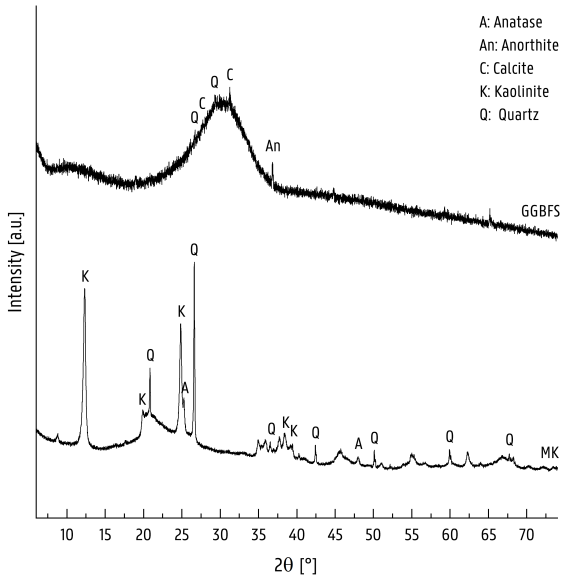

Figure 3: XRD pattern of MK and GGBFS

2.1.4. Recycled aggregates

Aggregates are one of the key factors in the strength and cost-effectiveness of geopolymer concrete. They can be used up to 75% by volume, with various options available. The chemistry of geopolymer concrete encourages the use of recycled aggregates (RA) and partially reactive aggregates such as waste sands [9].

Coarse RCA mixed with natural sand is commonly used to replace natural aggregates. However, the use of fine fraction RCA is often neglected due to its high water absorption coefficient, which negatively affects workability. Coarse RCA mixed with natural sand is commonly used to replace natural aggregates. Disregarding the fine fraction is counterproductive from both an environmental and economic point of view. Significant amounts of RCA are left unused in recycling platforms due to the crushing process of demolition waste. Therefore, the use of both fractions of RCA, either in combination or separately, is highly beneficial for sustainable construction [20, 21]. The fine fraction of RCA was distributed according to the EN 196-1 standard distribution.

While the use of geopolymer concrete to replace traditional concrete is widely promoted in the available literature, GPC waste is expected to increase rapidly in the coming decades as the first generation of GPC structures near their end-of-life. Although the application of GPC in the construction industry is still in its early stages, particular attention needs to be paid to understanding of the potential challenges of managing GPC waste. One potential method of managing this waste, as with traditional concrete, is to reuse the waste as aggregates [22]. In this research, recycled geopolymer aggregates (RGA) were produced from previous samples using a jaw crusher and also distributed according to the EN 196-1 standard distribution.

2.1.5. Sodium silicate solution

The used sodium silicate solution (SSS) for activation of the geopolymerization reaction is based on a commercially available solution. However since the ready-to-use SSS did not have a suitable SiO_2/Na_2O molar ratio (MR). The purchased SSS has a MR of approximately 3,4 while it is recommended to use a SiO_2/Na_2O MR within the range of MR=1,7 to 1,9 [11]. The used SSS has an adjusted MR by dissolving additional sodium hydroxide (NaOH). A a MR $\simeq$ 1,7 is achieved by adding 7,5 wt.-% of NaOH to the original solution and leaving it for 24 hours before use.

2.1.6. Geopolymer preparation

The GPC mixes were prepared according to the mix designs displayed in Table 2. It should be noted that the mixes with the RA have slightly higher water-to-solid ratio to achieve decent workability. The following mixing procedure was used to produce the GPC. The aggregates and GGBFS are mixed for three minutes at a low speed and when finished kept in a separate bowl. Next the MK and SSS are mixed at high speed for ten minutes to initiate the alkalination of the sialate groups. After that the mixed aggregates and GGBFS are added to the MK & SSS-mixture and mixed at low speed for five minutes together with the additional water. The obtained mixture was poured into standardised prism moulds (160x40x40 mm^3) and vibrated with a vibrating table for one minute.

Table 2: Mix designs used mixes [kg/m³]

	DM8	DM8-SW	DM8-RCA	DM8-RGA
MK	163,33	163,33	161,98	161,98
GGBFS	381,11	381,11	377,98	377,98
SSS	263,33	263,33	261,16	261,16
Sand EN 196-1	1 324,44	1 324,44	-	-
RCA	-	-	1 313,51	-
RGA	-	-	-	1 313,51
Water	110,00	-	110,00	110,00
SW	-	110,00	-	-

The filled moulds were kept sealed with plastic foil to avoid premature condensation and were cured at an elevated temperature (70°C) for the first 24 hours. At the end of the elevated curing the samples were removed from the moulds and kept sealed at ambient temperature to complete the 28-day test age.

2.2. Methods

2.2.1. Fresh density and workability

The density and workability of the fresh concrete mix was measured to give good insight of the fresh properties of the concrete mix. Density was measured according to the standard EN 12350-6, filled in as many layers as needed to achieve a full compaction. The concrete was compacted during each layer with a compacting rod. After full compaction, the filled recipient gets weighed and the density of the fresh concrete can be determined by the difference in mass [kg] divided by the known volume [m³].

The workability of fresh concrete is an important factor in determining its suitability. The flowtable test uses the Haegermann cone and was performed according to the standard NBN EN 1015-3:1999, to evaluate the workability of concrete.

2.2.2. Flexural and compressive strength

The flexural and compressive strength of the samples were determined after six different curing durations (2, 4, 8, 12, 24 hours and 28 days). The same curing process is used for all samples. The samples were cured at an elevated temperature (70°C) for the first 24 hours before being cured at ambient temperature. For the flexural tests, 160x40x40 mm^3 solid prisms were used, while the broken half-prisms were used for the compressive tests. These tests were carried out according to the standard EN 196-1:2016.

2.2.3. Mineralogy and microstructure

The mineralogy and microstructure of the samples were evaluated using XRD analysis. Each of the different mixes was analysed after 28 days of curing, one day at elevated temperature and 27 days at ambient temperature to assess the difference in mineralogy and microstructure due to the incorporation of alternative waste materials. The powders used for analysis were obtained by bowl grinding the samples which were crushed after the strength related tests.

3. Results and Discussion

3.1. Influence of seawater

The difference in density and workability of the mix in which seawater was used instead of additional water is shown in Table 3. As the specific gravity (S.G.) of seawater is only slightly higher than that of distilled water and the additional water present in the sample is minimal, the density of DM8-SW is equal to that of the reference mix (DM8). The literature and measurements confirm that the presence of salt in seawater affects the fresh properties, which explains the reduced workability [18, 19].

The early-age mechanical properties of DM8-SW are compared with the reference mix in Figures 4 and 5. The results indicate that the final strength is not significantly affected by replacing the additional water with seawater. It also shows that the mix with seawater as additional water has a fairly faster strength development in the first hours of elevated curing, but reaches a similar strength after full development. This effect could be related to the sodium in seawater, which slightly lowers the SiO_2/Na_2O molar ratio of the activator, thereby increasing reactivity. Thus, the seawater would act as an accelerator to speed up the geopolymerization process. The successful use of seawater and sea sand in GPC has also been successfully demonstrated in previous studies conducted in China. Previous studies conducted in China have also demonstrated the successful use of seawater and sea sand in GPC. Even seawater was used to produce the SSS, resulting in lightly reduced workability but little effect on compressive strength [23].

Furthermore, the XRD pattern in Figure 10 shows no significant changes in mineralogy due to the use of seawater compared to DM8. The illite ($(K,H_3O)(Al,Mg,Fe)_2(Si,Al)_4O_{10}[(OH)_2,(H_2O)]$) and microcline ($KAlSi_3O_8$) phases in DM8-SW were also observed in other reference patterns. More research is needed to fully understand the impact of seawater on the geopolymerization process, mineralogy and long-term effects.

Table 3: Fresh properties different mixes

Mix	Density of mix		Workability[1]	
	ρ [kg/m³]	S.G. [-]	D_{avg} [cm]	F_{avg} [-]
DM8	2 170	2,17	23,35	133,53
DM8-SW	2 170	2,17	22,81	128,13
DM8-RCA	2 140	2,14	14,96	49,58
DM8-RGA	2 040	2,04	19,00	90,00

[1] Tested with Hägermann flow table according to EN 1015-3

3.2. Influence of recycled aggregates

The effect of the RA can have a significant impact on the fresh properties of the mix as well as the mechanical properties of the hardened samples. Table 3 shows the effect of RA on the measured density and workability. Both mixes are lighter compared to DM8, but DM8-RGA is the lightest because the fine fraction of RGA are initially lighter than the RCA's. Both mixes also have a lower workability than DM8, which is not uncommon according to the literature. This results from a higher water demand of the recycled fine fractions and the different grain shapes compared to natural aggregates. This is the main reason why recycled fine fractions are rarely used as aggregates in concrete, while coarse recycled aggregates are already used in combination with natural aggregates to some extent [20, 21]. The difference between the used recycled aggregates and the standard distributed sand (natural aggregates) can be seen in Figures 6, 7 and 8. Both the recycled aggregates are more angular, and the difference in shape between RCA and RGA may be due to a different crushing method. In addition to the grain shape, there is less binder paste attached to the original sand of the RGA grains compared to the RCA grains. The presence of this paste on the aggregates can have a beneficial effect in the interfacial transition zone and can even lead to higher strengths.

Figures 9 and 11 compare the development and final strength of the mixes containing RA and DM8. Although strength development is slower in both cases, development of DM8-RGA appears to be even slower than the others. This may be attributed to some residual chemical components in the RGA slowing down the reaction rate, but this needs to be confirmed by further research. Both mixes containing RA show enhanced flexural strength due to the angular shape of the grains. The angular shape allows for better interlocking and therefore stronger bonds compared to DM8 with rounded grains.

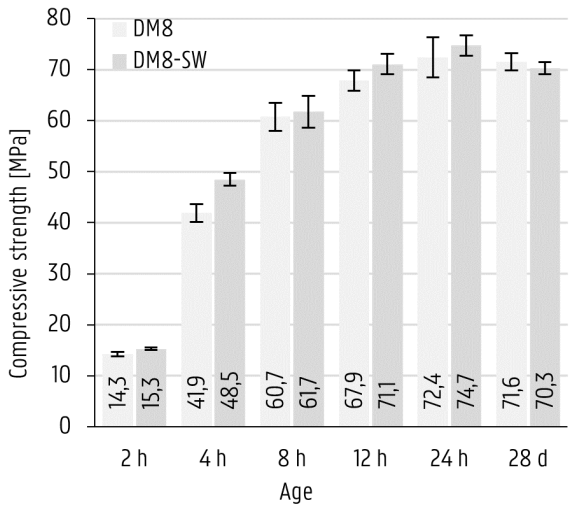

Figure 4: Compressive strength DM8 & DM8-SW

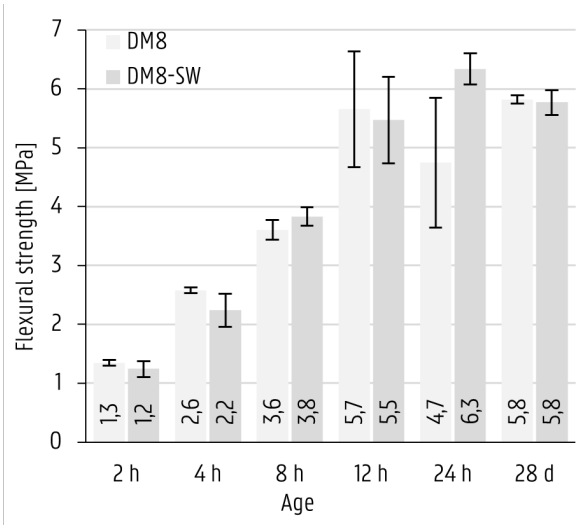

Figure 5: Flexural strength DM8 & DM8-SW

Figure 6: Grain shape standard distributed sand

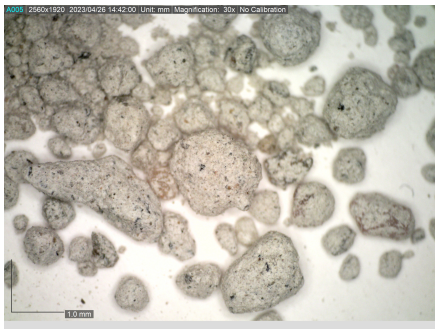

Figure 7: Grain shape RCA

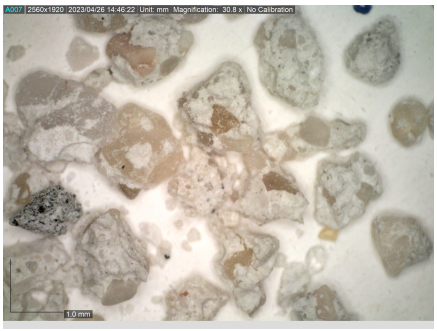

Figure 8: Grain shape RGA

The XRD patterns of both the mixes with different RA are shown in Figure 10. Analysis indicates that the majority of the phases detected in the samples are still quartz (SiO_2). The DM8-RGA pattern has no new peaks and contains additional traces of kaolinite and illite, which are also present in DM8. Analysis of DM8-RCA reveals the presence of new peaks, identified as anorthite ($CaAl_2Si_2O_8$), phlogopite ($KMg_3AlSi_3O_{10}F$) and calcium-silicate-hydrate (CSH), not detected in other mixes. The improved performance the mix with RCA compared to the mix with RGA may be explained by the presence of these phases which, given the composition, are likely to be present in the grains of RCA.

Additional research is required to confirm these results and to investigate the behavior of CSH in GPC and to ensure that these RA do not have a negative effect on the mineralogy, microstructure and the mechanisms of geopolymerization.

3.3. Comparative overview

The influence of different alternative waste materials on the reference mix are compared. The comparison will be based on two important factors: early-age strength development and the impact on the environment. The early-age strength properties are evaluated to gain insight into the impact of these alternative waste materials on the overall strength of the mix. Secondly, analysing the potential for these waste materials provides knowledge about their impact in terms of ecology, sustainability and the environment.

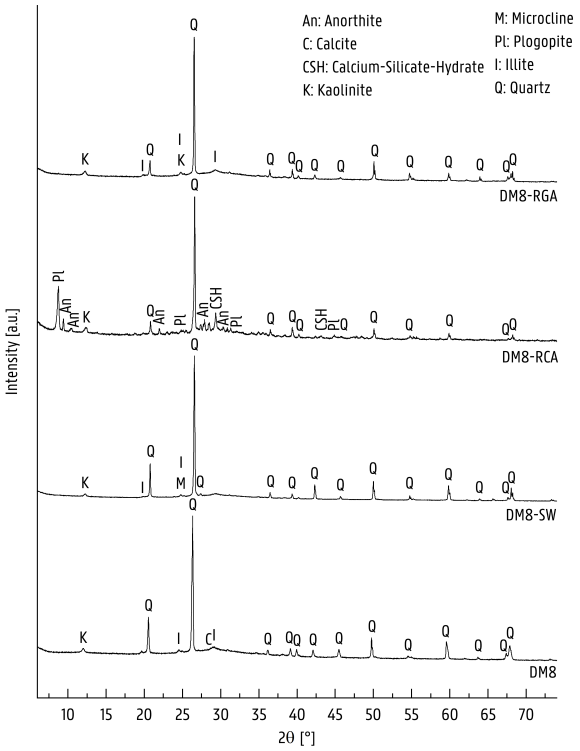

Figure 10: XRD patterns DM8, DM8-SW, DM8-RCA & DM8-RGA at 28 days

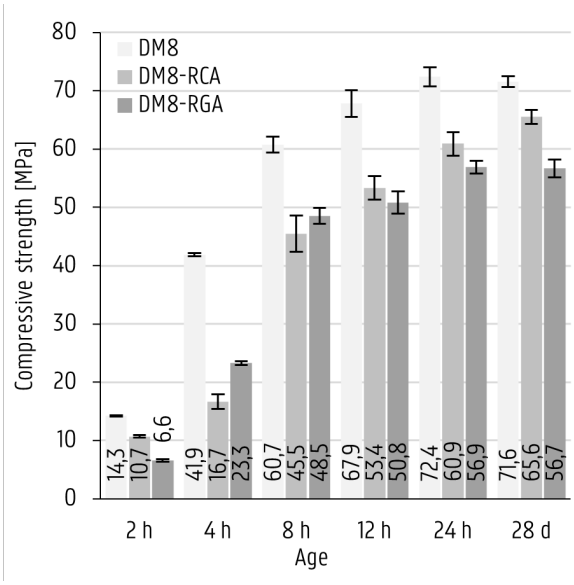

Figure 9: Compressive strength DM8, DM8-RCA & DM8-RGA

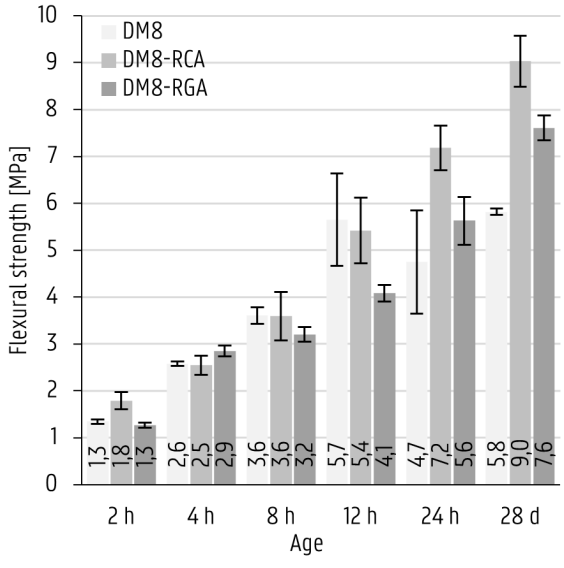

Figure 11: Flexural strength DM8, DM8-RCA & DM8-RGA

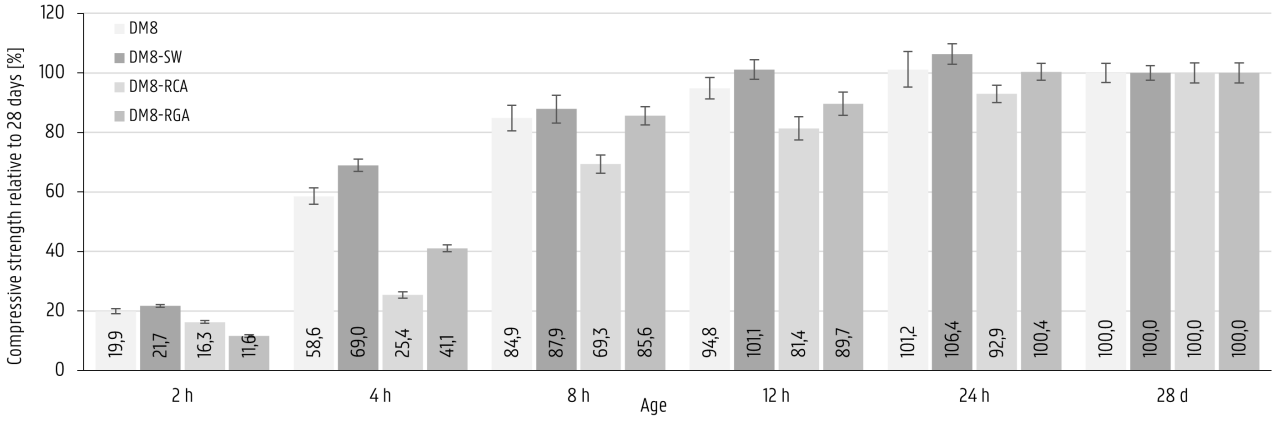

Figure 12: Influence of waste streams on compressive strength

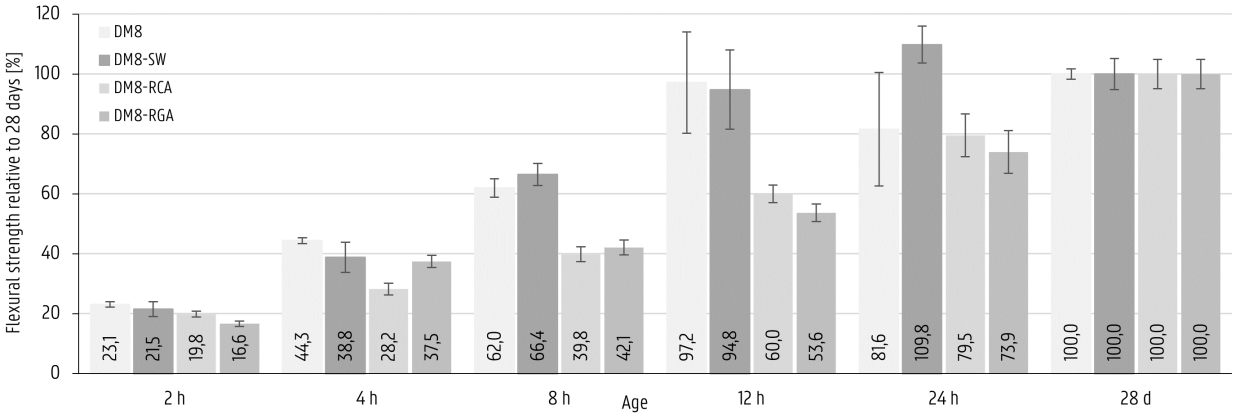

Figure 13: Influence of waste streams on flexural strength

3.3.1. Early-age strength development

The compressive and flexural strengths in Figures 12 and 13 compare the impact of the various alternative waste streams on the development of early-age strength. The strengths are relative to their strength after 28 days of curing. The use of alternative waste materials influences not only the final achieved strength, but also the rate of development. It is critical to remember that not all waste materials have the same effect on sample strength growth. In this study, the DM8 and SW mixes cured faster than the RCA and RGA mixes. This preliminary study demonstrates that the use of alternative waste materials has an effect on the early-age properties of geopolymers.

3.3.2. Ecological and environmental impact

In general, it is preferable to be one step ahead of a product's end of life. Only when waste streams can be used to create new products is it a win-win situation. Figure 14 illustrates the amount of waste materials that could potentially be used in a new GPC mixture. The DM8 reference mix, which includes GGBFS and MK, is the first. These are industrial by-products, so they are a waste material. When seawater is added to the mixture as a water replacement or to make SSS, the amount of waste in the mixture can reach up to 36,5%. The amount of waste increases significantly when aggregates are replaced with recycled aggregates. When everything is considered, the total amount of waste in the GPC mix is close to 94%. This demonstrates the tremendous potential for incorporating waste materials into geopolymer concrete. This will not only have significant environmental benefits by reducing landfill waste, conserving natural resources, and saving energy, but it will also significantly reduce the construction industry's carbon footprint.

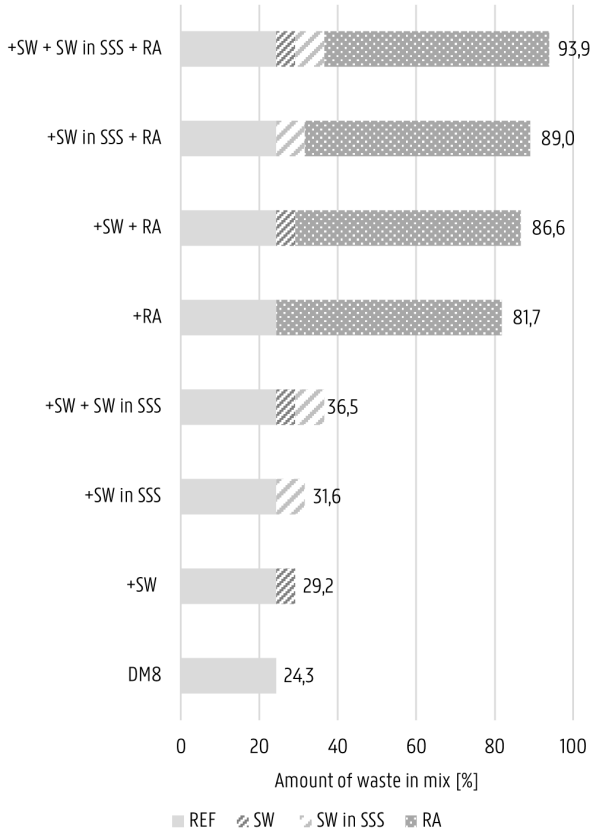

Figure 14: Potential amount of waste material in mix

4. Conclusions

An effect on early age properties was observed in this research by incorporating different alternative waste sources. Each different waste source showed at least some effect on the fresh or hardened properties, the rate of development and the mineralogy. Some mechanical properties were improved by the use of these alternative waste sources, while others were adversely affected. A change in mechanical properties did not always imply a significant change in mineralogy.

Recycled aggregates have a substantial effect on the properties of the mixes. Both DM8-RCA and DM8-RGA exhibit a lower workability due to a higher water demand and different grain shapes compared to natural aggregates. Strength development is in both cases slower than in the DM8. Recycled aggregates improve flexural strength due to their angular shape, providing better interlocking and stronger bonds. The use of RGA does not significantly change the mineralogy, while DM8-RCA shows new peaks identified as anorthite, plogopite and calcium silicate hydrate. This could possibly explain the improved performance of DM8-RGA and possibly also the reference mix if the same water-to-solid factor is used. Further research is needed to confirm these initial findings.

The use of seawater as a substitute for additional water in the reference mix slightly reduced workability due to the salt content, as confirmed and reported in the literature [18, 19]. However, the measured mechanical properties of the mix are not significantly affected by this substitution. DM8-SW shows a slightly faster strength development compared to DM8, but reaches a similar strength after full development, within the margin of error. This could possibly be attributed to the sodium content in seawater which affects the MR of the SSS. The XRD pattern shows no significant changes in mineralogy compared to DM8, but further research is required to fully understand the effects of seawater on the geopolymerization process, mineralogy, and long-term durability.

The initial results of this research show that the used alternative waste materials have the potential to be used in GPC. However the obtained results regarding mineralogy and microstructure are specific for the analysed samples. These results are highly influenced by the sample itself, the sample preparation and the software for analysis. Further research is required to confirm the observed findings and to gain more knowledge about the effects of these waste materials.

5. Further research

The used precursors, activators, aggregates and water sources have a strong influence on the results of this study, as well as the methods of quantifying them and the used curing methods. Further research is needed to draw more general conclusions, it could also focus on curing at different temperatures and the optimal duration of elevated curing. An optimal curing method can be obtained through dedicated and parameter based research.

It may also be worthwhile to further investigate the implementation of various waste based aggregates and the use of seawater. Substituting seawater can be further implemented to replacing the water in the sodium silicate solution. Anyhow, long term effects need to be evaluated before using outside the laboratory environment.

The obtained results in terms of mineralogy and microstructure are based on the specific samples and sample preparation methods used in this study. Further studies are needed to confirm the obtained results by XRD, with sufficient data to support them.

Additional techniques such as NMR and FTIR could be used to understand the development of the amorphous content better, as XRD does not easily detect amorphous phases. It could provide a more complete picture of the geopolymerization process, the resulting microstructure, its relationship to the development of mechanical properties and the impact of waste sources.

Author Contributions

Conceptualization, D.D.M., M.L.H., V.B. and I.N.; Data curation, D.D.M. and M.L.H.; Investigation, D.D.M, M.L.H., I.N. and V.B.; Writing - original draft, D.D.M. and M.L.H.; Supervision, V.B. and I.N.

Declaration of Conflict of Interests

The authors declare that they have no known competing financial interests or personal relationships that could have appeared to influence the work reported in this paper.

Acknowledgements

This research is included in the master's dissertation submitted in order to obtain the academic degree of Master of Science in de industriële wetenschappen: bouwkunde. It is part of the GEOSUMAT project, an international research project funded by M-ERA.NET.

The RCA fines used in this research were available from Nordland Betong (Norway).

References

[1] K. K. Poloju, *Advanced materials and sustainability in civil engineering*, 1st ed. Singapore, Singapore: Springer, 2021.

[2] N. Shehata, O. A. Mohamed, E. T. Sayed, M. A. Abdelkareem, and A. G. Olabi, "Geopolymer concrete as green building materials: Recent applications, sustainable development and circular economy potentials," *SCIENCE OF THE TOTAL ENVIRONMENT*, vol. 836, AUG 25 2022.

[3] A. 2030, "Why the built environment?" 2022. [Online]. Available: https://architecture2030.org/why-the-building-sector/The%20built%20environment%20generates%2040,for%20an%20additional%2013%25%20annually

[4] L. Rodgers, "Climate change: The massive co2 emitter you may not know about," Dec 2018. [Online]. Available: https://www.bbc.com/news/science-environment-46455844?fbclid=IwAR3UdWPQ3F2jBqMHiARsbG4AWWaYCwFJgDQzRhi4NKCFeF3E5piJp8hgobY

[5] Z. G. Ralli and S. J. Pantazopoulou, "State of the art on geopolymer concrete," *INTERNATIONAL JOURNAL OF STRUCTURAL INTEGRITY*, vol. 12, no. 4, pp. 511–533, AUG 9 2021.

[6] S. Qaidi, H. Najm, S. Abed, H. Ahmed, H. Al Dughaishi, J. Al Lawati, M. Sabri, F. Alkhatib, and A. Milad, "Fly ash-based geopolymer composites: A review of the compressive strength and microstructure analysis," *Materials*, vol. 15, p. 7098, 10 2022.

[7] A. Gholampour and T. Ozbakkaloglu, "8 - oven-cured alkali-activated concrete," in *Handbook of Advances in Alkali-Activated Concrete*, ser. Woodhead Publishing Series in Civil and Structural Engineering, F. Pacheco-Torgal, P. Chindaprasirt, and T. Ozbakkaloglu, Eds. Woodhead Publishing, 2022, pp. 157–186. [Online]. Available: https://www.sciencedirect.com/science/article/pii/B9780323854696000192

[8] D. Khale and R. Chaudhary, "Mechanism of geopolymerization and factors influencing its development: a review," *JOURNAL OF MATERIALS SCIENCE*, vol. 42, no. 3, pp. 729–746, FEB 2007.

[9] Z. G. Ralli and S. J. Pantazopoulou, "State of the art on geopolymer concrete," *INTERNATIONAL JOURNAL OF STRUCTURAL INTEGRITY*, vol. 12, no. 4, pp. 511–533, AUG 9 2021.

[10] L. Yun-Ming, H. Cheng-Yong, M. M. Al Bakri, and K. Hussin, "Structure and properties of clay-based geopolymer cements: A review," *PROGRESS IN MATERIALS SCIENCE*, vol. 83, pp. 595–629, OCT 2016.

[11] J. Davidovits, "About geopolymerization," Apr 2006. [Online]. Available: https://www.geopolymer.org/science/about-geopolymerization/

[12] D. K. Panesar, "3 - supplementary cementing materials," in *Developments in the Formulation and Reinforcement of Concrete*, 2nd ed., ser. Woodhead Publishing Series in Civil and Structural Engineering, S. Mindess, Ed. Woodhead Publishing, 2019, pp. 55–85. [Online]. Available: https://www.sciencedirect.com/science/article/pii/B9780081026168000034

[13] J. M. Khatib, O. Baalbaki, and A. A. ElKordi, "15 - metakaolin," in *Waste and Supplementary Cementitious Materials in Concrete*, ser. Woodhead Publishing Series in Civil and Structural Engineering, R. Siddique and P. Cachim, Eds. Woodhead Publishing, 2018, pp. 493–511. [Online]. Available: https://www.sciencedirect.com/science/article/pii/B9780081021569000158

[14] D. Moro, R. Fabbri, J. Romano, G. Ulian, A. Calafato, A. Solouki, C. Sangiorgi, and G. Valdrè, "Thermal, x-ray diffraction and oedometric analyses of silt-waste/naoh-activated metakaolin geopolymer composite," 2021. [Online]. Available: https://www.mdpi.com/2504-477X/5/10/269

[15] J. Ahmad, K. J. Kontoleon, A. Majdi, M. T. Naqash, A. F. Deifalla, N. Ben Kahla, H. F. Isleem, and S. M. A. Qaidi, "A comprehensive review on the ground granulated blast furnace slag (ggbs) in concrete production," *Sustainability*, vol. 14, no. 14, 2022. [Online]. Available: https://www.mdpi.com/2071-1050/14/14/8783

[16] A. Nourredine and R. Jauberthie, "Calcium silicate materials: Substitution of hydrated lime by ground granulated blast furnace slag in autoclaving conditions," *Journal of Materials in Civil Engineering*, vol. 24, pp. 1230–1236, 09 2012.

[17] Y. Jun, J. H. Kim, S. H. Han, and T. Kim, "Influence of seawater on alkali-activated slag concrete," *Materials and Structures*, vol. 54, no. 3, May 2021. [Online]. Available: https://doi.org/10.1617/s11527-021-01719-5

[18] A. Younis, U. Ebead, P. Suraneni, and A. Nanni, "Fresh and hardened properties of seawater-mixed concrete," *Construction and Building Materials*, vol. 190, pp. 276–286, 2018. [Online]. Available: https://www.sciencedirect.com/science/article/pii/S0950061818323055

[19] S. Luhar, , and I. L. and, "Application of seawater and sea sand to develop geopolymer composites," *International Journal of Recent Technology and Engineering (IJRTE)*, vol. 8, no. 5, pp. 5625–5633, Jan. 2020. [Online]. Available: https://doi.org/10.35940/ijrte.e5681.018520

[20] P. Nuaklong, V. Sata, A. Wongsa, K. Srinavin, and P. Chindaprasirt, "Recycled aggregate high calcium fly ash geopolymer concrete with inclusion of OPC and nano-Si02," *Construction and Building Materials*, vol. 174, pp. 244–252, Jun. 2018. [Online]. Available: https://doi.org/10.1016/j.conbuildmat.2018.04.123

[21] A. Hasnaoui, E. Ghorbel, and G. Wardeh, "Performance of metakaolin/slag-based geopolymer concrete made with recycled fine and coarse aggregates," *Journal of Building Engineering*, vol. 42, p. 102813, Oct. 2021. [Online]. Available: https://doi.org/10.1016/j.jobe.2021.102813

[22] S. Mesgari, A. Akbarnezhad, and J. Xiao, "Recycled geopolymer aggregates as coarse aggregates for portland cement concrete and geopolymer concrete: Effects on mechanical properties," *Construction and Building Materials*, vol. 236, p. 117571, Mar. 2020. [Online]. Available: https://doi.org/10.1016/j.conbuildmat.2019.117571

[23] X. Lyu, N. Robinson, M. Elchalakani, M. L. Johns, M. Dong, and S. Nie, "Sea sand seawater geopolymer concrete," *Journal of Building Engineering*, vol. 50, p. 104141, Jun. 2022. [Online]. Available: https://doi.org/10.1016/j.jobe.2022.104141

Table of contents

List of Figures

List of Tables

List of Acronyms

0/2 Sand Non-standard distributed sand

AAM Alkali-activated material
AMB Ambient temperature
ASR Alkali-silica reaction

CEN European Committee for Standardization
CEN Sand Standard distributed sand according to EN 196-1
CF Conversion factor
CL Clinker

DM8-REF DM8-R50-MK2.GGBFS6.SSS1,7-1.S.70°C-27.S.AMB

EDXRF Energy dispersive X-ray fluorescence
EN European norm

FA Fly ash

GGBFS Ground granulated blast-furnace slag
GPC Geopolymer concrete

IR Infrared
ISO International Organization for Standardization
ITZ Interfacial transition zone

LDM Laser diffraction method

MBS Micronized biomass silica
MK Metakaolin
MK-750 Metakaolin 750
MR Molar ratio

OPC Ordinary Portland cement

PSA Particle size analysis

RCA Recycled concrete aggregates
RGA Recycled geopolymer aggregates
RH Relative humidity
RHA Rice husk ash
rpm Rotations per minute

S Sealed mould or sample
S.G. Specific gravity
SF Silica fume
SS Soluble silicate
SSS Sodium silicate solution
SW Seawater

TDS Technical data sheet

U Unsealed mould or sample

WDXRF Wavelength dispersive X-ray fluorescence
WR Weight ratio
WWA Waste wood ash

XRD X-ray diffraction
XRF X-ray fluorescence

List of Symbols

D_{avg}	Average diameter from flowtable test using Haegermann cone [cm]
F_{avg}	Average Flow
K	Blaine apparatus constant
$pH_{electrical}$	PH value using pH electrode
pH_{lit}	PH value found in literature
pH_{strip}	PH value using pH strips
S_{avg}	Average specific surface area [cm^2/g]
S_{Blaine}	Specific surface area using Blaine method [cm^2/g]
$S_{Blaine,TDS}$	Specific surface area from technical data sheet using Blaine method [cm^2/g]
S_{Laser}	Specific surface using laser diffraction method [cm^2/g]
$S_{Laser,TDS}$	Specific surface area from technical data sheet using Laser diffraction method [cm^2/g]
k	Absorption index
k_{est}	Estimated absorption index
n_d	Refractive index
$n_{d,est}$	Estimated refractive index
ρ	Density [g/cm^3 or kg/m^3]
ρ_{lit}	Density found in Literature [g/cm^3 or kg/m^3]
ρ_{avg}	Average density [g/cm^3 or kg/m^3]
σ_c	Compressive strength [MPa]
$\sigma_{c,avg}$	Average compressive strength [MPa]
σ_f	Flexural strength [MPa]
$\sigma_{f,avg}$	Average flexural strength [MPa]

Part I

Preliminary

1

Introduction

1.1 Context

Geopolymer concrete uses waste and industrial by-products, including materials such as fly ash (FA), ground granulated blast-furnace slag (GGBFS) and metakaolin (MK), as substitutes for ordinary Portland cement (OPC). This reduces the carbon footprint of concrete since the production of Portland cement, the primary binder in traditional cement-based concrete, contributes significantly to CO_2 emissions and has a negative impact on the environment.

The production of geopolymer concrete (GPC) is based on a complex chemical reaction between an alkaline solution and alumino-silicate materials. The resulting product is a strong and durable three-dimensional networked structure that provides strength and durability. With advantages like high early strength, superior acid and fire resistance, GPC is an ideal material for numerous construction applications, outperforming traditional cement-based concrete.

Research on geopolymers has gained significant attention in the last few years due to its potential as a sustainable alternative to traditional cement-based concrete. The research conducted in this thesis is part of the GEOSUMAT project, an international research project funded by M-ERA.NET, that is focused on developing new materials that support circular economy. GEOSUMAT is driven by the re-use of local waste resources, to reduce CO_2 production, encouraging preservation of natural resources, etc. The aim is to develop a new fiber reinforced eco-friendly geopolymer composite for civil engineering applications.

1.2 Scope of the research

The scope of this research is limited to the analysis of the early-age properties of geopolymers and the influence on these properties by the use of alternative waste materials. In a first part, a reference mix is designed using available alumino-silicate source materials. The development of this mix is analysed in terms of mechanical properties as well as mineralogy and microstructure. The second part consists of implementing alternative waste materials. After thorough analysis, the available waste materials are used to produce a geopolymer concrete. The influence of using these waste materials is closely monitored and the changes in mechanical properties, mineralogy and microstructure are studied.

1.3 Methodology

The research is divided into two distinct phases, corresponding to the first and second semester of this academic year. Each phase is divided into different workloads, as shown in Figure 1.1, each having their own focus area. The actual research is conducted in the second semester, which is also the semester when the master's thesis is completed at UiT, The Arctic University of Norway campus Narvik.

In the first phase, practical preparations are made in combination with a theoretical review. This phase involves the collection of relevant literature and research material on geopolymerization, including the involved chemical reactions, the types of raw materials that can be used and possible applications of the resulting material. During the second phase, the theoretical review continues alongside with the quantification of materials using suitable tests. Additionally, the evolution of the mixes is closely monitored throughout this stage. The properties of the resulting mixture changes as the process progresses, it is essential to monitor and document these changes. Both the quantification and evolution of the mixes are closely tracked and processed to obtain accurate schematics and visualizations of the mechanism of geopolymerization over a certain timeline.

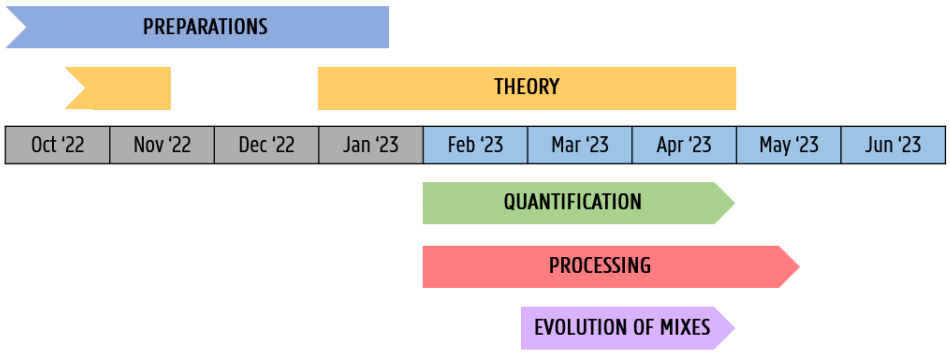

Figure 1.1: Scheme of research methodology

1.3.1 Detailed overview

In this part, a detailed description is provided for each phase and workload, along with its respective tasks connected to the research on geopolymer concrete.

Preparations

During the first semester, the focus was on the preparation of the research. This phase, illustrated in Figure 1.2, can be divided into three main tasks. First, it was crucial to become familiar with the state of the art of geopolymer concrete. Through laboratory practice, various mixes were prepared and the mixing procedure and the properties of the fresh and hardened product became more understandable and tangible. The research conducted during this period helped to gain practical knowledge about GPC and the mechanisms that can occur during the curing.

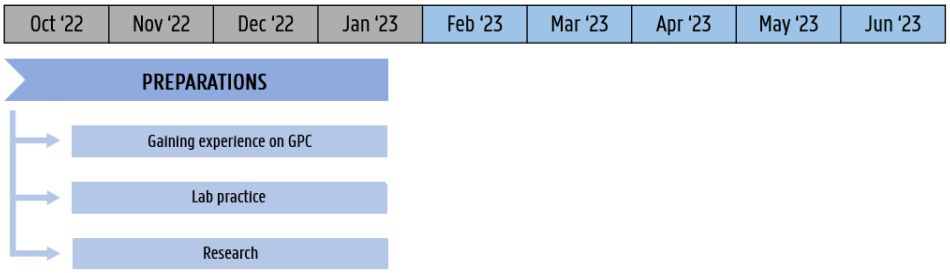

Figure 1.2: Workload preparations

Theory

The theoretical part plays a crucial role in understanding and executing the research. This workload is divided into three parts, as shown in Figure 1.3. At first, it was important to provide a general overview and introduction to GPC. Understanding the ways of quantifying the resources helped to identify and monitor important parameters. Finally, the aim was to deepen the subject matter and gain further knowledge along with the research.

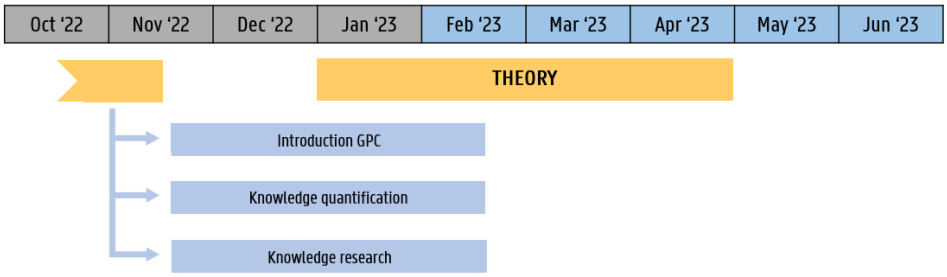

Figure 1.3: Workload theory

Quantification

Since most of the materials used as resources for geopolymer concrete are waste or industrial by-products, the quantification phase, shown in Figure 1.4, is necessary to have an idea of the composition and potential use of the resources. The physical and chemical properties of the used waste materials are analysed in this workload. These properties, such as the grain distribution, specific density, pH and chemical composition, can vary depending on the source and batch of the resource. Not incorporating the actual properties of the used materials in the mix design of geopolymers could have tremendous effects on the final product, hence demonstrating the importance of quantification.

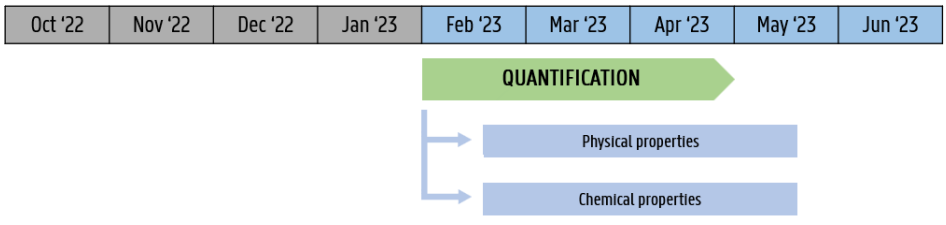

Figure 1.4: Workload quantification

Evolution of mixes

The workload visualised in Figure 1.5 is the most intensive and time-consuming of the entire research. The evolution of the early-age properties of mixes is the main topic of this research on geopolymer concrete. First of all, a reference mix will be designed using available alumino-silicate source materials, such as calcinated clays and blast-furnace slags. All changes regarding the mechanical, physical and chemical properties at of the geopolymers will be documented and analysed to gain knowledge on the development of the early-age properties of geopolymer concrete. Also adding to this workload is the usage of various waste materials into the mix design. These mixes will also be evaluated in the same order as the reference mix, allowing to make a comparison between the different waste streams and their impact on the final product. Hopefully promoting, or at least give some insight on the use of alternative waste materials in geopolymer concrete.

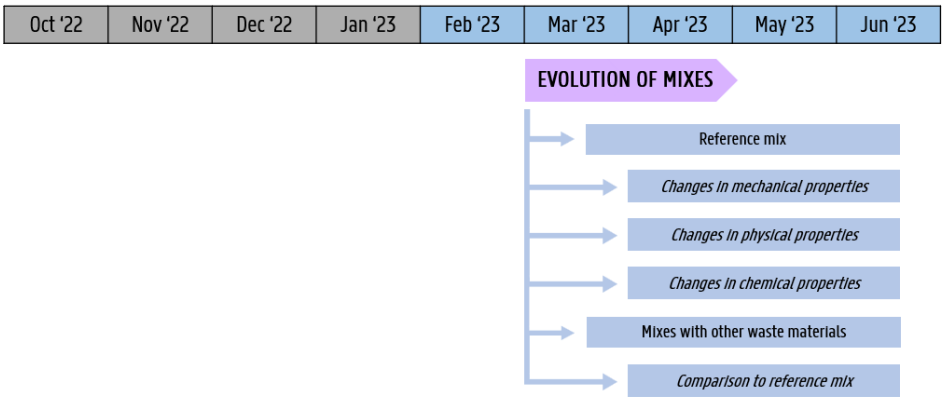

Figure 1.5: Workload evolution of the mixes

Processing

This workload is devoted towards processing between various phases, illustrated in Figure 1.6. The quantified resources are analysed and used to design different mixes. The gained knowledge and measured properties of the different mixes lead to a reference mix and a couple of feasible mixes with alternative waste materials. The evolution of the early-age properties for the reference mix and the other mixes will be compared and discussed. Allowing to gain knowledge on the evolution of geopolymer concrete.

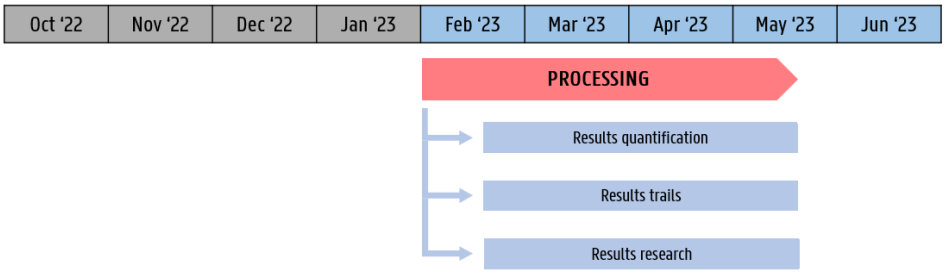

Figure 1.6: Workload processing

1.3.2 Into practice

While the methodology is a useful tool to have a good overview and idea of the workloads, it is crucial for the research to translate this into a realistic schedule. Making a schedule helps to think about the goals as well as the process and tasks that are needed to achieve them. The research schedule is illustrated in Figure 1.7. Progress and delays were assessed every two weeks in comparison to the original schedule and adjusted accordingly. The minutes of meetings recorded these changes are available for reference in Appendix A.

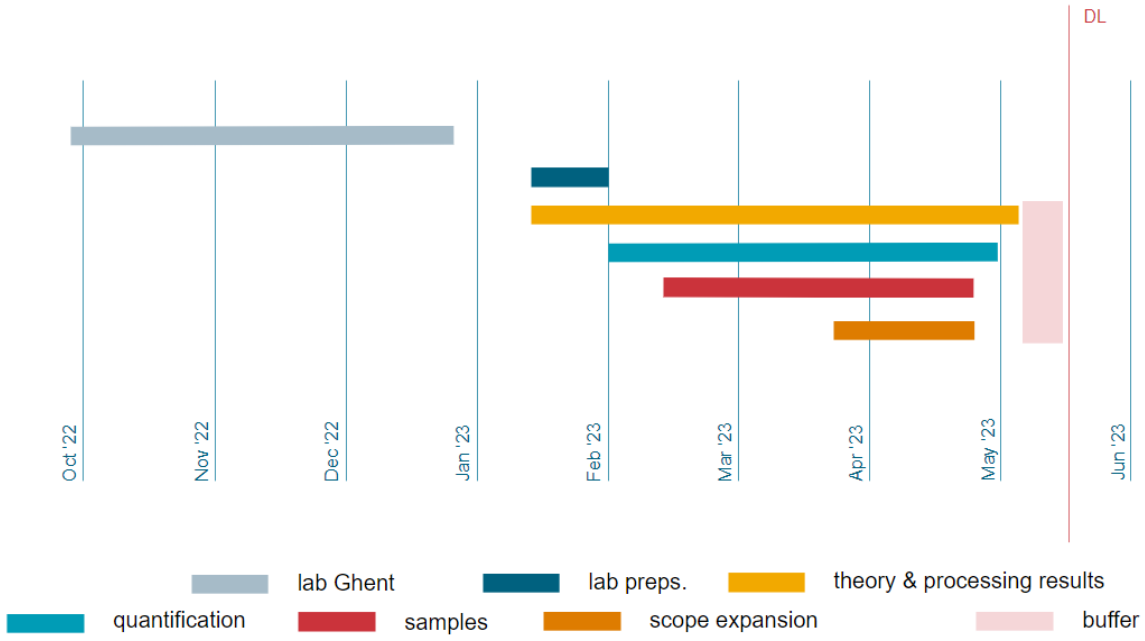

Figure 1.7: Final research schedule

1.4 Health and safety

When performing laboratory work involving various machines and substances, it is critical that health and safety measures take precedence. The production of GPC requires cautious handling of substances such as waste wood ash, blast-furnace slags and other waste and industrial by-products, to prevent harm to workers and the environment. In addition, the involved people are exposed to potentially hazardous substances when testing the durability of GPC and determining its physical and chemical properties. Therefore, implementing proper safety protocols, such as wearing protective clothing and ensuring adequate laboratory ventilation is crucial.

Observing health and safety measures while working in the laboratory can ensure the well-being of everyone involved. Creating a culture of safety in the laboratory is critical to preventing accidents and promoting a safe work environment. A health and safety course is taken as part of the research to raise awareness and address the importance of these measures.

1.4.1 Risk assessment

A risk assessment is a systematic process for identifying, evaluating and minimize potential risks or hazards associated with a particular activity or research. In the context of research, a risk assessment involves the evaluation of potential risks associated with the research design, materials or equipment used, participants or other factors that could affect the safety of the researcher.

Conducting a risk assessment aims to minimize, eliminate or at least raise awareness to the potential risks. This is done through proactive planning and risk management strategies to ensure that the activity or project can be conducted safely and effectively. A proper risk assessment for this research was executed based on the 5x5 risk matrix. It is based on two parameters for each risk, the likelihood of it happening and the severity of the risk. These parameters give the risk a combined score out of 25, based on this score the risk is visualised and proper precautions can be taken. The matrix and the different combined scores are shown in Figure 1.8. The risk assessment for this research can be consulted in Appendix B.

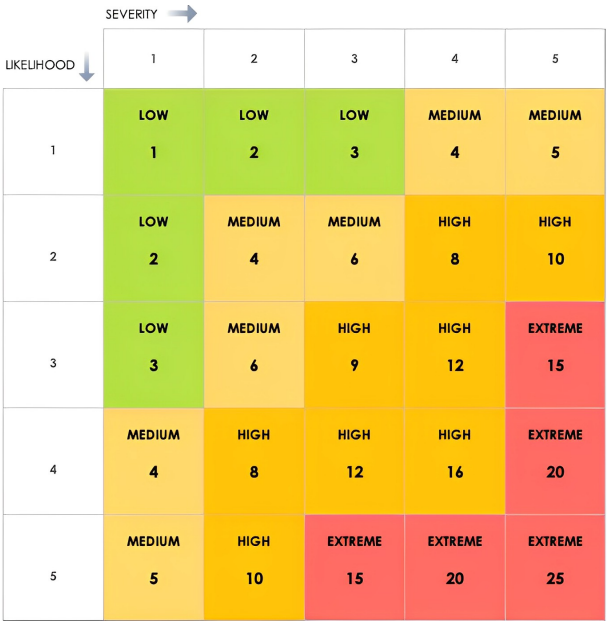

Figure 1.8: 5x5 risk matrix [1]

1.5 Thesis outline

The thesis is divided into four main parts. In the first part, Chapter 1 introduces the research objectives, research methodology and discusses the precautions towards health and safety, while Chapter 2 explores the theory about geopolymer concrete. The second part, covers methods of analysing the resources and the geopolymer concrete (Chapter 3), including the quantification of the resources (Chapter 4), developments towards the reference mix (Chapter 5) and the influence of alternative waste materials (Chapter 6). The third part presents the results and discussion, including the evolution of early-age properties of the reference mix (Chapter 7) and the impact of alternative waste materials on these early-age properties (Chapter 8). Finally, the fourth part gives the conclusions and further perspectives of the research.

2

About geopolymer concrete

The first chapter will provide some essential background information about the discussed topics. The reader can learn about the most frequent concepts and mechanisms within the world of geopolymer concrete. It covers the most frequently asked questions that come to mind when discussing such a topic including the potential applications, properties, durability, components of geopolymer concrete.

2.1 Introduction

Geopolymer concrete is a type of high-strength and lightweight material that is attracting a lot of attention as a more sustainable alternative to traditional cement-based concrete. Unlike traditional concrete which uses ordinary Portland cement as a binding agent, GPC uses waste and industrial by-products as its binder, making it a more environmentally friendly option. With an expected increase in demand for construction materials due to the growing global population and urbanization, it is crucial to consider more sustainable options in the building industry [23, 24].

The building industry is a significant contributor to the world's carbon dioxide (CO_2) emissions in the atmosphere, accounting for approximately 40% of the world's emissions [25]. The cement production is responsible for a substantial portion of the world's CO_2 emissions, accounting for around 8% of the total [2]. The chemistry behind the production of OPC highlights its significant contribution to global warming. The production of cement involves the calcination of limestone ($CaCO_3$) and silico-aluminous materials, which results in the following chemical reaction [11]:

$$5CaCO_3 + 2SiO_2 \Longrightarrow (3CaO.SiO_2)(2CaO.SiO_2) + 5CO_2 \tag{2.1}$$

For every ton of cement produced, this reaction produces 0,55 tons of CO_2. Additionally, the combustion of carbon-fuel releases an additional 0,4 tons of CO_2. This means that each ton of cement produced results in the generation of approximately one ton of CO_2 [11]. The global cement production and the associated pollution levels for the biggest consumers between 2010 and 2017 are illustrated in Figure 2.1. The substantial CO_2 emissions associated with the production of ordinary Portland cement pose a significant challenge to reaching sustainability goals and further contribute to negative environmental impacts [26].

GPC offers a solution to this issue by eliminating the use of OPC as a binding agent. Instead, it uses an alkali or acidic medium to activate alumino-silicate precursors through a process called geopolymerization, resulting in a significant reduction of

CO_2 emissions by 22-72%. The environmental impact of cement production and the need for more sustainable alternatives has been marked as a priority in the Paris Agreement signed in December 2015. GPC does not only reduces CO_2 emissions but also provides an effective way to manage waste, which could have positive effects on our health and environment [2, 26, 27].

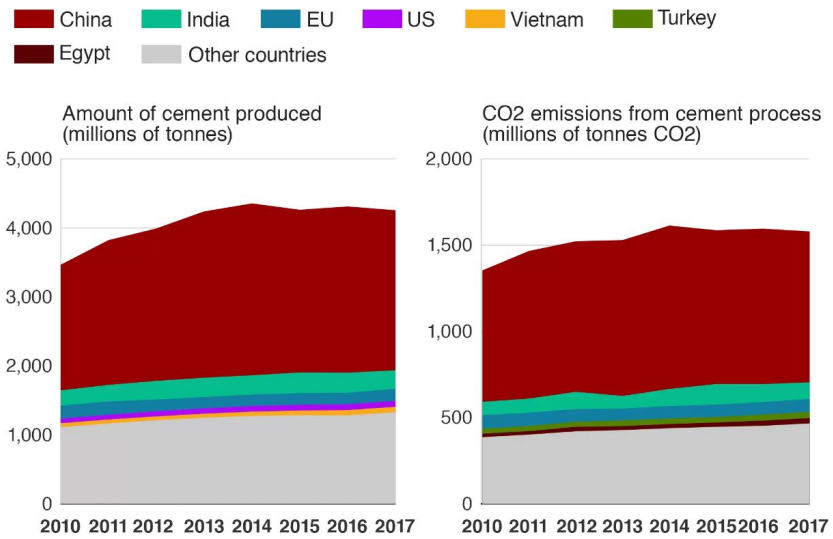

Figure 2.1: Global cement production and process-related CO_2 emissions [2]

Studies have shown that GPC has similar mechanical characteristics as traditional concrete, while being able to reduce CO_2 emissions. In addition, GPC also boasts superior characteristics such as adjustable thermal expansion, high-temperature resistance and acid resistance. This makes it a versatile material that can be used in various construction applications and is especially well-suited for environments with high levels of heat and acidity [2, 27].

Overall, geopolymer concrete is a promising alternative to traditional concrete that can help to reduce CO_2 emissions and improve sustainability in the building industry. With its high strength and lightweight characteristics, as well as its ability to reduce emissions and manage waste, GPC has the potential to play a significant role in building a greener future [23].

2.2 What is geopolymer concrete?

Geopolymers are mineral chemical compounds or mixtures of such. They consist of repeating units created by a polymerization process. In geopolymerization, a large number of small molecules are combined to form a covalently bonded three-dimensional macromolecular network. Geopolymers are considered as a type of alkali-activated material (AAM), where the binding phase primarily exists of alumino-silicate and happens rather coordinated. The used activator is usually an alkali metal hydroxide or silicate. The most used precursors, the source of alumino-silicate, in geopolymer synthesis are low-calcium fly ashes and calcined clays. For the sake of simplicity and to avoid further discussions, the previously stated definition is used. It is important to note that the term "geopolymer" is sometimes used in a broader sense by some academic and commercial entities, primarily for marketing purposes and not for scientific accuracy [3, 11].

The classification difference between AAM and GPC is shown in Figure 2.2. This representation of the chemistry of concrete-forming systems is a greatly simplified view. M^+ being an alkali metal cation, that gets activated under high pH conditions. Nevertheless the image does provide a helpful illustration of the classification of AAM's and their relationship to OPC and sulfoaluminate cement systems. In this illustration, geopolymers are depicted as a subcategory of AAM's, with high aluminium concentrations and low calcium concentrations [3].

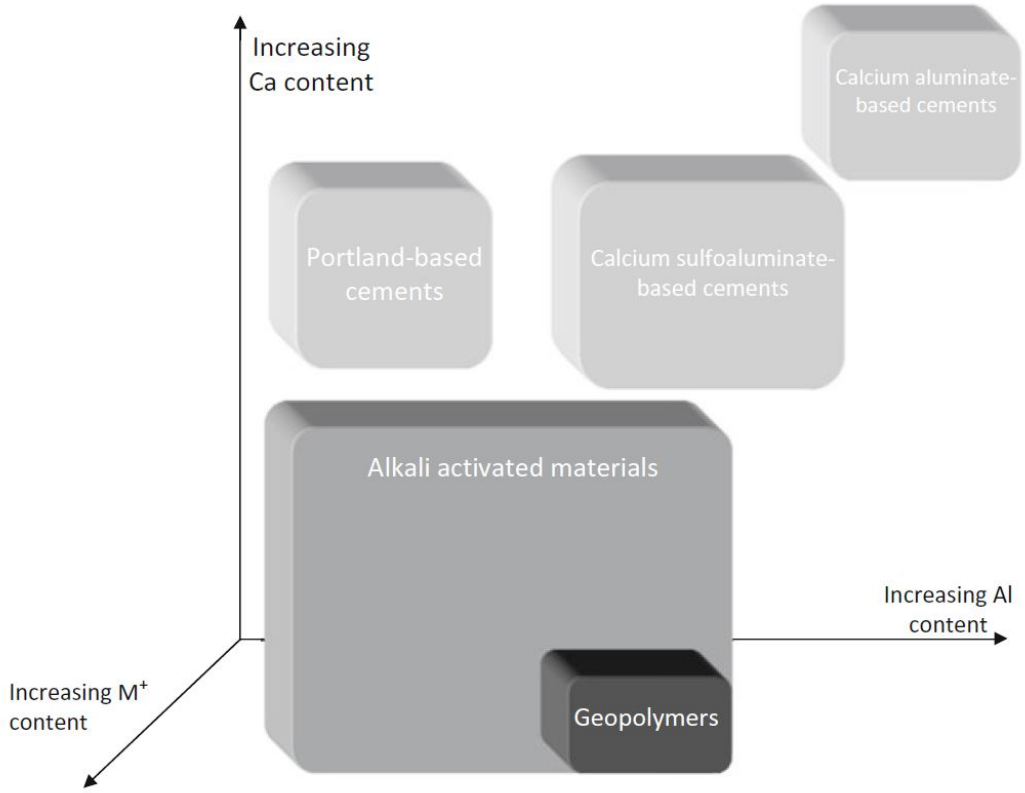

Figure 2.2: Classification of AAMs compared to OPC and calcium sulfoaluminate binder chemistry diagram [3]

2.2.1 Compared to traditional cement-based concrete

Geopolymer concrete is a reliable construction material that outperforms traditional cement-based concrete in several ways. While GPC is considered to be environmentally sustainable, OPC-based concrete is not. The production of GPC is also more efficient and energy-saving. In addition, geopolymer concrete is more resistant to chemicals, temperature changes and corrosion than traditional concrete. Although still in the early stages of growth, the widespread use of geopolymer concrete in the construction industry is yet to be seen. The toughness of GPC makes it a viable option for high-cost, demanding environmental applications. A transition from traditional concrete to geopolymer concrete would benefit both the environment and the people. Over time, GPC is expected to replace OPC-based concrete as the world's most widely used man-made material [11, 23].

2.2.2 History of geopolymer concrete

Geopolymer materials were a breakthrough in alumino-silicate chemistry, which was first investigated in the 1930s. At that time and for the next two decades, research focused on developing alkali activated materials by reacting alumino-silicates with alkali hydroxides. Later in the 1970s, the French professor and engineer Joseph Davidovits established the field of geopolymer chemistry with his work on kaolinite. This work opened the door for further research and development in this area. The first fire-resistant mineral resin made from metakaolin and soluble alkali silicate was patented in 1975, but the word "geopolymer" was not introduced until 1978 [11, 28].

The first geopolymer cement was developed and patented by Davidovits and Sawyer in 1984 in the United States under the name "Early High-Strength Mineral Polymer". It is worth mentioning that evidence of geopolymer synthesis can be found in ancient structures around the world. For example, some claim that the pyramids of Cheops and Chephren (2700 BC) contain stones with a microstructure very similar to that of modern geopolymer materials. Davidovits even formulated a hypothesis about the use of geopolymer bindings during the construction of ancient monuments. Stating that the "concrete" technology was used during the construction of the Egyptian pyramids by using geopolymer mixes with limestone aggregate in formwork to create individual blocks. Similarities can also be seen in Roman concrete (300 BC) and South American monuments (600 AD) [3, 11, 29].

2.3 Potential applications

Geopolymer concrete has several advantages over traditional cement-based concrete, making it a desirable choice for the construction industry. Because of its wide range of applications and many promising properties. It should be mentioned that a single batch of geopolymer concrete will not necessarily have all the specific required properties for each of the applications listed below [23, 24, 30].

2.3.1 Infrastructure and building developments

The growing use of geopolymer concrete in construction projects can be traced to its many advantages over traditional concrete. With its high strength and durability, GPC is ideal for construction applications that require robustness, such as roads, bridges, tunnels, pipes and other infrastructure structures exposed to harsh conditions [24, 30].

Roads

Geopolymer concrete has been used to construct a number of footpaths and bikeways across Australia, including those on Brady Street, Taylers Lake, South Malboure and Kings Road. In addition, the pavements on the Westgate Freeway in Victoria were constructed using geopolymer concrete [31, 32]. In the heart of Sydney, an experiment was conducted to test the durability of geopolymer concrete. Two pavement structures were built on Wyndham Street, each measuring 15 meters in length and 3 meters in width. The pavements were constructed using geopolymer and traditional cement-based concrete. To determine the performance of GPC, the duplicate pavement was placed next to the other one, providing a side-by-side comparison of the durability and behaviour of the material. The purpose of this experiment was to demonstrate that GPC is a suitable material for pavement structures in an urban environment [33]. Since geopolymer concrete is highly resistant

to chloride, it will experience less damage than ordinary concrete roads and highways when calcium chloride road salts are used in the winter season [23].

Buildings

One of the first residential applications of GPC occurred in 1989, when a residential building was constructed in Lieptsk, Russia, using an alkali-activated concrete that did not contain OPC [30]. During construction of the University of Queensland in 2012, a research organization focused on global sustainability issues utilized precast GPC floor beams as structural floor elements [34, 35]. The Brisbane West Well-camp Airport is considered a major engineering accomplishment, especially because it features the largest use of GPC in the world. Taking nearly 50 years to build, this new public airport in Australia started offering commercial flights by Qantas Link in November 2014 [36]. One of the latest development in the use of GPC in residential construction is 3D printed concrete, the first 3D printed house made of GPC was built in Siberia in 2018 [11].

Bridges

In Port Melbourne, Australia, 180 units of precast GPC were utilized to build the Salmon Street Bridge over the Westgate Freeway [31]. A little bit further in Melbourne, two landscape retaining walls were created in-situ, as part of the bridge construction over the Yarra River. Some of the elements that make up the bridge over the Yarra River, such as the retaining wall, footway and footpath panels are shown in Figure 2.3 [4]. A similar project was realized in Russia, where a GPC-based pedestrian bridge was constructed in the city of Skolkovo [11].

Figure 2.3: Geopolymer concrete, retaining wall (left), footway pannels (center) and footpath (right) [4]

Pipes

The high resistance to GPC to acids and toxic waste makes it suitable for use in hazardous conditions such as sewer pipes and landfills. Using geopolymers can create long-lasting structures that prevent contamination. Corrosion prevention is crucial in sewer pipes, as repairing them is expensive and difficult, especially if the pipe is located under a road [23]. Pipes made from GPC were successfully utilized and installed in the Princess Highway Duplication project in Winchelsea, Southwestern Victoria. Other installations using this type of pipes have also been carried out, such as in drainage projects in Harley Street in the City of Greater Bendigo and at the Bendigo Airport in Victoria [31].

2.3.2 Other developments

In addition to conventional construction, geopolymer concrete is used in a variety of ways, such as marine projects, fire-proofing, and coatings. Its remarkable tolerance to salt and immunity to chlorine corrosion makes it a superior choice for constructing saltwater-exposed structures like piers and coastal bridges. Its fire-resistant qualities makes it a good material for improving the fire safety of concrete structures. The application of geopolymer concrete coatings has become well-known for their strength, protection against corrosion and ability to smooth concrete surfaces and resist against chemicals [23].

Marine developments

GPC is a suitable material for the use in marine environments due to its high salt resistance. Making it ideal for the construction of structures such as piers, coastal bridges and underwater concrete supports that are exposed to the mild alkaline salt water. One of the major challenges in maritime concrete structures, such as bridges, is steel corrosion caused by contact with seawater, which has a low pH. GPC can effectively address this issue by providing a protective barrier to the steel supports and preventing chloride corrosion. The technology of geopolymer concrete has recently been used in Australia to develop breakwater armour units, illustrated in Figure 2.4, to protect the northern breakwater of the harbour [5, 23, 37].

Figure 2.4: Placement of the armour units on the breakwater (left), aerial view of the breakwater (right) [5]

Fireproofing

GPC has excellent heat and fire resistance, able to withstand extremely high temperatures exceeding 1200°C without undergoing significant changes. Though no type of concrete is flammable, exposure to excessive heat from fires can reduce its strength and increase the risk of spalling. Spalling is the cracking of concrete layers that can produce a popping noise. The high resistance of geopolymer concrete makes it suitable for use in high-heat environments [23, 28].

Coatings

The market offers several options for geopolymer coatings, one of which is GeoSpray®. This geopolymer-based mortar can be used to repair pipes or sewer lines without having to dig trenches, making it a convenient solution for such repair work [38]. A public facility in Ohio utilized geopolymer mortars in 2019 to fix a damaged sewer lining, demonstrating its effectiveness as a repair material [11]. While in Thailand, the damaged roads were repaired using GPC. The product was chosen for its superior strength and durability. This highlights the flexibility and value of this innovative material in a range of applications [39].

2.4 Mechanism of geopolymerization

Geopolymerization is a reaction that chemically integrates minerals. The strength of the geopolymer concrete is developed through this reaction between alumino-silicate source materials and alkaline or acidic activators. Various amounts of different source materials have been used in the production of geopolymer concrete. In addition, different types of activators are used to activate those alumino-silicate materials. A proper selection of the alumino-silicate materials and activators will benefit the desired properties of the geopolymer concrete [11, 40, 41, 42].

To illustrate the procedure and kinetics of the geopolymerization reaction, an example geopolymer product is used. It is a result of the reaction between Metakaolin 750 (MK-750) and sodium silicate (Na_2SiO_3), an alkaline activator. The reaction can be divided into three phases: (1) alkaline depolymerization of the poly(siloxo)layer of kaolinite, (2) formation of the ortho-sialate and (3) polymerization into higher oligomers and polymers [6, 11].

The alkalination of metakoalin particles starts geopolymerization mechanism. The chemistry of alkalination is determined by the nature of both the alumino-silicate sources and the used activators. However, the geopolymerization reaction relies on the same mechanisms regardless of the initial materials. Due to alkalination, the Al atom has a valency of 4 and becomes tetravalent in the side group sialate Si-O-Al-$(OH)_3Na^+$, as illustrated in Figure 2.5 [6, 11, 42].

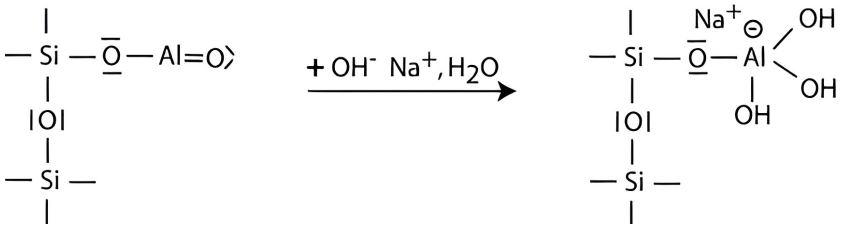

Figure 2.5: Alkalination of sialate group [6]

Since the aluminium atom either acts as an acid or a base, depending on the substance it's reacting with, it qualifies as amphoteric. This implies that the Al atom can either be trivalent or tetravalent by respectively giving up or accepting protons from other atoms. In the following stage, shown in Figure 2.6, the pentavalent silicon atom is formed by interaction with the OH^-cation. This initiates the alkali dissolution on the particle edges [6, 11, 43].

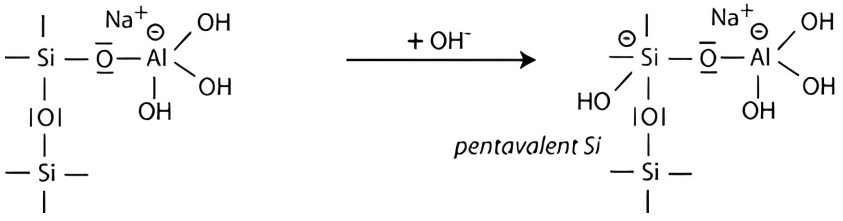

Figure 2.6: Initiation of superficial alkali dissolution [6]

Following in the reaction of geopolymerization, the separation of siloxane oxygen (Si-O-Si) occurs through transfer of the electron from Si to O. Causing the silicon atom to return to a tetravalent state. This leads to the formation of intermediate silanol (Si-OH) and basic siloxo ($Si-O^-$) as illustrated in Figure 2.7 [6, 11].

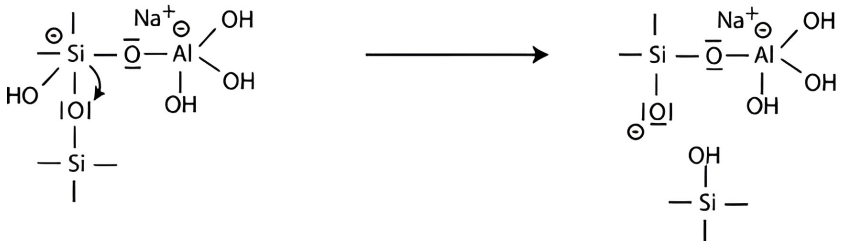

Figure 2.7: Formation of intermediate silanol (Si-OH) and basic siloxo ($Si-O^-$) [6]

The process continues with the formation of silanol groups (Si-OH) and isolation of the ortho-sialate molecule, shown in Figure 2.8, which is the primary unit in geopolymerization [6, 11].

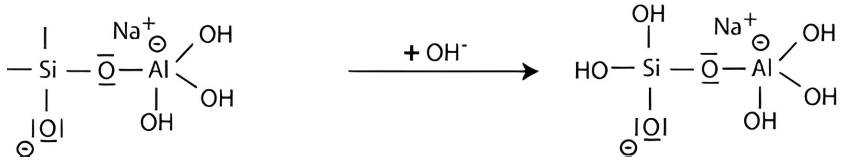

Figure 2.8: Formation of primary unit of geopolymerization [6]

A reaction between the basic siloxo ($Si-O^-$) and the sodium cation Na^+, causes the formation of the Si-O-Na terminal bond. The terminal atom Na^+ is connected to the central oxygen atom, visible in Figure 2.9. An atom, with the exception of the hydrogen atom, is considered to be terminal if it's connected to a central atom. While a central atom has two or more atoms attached to it [6, 11, 44].

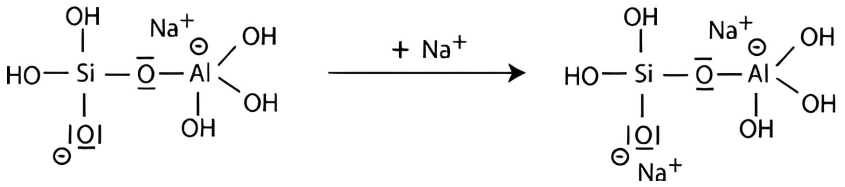

Figure 2.9: Formation of orthosialate molecule [6]

A cyclo-tri-sialate structure is created by condensation between the ortho-sialate molecules, the reactive groups (Si-O-Na) and the aluminum hydroxyl molecules (OH-Al). The condensation produces the alkaline substance NaOH. As the cyclic structure is formed, the alkali is released and again available for reaction, responsible for further polycondensation into the Na-poly(sialate) nepheline backbone as can be seen in Figure 2.10 [6, 11].

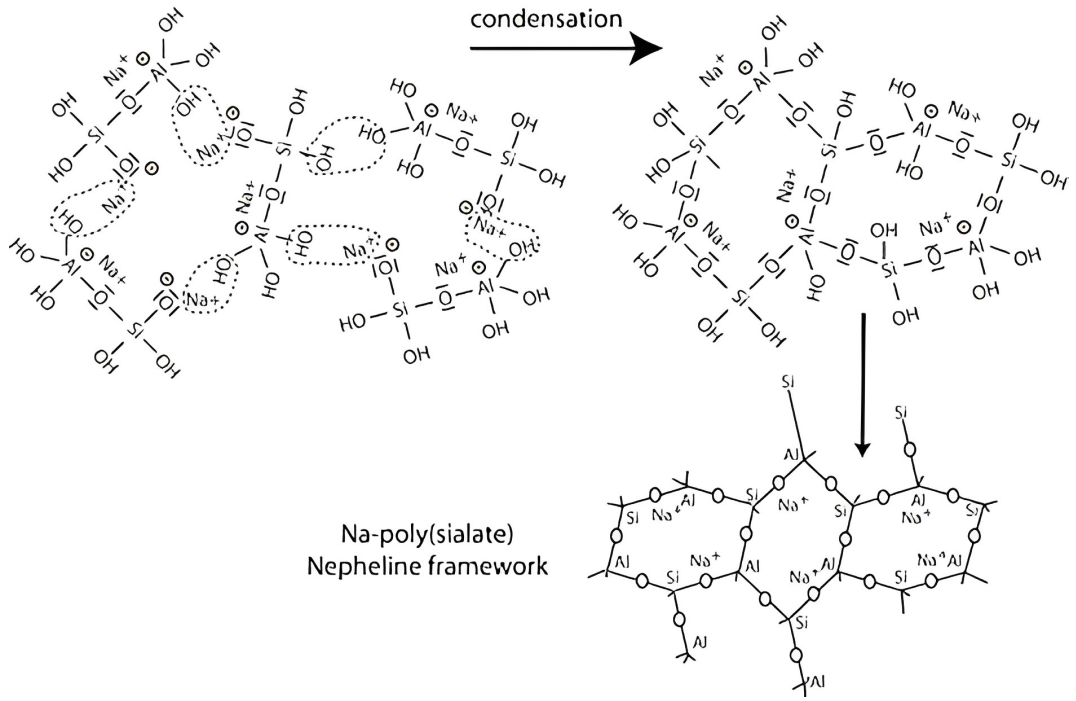

Figure 2.10: Condensation of the ortho-sialates [6]

Condensation takes place between di-siloxinate and ortho-sialate molecules, due to the presence of waterglass. These molecules are respectively shown at the top and bottom in the left side of Figure 2.11. The reactive groups Si-O-Na, Si-OH and OH-Al$^-$ form the cyclic ortho-sialate-disiloxo structure through which the alkali NaOH is released and reacts a second time [6, 11].

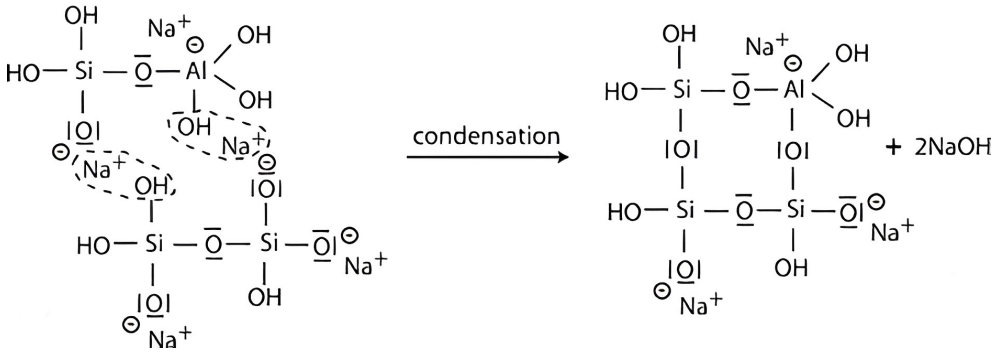

Figure 2.11: Condensation into cyclic ortho-sialate-disiloxo [6]

Through further polycondensation, the formed chains interact through hydrogen bonds to form the three-dimensional geopolymer network. The free NaOH is fully consumed towards the formation of the network and a Na-poly (sialate-disiloxo) albite framework with a typical feldspar crankshaft chain structure, as shown in Figure 2.12, is created. The hydrogen bonds result in dehydroxylation, causing water to evaporate and form the final stable network through solidification [6, 11].

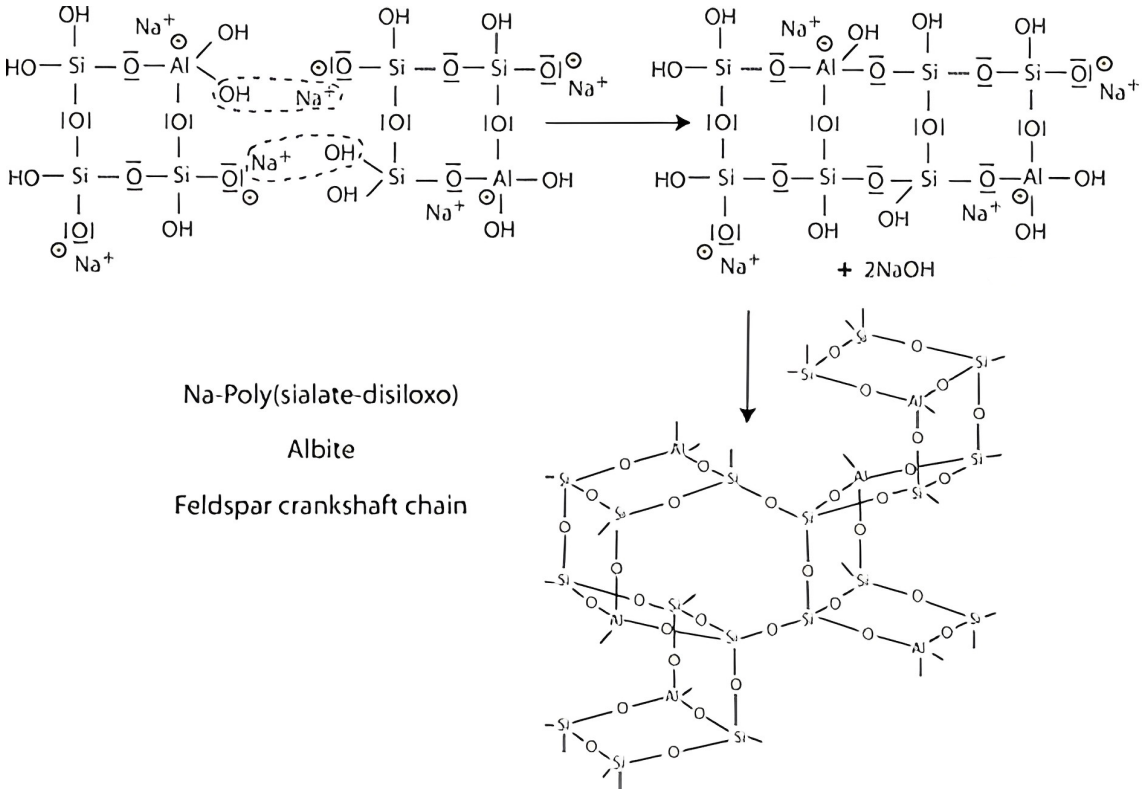

Figure 2.12: Formation of 3D geopolymeric network [6]

2.5 Components

The geopolymer's application, with a wide range from ceramics to high-tech heat resistant composites used in the aircraft and automobile industry, is determined by the atomic ratio Si/Al in the molecular structure. A three-dimensional network of Si/Al=2 units characterizes geopolymer concrete. Regardless of its application, a combination of material sources is required for the composition of a geopolymer material. These sources are included in the following groups: precursor, activator, aggregates, water and possible additives [11].

2.5.1 Precursor

Alumino-silicate source materials are used as precursors and are essential to develop geopolymer concrete. The properties of geopolymers are primarily influenced by the availability of aluminium in the precursor and its ability to release during the reaction as it determines the strength, setting, acid resistance, microstructure, etc., of the geopolymer. While presence of silicon in the precursor is also significant for the properties of geopolymers, it is less critical as aluminium since an insufficiency in the precursor can be compensated by adding supplementary soluble silicate to the activating solution. This is also known as the activator, and is further described in section 2.5.2 [41, 45].

Achieving criteria such as high performance and sustainability requires an in-depth understanding of the physicochemical material properties. Besides possessing and releasing aluminium efficiently, source materials for geopolymer concrete should be highly amorphous and contain sufficient reactive glassy content while also having a low water demand. Numerous alumino-silicate raw materials, such as metakaolin or industrial by-products such as fly ash and ground granulated blast-furnace slag, have been used alone or in various combinations as precursors for geopolymer concrete [41].

The following sections summarize the alumino-silicate source materials that have already been or have the potential to be a part of a geopolymeric precursor with reference to cost, availability, suitability, performance. The summary is limited to MK, GGBFS, FA and other waste products since these are mainly used as precursors in research.

Metakaolin

Metakaolin is an amorphous alumino-silicate source material that is a highly reactive natural pozzolan. MK is the result of calcination and dehydroxylation of kaolinitic clay at temperatures between 500°C and 900°C. Metakaolin 750 (MK-750) is the most common type of MK used for geopolymer concrete, it is a product of kaolinite calcination at 750°C. Metakaolin is a porous, angular-shaped, platy particle with a mean size that can range from 1 to 20 µm with a specific gravity (S.G.) from 2,20 to 2,60 [11, 46, 47].

The main components of metakaolin are silicon dioxide (SiO_2) and alumina oxide (Al_2O_3), the exact amount can vary according to the sources of kaolin. Other components present in MK are ferric oxide (Fe_2O_3), calcium oxide (CaO), magnesium oxide (MgO), potassium oxide (K_2O) and sodium oxide (Na_2O). Accurate component analysis of MK can be performed by either X-ray fluorescence (XRF), X-ray diffraction (XRD) or other viable methods. Typical results, including common sums and weight ratios, regarding the chemical composition of metakaolin, as reported in literature, are shown in Table 2.1 [46, 48].

Table 2.1: Chemical composition of metakaolin according to literature [wt. -%]

Source	SiO_2	Al_2O_3	Fe_2O_3	CaO	MgO	K_2O	Na_2O	$SiO_2 + Al_2O$	SiO_2/Al_2O_3
[49]	60,39	32,41	1,10	-	2,11	1,46	2,50	92,80	1,86
[50]	54,50	40,20	1,80	<0,10	0,20	0,30	0,30	94,70	1,36
[51]	55,70	38,60	2,03	-	-	2,43	-	94,30	1,44
[52]	40,02	34,00	2,00	0,10	0,60	1,70	0,10	74,02	1,18
[53]	53,00	43,80	0,43	0,02	0,03	0,19	0,23	96,80	1,21
[54]	49,80	19,30	6,30	2,20	-	2,40	-	69,10	2,58
[55]	49,86	30,51	0,69	1,49	1,07	0,59	0,45	80,37	1,63
[56]	43,90	38,50	0,98	-	0,03	0,07	-	82,40	1,14
[56]	45,10	37,70	1,40	0,06	0,06	0,05	0,03	82,80	1,20
[56]	48,50	38,20	0,93	0,03	0,40	2,06	-	86,70	1,27
[56]	46,80	36,60	1,02	0,50	0,30	0,22	0,36	83,40	1,28
[57]	57,37	38,63	0,77	0,03	0,07	0,49	0,39	96,00	1,49
[58]	51,52	40,18	1,23	2,00	0,12	0,53	-	91,70	1,28
[59]	52,80	36,30	4,21	<0,10	0,81	1,41	-	89,10	1,45
[60]	57,40	35,26	0,94	0,02	0,18	3,17	<0,01	92,66	1,63
[61]	54,30	38,30	4,28	0,39	0,08	0,50	0,12	92,60	1,42
[62]	51,52	40,18	1,23	2,00	0,12	-	0,08	91,70	1,28
[63]	55,62	39,68	0,96	1,49	0,18	0,88	-	95,30	1,40
[64]	55,80	27,40	1,10	1,10	0,06	0,17	0,23	83,20	2,04
[65]	59,59	34,91	1,52	0,20	0,05	0,80	0,07	94,50	1,71
Minimum	40,02	19,30	0,43	0,02	0,03	0,05	0,03	69,10	1,14
Maximum	60,39	43,80	6,30	2,20	2,11	3,17	2,50	96,80	2,58
Median	52,90	37,95	1,17	0,20	0,15	0,59	0,23	91,70	1,41
Mean	52,17	36,03	1,75	0,71	0,36	1,02	0,41	88,21	1,49

MK-750, a manufactured pozzolan, undergoes rigorous quality control and standardization, resulting in an excellent candidate for geopolymers. The high reactivity and fine size contribute to the high strength and durability of the geopolymer. When used in combination with industrial by-products as a geopolymer binder, it can extend the mixing and setting time. The disadvantage is the high cost of MK-750, therefore it is mainly used in small quantities to improve the properties of geopolymers based on industrial by-products [11].

Ground granulated blast-furnace slag

Ground granulated blast-furnace slag is a major byproduct of the steel and iron production. A carefully regulated combination of limestone, iron ore and coke are melted together in a blast furnace. This produces iron and slag in a molten state. This molten slag is rapidly cooled with powerfull water jets. Converting it to GGBFS, a finer, granular and glass-like material. Only highly amorphous slags can be used as a geopolymer precursor. The small particle size, ranging from 5–25 µm, increases the specific surface area and its reactivity. The grains are angular and irregular resembling fractured glass particles. Its specific gravity ranges from 2,50 to 2,90, which is approximately the same as cement [11, 66].

In general, GGBFS contains a high amount of CaO, followed by SiO_2, Al_2O_3 and MgO molecules. These chemical compounds typically account for 95% of the total composition, with exact concentrations depending on the ore, fluxing stone and impurities in the coke supplied to the blast furnace. A trace amount of other compounds such as Na_2O and K_2O have been reported. Table 2.2 consists of several different chemical compositions of GGBFS found in literature. Techniques such as XRF and XRD can be used to accurately determine the chemical components of GGBFS and their relative quantities [11, 66, 67].

Table 2.2: Chemical composition of ground granulated blast-furnace slags according to literature [wt. -%]

Source	SiO_2	Al_2O_3	Fe_2O_3	CaO	MgO	K_2O	Na_2O	SiO_2 + Al_2O	SiO_2/Al_2O_3
[52]	45,18	10,78	2,30	32,73	5,38	0,93	0,14	55,96	4,19
[68]	36,40	13,60	-	41,40	6,80	-	-	50,00	2,68
"	36,60	12,00	-	42,00	6,94	-	-	48,60	3,05
"	37,60	9,61	-	40,90	6,40	-	-	47,21	3,91
"	37,00	9,41	-	42,10	6,12	-	-	46,41	3,93
"	37,10	12,90	-	38,40	7,32	-	-	50,00	2,88
"	35,60	11,00	-	41,20	6,84	-	-	46,60	3,24
"	36,70	11,50	-	41,70	6,35	-	-	48,20	3,19
"	36,60	11,20	-	40,90	6,84	-	-	47,80	3,27
"	37,40	11,00	-	39,50	6,64	-	-	48,40	3,40
"	38,00	10,10	-	41,70	6,46	-	-	48,10	3,76
"	36,30	11,80	-	43,20	6,30	-	-	48,10	3,08
"	36,80	11,70	-	42,00	6,60	-	-	48,50	3,15
"	39,20	11,20	-	33,90	10,40	-	-	50,40	3,50
"	34,60	13,70	-	38,90	8,36	-	-	48,30	2,53
"	34,60	20,10	-	29,00	11,60	-	-	54,70	1,72
"	36,70	6,80	-	37,40	11,10	-	-	43,50	5,40
[69]	33,78	13,11	0,51	42,47	7,46	0,32	0,16	46,89	2,58
[70]	27,50	7,60	1,66	48,43	5,27	0,60	-	35,10	3,62
[71]	40,10	7,00	0,30	44,80	5,90	0,49	0,23	47,10	5,73
Minimum	27,50	6,80	0,30	29,00	5,27	0,32	0,14	35,10	1,72
Maximum	45,18	20,10	2,30	48,43	11,60	0,93	0,23	55,96	5,73
Median	36,70	11,20	1,09	41,30	6,72	0,55	0,16	48,15	3,25
Mean	36,69	11,31	1,19	40,13	7,25	0,59	0,18	47,99	3,44

Unfortunately, knowing the chemical composition of the slag is not sufficient to determine whether it is suitable to be used for geopolymers. The mineral composition, can be analysed through XRD, determines the suitability of GGBFS as a precursor. The glassy content of GGBFS should include the mineral gehlenite. Gehlenite ($2CaO\text{-}Al_2O\text{-}3SiO_2$) and akermanite ($2CaO\text{-}MgO\text{-}2SiO_2$) form a solid mixture which is know as the melilite. Typically, the mineral merwinite ($3CaO\text{-}MgO\text{-}2SiO_2$) is also present in blast-furnace slag. Among the minerals mentioned, gehlenite is the most reactive. This is because aluminium is more favorable for geopolymerization than magnesium. A typical XRD pattern for ground granulated blast-furnace slag is shown in Figure 2.13, with annotation of the discussed minerals [11, 66, 67].

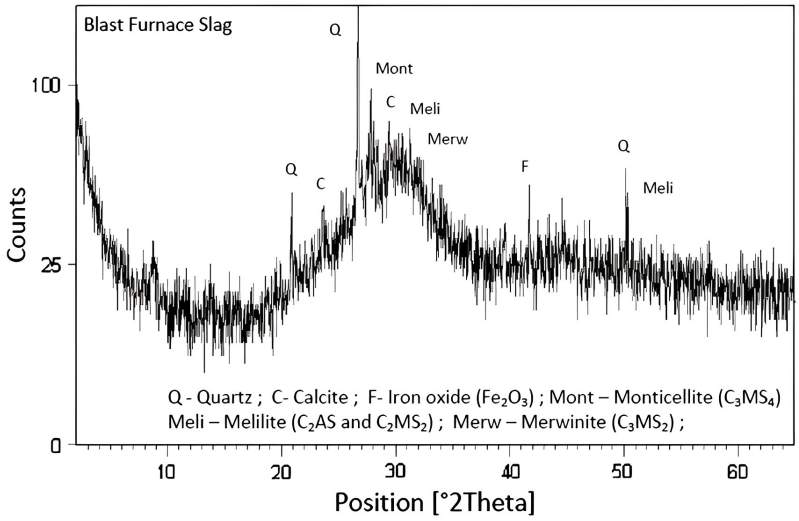

Figure 2.13: Example XRD pattern of GGBFS with annotation of present minerals [7]

Due to the highly reactive nature of GGBFS, this alumino-silicate source material does not have the right mineralogy to be used as the main precursor in a geopolymer. The lack of molecular structures in GGBFS, as opposed to MK or even FA, makes it challenging to form the three-dimensional geopolymer network. The absence of the structures present in MK or FA would result in an incomplete final product, consisting of chains rather than a complete geopolymer block. This is unfortunate since this alumino-silicate source material is so widely and easily available [11, 72, 73].

Fly ash

Fly ash is a precipitation ash product from exhaust gases of coal-based power plants. The ash is removed from the combustion gases by the dust collection system before the gases are released into the atmosphere. It is the most common artificial pozzolan and is sometimes considered a lower quality natural MK due to its high amorphous silica content. Combustion temperature, coal source and furnace oxygen supply all have an effect on FA particle morphology. Depending on these parameters, the particles can be fine or coarse and have a range of possible surface texture characteristics in terms of angularity and porosity. In general, a high combustion temperature of around 1500° C produces a finer FA. It consists mainly of hollow particles, amorphous in nature and spherical in shape. These are very suitable for geopolymerization. Particle size also depends on processing parameters, ranging from 5 µm to 300 µm. The specific gravity of FA, according to the literature, has a wide range going from 1,90 to 2,96. This is also affected by the previously mentioned parameters [11, 74, 75].

The composition of the FA will vary considerably depending on the source of the coal. A different source may lead to a variety of XRD patterns. It typically consists of SiO_2, Al_2O_3, CaO and Fe_2O_3 in the form of amorphous and crystalline oxides or minerals. In addition to its main components, FA can contain several other trace elements, including Ti, V, Cr, Mn, Co, As, Sr, Mo, Pb, and Hg. Depending on the chemical composition, FA can be classified into Class C and Class F. The Class C is also known as high-calcium fly ash because it typically contains more than 20 mass percent of CaO. The chemical composition of these found in literature are shown in Table 2.3. The concentrations of toxic trace elements are up to 4-10 times higher than those found in coal. Fly ash is considered hazardous and its improper disposal can result not only in loss of usable space, but also in environmental and ecological degradation [11, 74, 76].

Table 2.3: Chemical composition of fly ash according to literature [wt. -%]

Source	SiO_2	Al_2O_3	Fe_2O_3	CaO	MgO	K_2O	Na_2O	$SiO_2 + Al_2O$	SiO_2/Al_2O_3
[77]	59,04	34,08	2,00	0,22	0,43	0,76	0,50	93,12	1,73
[78]	49,45	29,61	10,72	3,47	1,30	0,54	0,31	79,06	1,67
[79]	59,03	25,86	5,81	1,07	0,68	1,89	0,07	84,89	2,28
[80]	48,94	27,76	7,90	6,03	1,77	0,84	0,58	76,70	1,76
[81]	59,94	22,87	4,67	3,08	1,55	2,19	0,62	82,81	2,62
[82]	55,90	27,80	7,09	3,95	-	1,55	-	83,70	2,01
[83]	60,83	26,63	4,19	3,03	0,80	0,90	-	87,46	2,28
[84]	57,80	20,00	11,70	3,28	1,95	3,88	0,30	77,80	2,89
[65]	59,57	24,48	3,94	2,77	0,78	1,02	0,60	84,05	2,43
[85]	62,24	21,50	9,20	1,42	1,46	1,05	0,47	83,74	2,89
[86]	50,30	25,10	9,33	2,31	2,01	3,22	0,48	75,40	2,00
[87]	54,40	26,50	4,80	3,50	2,50	0,60	0,40	80,90	2,05
[88]	63,60	28,19	2,99	1,57	0,54	0,01	0,05	91,79	2,26
[88]	31,62	30,11	8,94	17,17	0,71	0,10	0,74	61,73	1,05
[89]	30,10	16,60	7,00	36,90	1,40	0,30	0,60	46,70	1,81
[89]	30,70	15,70	6,50	34,70	1,00	0,30	1,80	46,40	1,96
[89]	30,70	8,20	8,90	30,20	2,60	0,90	4,10	38,90	3,74
[89]	35,00	24,50	24,50	0,90	-	3,20	-	59,50	1,43
[89]	59,40	21,40	21,40	3,80	0,20	4,60	-	80,80	2,78
[90]	20,50	9,11	32,10	26,90	2,16	2,61	1,10	29,61	2,25
Min	20,50	8,20	2,00	0,22	0,20	0,01	0,05	29,61	1,05
Max	63,60	34,08	32,10	36,90	3,71	4,60	4,10	93,12	3,74
Median	55,15	24,80	7,50	3,38	1,40	0,96	0,49	79,93	2,15
Mean	48,95	23,30	9,68	9,31	1,41	1,52	0,71	72,25	2,20

Essential characteristics for potential waste and industrial by-products

As the emphasis shifts towards utilizing alternative energy sources for sustainability, it is expected that coal burning will be eliminated. Eliminating the coal burning industry will terminate the production of FA. On the other hand GGBFS is mineralogically unsuitable to serve as the main geopolymer precursor. Therefore, it cannot fully replace fly ash, and the high cost of MK certainly prevents its use in large quantities. This motivates the use and research of various alternative alumino-silicate source materials which is also beneficial from a sustainability perspective [11, 91].

A major difficulty is the unknown mineralogy, physical and chemical properties which vary from the variety of alumino-silicate source materials and their topography. Therefore, the compatibility of each non-standard precursor should be assessed through a series of tests, with a particular focus on determining the microstructure, chemical composition, mineral phases and the pH. The last one is rather important, as a higher pH value increases the risk of flash setting or rapid hardening, potentially harming the geopolymarization.

To address the need for analyzing the waste and industrial by-products, the following Table 2.4 summarizes the chemical composition of different waste wood ash materials found in the literature. The wide range of possibilities in terms of chemical composition and therefore the potential use for GPC is noteworthy [11, 91, 92, 93, 94].

Table 2.4: Chemical composition of waste wood ash according to literature [wt. -%]

Source	SiO_2	Al_2O_3	Fe_2O_3	CaO	MgO	K_2O	Na_2O	$SiO_2 + Al_2O$	SiO_2/Al_2O_3
[94]	41,00	9,30	2,60	11,40	2,30	3,90	0,90	50,30	4,41
"	28,00	6,20	2,20	25,40	5,00	3,20	3,30	34,20	4,52
"	37,49	12,23	8,09	26,41	4,04	6,10	1,81	49,72	3,07
"	26,06	1,91	2,65	45,76	2,33	10,70	2,65	27,97	13,64
"	12,40	0,12	1,10	68,20	11,50	2,60	0,90	12,52	103,33
"	4,38	0,55	2,24	69,06	5,92	8,99	1,85	4,93	7,96
"	39,91	15,12	9,54	9,75	2,59	8,06	0,54	55,03	2,64
"	4,48	0,12	0,37	83,46	2,49	5,47	0,87	4,60	37,33
"	10,04	3,10	1,12	57,74	10,91	9,29	1,56	13,14	3,24
"	19,26	5,02	8,36	15,10	5,83	8,89	29,82	24,28	3,84
"	20,65	2,99	1,42	47,55	7,20	10,23	1,60	23,64	6,91
"	2,34	2,34	1,45	59,62	14,57	5,12	1,22	4,68	1,00
"	65,82	14,85	1,81	5,79	1,81	2,19	2,70	80,67	4,43
"	8,95	3,98	1,43	67,36	6,59	7,03	1,76	12,93	2,25
"	29,93	4,27	4,20	15,56	5,92	31,99	2,00	34,20	7,01
"	48,95	9,49	8,49	17,48	1,10	9,49	0,50	58,44	5,16
"	10,24	2,02	0,88	41,47	3,03	25,16	3,67	12,26	5,07
"	9,20	7,20	2,79	56,83	6,19	7,78	1,97	16,40	1,28
"	68,18	7,04	5,45	7,89	2,43	4,51	1,20	75,22	9,68
"	7,76	2,75	1,25	44,10	11,33	22,32	0,42	10,51	2,82
"	9,71	2,34	2,10	48,88	13,80	14,38	0,35	12,05	4,15
"	3,87	0,68	1,16	57,33	13,11	18,73	0,22	4,55	5,69
"	1,86	0,62	0,74	77,31	2,36	8,93	4,84	2,48	3,00
"	26,17	4,53	1,82	44,11	5,34	10,83	2,48	30,70	5,78
"	6,13	0,68	1,90	72,39	4,97	7,22	2,02	6,81	9,01
"	49,30	9,40	8,30	17,20	1,10	9,60	0,50	58,70	5,24
"	7,77	8,94	3,83	53,50	9,04	5,64	3,40	16,71	0,87
"	6,10	1,96	0,74	46,09	4,03	23,40	1,61	8,06	3,11
"	23,15	5,75	3,27	37,35	7,26	11,59	2,57	28,90	4,03
"	53,15	12,64	6,24	11,66	3,06	4,85	4,47	65,79	4,20
[95]	32,40	17,10	9,80	3,50	0,70	1,10	0,90	49,50	1,89
"	13,00	7,80	2,60	13,70	2,60	0,40	0,60	20,80	1,67
"	50,70	8,20	2,10	19,60	6,55	2,80	2,10	58,90	6,18
"	30,00	12,30	14,20	2,20	0,70	2,00	0,50	42,30	2,44
"	8,10	7,50	3,00	25,30	4,50	2,70	3,30	15,60	1,08
Minimum	1,86	0,12	0,37	2,20	0,70	0,40	0,22	2,48	0,87
Maximum	68,18	17,10	14,20	83,46	14,57	31,99	29,82	80,67	103,33
Median	19,26	5,02	2,24	41,47	4,97	7,78	1,76	23,64	4,20
Mean	23,33	6,03	3,69	37,32	5,49	9,06	2,60	29,36	8,23

Once the chemical composition of an unknown waste material of industrial by-products has been determined, Figure 2.14 can be used to gain insight into its potential as a precursor. The ternary graph has three axes, representing the weight contribution of SiO_2, Al_2O_3 and CaO, as well as a marked area where common precursors and others (silica fume,SF, and OPC) are situated. Plotting the composition of the unknown waste material of industrial by-product in the ternary graph could potentially provide some initial information about the potential in geopolymers compared to common precursors [11, 91, 93].

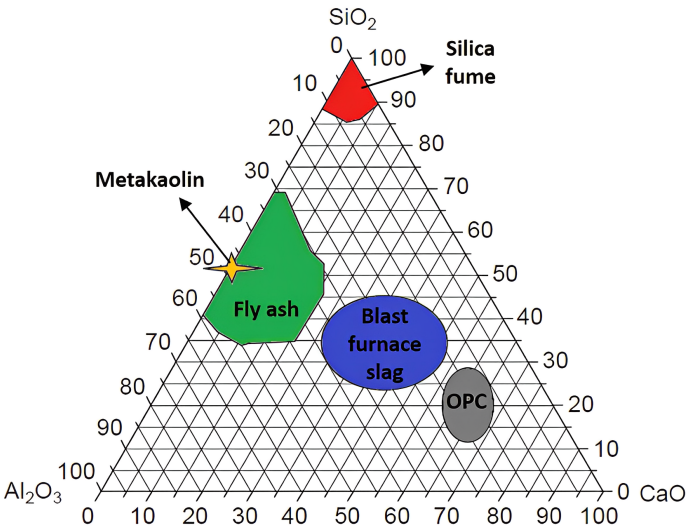

Figure 2.14: Ternary graph common precursors and OPC [8]

2.5.2 Activators

Activators or soluble silicates (SS) act as initiators of the geopolymerization mechanism. The class of minerals known as silicates is the largest and most complex. This is not surprising when you consider that oxygen and silicon, the chemical components of silica, are the two most commonly found elements on Earth. They make up about 75% of the Earth's crust, as shown in Figure 2.15. The combination of their wide availability, low cost and user-friendly nature makes them a suitable material for the geopolymerization of various alumino-silicate source materials. Some silicates are formed deep below the Earth's surface. Today, however, silicates are mainly produced either by the furnace route or the hydrothermal process. In the furnace route, sodium silicate is produced by melting primary sand and sodium carbonate (Na_2CO_3) or potassium carbonate (K_2CO_3) at a temperature between 1350°C and 1450°C. The resulting product is then dissolved in water to form a solution. The silicates are formed through direct dissolution of siliceous materials such as sand in caustic soda (NaOH) or potassium hydroxide (KOH) [11, 73, 96, 97, 98].

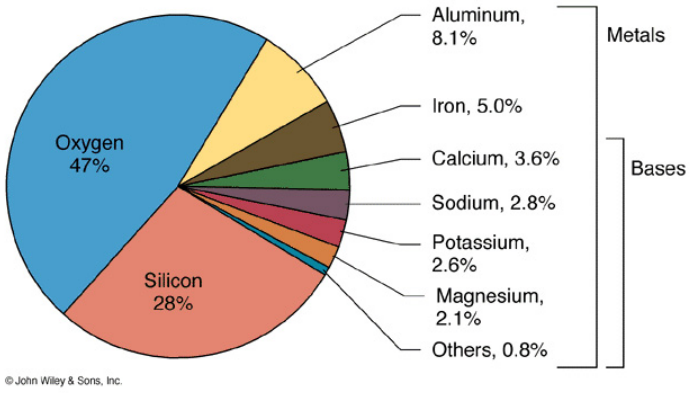

Figure 2.15: Elements in the Earth's crust [9]

With respect to the chemical composition, silicates are basically combinations of alkali metal oxide (M_2O), silica (SiO_2) and water. The alkali metal M^+, previously mentioned in section 2.1, can be either sodium (Na), potassium (K), lithium (Li), magnesium (Mg), calcium (Ca), or cesium (Cs), with the first two being the most common. The general formula of a silicate is $xSiO_2.M_2O.zH_2O$, where x is the degree of polymerization and z the number of water molecules. These two parameters are very important in choosing the right activator for the production of geopolymer concrete [11, 99].

The parameters used to define commercially available silicates are the weight ratio (WR) and the molar ratio (MR). These ratios are often confused as being the same. WR is the weight of SiO_2 to the weight of M_2O, while MR represents the molar quantities of SiO_2 to M_2O. Commercially available silicates have MR values ranging from 0,4 to 4,0. Silicates with values less than 1,45 are highly corrosive and unstable due to their high causticity and lack of a three-dimensional structure. On the other hand, silicates with high MR values, such as 3 or 4, are less reactive. Viscosity, causticity, pH, solubility, and dissolution rate are other important properties in selecting an appropriate activator. These properties, depending on the molar ratio, are summarized in Figure 2.16. All of these are mainly influenced by the MR, density and temperature. In general, a commercially available activator with a molar ratio SiO_2/K_2O between MR=1,5 and 1,7 or a sodium silicate with a molar ratio SiO_2/Na_2O between MR=1,7 and 1,9 is preferred because it is easy to use, reproducible and stable. The research industry will avoid producing the activator in-house and instead purchase the K-silicate and Na-silicate solution with a viable MR that are specifically manufactured and marketed for geopolymer applications. Other available ratios are not made specifically for geopolymers [11, 73, 99].

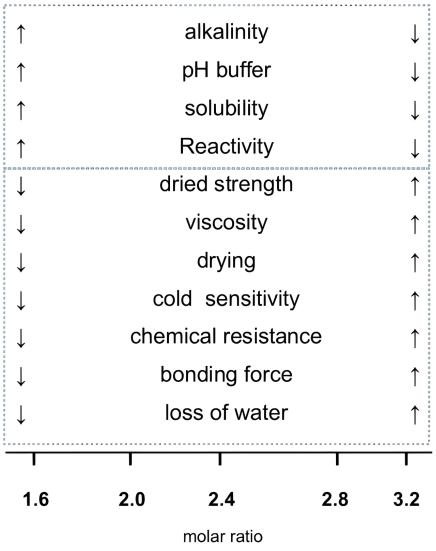

Figure 2.16: Properties according to MR of activator [10]

Because of their wide availability, potassium (K) and sodium (Na) based silicates are the most commonly used silicates. The Na-silicate has become more popular due to its lower cost and ability to produce higher compressive strengths, but its lower atomic mass can result in durability issues due to the Na^+ cation being more prone to migration. In addition, the viscosity of Na-silicate is more sensitive to temperature changes than that of K-silicate, which may require the use of greater amounts of water to increase fluidity. Which will also increase the porosity of the hardened material [11, 73].

2.5.3 Aggregates

Similar to conventional concrete, aggregates are crucial in geopolymer concrete, where they can be used up to 75% of the volume and serve the same function in the hardened state. They provide strength, volume stability, workability, lower cost, etc. There are numerous options of available aggregates, from well-graded coarse to fine grians with angular or round shapes. Typically the fine and coarse aggregates are mixed in such a way that it gives minimal voids in the concrete, achievable by grading the fine aggregate and selecting a suitable fine-to-total aggregate ratio [11, 100].

Geopolymer concrete does not carry the risk of alkali-silica reaction (ASR) because it is based on a different mechanism than that of conventional concrete. Some aggregates with a reactive surface and inert core, such as waste sands, even improve the geopolymer matrix due to a better bond with the reactive surface. Besides the research community being suspicious due to the risks, geopolymer concrete should encourage the use of partially reactive aggregates [11].

2.5.4 Water

From the chemical perspective, it was observed that formed geopolymer chains interact with each other through hydrogen bonds to create the three-dimensional geopolymer network. Adding water to a hydroxyl group results in free water and an alkyl group (dehydroxylation), this means that water is only needed during the polymerization process. Once the network is formed, evaporation of the water occurs and results in solidification. This process, briefly discussed in section 2.4 and shown in Figure 2.17, causes the final stable geopolymer network [11, 100, 101].

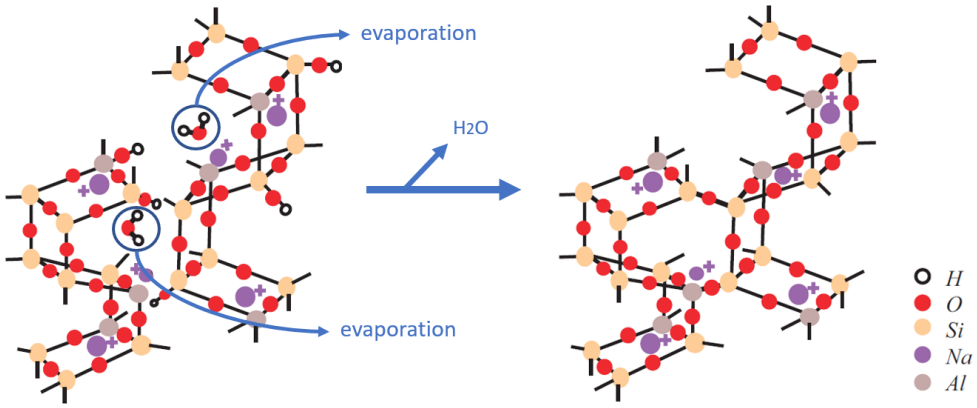

Figure 2.17: Evaporation of water during the solidification [11]

The evaporation indicates that the role of water in the geopolymer only contributes to the workability of the concrete in a liquid state and not to the strength in a hardened state. For the same degree of workability, the demand for water increases when the fineness of the precursor increases. Therefore the minimum quantity of water required to achieve the requested workability is determined by the basic degree of workability, fineness of the precursor and the grading of the fine aggregates. However, the addition of extra water should be handled with caution. Adding too much water to the mixture promotes high porosity and will reduce the compressive strength in the hardened state [11, 100].

In addition to the water that is needed for the chemical reaction, it is also needed to increase the workability of the geopolymer concrete. This water forms a thin layer around all the aggregate grains and reduces the frictional resistance between them, allowing the concrete to flow more easily. The water amount needed to wet all the grains can be estimated from the indicatory values in Table 2.5 [102].

Table 2.5: Water demand for wetting of the grains [102]

Material	Grainsize [mm]	Water demand [%m/m]
Cement	<0,063	25 to 30
Additives	<0,063	22,5 to 25
Fine sand	0,063 - 1	7 to 10
Semi-coarse sand	0,063 - 2	5 to 7
Coarse sand	0,063 - 4	4 to 6
Fine gravel	2 - 8	2,5
Semi-coarse gravel	8 - 16	2
Coarse gravel	16 - 22	1,5
Very coarse aggregates	22 - 63	0,5

2.5.5 Possible additives

Geopolymer concrete, much like conventional concrete, can use additives to enhance the durability and performance of the material. This may involve improving its strength and ductility, or introduce new properties such as antimicrobial action, self-cleaning and the capability of self-healing [11].

Although no additives are used in this research, the following section discusses the most prominent additives used in geopolymer concrete.

Fibers

While GPC exceeds the performance of traditional cement-based concrete, it is still very brittle in tension and has a low resistance to cracking. Therefore, it can only be used in reinforced structural members. In the last few years, fiber-reinforced geopolymer concrete has been developed in which fibers have a similar function as those in traditional fiber-reinforced concrete. The fibers increase the ductility, tensile strength and strain capacity of the concrete, but it requires an adapted mixing method to prevent the fibers from breaking and forming a lump in the fresh mix [11, 103].

A variety of fiber materials have been researched. Carbon fibers have shown to improve the mechanical properties of geopolymer composites, but have a negative effect on workability. There is an improvement in the compressive and flexural strength, impact resistance, hardness, toughness and modulus of elasticity. On several occasions, steel fibers have also been introduced into the geopolymer mix, reducing workability but improving mechanical properties and durability. Some studies have investigated the effect of using a hybrid combination of fibers, such as a combination of steel and carbon. The results showed that hybridization of steel fibers up to a dosage of 1,5% resulted in superior mechanical properties in comparison to those with a single fiber type [11, 103].

Silica fume

Silica fume, or microsilica, is a noncrystalline polymorph of SiO_2 that is produced as a by-product of silicon and ferrosilicon alloy production in electric arc furnaces. Due to its fine spherical particles and high silica content, SF is a highly effective pozzolanic material, highly reactive and improves the packing of the binder [11, 104].

Silica fume is already used in GPC to improve its properties such as compressive strength, bond strength and to reduce permeability, which helps to protect the reinforcing steel from corrosion. A study from India, researching the effect of SF on the mechanical properties of FA-based GPC, found that the workability of the paste decreases in the presence of SF. Compared to their reference mix M40, the geopolymer concrete containing SF showed higher compressive, tensile and flexural strengths. Figure 2.18 shows that these values increase with increasing silica fume content, with 40% of SF giving the best results. The increased compressive, tensile and flexural strengths is associated to an increased compactness and denser microstructure [11, 12, 104].

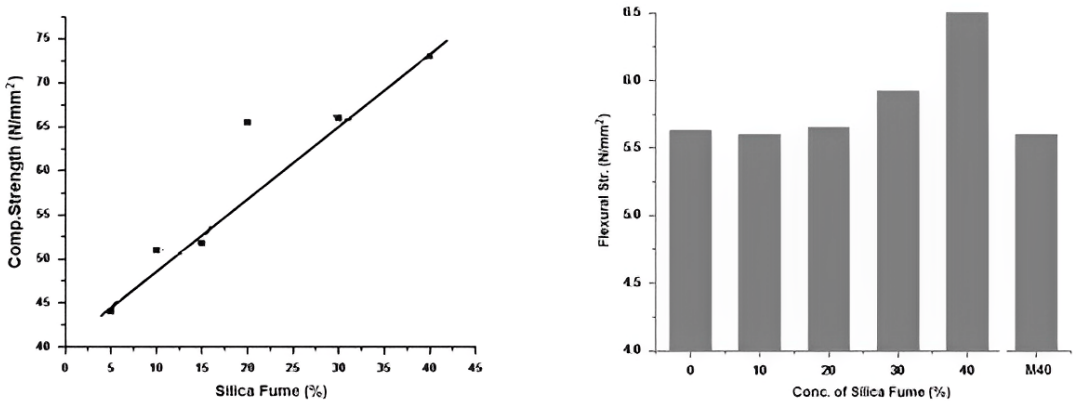

Figure 2.18: Increased parameters due to increase in SF [12]

Chemical admixtures

The plasticizers that have been used in geopolymers are typically based on carboxylate ethers and on lignosulfonates or naphthalene sulfonates. The naphthalene sulfonate plasticizers are very effective in advanced OPC-based concretes. Although, the organic polymers in these plasticizers can interfere with the geopolymerization and thus the strength development of the geopolymer. Naphthalene sulfonate-based plasticizers produce small bubbles that improve workability without interfering with the geopolymerization mechanism. However, the use of plasticizers can be avoided by adding some drops of water at the end of mixing. As with conventional concrete, the optimal dosage for water is in the range of 1-1.5% by weight of the geopolymeric binder [11].

Another issue with geopolymer concrete is the rapid setting time caused by the high alkalinity of the binder. While retarders are used in conventional concrete to extend the setting time, they are not effective in geopolymer concrete and can actually cause unpredictable behavior because the retarders are based on the hydration mechanism [11, 105].

2.6 Mix procedure

The mixing procedure is critical to the realization of geopolymer concrete. The mixing process for most AAM-based concrete is similar to that of OPC-based concrete. Typically, the process begins with combining a dry mix of alumino-silicate materials and aggregates, followed by the addition of soluble silicates, water and any admixtures. The GPC mixing process on the other hand is completely different [3, 11].

2.6.1 Different mixing methods

Various techniques are available for the mix procedure. Literature suggests two different kind of methods [3, 11]:

In the first method, the activator is added to the mixing water. Initially, the fine and coarse aggregates are premixed together with a small amount of activator solution for a specified time, t_1. After that, the mineral components are added, and the remaining activator solution is gradually introduced. The components are mixed for a duration of t_2, followed by a rest period of t_3. Then mixing is resumed and continued for a duration of t_4. The time values of t_1 to t_4 must be predetermined based on the activators solubility in the mixing water and issues related to the initial setting time [3].

The second method is similar to the first one, with the only difference that the mineral components are added to a mixing water solution (water with well-dissolved activator) and are mixed to initiate the activity of the mineral components. Moving forward with the same sequence mentioned in the first method [3].

2.6.2 Importance of the mixing time

To achieve the highest stability, the soluble silicate must be mixed with water before the start of mixing, ideally at least 24 hours prior. The mixing process should initiate by mixing the precursors with the silicate for a minimum of 5 minutes, taking into account the mixer's speed. After the geopolymeric slurry is prepared, the aggregates should be added and mixed for 2 to 3 minutes. To ensure a better workability, water can be added to the mixture, but, the strength will be effected. When there is too much or too little water added, the strength will be lower, respectively due to the increasing water/solid factor or the difficult to compact mixture [3, 11].

In the literature, the second mixing method was used to test the effects of different mixing durations on geopolymer concrete performance. Two different mixing times were used, a short duration (1 minute) and a long duration (10 minutes). It was observed that the mixing time of the geopolymer concrete has an impact on its workability and curing rate. When GPC was mixed with a 1 minute duration, the mix remained workable for slightly over 15 minutes after discharge and then hardened rapidly. For the tests with a 10 minute mixing duration, the geopolymer concrete remained workable for approximately 90 to 120 minutes after which it started to harden [106].

2.7 Properties

The focus of this section is to discuss the most important properties related to the specific parameters used, rather than to provide a comprehensive list of properties. It's important to measure and track the various parameters to accurately identify

and quantify the properties of the concrete. The same tests used to evaluate OPC-based concrete can also be used for GPC. The properties of fresh concrete are discussed first, followed by a discussion of the hardened properties.

2.7.1 Fresh properties

Workability

The concept of workability refers to a crucial characteristic of cementitious materials, namely their ability to be easily molded and shaped when fluid. The same concepts can be applied to GPC. To achieve the desired workability of concrete, the amount of water required depends largely on the properties and quantity of the fine aggregates. It has been shown that a geopolymer concrete with a slump of 193 mm can be achieved, indicating optimum workability. According to the requirements in EN 1015-6, a geopolymer with this degree of workability falls under the classification of a plastic mortar, as it falls within the range of 140-200 mm [30].

Several studies have shown that the addition of GGBFS to the concrete results in an increase in slump, the fine particle size of GGBFS can be the explanation. Furthermore, the addition of MK to the mix has a significant effect on workability. Research shows that using a lower percentage of MK leads to an improved workability [107, 108].

2.7.2 Hardened properties

Density

The density of geopolymer concrete is significantly influenced by the ratio of silica to alumina. Silica, a hard and strong compound, can affect the density of GPC because it fills the pores between the grains and prevents excessive grain growth, resulting in a higher density. On the other hand when alumina is added, it can affect density by forming additional pores. Reducing the alumina content can lead to a reduction in porosity and thus a higher density. This suggests that a decrease in alumina content can lead to a decreased porosity and an increased density [109].

Strength

GPC can achieve a very high compressive strength exceeding conventional concrete. Numerous research studies have shown that geopolymer concrete can withstand over 10 MPa more than conventional concrete when given sufficient time to cure. A disadvantage of conventional concrete is its low flexural strength, which makes it brittle. For example, in earthquakes where it is subjected to numerous compressive and flexural forces. In contrast, geopolymer concrete not only has impressive compressive strength, but also high flexural strength. Although GPC has a higher flexurial strength, it does not mean that GPC is earthquake resistant, it still can be an advantage over conventional concrete [23].

A geopolymer concrete containing alumino-silicate starting material, activator, water, fine sand, and coarse aggregates typically achieves a compressive strength in the range of 60 MPa, with a E-modulus of 27 GPa. Similar to conventional concrete, GPC has a Poisson's of 0,17 [11].

2.8 Mineralogy and microstructure of geopolymers

GPC consists of phases that are either amorphous or semi-crystalline. The primary phase is a geopolymer gel formed by the chemical reaction between the alkaline activator and precursor. Depending on the alkaline activator, the geopolymer gel can either be sodium or potassium-based. The gel has a three-dimensional polymer network structure formed by tetrahedral and octahedral units of Si, Al and O. With its high specific surface area, it can absorb water and other chemicals, which contributes to the strength and durability of the concrete. In addition to the geopolymer gel, geopolymer concrete may contain secondary crystalline phases, such as zeolites and alumino-silicate hydrates, similar to those found in OPC-based concrete. Geopolymers typically contain alumino-silicate hydrates such as sodium alumino-silicate hydrate (N-A-S-H) or potassium alumino-silicate hydrate (K-A-S-H), depending on the alkaline activator. Calcium alumino-silicate (C-A-S-H) can also be present if the precursor, like FA or GGBFS, has a high calcium content. All of these contribute to the strength of geopolymer concrete. However, the contribution of C-A-S-H is rather limited compared to the others [14, 73, 110, 111, 112].

Compared to OPC-based concrete, GPC has a different microstructure due to geopolymerization. It results in a denser, more homogeneous material with a lower porosity and a more uniformly distributed binder phase. The microstructure is mainly composed of three types of features: the geopolymer gel, the aggregates and the interfacial transition zone (ITZ). These are visualized in Figure 2.19 through a microscopic image. The gel forms a continuous matrix around the aggregates and fills the voids between them, while the aggregates provide most of the mechanical strength to the concrete. The ITZ is the region where the gel and aggregates meet, it plays an important role in the mechanical properties [3, 13, 113, 114].

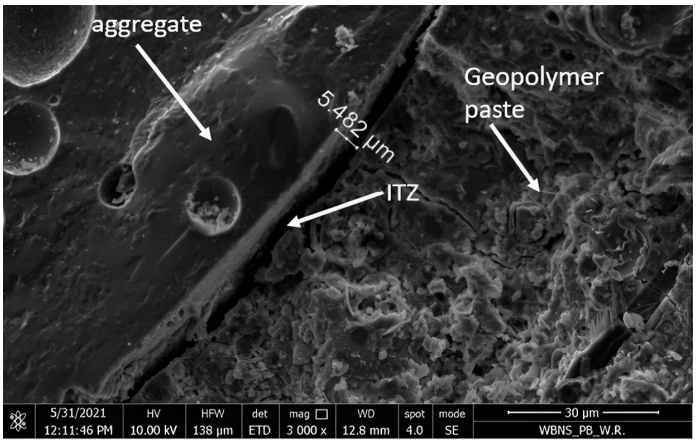

Figure 2.19: Interfacial transition zone between coarse aggregate and geopolymer paste [13]

2.8.1 Mineralogy based on literature

Studies have shown that minor changes in the mixture components can greatly impact the mineralogy and evolution of GPC, as can be observed in the diffraction patterns (Figure 2.20), affects its microstructure and physical properties. Thus, a precise selection of precursors and mix design is critical when designing GPC. Valuable insight can be obtained by analyzing the mineralogy of the components to understand the results of the geopolymer. To provide some background on the possible mineralogy of common precursors and different mixtures of GPC, the following Tables 2.6 and 2.7 give an overview based on diffraction data derived from literature.

Table 2.6: Mineral composition frequent precursors

		Minerals																							
Precursor	**Source**	Akermanite	Albite	Alunite	Anatase	Anhydrite	Anorthite	Calcite	Dolomite	Gehlinite	Gibbsite	Gypsum	Hematite	Illite	Kaolinite	Lime	Magnesite	Magnetite	Melilite	Merwenite	Microcline	Mullite	Muscovite	Portlandite	Quartz
MK	[115]													x	x								x		x
	[116]				x																				
	[117]														x										x
	[118]												x	x								x			x
	[119]				x									x											x
	[120]				x																				x
	[121]				x									x	x						x		x		x
	[122]														x								x		x
	[123]												x	x											x
	[124]			x											x										x
	[125]																				x		x		x
	[126]														x										x
	[127]				x									x											x
	[128]				x						x				x										x
	[129]			x										x	x										x
GGBFS	[130]							x		x															x
	[7]							x											x	x					x
	[131]					x		x				x													x
	[132]	x						x																	
	[133]											x													
	[134]							x		x							x								x
	[135]							x																	
	[136]							x				x													
	[137]	x				x	x	x				x													x
	[138]					x		x				x				x									x
	[11]	x								x										x					
FA	[139]							x				x	x									x			x
	[140]							x											x	x		x			x
	[141]																					x			x
	[142]												x					x				x			x
	[142]												x			x		x	x	x		x			x
	[143]						x	x			x		x									x		x	x
	[144]												x					x				x			x
	[145]												x									x			x
	[146]							x								x		x				x			x
	[147]						x						x					x				x			x
	[148]		x					x													x	x			x
	[149]												x									x			x
	[150]							x	x				x									x			x
	[151]												x			x		x				x			x

Table 2.7: Mineral composition frequent GPC mixes

		Minerals																						
Precursor	**Source**	Albite	Anatase	Calcite	Ca-silicate	CASH	CH	CSH	Ettringite	Feldspars	Hematite	Hydrotalcite	Illite	Kaolinite	Larnite	Leucite	Magnesite	Magnetite	Mullite	NASH	Nepheline	Portlandite	Quartz	Tobermorite	Wuestite
FA	[152]			x		x			x									x	x				x		
	[153]							x											x				x		
	[154]					x													x		x		x		
	[155]			x							x								x			x	x		
	[156]									x			x			x			x				x		
	[157]				x													x	x				x		
	[158]					x		x											x	x	x		x		
	[58]																		x				x		
	[159]	x									x								x				x		
	[145]										x								x				x		
	[160]							x			x							x	x				x		
FA, GGBFS	[161]																		x	x			x		
	[134]			x	x	x											x			x			x		
	[160]			x				x											x				x		
	[136]			x		x		x			x	x							x	x			x		
FA,WWA	[159]	x		x							x								x				x		
	[162]	x		x				x											x				x	x	
GGBFS	[163]					x		x	x			x								x			x		
GGBFS, MK	[164]					x																	x		
	[165]					x	x	x												x			x		
	[116]		x	x	x												x								x
MK	[166]									x			x			x							x		
	[160]		x										x	x					x				x		
MK, WWA	[115]			x									x	x	x						x	x	x		

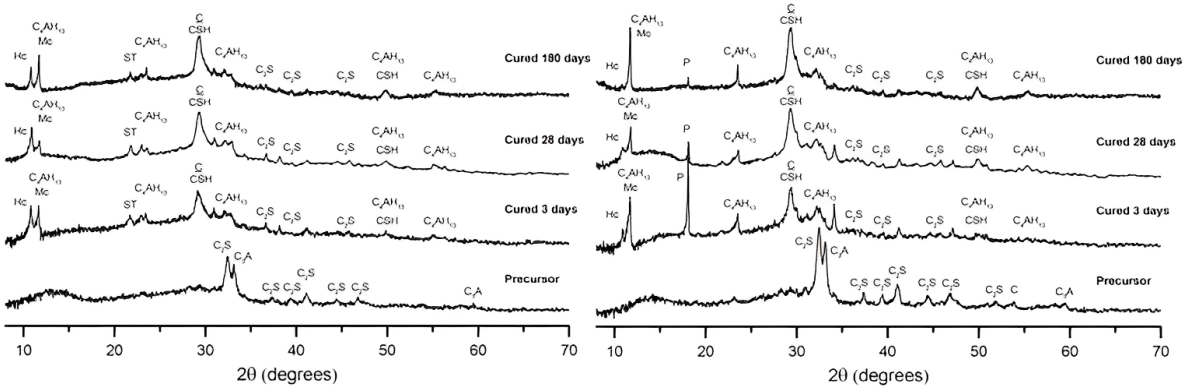

Figure 2.20: Change in diffraction pattern due to change in chemical composition precursor [14]

2.9 Durability

The existence of historical geopolymer monuments, such as the ruins of Tiwanaku and the Egyptian pyramids (Figure 2.21), serves as compelling proof that geopolymer composites surpass traditional concrete as well as alkali-activated materials in terms of durability. This suggests that geopolymer applications could have extensive potential in the construction industry [11, 15, 167].

Figure 2.21: Historical geopolymer monuments, Tiwanaku ruins (left) and Egyptian pyramids (right) [15, 16]

The following topics cover some of the fundamental durability aspects along with a comparison to alkali-activated materials and OPC-based concrete.

2.9.1 Acid resistance

As previously stated in the introduction, Section 2.1, the mechanism of geopolymerization can take place either in an alkali or acidic medium. Therefore, in an acidic environment, the destruction of the geopolymer chain is limited in comparison to ordinary Portland cement and Ca-rich alumino-silicates such as GGBFS. The strength loss of geopolymers in the presence of strong mineral acids such as HCl and H_2SO_4 is limited, while Portland cement is highly sensitive to both acids and has losses ranging from 80 to 100% [11, 168].

Research was done on the acid resistance of fly ash based geopolymer concrete in sulfuric acid. The study involved submerging samples in solutions of varying sulfuric acid concentrations for 24 weeks. The results indicated that 0,5% concentration had no significant effect on compressive strength, while 1% and 2% concentrations caused reductions of approximately 35% and 60%, respectively. Bakharev observed that exposure to acidic media causes alumino-silicate polymers to depolymerize. This leads to the release of a silicic acid and the replacement of sodium and potassium cations with hydrogen or hydronium ions, which in result into the dealumination of the geopolymer structure [11, 168].

2.9.2 Sulfate resistance

The significance of sulfate resistance as a measure of durability is not negligible. In the case of OPC, its highly sensitive to sulfate attack, this is due to the formation of expansive gypsum and ettringite. This often results in expansion and cracking of the material. Geopolymers, on the other hand, have a different chemical mechanism than OPC and therefore do not form gypsum or ettringite. However, Ca-rich binders may pose a minor risk in this regard [11, 169].

The sulfate resistance of geopolymer concrete has also been investigated in several studies. An experiment, involving immersion in a 5% sodium sulfate solution for varying periods of time, was conducted to evaluate the sulfate resistance of heat-cured, low-calcium FA-based concrete. Mass, length, and compressive strength measurements were used to evaluate the durability of the material. The results showed that the geopolymer concrete outperformed conventional concrete in terms of sulfate resistance, with no evidence of erosion, cracking, or spalling even after one year of immersion in the solution. In fact, it is noteworthy that immersion resulted in a slight increase in compressive strength [11, 169].

2.9.3 Alkali-silica reaction

The use of high levels of alkalis in the mixing of geopolymers has raised concerns about the potential for alkali-silica reaction in structures. In traditional concrete the alkalis and hydroxyl ions from the OPC paste react with reactive siliceous minerals in aggregates and form an expansive gel. The volumetric expansion of the silica gel creates internal stresses in the concrete and leads to loss of strength, cracking and failure of the structure. A schematic representation of the ASR is illustrated in Figure 2.22. Unlike traditional OPC-based materials, there are no free hydroxyls or alkalis in the geopolymer because they are trapped in the stable 3D geopolymer network. As a result, the siliceous minerals in the aggregates help to improve the chemical bond between the aggregates and the binder, eliminating the risk of ASR and promoting the use of reactive aggregates [11, 17, 170].

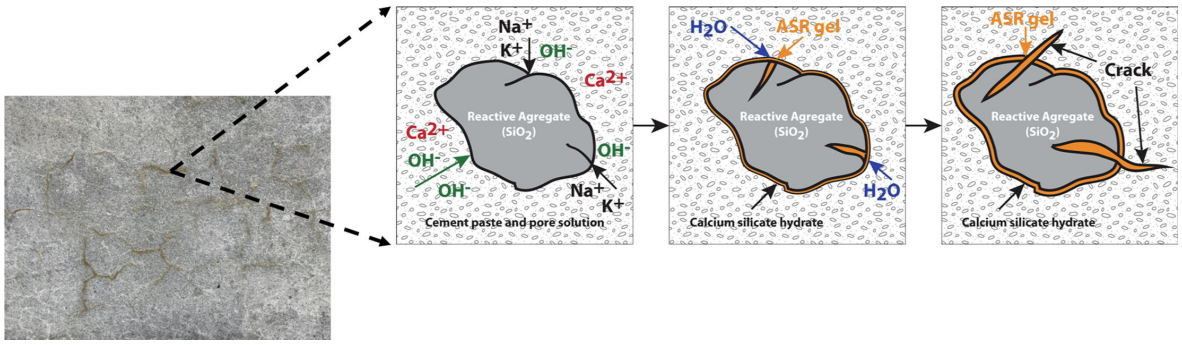

Figure 2.22: Schematic representation of the mechanism of the ASR in traditional concrete [17]

A lack of thorough understanding of geopolymer chemistry in the civil engineering research community, combined with the concerns regarding ASR, led to the delayed development of geopolymer concrete. As a response to the concrete industry's ASR concerns regarding geopolymer concrete, research has been conducted using accelerated expansion tests in saturated NaCl baths. The results showed that geopolymer binders outperformed conventional OPC. Even at alkali contents as high as 10%, the geopolymer materials did not generate any hazardous silica gel [11, 170].

2.9.4 Corrosion

While AAMs can have pH values as high as 13 to 14, geopolymer concrete is not as highly alkaline. The pH range of geopolymer cement is between 11,5 and 12,5, which is very close to that of ordinary Portland cement (pH 12-13), leading to be effective in the protection of reinforced steel. The highly alkaline environment forms a thin passive protective layer around the steel

reinforcement, protecting it from the action of oxygen and water. As long as steel is in this highly alkaline state, it will not corrode due to the condition called passivation. Research has shown that this passive protective film is formed around the reinforced steel once the dissolved silicates have stabilized in the high alkali geopolymer matrix [11, 18, 171].

Once the protective film is compromised, the steel (Fe) will naturally return to its initial state of lower energy (Fe_2O_3). Thus the corrosion process begins. The following Figure 2.23 summarizes the corrosion phenomenon and reactions in an environment where the oxidized form is the preferred state of lower energy due to the presence of an electrolyte. Since rust is created inside the concrete, the lack of space will increase the internal pressure. As a result, cracks are formed to release the pressure outside. This allows the atmosphere to further react with the internal environment of the reinforced concrete and increase the danger of failure. The cracks will continue to grow and cause the concrete to fall off and if not treated properly the corrosion will keep spreading [18, 171, 172].

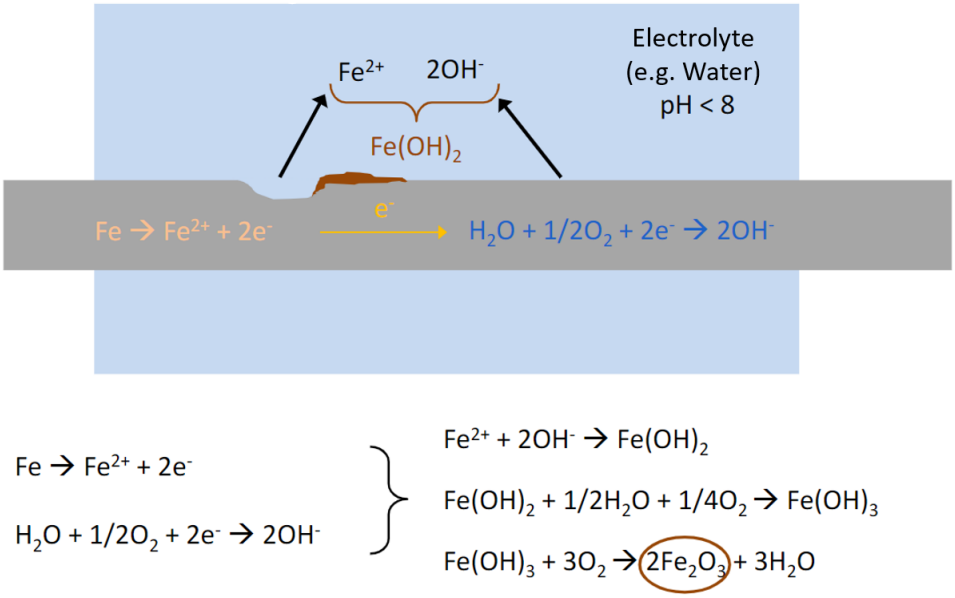

Figure 2.23: Corrosion of steel in suitable environment [18]

2.9.5 Carbonation

Carbonation increases the risk of corrosion due to the decrease in alkalinity of the OPC. The carbonation reaction occurs when certain hydrates ($Ca(OH)_2$) react with free hydroxyl ions in the presence of CO_2 to form calcium carbonate ($CaCO_3$). Consuming the hydroxyl ions lowers the pH of the concrete, creating a low pH zone in the concrete. The depth of this zone depends on how the deep CO_2 can diffuse, as shown in Figure 2.24. It is important to evaluate this depth as once it reaches the reinforcement, the passive protecting layer of the steel will be compromised. Besides the amount of CO_2 in the atmosphere, the rate at which the carbonation depth increases depends on the relative humidity (RH) [11, 18, 171].

Carbonation in GPC produces different products than in OPC-based concrete, resulting in the formation of potassium or sodium carbonate with a pH in the range of 10 to 10,5, as opposed to $CaCO_3$ with a pH of 7 to 8. Despite their presence, the alkalinity of the carbonated products in geopolymerized concrete remains high enough to maintain the passive protective layer of the steel reinforcement [11, 171].

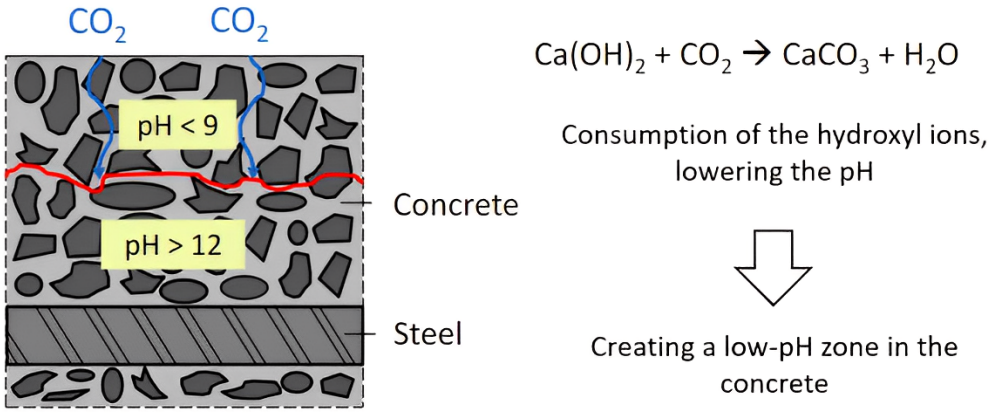

Figure 2.24: Mechanism of carbonation [18]

2.10 Influencing factors

In order to achieve a geopolymer concrete with a high compressive strength, source materials with a high reactivity are required. It is also important to consider the interactions between the source materials as well as the source materials themselves, the conditions they are in and other factors that influence the compressive strength [41]

2.10.1 Curing temperature

When concrete is cured at ambient temperature, the reaction of FA and other precursors is extremely slow. By initiating the curing process at elevated temperatures, the appropriate system chemistry is catalyzed, resulting in the formation of concrete. Curing the material at 70°C for the same amount of time resulted in better strength than curing at 30°C. However, curing at higher temperatures for longer periods of time may potentially affect the development of compressive strength. Another study examined the use of FA and MK in geopolymeric material. The sample that was heated at 60°C for 48 hours exhibited the highest compressive strength after 7 and 28 days. Curing at an elevated temperature can result in the higher compressive strength, as confirmed by other research. This is not the case for OPC based concrete. When cured at elevated temperatures, OPC exhibits expansion behavior and leads to cracking, resulting in loss of strength, reduced service life or other durability problems. It can be concluded that curing at higher temperatures is an effective method and plays a greater role in promoting the mechanism of geopolymerization [41, 173, 174].

2.10.2 Curing time

Research has shown that a longer curing time will enhance the polymerization process, resulting in an increase in compressive strength. However, strength gains from curing beyond 48 hours were not substantial. It is not uncommon for GPC to have a developed compressive strength of 45 MPa in just 24 hours, especially when cured at a higher temperature. Increasing the temperature favors the dissolution of reactive species, mainly GGBFS and FA, to the same extent. However, curing the geopolymer mixture at higher temperatures for longer periods of time can lead to a reduction in compressive strength

because it can disrupt the granular structure. Such disruptions result in dehydration and excessive shrinkage caused by contraction of the gel without transitioning to a more semi-crystalline form. It is noteworthy that the crystalline component of the geopolymer remains unaffected by longer curing times, which suggests that the changes that lead to differences in strength take place within the amorphous phase of the structure [41, 175].

2.10.3 Curing conditions

Research has proven that samples cured at higher humidity did not significantly improve strength. This behavior is contrary to what is expected from the curing of traditional cementitious products, cement-based products gain strength when cured at higher humidity. This behavior, measured in the research, is also supported by the infrared (IR) absorption peaks around 1033 cm^{-1}, corresponding to the asymmetric stretching of Si-O and Al-O bonds, which were affected by the curing of the samples in sealed bags. Their wave numbers were slightly lower than for the samples cured without bags. Lower wave numbers indicate weaker inter-tetrahedral bonding and could contribute to the lower strength of the samples cured in the sealed bags. The saturated atmosphere in the bags results in conditions more conducive to the formation of the slightly weaker bonds. Other studies on the compressive strength of metakaolin based geopolymers have shown that the best performance of geopolymerization for the development of a high compressive strength is when the value of relative humidity is 85%. [41, 173, 175].

2.10.4 PH

In general, the pH scale is a measure of the acidity or alkalinity of a solution. The pH scale ranges from 0 to 14, with a pH of 7 considered neutral. A pH below 7 indicates an acidic solution, while a pH above 7 indicates a basic (or alkaline) solution. Acids are substances that release hydrogen ions (H^+) into water, while bases are substances that release hydroxide ions (OH^-) into water. The concentration of these ions in a solution determines its pH. Solutions with a high concentration of H^+ ions have a low pH and are considered acidic, while solutions with a high concentration of OH^- ions have a high pH and are considered basic. The pH scale is logarithmic, meaning that a change of one pH unit corresponds to a tenfold change in the concentration of H^+ or OH^- ions. For example, a solution with a pH of 5 is ten times more acidic than a solution with a pH of 6 and 100 times more acidic than a solution with a pH of 7 [176].

The pH is the most important factor affecting the compressive strength of geopolymeric mixtures. When the pH of the activating solution is increased, the setting time of the concrete is shortened. At lower pH values, the geopolymeric mixture is thick and behaves like cement. At higher pH values, the mixture becomes more fluid and is easier to process. The strength of the geopolymer matrix with cement as the setting admixture is much higher at a pH of 14 than at a pH of 12 [41].

As the pH increases, there is a higher concentration of small chain oligomers and monomeric silicate that can react with soluble alumina. This leads to an increase in soluble alumina reacting with calcium available for reaction, thus increasing the strength. A lower pH of the solution results in a lower monomer concentration. The pH of the simple alkaline solution varies in concentration and type of alkali ions. From these observations, it appears that the pH range 13-13,5 is most suitable for the formation of geopolymers with better mechanical strength. A higher pH can indicate an increased risk of flash setting [11, 41].

2.10.5 Silicate and aluminium ratio

To achieve a strong interparticle bonding and physical strength in geopolymers, a significant amount of soluble silicate is required to synthesize the alumino-silicate binder. A higher amount of reactive silica promotes the formation of a greater amount of the alumino-silicate gel, resulting in the development of higher mechanical strength in the final product. A higher concentration of sodium silicate has also been found to be beneficial to the geopolymerization process of an MK/sand mix. As part of the research on the effects of the alkaline solution on the properties of geopolymer mortars, it was concluded that the compressive strength of the mortar is directly proportioned to the Si/Al ratio. A 10% increase in the Si/Al ratio resulted in a 20 to 40% increase in the strength of the geopolymer mortar after 3 days. However, the effect on strength after 28 days was less significant, with an increase of only 10 to 25% [41, 177].

2.10.6 Aluminium source

Geopolymer concretes containing clays, such as MK, were found to be the strongest in compressive strength tests, while FA alone lacked significant strength. A small amount of clay content is fully digested to participate in the geopolymerization reaction, whereas at larger additions, clay becomes partially reactive filler and serves to weaken the structure. Replacement with MK induced a decrease in mechanical strength during the first day, but an equal resistance after 28 days. More than 15% replacement induced a decrease in bond strength and compressive strength. MK increased the geopolymerization of FA as a secondary source of silicate and aluminum. This was explained by the fact that metakaolin tends to dissolve to a greater extent than FA. Due to the fineness of the MK grain, the consistency of the mix design is reduced. 5% MK results in a 14,6% decrease in consistency, while 15% results in a 34% decrease in consistency. Therefore, the optimum reactivity seems to be between 10 and 15% in terms of low workability, best mechanical performance and inhibiting effect on chloride diffusion and sulfate attack [41, 178].

2.10.7 Age of concrete

Research has shown that approximately 70% of the final compressive strength of geopolymer concrete is achieved within the first 4 hours of curing at an elevated temperature of 75°C. This is due to the fact that the chemical reaction involved in GPC is a rapid polymerization process. After curing the GPC for 24 hours, the compressive strength does not appear to vary with the age of the concrete. This is in contrast to traditional OPC-based concrete, where the hydration process takes place over a longer period of time, resulting in a gradual increase in strength over time [41, 179].

2.10.8 Impact of influencing factors on strength

Each mentioned factor plays a unique role in the development of the final product. In order to provide a thorough understanding of the influence of various factors on the measured strength of GPC, during the period of 1 day to 28 days, an extensive list has been made from published research studies. The list, presented in the table below, is categorized based on the most commonly used precursors. Each row represents a different sodium silicate solution (SSS) based mix design cured at a specified temperature.

Table 2.8: Early-strength development with various precursors and curing conditions

Mix information			Compressive strength [MPa]							
Precursor	Source	Curing temperature	1 d	2 d	3 d	4 d	7 d	14 d	21 d	28 d
CL[1], GGBFS	[68]	Ambient	3,1	11,0	-	-	33,8	-	-	44,6
			3,9	11,2	-	-	37,3	-	-	47,5
			2,6	8,2	-	-	32,3	-	-	48,5
			2,8	9,4	-	-	32,4	-	-	48,9
			2,7	9,2	-	-	32,2	-	-	45,5
			2,4	9,2	-	-	28,1	-	-	45,5
			2,8	11,2	-	-	34,8	-	-	44,4
			2,1	10,3	-	-	31,4	-	-	43,8
			2,0	4,3	-	-	18,0	-	-	37,9
			2,5	7,4	-	-	32,7	-	-	46,3
			3,9	15,6	-	-	40,0	-	-	54,3
			3,1	10,6	-	-	39,2	-	-	50,6
			2,2	5,1	-	-	23,4	-	-	44,6
			3,0	14,8	-	-	35,1	-	-	49,2
			-	17,1	-	-	29,3	-	-	38,2
			-	3,7	-	-	12,0	-	-	26,5
FA	[180]	Ambient	38,4	-	-	-	-	-	-	-
			41,4	-	-	-	-	-	-	-
			40,0	-	-	-	-	-	-	-
	[181]	Ambient	26,7	-	-	-	-	-	-	-
	[182]	Ambient	41,7	-	-	-	-	-	-	-
	[183]	Ambient	41,1	-	-	-	-	-	-	-
	[184]	Ambient	47,0	-	-	-	-	-	-	-
			39,0	-	-	-	-	-	-	-
	[180]	60°C	68,0	-	-	-	-	-	-	-
			63,0	-	-	-	-	-	-	-
			45,0	-	-	-	-	-	-	-
			44,0	-	-	-	-	-	-	-
			36,0	-	-	-	-	-	-	-
		30°C	35,0		-	-	-	-	-	-
	[185]	Ambient	-	-	28,6	-	-	-	-	
	[157]	Ambient	-	-	-	-	40,2	71,6	-	75,3
			-	-	-	-	44,7	67,3	-	73,0
			-	-	-	-	44,0	56,0	-	56,6
	[186]	Ambient	-	-	-	-	28,0	-	-	55,3
	[187]	75°C	-	-	-	-	10,5	-	-	31,1
		Ambient	-	-	-	-	4,5	-	-	10,0
	[188]	Unknown	-	-	-	-	11,8	-	-	13,5
	[189]	70°C	32,22	-	32,9	-	33,5	-	-	-
FA, GGBFS	[190]	Ambient	-	-	39,9	-	45,3	-	-	49,0
			-	-	34,0	-	42,7	-	-	46,3
			-	-	26,6	-	31,5	-	-	33,4

Continued on next page

Table 2.8: *(Continued)* Early-strength development with various precursors and curing conditions

Mix information			Compressive strength [MPa]							
Precursor	Source	Curing temperature	1 d	2 d	3 d	4 d	7 d	14 d	21 d	28 d
FA, GGBFS	[190]	Ambient	-	-	46,3	-	42,7	-	-	57,2
			-	-	34,0	-	42,7	-	-	46,3
			-	-	29,5	-	32,0	-	-	34,2
	[191]	80°C	-	70,9	71,4	72,1	73,2	72,5	73,8	74,3
	[186]	Ambient	10,5	-	25,5	-	37,0	-	-	63,1
FA, GGBFS, MK	[188]	Unknown	-	-	-	-	12,5	-	-	18,9
			-	-	-	-	14,8	-	-	21,3
			-	-	-	-	16,7	-	-	26,4
			-	-	-	-	18,6	-	-	29,8
			-	-	-	-	22,8	-	-	35,7
			-	-	-	-	21,5	-	-	33,6
FA, WWA[2]	[159]	Ambient	-	-	21,7	-	29,0	-	-	38,9
	[162]	70°C	38,2	-	38,4	-	39,5	-	-	-
			40,7	-	46,8	-	47,1	-	-	-
			43,7	-	45,0	-	45,1	-	-	-
			41,7	-	42,0	-	42,0	-	-	-
			47,6	-	48,1	-	48,5	-	-	-
			40,0	-	39,0	-	39,5	-	-	-
GGBFS	[163]	60°C	-	-	7,6	-	39,5	-	-	42,2
			-	-	3,9	-	18,6	-	-	33,2
	[192]	Ambient	-	-	-	-	13,6	-	38,7	39,4
			-	-	-	-	16,1	-	41,2	42,9
	[107]	Ambient	4,0	-	23,0	-	34,0	-	-	38,0
GGBFS, MBS[3]	[193]	Ambient	-	-	36,3	-	41,4	-	-	47,4
			-	-	42,1	-	50,4	-	-	55,3
			-	-	32,0	-	39,8	-	-	52,1
			-	-	9,1	-	11,7	-	-	19,6
			-	-	38,2	-	43,9	-	-	52,7
			-	-	41,9	-	45,8	-	-	53,5
			-	-	36,8	-	43,9	-	-	52,8
			-	-	15,7	-	20,2	-	-	25,5
			-	-	41,5	-	45,3	-	-	51,3
			-	-	44,0	-	47,6	-	-	53,0
			-	-	32,5	-	41,1	-	-	47,9
			-	-	17,7	-	25,6	-	-	29,9
GGBFS, MK	[107]	Ambient	7,0	-	26,0	-	36,0	-	-	41,0
			9,0	-	28,0	-	39,0	-	-	43,0
			10,0	-	32,0	-	41,0	-	-	46,0
			11,0	-	35,0	-	42,0	-	-	47,0
			14,0	-	37,0		45,0	-	-	52,0
	[116]	Ambient	-	-	1,6	-	2,1	-	-	2,8

Continued on next page

Table 2.8: *(Continued)* Early-strength development with various precursors and curing conditions

Mix information			Compressive strength [MPa]							
Precursor	Source	Curing temperature	1 d	2 d	3 d	4 d	7 d	14 d	21 d	28 d
GGBFS, MK	[116]	Ambient	-	-	1,7	-	1,7	-	-	2,5
			-	-	1,3	-	1,6	-	-	2,1
			-	-	0,3	-	0,6	-	-	1,9
			-	-	1,5	-	1,8	-	-	2,7
			-	-	16,9	-	17,6	-	-	20,1
			-	-	14,5	-	15,8	-	-	15,8
			-	-	18,4	-	19,1	-	-	21,2
			-	-	40,4	-	41,0	-	-	41,6
	[194]	80°C	-	-	60,1	-	64,8	-	-	70,5
			-	-	62,4	-	66,8	-	-	73,6
			-	-	63,0	-	66,9	-	-	75,3
			-	-	63,4	-	68,0	-	-	76,8
			-	-	61,2	-	65,4	-	-	74,7
	[108]	Ambient	-	-	-	-	-	-	-	52,7
			-	-	-	-	-	-	-	49,6
			-	-	-	-	-	-	-	51,1
			-	-	-	-	-	-	-	47,1
			-	-	-	-	-	-	-	56,3
			-	-	-	-	-	-	-	51,1
			-	-	-	-	-	-	-	50,7
			-	-	-	-	-	-	-	52,5
			-	-	-	-	-	-	-	56,0
			-	-	-	-	-	-	-	52,8
			-	-	-	-	-	-	-	54,8
			-	-	-	-	-	-	-	55,5
			-	-	-	-	-	-	-	57,5
			-	-	-	-	-	-	-	58,1
	[192]	Ambient	-	-	-	-	9,5	-	13,6	24,7
			-	-	-	-	10,4	-	24,9	32,8
GGBFS, MK, RHA[4]	[192]	Ambient	-	-	-	-	8,2	-	11,5	18,6
			-	-	-	-	9,7	-	15,7	33,8
MK	[195]	Ambient	19,3	-	28,5	-	-	-	-	-
	[107]	Ambient	12,0	-	32,0	-	37,0	-	-	46,0

[1] CL = Clinker

[2] WWA = Waste wood ash

[3] MBS = Micronized biomass silica

[4] RHA = Rice husk ash

Part II

Research

3

Methods of analysing

Analysis is an important process in various fields, including science and engineering and manufacturing. It involves examining a sample to determine its composition, properties, etc. There are various methods, each with its strengths and limitations. In this chapter, some common methods for analyzing samples are presented. Understanding these methods, it is possible to gain valuable insight into the properties and behaviour of materials, which helps to make informed decisions and improve processes.

3.1 Resources

Geopolymer concrete uses waste or industrial by-products as resource materials. It is critical to analyze the chemical and physical properties of the material. Neglecting the actual properties of the used resources in the mix design can greatly affect the final product, highlighting the importance of resource analysis.

3.1.1 Particle size analysis

Accurate determination of particle size is essential for predicting product performance, quality and behaviour. There are several methods for measuring particle or grain size, including the sieving method, the Blaine method and the laser diffraction method (LDM).

Sieving method

The sieving method is commonly used to determine the size distribution of grains. It involves passing a sample of the material through a series of sieves with progressively smaller openings. The grains that are too large to fit through the openings are left on the sieve, while the ones that are small enough to pass are collected. Those left on the sieves are weighted and the results are used to calculate the size distribution of the grains. The sieving method is standardized in the EN 933-1 norm and the used instrument is shown in Figure 3.1a [196]. The following sieves are used: 2 mm - 1 mm - 0,5 mm - 0,25 mm - 0,125 mm - 0,063 mm.

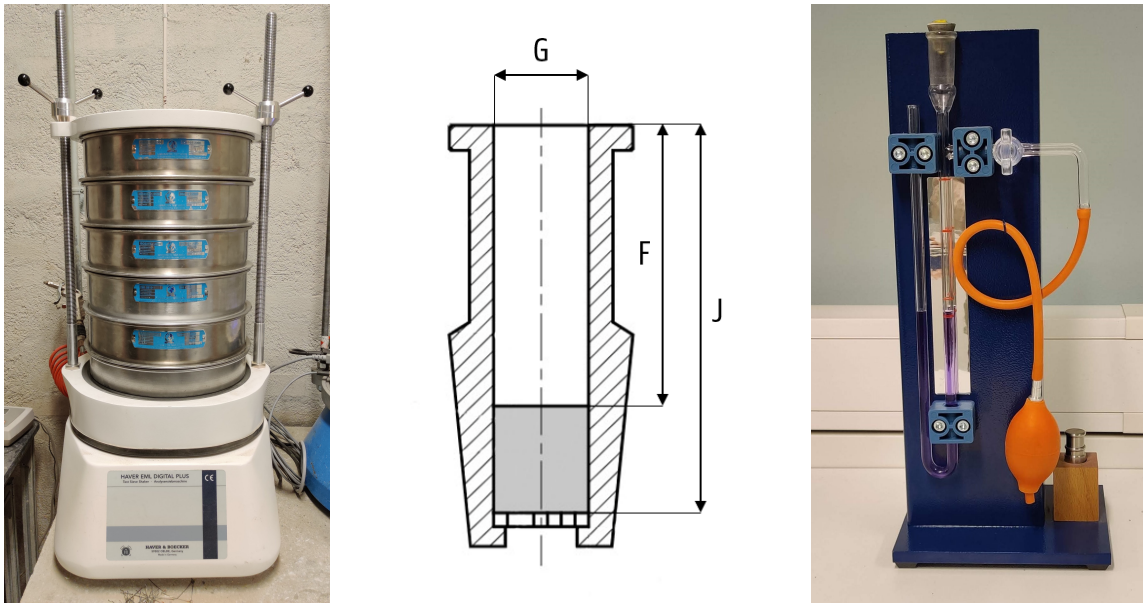

(a) (b) (c)

Figure 3.1: Sieving instrument (a); Blaine apparatus cell (b); Blaine air permeability apparatus (c)

Blaine method

The Blaine method is used to determine the specific surface area of powders. It involves measuring the time it takes for air to pass through a compacted material sample. The Blaine method is based on the principle that the specific surface area of a powder is inversely proportional to the time it takes for air to flow through the sample. The greater the specific surface area, the longer it takes for the air to flow through the sample. This method is used in the cement industry to determine cement fineness. It is relatively simple and inexpensive, making it popular in industries that need a quick and easy method to determine the specific surface area of a sample [197]. The Blaine method is standardized in the EN 196-6 norm and shown in Figure 3.1c [196].

Calculations towards specific surface area

Some calculations are necessary to determine the specific surface area of a sample using the Blaine method. The first step involves obtaining the K value, the apparatus constant. The determination of this K is different for each apparatus and setup, it is achieved by using a standardized reference material. To calculate the K value, the total volume of the bed, V, is required. The volume, in cm^3, can be determined based on Figure 3.1b using the following formula:

$$V = (J - F).(\frac{G}{2})^2.\pi \tag{3.1}$$

With:

J	Total height inside cell [cm]
F	Remainder height in cell [cm]
G	Diameter cell [cm]

With a known density of the resource material and assuming a porosity of 0,5 for the bed (e), the total needed mass of the reference sample is calculated.

$$m_i = (1 - e).\rho.V \tag{3.2}$$

With:

e	Porosity of the bed [-]
ρ	Density of material [g/cm³]
V	Volume of the bed [cm³]

For the computation of the K value, the Blaine test is performed with the mass calculated in Formula 3.2. Out of three repetitions, the average flow time t_0 and average air viscosity η_o is calculated and used as input for Formula 3.3. The air viscosity can be determined using the standard EN 196-6. Together with the other known values, the K value can be determined.

$$K = S_0.\rho_0.\frac{(1 - e)}{\sqrt{e^3}}.\frac{\sqrt{10.\eta_0}}{\sqrt{t_0}} \tag{3.3}$$

With:

S_0	Specific surface area of reference material [cm²/g]
ρ_o	Density of reference material [g/cm³]
t_0	Mean of 3 flow times [s]
η_o	Mean of 3 air viscosities [Pa.s]

After calculating the K value of the apparatus, the testing of the samples can start. Formula 3.2 must be used to calculate the porosity for each sample. To determine the specific surface area of the sample material, the previously found K value should be used in the next formula together with the measured flowtime and air viscosity.

$$S_i = \frac{K}{\rho}.\frac{\sqrt{e^3}}{(1 - e)}.\frac{\sqrt{t}}{\sqrt{10.\eta}} \tag{3.4}$$

With:

S	Specific surface area of resource material [cm²/g]
K	Apparatus constant [-]
η	Air viscosity at operating temperature [-]
t	Recorded flowtime [s]

The Blaine test towards the calculation of the specific surface area is performed three times, each with a new sample. The average of the three values is computed using the following formula and can be rounded to the closed 10 cm²/g according to the standard EN 196-6.

$$S = \frac{S_1 + S_2 + S_3}{3} \tag{3.5}$$

Laser diffraction method

Laser diffraction can accurately determine the size distribution of particles in the sample. It uses a laser beam to study the diffraction pattern produced by particles in a given sample. The analysis of the scattering pattern generated by the laser beam is influenced by both Fraunhofer and Mie's theories. A schematic representation of this concept is shown in Figure 3.2 [19].

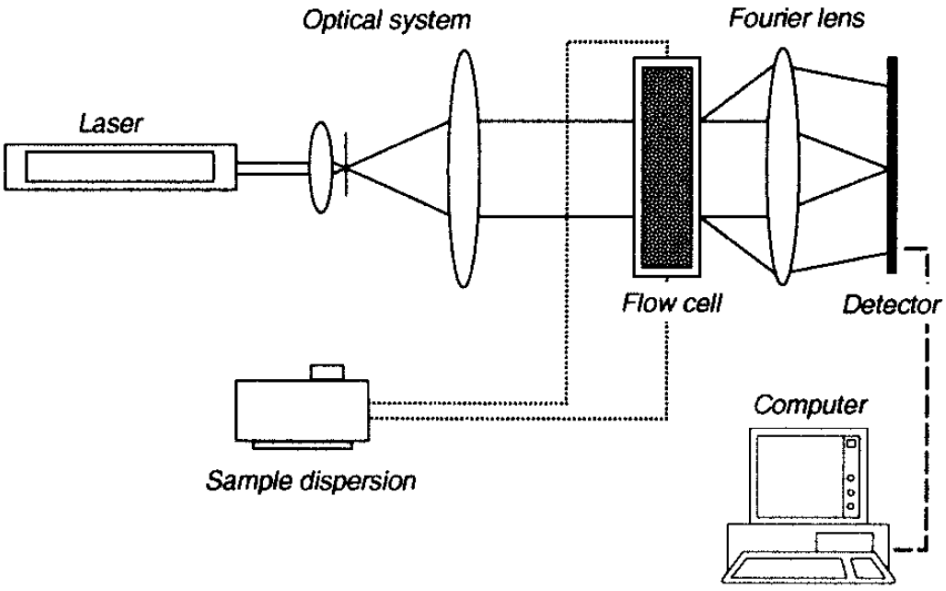

Figure 3.2: Schematic overview of a laser diffraction spectrometry instrument [19]

It is important to consider input values such as the refractive index and absorption index. These indices have a significant impact on the result. The standard ISO 13320: 2020 has standardized the laser diffraction method. There are two different methods that can be used, the wet and dry method, in this research the wet method is used [19].

Some modern laser diffraction spectrometry instruments (e.g. Malvern Mastersizer 3000) allow optimization of the refractive index (n_d) and the absorption index (k). First, the test is run with an estimated value for n_d and k, the results are used to optimise these indices. In Table 3.1 the estimated values are collected together with the source of information.

Table 3.1: Estimated indices laser diffraction spectrometry

Precursor	$n_{d,est.}$	Source	$k_{est.}$	Source
MK	1,53 - 1,65	[198]	0,100	[198]
GGBFS	1,60 - 1,70	[199, 200]	0,100 - 1,000	[198, 201]
WWA	1,50 - 1,73	[198, 199, 202]	0,003 - 1,000	[198, 199, 201]

3.1.2 Density

One of the methods of measuring density is by using a pycnometer, which is a glass container with a precisely known volume and a ground glass stopper to seal the container. The used pycnometers have a known volume of 500 ml. The procedure for using a pycnometer to measure density is described in the standard EN ISO 1675 and EN 1097-6. The pycnometer is first filled with a known mass of the sample of the solution. After which the mass of the filled pycnometer, with the sample, is measured. Then the pycnometer is emptied, filled with a known volume of a liquid that is denser than the sample, and then the mass of the pycnometer filled with the liquid is measured. The density of the sample can then be calculated using the following formulas depending if the density of a liquid (3.6) or a powder (3.7) is measured. The density ranges found in literature for the materials (SS, MK, GGBFS and seawater (SW)) are listed in Table 3.2, along with the cited sources.

$$\rho_{\text{liquid}} = \frac{m_1 - m_0}{V} + \rho_a = \frac{(m_1 - m_0).(\rho_e - \rho_a)}{(m_2 - m_0)} + \rho_a \tag{3.6}$$

$$\rho_{\text{powder}} = \rho_e \frac{m_p}{m_p - (m_1 - m_2)} \tag{3.7}$$

With:

m_p	Mass of powder [g]
m_0	Mass of empty pycnometer [g]
m_1	Mass of filled pycnometer[g]
m_2	Mass of filled pycnometer with distilled water [g]
ρ_a	Density of air (air buoyancy correction) [g/ml]
ρ_e	Density of distilled water [g/ml]
V	Volume of the pycnometer [ml]

Table 3.2: Overview range of density values found in literature

Resource	$\rho_{lit.}$[g/cm³]	Source
SS	1,34	[203]
MK	2,60	[C.2]
GGBFS	2,80 - 3,00	[C.4, C.3]
SW	1,02 - 1,03	[137, 204]

3.1.3 PH

From the different methods available to determine the pH of materials, the first technique involves using pH test strips. These are small pieces of paper or plastic with pH-sensitive coatings. When in contact with the solution these compounds change color. The pH is determined using a color chart. Using an pH electrode is a more accurate way to determine the pH. The device measures how well the solution conducts an electric current [205]. Since most of the materials regarding GPC are insoluble in water, measuring the pH directly would give incorrect results. A method is deviated from standard operating procedures for soil pH determination. Since soil is also insoluble, the described methods can be adapted for the materials in this research, allowing for a more correct determination of the pH. For the measurement of a sample of 10 g is added to 25

ml of water. The material-water mixture needs to be stirred for 60 minutes until complete homogenization. After this, the mixture needs to rest for 60 minutes and before taking the pH measurement the suspension needs to be stirred again for 10 seconds. The pH ranges found in literature for the various materials are listed in Table 3.3, along with the cited sources.

Table 3.3: Overview range of pH values found in literature

Resource	$pH_{lit.}$	Source
SS	9,00 - 11,56	[206]
MK	6,00 - 7,00	[11]
GGBFS	8,00 - 12,50	[C.4], [11]
WWA	2,00 - 14,00	[207, 208]
GPC	11,50 - 12,50	[11]
SW	7,50 - 8,40	[137, 204]

3.1.4 Chemical composition

It is important to know the chemical composition of the resource materials used in geopolymer concrete because the properties and performance of the final product depend on the chemical reactions that occur during its formation. Analysis of the chemical composition of the waste and industrial by-products used in geopolymer concrete can provide useful knowledge into the performance of the resulting concrete. The amount of alumino-silicates present in the resources can have a big impact on the strength and durability of the concrete, while the presence of contaminants such as heavy metals can pose health and environmental hazards [209, 210]

X-ray fluorescence spectroscopy

X-ray fluorescence is an analytical technique used to non-destructively determine the elemental composition of materials. In this technique, atoms are brought to an excited state by high-energy radiation that ejects electrons from their innermost orbitals. As the atoms relax and the outer electrons fix the unstable state, filling the inner shells, they emit XRF radiation. The radiation emitted by the XRF process can be interpreted as a unique atomic signature. As an illustration, the fluorescence of copper looks very different from the fluorescence of zinc, as well as from the fluorescence of any other element in the periodic table. As a result, XRF is one of the simplest and most convenient methods for elemental analysis and is used in a wide range of applications. The data obtained through XRF can be used to extract qualitative, semi-quantitative, and quantitative information about the major, minor and even trace elements present in a sample [20, 211].

The X-ray fluorescence process, illustrated in Figure 3.3, begins by irradiating a solid or liquid sample with high energy X-rays emitted from a controlled X-ray tube. As the sample is irradiated by these X-rays, atoms within the sample are struck by an X-ray of sufficient energy, typically greater than the atom's K- or L-shell binding energy, to cause an electron to be released from one of the atom's inner orbital shells. To regain stability, the atom fills the vacancy left in the inner orbital shell with an electron from one of its higher energy orbital shells. Doing so, the electron drops to a lower energy state, releasing a fluorescent X-ray with an energy equal to the specific difference in energy between two quantum states of the electron [211].

Every XRF instrument available today contains an X-ray tube to excite the atoms in the sample and a detector to register the fluorescent radiation. The tubes can be water-cooled high-power tubes with 4000 W output, or tiny thumb-sized 4 W

tubes for mobile devices. On the detection side, there are basically two different technologies: energy dispersive (EDXRF) or wavelength dispersive (WDXRF). Although the energy E of a photon and its wavelength λ are virtually interchangeable due to Planck's relation (Formula 3.8), the way the photons are sorted with respect to either E or λ is quite different [20, 211].

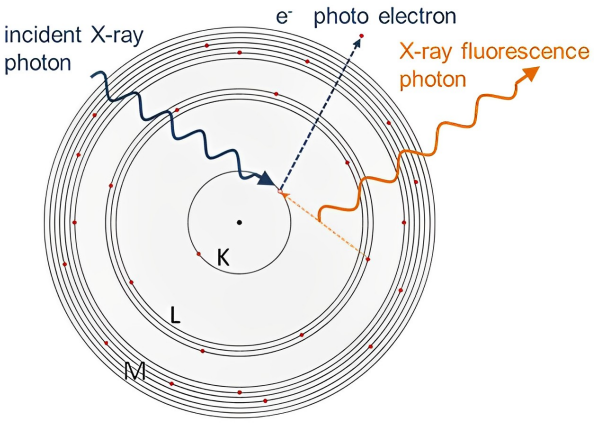

Figure 3.3: Schematic overview of the X-ray fluorescence (XRF) process [20]

$$E = \frac{c.h}{\lambda} \tag{3.8}$$

With:

E	Energy of a photon [J]
c	Speed of light in vacuum; $2{,}99792.10^{8}$ [$m.s^{-1}$]
h	Planck constant; $6{,}62607.10^{-34}$ [J.s]
λ	Wavelength [m]

A WDXRF spectrometer treats the X-rays as waves and uses some regular structure to create interference patterns that allow remarkably high spectral resolution. EDXRF detectors treat X-rays as particles. By analogy, the process can be compared to throwing bowling balls (represented by the photons) into a ball pit (the detector) to observe the number of small plastic balls (the electrons) discharged by each collision. The higher the energy of the bowling ball (heavier or faster), the greater the number of plastic balls emitted [20].

Handheld-XRF spectrometers, the smallest possible, is small enough to be run on batteries and carried in one hand. Nevertheless, it can still do a full positive material identification within seconds. A handheld-XRF, shown in Figure 3.4, has the same components as a larger EDXRF instrument but packed into a much smaller volume. Despite of the smaller size, these instruments are very accurate and can detect all elements starting from magnesium. This implies that some of the common elements found in a sample, such as hydrogen, carbon, oxygen, nitrogen and sodium, will not be detected. That's because the tube and the detector, due to the configuration of the handheld-XRF analyzer, are very close to the sample [20, 21].

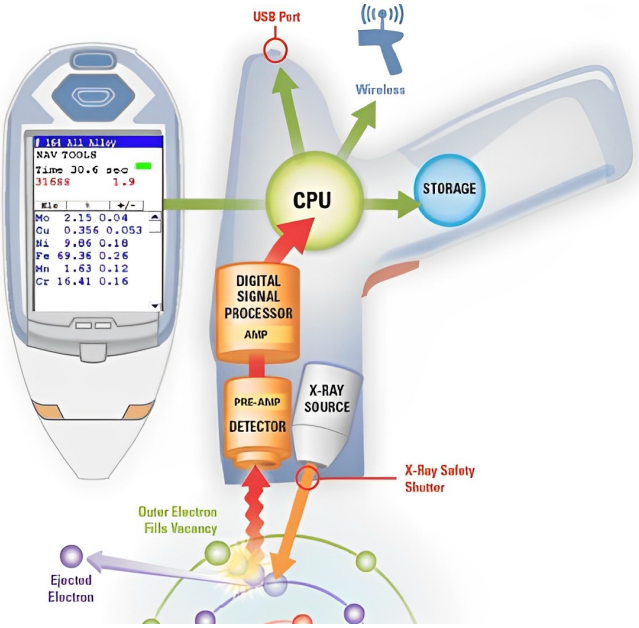

Figure 3.4: Handheld XRF-analyzer and its basic function [21]

Calculations towards an oxide composition

As mentioned earlier, XRF spectroscopy is used to determine the elemental composition of materials. A handheld XRF allows for a quick analysis of the sample, but due to its configuration it cannot detect elements below magnesium (this includes oxygen and other common elements). Since materials are usually composed of oxide compounds, due to their more stable configuration, it is more convenient to analyze and compare the chemical composition according to their oxide based composition. This requires converting the element mass percent ($\%m_{element}$) to an oxide mass percent ($\%m_{oxide}$), as shown in the expression below [21, 212, 213].

$$\%m_{element} \longrightarrow \%m_{oxide} \tag{3.9}$$

Since $\%m_{oxide}$ is the desired output and $\%m_{element}$ is given through the handheld-XRF spectrometer, an expression needs to be formulated between the two using a conversion factor (CF).

$$\%m_{oxide} = CF.\%m_{element} \tag{3.10}$$

Previous formula is adapted for notation purpose and to avoid differences in terminology. Adapted Formula 3.11 relies on the following notation, element A and oxide compound A_nO_m.

$$\%m_{A_nO_m} = CF.\%m_A \tag{3.11}$$

With:

CF	Conversion factor
$\%m_A$	Element mass percent
$\%m_{A_nO_m}$	Oxide mass percent

For the determination of the conversion factor (CF), the oxide compound gets divided into two imaginary parts. These being $\%_{Cation}$ and $\%_{Oxygen}$, respectively accounting for the mass of the cation and oxygen atoms in the oxide compound. The sum of the two should always be 100% when calculated according to Formula 3.12 and 3.13.

$$\%_{Cation} = \frac{n.MM_A}{n.MM_A + m.MM_O} = \frac{n.MM_A}{MM_{A_nO_m}} \tag{3.12}$$

$$\%_{Oxygen} = \frac{m.MM_O}{n.MM_A + m.MM_O} = \frac{m.MM_O}{MM_{A_nO_m}} \tag{3.13}$$

With:

n	Number of element A atoms in oxide compound
m	Number of oxygen atoms in oxide compound
MM_A	Molar mass element A
$MM_{A_nO_m}$	Molar mass oxide compound

The mass percent of the element, $\%m_A$, detected by the XRF spectrometer only accounts for the $\%_{Cation}$ part of the oxide compound. Based on the mathematical relationship between percentages and inverse percentages, a division of $\%m_A$ by $\%_{Cation}$ gives the mass percentage of the oxide compound, $\%m_{A_nO_m}$, resulting in a CF that can be calculated according to Formula 3.14:

$$CF = \frac{1}{\%_{Cation}} = \frac{MM_{A_nO_m}}{n.MM_A} \tag{3.14}$$

Applying the conversion factor to the initial Formula 3.11, gives a direct relation between $\%m_A$ and $\%m_{A_nO_m}$. Formula 3.15 allows for a computation from the output of a handheld-XRF spectrometer towards the chemical composition of a material in a stable oxide state.

$$\%m_{A_nO_m} = \frac{MM_{A_nO_m}}{n.MM_A}.\%m_A \tag{3.15}$$

3.2 Geopolymer concrete

Analysis of the geopolymer concrete is important to gain valuable insight into the early-age evolution of various parameters as a function of curing time. Samples are tested for compressive and flexural strength, density and others to analyze these early-age parameters of geopolymers, while also looking at the changes that occur in the mineralogy and microstructure of the concrete samples.

3.2.1 Workability

The workability of fresh concrete is an important factor in determining its suitability, as previously discussed in 2.7.1. The standardised test is performed according to the standard EN 1015-3:1999, to evaluate the workability of concrete. This standardised flowtable test, uses the Haegermann cone. With this method, the workability of fresh concrete can be measured accurately, and the results can be compared to ensure consistency and quality.

3.2.2 Density

Measuring the density of GPC is a good way of analyzing the curing of a concrete mix. As briefly discussed in Sections 2.4 and 2.5.4, it is known that the water present in the fresh concrete evaporates at some stage of the geopolymerization process. Information on the evolution of the mix during this process can be obtained from the measured density. Although the principle of measuring the densities is similar, a distinction must be made between fresh and hardened concrete.

The density of fresh concrete is tested according to the European standard EN 12350-6. It relies on the principle of a density container, while in this research a recipient with a known volume and mass is used instead. The recipient gets filled in as many layers as needed to achieve full compaction. The concrete needs to be compacted with each layer, either with a vibrating table or with a compacting rod. After full compaction, the filled recipient gets weighed and the density of the fresh concrete can be determined by the difference in mass [kg] divided by the known volume [m^3].

European standard EN 12390-7 describes testing the density of hardened concrete. The hardened geopolymer samples will be tested according to this standard. There are different possible procedures for determination of the density, in this research the weighed mass of the samples will be divided by the volume, calculated by using actual measurements.

3.2.3 Strength of samples

The strength of a material is an important property that needs to be accurately determined for various applications. To achieve this, different test methods are used for different types of strength, such as compressive strength and flexural strength. These tests are performed according the standard (EN 196-1:2016) to ensure consistent and reliable results. Comparison of the results of these tests is necessary to understand the overall strength properties of the material. By using different test methods and comparing the results, a better understanding of the strength properties of a material can be gained and make reasoned decisions about its use in various applications [196].

3.2.4 Mineralogy and microstructure

Geopolymer concrete has a mineralogy consisting of amorphous and crystalline phases, including C-S-H and geopolymer gel formed by polycondensation. Its microstructure is porous with interconnected gel and capillary pores that contribute to its unique mechanical and durability properties. X-ray diffraction is one of the techniques available to evaluate mineralogy and microstructure during geopolymer development.

X-ray diffraction analysis

X-ray diffraction is a broadly applicable, non-destructive analytical technique that is used to analyze physical properties such as phase composition and quantification, crystallographic structure, phase purity, unit cell dimensions and so much more of powder, solid and liquid samples. XRD works by exposing a sample of material with incident X-rays and then measuring the intensities and scattering angles of the X-rays leaving the sample. The intensity of the scattered X-rays then is plotted as a function of the scattering angle, giving the typical XRD patterns. By analyzing the location and intensity of the scattered intensity peaks, the structure of the sample can be determined [22, 214].

As the beam passes through the sample, it collides with an atom in the structure, bouncing off and changing direction at a different angle θ as opposed to the original beam, illustrated in Figure 3.5. Some of these diffracted beams will cancel each

other out, but if they have similar wavelengths, constructive interference will occur. Constructive interference occurs when the X-ray beams, which are whole number integers of the same wavelength, are added to create a new one with a higher amplitude. A greater amplitude of the wave translates into a more intense signal for that particular diffraction angle. That angle can be used to determine the distance between the atomic planes using Bragg's Law:

$$2d \sin \theta = n\lambda \tag{3.16}$$

With:

d	Distance between atomic plates [Å]
θ	Diffraction angle [°]
n	Whole number integer [-]
λ	Wavelength of beam [m]

The distance between atomic plates can then be used to determine the composition or crystalline structure of the sample. X-rays are used because their wavelength resembles the spacing between the atoms in the sample. Thus the diffraction angle is affected by the distance between atomic plates in the molecule. When using much larger wavelengths, they would not be affected by the distance [22, 214, 215].

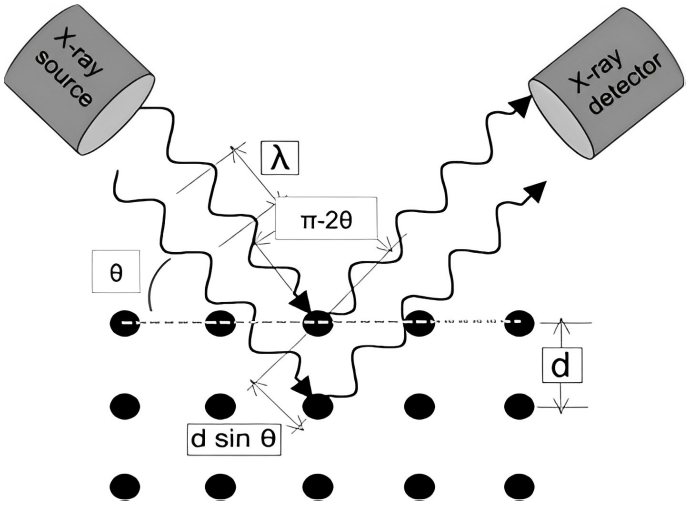

Figure 3.5: Schematic illustration of Bragg's Law applied to XRD [22]

A typical result of X-ray diffraction was previously shown in Figure 2.13, it plots the intensity of the beams for various diffraction angles at their respective 2θ positions. The 2θ positions, for powders typically varies from 5° to 70°, correspond to a certain spacing between the atoms in the samples. The intensity of the peaks reflects the number of atoms or crystals in that phase or at that particular spacing. As the intensity of the peak increases, so does the number of crystals with that particular spacing. The width of the peaks is indirectly proportional to the size of the crystal. A thinner peak corresponds to a larger crystal. A broader peak means that there may be a smaller crystal, a defect in the crystalline structure, or that the sample is amorphous. For smaller samples, the patterns determined by XRD analysis can be used to determine the chemical composition [22, 215].

There is a large database available of elements, compounds, and minerals that contains their diffraction patterns. The pattern for an unknown compound can be compared to literature and experimentally determined values to verify the identification of an element or compound. This is done by matching the position, width and relative heights of the diffraction patterns [22, 214, 215].

Proper sample preparation is critical to obtaining high-quality XRD data. Failure to do so can result in errors that can make it difficult or impossible to identify the phases and lead to incorrect results. There are a number of conditions that must be met to ensure good data, but the best approach is to use fine powdered samples. There are numerous methods to grind the samples into powder, but hand grinding by using a mortar and pestle is usually used the most [216].

4

Quantification of resources

The chemical and physical properties of the resources are examined in this chapter. This is necessary to obtain an accurate and complete picture of the used materials. When examining chemical properties, various factors such as chemical composition, mineralogy and pH are taken into account. For the physical properties, density, specific surface area and particle size distribution are being studied.

4.1 Overview resources

The production of geopolymer concrete requires precursors, a silicate solution, aggregates and, if necessary, additional water. Among the precursors analysed, the first group consists of metakaolin, the second group includes various types of ground granulated blast-furnace slag and the third group includes waste or industrial by-products researched as alternative precursors for geopolymer applications. The last group consists of waste wood ash and steel grit. The used seawater and sodium silicate solution undergo analysis. Additional information about the resources can be derived from the available technical data sheets in Appendix C.

4.2 Precursor analysis

X-ray fluorescence is used to determine chemical composition, while X-ray diffraction is used to analyze mineralogy. Both techniques are discussed in Sections 3.1.4 and 3.2.4 respectively. Two methods, standard and non-standard, are used to determine the pH of the resources. These methods are performed as described in Section 3.1.3.

4.2.1 Chemical composition

Table 4.1 presents the oxide composition of the resources identified by handheld-XRF. Values are expressed as weight percent and are the result of 10 x 1 minute XRF analyses. As mentioned in Section 3.1.4, a handheld-XRF spectrometer has its limitations. Due to the configuration of the handheld-XRF analyzer, the tube and detector are very close to the sample. Consequently, only elements starting from magnesium can be detected. The chemical composition cannot be expressed directly in terms of oxides because the spectrometer does not detect oxygen. A conversion is required to express the handheld-XRF results in oxide notation. Based on chemical compositions found in the literature, there should be Na_2O in the resources, but the atomic weight of sodium is lower than magnesium, so it cannot be detected by a handheld-XRF spectrometer.

Table 4.1: Chemical composition of the resources [wt. -%]

Precursor ID	SiO_2	Al_2O_3	Fe_2O_3	CaO	MgO	K_2O
MK 1	53,39 ± 0,26	29,75 ± 0,28	4,79 ± 0,21	0,96 ± 0,17	-	0,67 ± 0,03
MK 2	53,09 ± 0,20	29,89 ± 0,41	4,80 ± 0,22	0,83 ± 0,01	-	0,75 ± 0,07
MK 3	52,88 ± 0,11	32,03 ± 0,15	4,42 ± 0,17	0,37 ± 0,01	-	0,45 ± 0,02
GGBFS 1	24,70 ± 0,19	5,86 ± 0,09	0,87 ± 0,03	52,46 ± 0,46	4,74 ± 0,36	0,68 ± 0,01
GGBFS 2	25,41 ± 0,37	6,38 ± 0,24	0,84 ± 0,02	50,81 ± 0,80	5,49 ± 0,30	0,66 ± 0,02
GGBFS 3	23,77 ± 0,78	6,63 ± 0,18	0,74 ± 0,05	51,15 ± 0,67	5,18 ± 0,31	0,88 ± 0,14
GGBFS 4	22,83 ± 0,27	5,98 ± 0,20	0,89 ± 0,02	52,93 ± 0,55	5,08 ± 0,31	0,88 ± 0,01
GGBFS 5	23,93 ± 0,40	7,15 ± 0,32	0,79 ± 0,02	50,00 ± 1,08	6,03 ± 0,10	0,90 ± 0,01
GGBFS 6	24,97 ± 0,04	6,65 ± 0,06	0,74 ± 0,02	48,02 ± 0,10	6,14 ± 0,15	1,13 ± 0,01
SG 1	26,18 ± 0,99	2,51 ± 0,04	53,22 ± 1,64	3,92 ± 0,20	4,60 ± 0,34	1,03 ± 0,03
WWA 1[1]	3,86 ± 0,13	1,04 ± 0,08	6,66 ± 0,27	36,95 ± 0,49	2,13 ± 0,56	3,91 ± 0,03
WWA 2[1]	3,79 ± 0,06	1,31 ± 0,04	2,30 ± 0,05	49,95 ± 0,34	3,51 ± 0,47	17,04 ± 0,12

[1] Heavy metals detected by XRF

Table 4.1 shows the chemical compositions derived from the conversion of the handheld XRF data from elements to oxides. The original elemental composition and calculations to oxide composition are provided in Appendix F. Despite the difference between the chemical composition of the metakaolin samples and the composition shown in the technical data sheet (Appendix C.2). They are consistent with the average composition reported in the literature, with a total weight percentage of about 80% for SiO_2 and Al_2O_3 with a little higher SiO_2/Al_2O_3 mass ratio of almost 1,80.

Throughout the samples of GGBFS from different manufacturers and batches, the chemical composition does not vary much. They consist mainly of CaO, SiO_2, Fe_2O_3 and Al_2O_3, the sum of which is close to 85% of the total weight. That total is slightly lower than reported in the literature, partly because both the detected SiO_2 and Al_2O_3 are lower than the minimum value found in literature.

The chemical composition of steelgrit mainly (± 80 wt.-%) consists of SiO_2 and Fe_2O_3. Not unusual since it is a waste product originating from sandblasting structures to remove paint and rust. The chemical composition has a low Al_2O_3 and CaO content, making it unlike MK and GGBFS.

As reported in the literature, the chemical composition of WWA contains a variety of elements in a wide range of possible compositions. It depends on the source of the waste wood that is burned, the process by which it is burned and how the ash is collected, etc. Based on the detected composition both waste wood ashes are not fully suitable as a precursors. The low SiO_2 and Al_2O_3 content makes them inefficient since a lot more ashes would be needed to achieve the same amounts of SiO_2 and Al_2O_3. However, as they are slightly similar to the chemical composition of GGBFS, they may have the potential to (partially) replace ground granulated blast-furnace slag, but this need to be confirmed by the other parameters.

4.2.2 Mineralogy

X-ray diffraction analysis was used to determine the minerals or phases that are present in the samples. Figure 4.1 shows the XRD patterns of the metakaolin samples (MK 1, MK 2 & MK 3). The XRD data collected are consistent with the literature review (see Table 2.6) and confirmed the presence of several major crystal phases. The major phases identified in all MK

patterns are kaolinite ($Al_2Si_2O_5(OH)_4$) and quartz (SiO_2). In addition small traces of anatase (TiO_2) are also detected. The presence of an amorphous phase is detected by a slightly higher background on the patterns in the range of 17,5-30° 2θ. This broad amorphous hump is a typical feature of metakaolin and is caused by the thermal calcination process [217].

Figure 4.2 shows the XRD patterns of the six examined GGBFS samples. As mentioned in the literature, the crystal structure of GGBFS is almost entirely amorphous, which makes it difficult to identify peaks in the patterns. Literature suggests that the angular band in the range of 25-35° 2θ could be attributed to a significant proportion of amorphous structure, such as glass. Some small traces of merwinite ($Ca_3Mg(SiO_4)_2$) and the mililite mineral akermanite ($Ca_2Mg(Si_2O_7)$) can be identified on more crystallized portions of the ground granulated blast-furnace slag. According to Arabi and Jauberthie, it is likely that some of the slag agglomerates partially crystallized during the cooling process [7]. Besides these minerals, some minor traces of calcite ($CaCO_3$), quartz (SiO_2) and anorthite ($CaAl_2Si_2O_8$) have been detected. The identified phases are consistent with the literature.

The XRD patterns of the samples from the alternative waste materials whose potential as precursors is investigated are shown in Figure 4.3. The major phases identified in WWA 1 are calcite ($CaCO_3$) and clinozoistite ($Ca_2Al_3(Si_2O_7)(SiO_4)O(OH)$). Other small traces of calcium-based phases, such as rustumite ($Ca_{10}(Si_2O_7)_2(SiO_4)Cl_2(OH)_2$), hydroxylapatite ($Ca_5(PO_4)_3OH$) and flamite ($(Ca,Na,K)_2(Si,P)O_4$) have also been detected. On the other hand, the sample of WWA 2 mainly consists of calcite ($CaCO_3$), anorthite ($CaAl_2Si_2O_8$) and simonkolleite ($Zn_5(OH)_8Cl_2.H_2O$). Given the high calcium content in WWA and the heavy metals detected by XRF, the identified phases are not unusual. From the sample of SG, quartz (SiO_2) and forsterite (Mg_2SiO_4) can be identified as the major phases, with additional traces of diopside ($CaMgSi_2O_6$), fayalite (Fe_2SiO_4) and calcite ($CaCO_3$) detected. These identified phases consist mainly of silica and iron, which is not unexpected given the original function of SG. Since none of these materials are commonly used in this context, there is no data to compare the identified phases and additional XRD analyses is recommended.

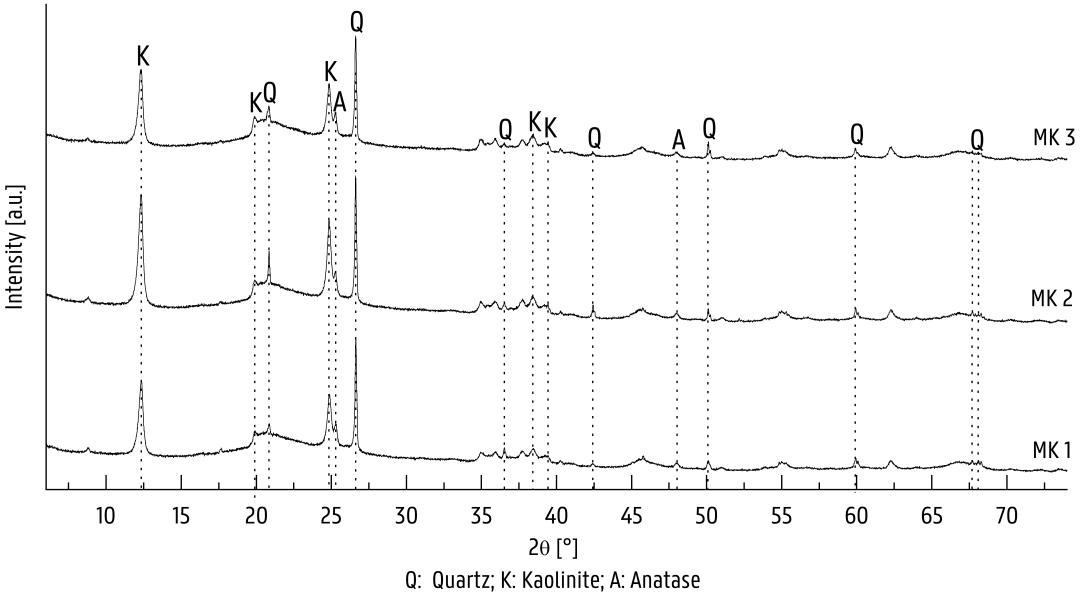

Figure 4.1: XRD patterns of MK 1, MK 2 and MK 3

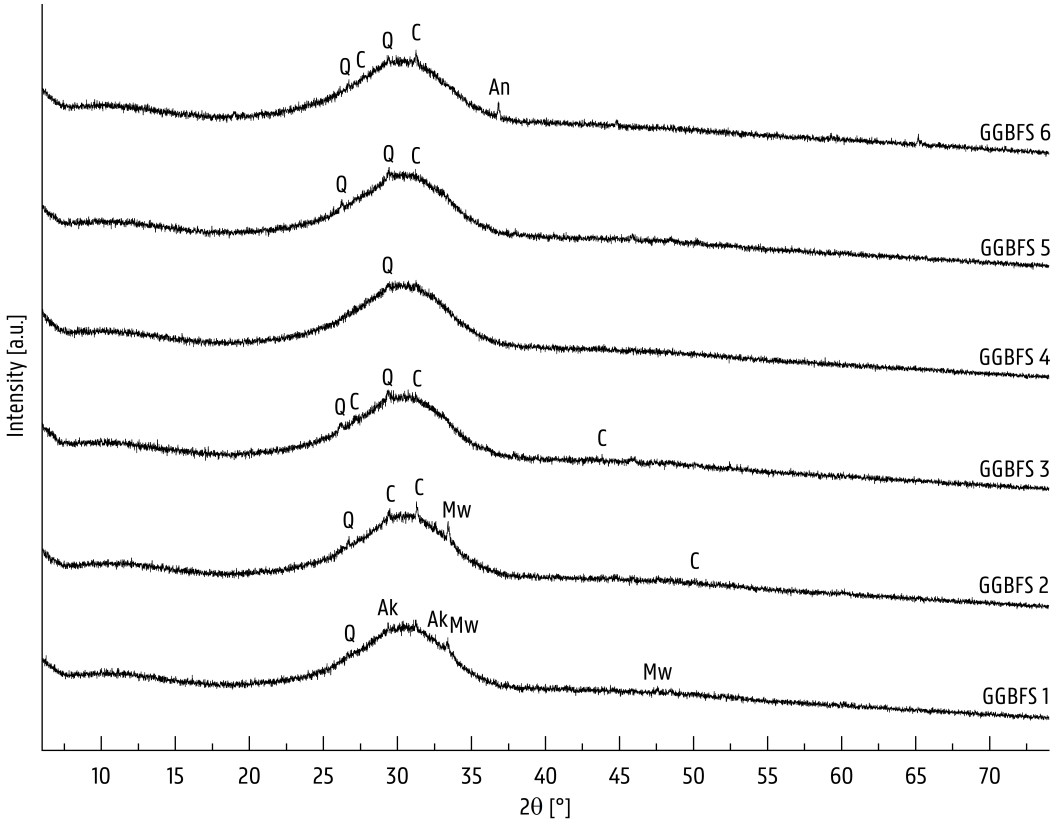

Q: Quartz; C: Calcite; Ak: Akermanite; Mw: Merwinite; An: Anorthite

Figure 4.2: XRD patterns of GGBFS 1, GGBFS 2, GGBFS 3, GGBFS 4, GGBFS 5 and GGBFS 6

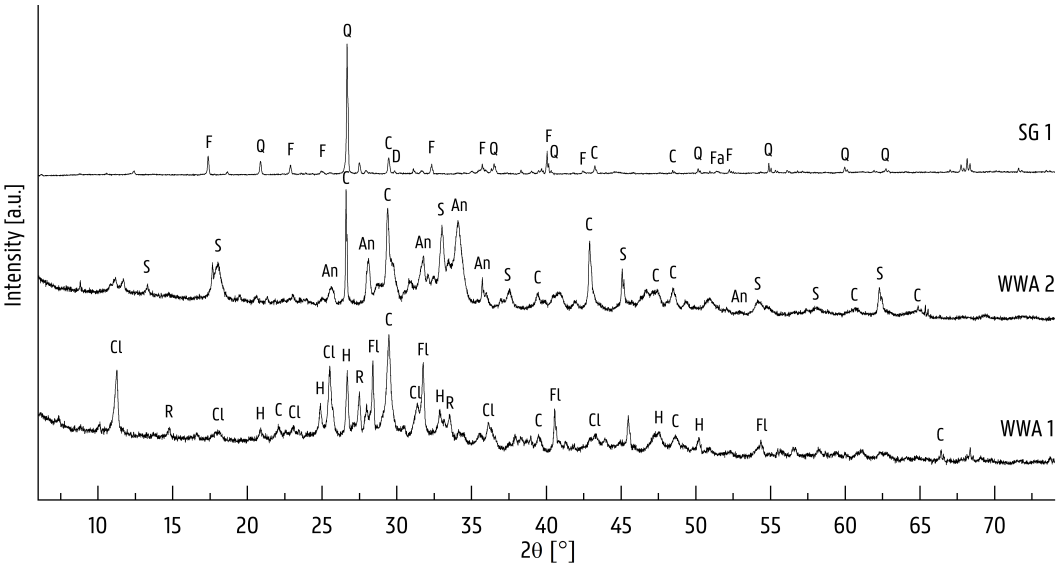

F: Forsterite; Q: Quartz; C: Calcite; D: Diopside; Fa: Fayalite; Cl: Clinozoistite;
Fl: Flamite; R: Rustumite; H: Hydroxylapatite; S: Simonkolleite; An: Anorthite

Figure 4.3: XRD patterns of WWA 1, WWA 2 and SG 1

4.2.3 PH

The pH tests were carried out using both a pH electrode and pH strips, and the results are shown in Table 4.2. To provide a more accurate representation of the pH values, the electrode measurements were averaged. Theoretical pH values from the literature (Table 3.3) were also included for comparison. Where the pH strip can be used as a first indicator, the pH electrode is a confirmatory test.

The readings from the pH electrode were found to be close, or within the range of error, to the theoretical pH values. In contrast, the pH strip measurements are sometimes deviated from the expected values. It should be noted that the pH strips are not always easy to read, especially when the substance being measured is still on the strip. In the case of the WWA, for example, the strip can become almost completely black, making it difficult to read the pH value accurately. Similar to the MK, where the strip is covered with a beige layer. Also, the pH strip values are discrete and do not include values in between the whole numbers. However, some measurements showed values that were in between two whole numbers.

The pH value is important to take in account, since the pH value of the GPC mixture has a big influence on the possibility of flash settings. For example, WWA 2 has a pH of 13,50 and is more likely to undergo flash setting than WWA 1, which has a pH of 11,13.

Table 4.2: Overview pH values

ID	pH_1	pH_2	pH_3	$pH_{electrical}$	pH_{strip}	$pH_{lit.}$
MK 1	5,28	5,22	5,16	5,22 $\pm$ 0,05	5	6,00 - 7,00
MK 2	5,08	5,07	5,15	5,10 $\pm$ 0,04	5	6,00 - 7,00
MK 3	5,03	5,25	5,21	5,16 $\pm$ 0,10	5	6,00 - 7,00
GGBFS 1	11,55	11,35	11,49	11,46 $\pm$ 0,08	11	8,00 - 12,50
GGBFS 2	11,46	11,49	11,41	11,45 $\pm$ 0,03	11	8,00 - 12,50
GGBFS 3	9,76	9,94	9,78	9,83 $\pm$ 0,08	10	8,00 - 12,50
GGBFS 4	11,60	11,56	11,53	11,56 $\pm$ 0,03	11	8,00 - 12,50
GGBFS 5	10,18	10,25	10,13	10,19 $\pm$ 0,05	10	8,00 - 12,50
GGBFS 6	11,65	11,65	11,71	11,67 $\pm$ 0,03	11	8,00 - 12,50
SG 1	9,77	9,67	9,72	9,72 $\pm$ 0,04	8	-
WWA 1	11,09	11,18	11,13	11,13 $\pm$ 0,04	12	2,00 - 14,00
WWA 2	13,45	13,54	13,51	13,50 $\pm$ 0,04	14	2,00 - 14,00
SW	8,28	8,29	8,33	8,30 $\pm$ 0,02	8	7,50 - 8,40
$SSS_{Original}$	11,85	11,80	11,78	11,79 $\pm$ 0,05	13	9,00 - 11,56
SSS	13,47	13,48	13,50	13,48 $\pm$ 0,01	14	9,00 - 11,56

4.3 Physical properties

The density of the different precursors and activators are determined based on the methods described in Section 3.1.2. The particle size analysis (PSA) is divided in two parts: specific surface area and particle size distribution. The specific surface area is determined by using the results of the Blaine method. The particle size distribution can be determined with the LDM for the finer particles between 0,002 and 200 µm. While the sieving method is used for coarser aggregates. These procedures are carried out as described in Section 3.1.1.

4.3.1 Density

The density of the various resources, as well as the densities found in literature, are presented in Table 4.3. Appendix H contains the calculated densities for each material. A pycnometer is used to determine these results. The practical determined densities for the GGBFS, SW and $SSS_{original}$ have a good correlation between the TDS values and fall within the margin of error. The experimental density on the MK is slightly different from the density on the TDS.

The density of the used materials will have an effect on the concrete. When using denser materials, the mixture will be heavier and the density of the fresh concrete will also be slightly higher.

Table 4.3: Comparison results density [g/cm^3]

ID	ρ_1	ρ_2	ρ_3	ρ_{avg}	$\rho_{lit.}$
MK 1	2,65	2,71	2,62	2,66 $\pm$ 0,04	2,60
MK 2	2,66	2,66	2,73	2,68 $\pm$ 0,03	2,60
MK 3	2,67	2,62	2,73	2,67 $\pm$ 0,05	2,60
GGBFS 1	2,94	2,76	2,86	2,85 $\pm$ 0,07	2,80 - 3,00
GGBFS 2	2,77	2,89	2,98	2,88 $\pm$ 0,09	2,80 - 3,00
GGBFS 3	2,92	2,74	2,89	2,85 $\pm$ 0,08	2,80 - 3,00
GGBFS 4	2,92	2,83	2,87	2,87 $\pm$ 0,04	2,80 - 3,00
GGBFS 5	2,80	2,72	2,90	2,81 $\pm$ 0,08	2,80 - 3,00
GGBFS 6	2,96	2,80	2,90	2,89 $\pm$ 0,06	2,80 - 3,00
SG 1	3,75	3,24	3,34	3,45 $\pm$ 0,22	-
WWA 1	2,48	2,31	2,57	2,45 $\pm$ 0,11	-
WWA 2	2,81	2,96	2,89	2,89 $\pm$ 0,06	-
SW	1,02	1,02	1,02	1,02 $\pm$ 0,01	1,02 - 1,03
$SSS_{original}$	1,35	1,35	1,35	1,35 $\pm$ 0,01	1,34
SSS	1,31	1,46	1,46	1,41 $\pm$ 0,07	-

4.3.2 Specific surface area

The Blaine method was used to calculate the specific surface area and these results are presented in this research. The results by LDM are included in Appendix D, they were not further used because the processed data showed differences between the measured value and those reported in the literature. The Blaine method was chosen as a trustworthy and validated alternative method for determining the specific surface area. These values are used in the further research.

Table 4.4 shows the results of the Blaine method for determining the specific surface area of the precursors, as well as TDS values. The detailed calculations towards these values can be found in Appendix I.

The GGBFS results show a good correlation between the TDS values and the experimental determined values, both of which fall most within the margin of error. The experimentally determined results for MK, on the other hand, are further away from the TDS values. It is important to note that because the Blaine method is based on time measurement, a small difference can result in a significant difference in specific surface area value.

SG 1 has a very small specific surface area. This could be because the Blaine method for determining specific surface area was designed primarily to determine the specific surface area of cement. Since there are a lot of coarse particles in SG 1, it is not a fine powder. As a result, the Blaine method is unlikely to be the best method for calculating the specific surface area of SG 1.

Table 4.4: Results specific surface area Blaine method [cm²/g]

Precursor ID	S_1	S_2	S_3	S_{avg}	S_{Blaine}	$S_{Blaine,TDS}$
MK 1	21 094,53	20 724,63	20 955,80	20 924,75	20 920	26 000
MK 2	21 964,97	21 733,84	21 425,33	21 708,05	21 710	26 000
MK 3	21 707,87	21 535,02	21 865,92	21 702,94	21 700	26 000
GGBFS 1	4 606,27	4 594,77	4 714,96	4 638,67	4 640	4 400 $\pm$ 200
GGBFS 2	4 549,76	4 511,51	4 573,12	4 544,80	4 540	4 400 $\pm$ 200
GGBFS 3	4 587,57	4 646,15	4 688,06	4 640,59	4 640	4 400 $\pm$ 200
GGBFS 4	4 609,67	4 574,21	4 591,13	4 595,00	4 600	4 400 $\pm$ 200
GGBFS 5	4 599,66	4 763,48	4 751,89	4 705,01	4 710	4 400 $\pm$ 200
GGBFS 6	4 433,84	4 374,12	4 386,74	4 398,23	4 400	4 200 $\pm$ 200
SG 1	0,04	1,86	41,46	14,45	10	-
WWA 1	7 420,67	7 599,31	7569,43	7529,80	7530	-
WWA 2	3 315,84	3 238,44	3 317,51	3290,60	3290	-

The specific surface area of the mixture is directly proportional to the mixture's water requirement. The finer the particles in the mixture, the greater the specific surface area and the greater the amount of water required to obtain good workability. The results show that WWA 1 has a much higher specific surface area than WWA 2. This implies that a WWA 1 mix with good workability will require more water than a mix with WWA 2. As a result, the WWA 1 mixture's water solid factor (W/S) will be greater than that of WWA 2. A higher W/S ratio indicates that the final mixture will be weaker [196].

4.3.3 Particle size distribution

Laser diffraction method

Table 4.5 shows the optimized refractive index and absorption index for the measured resources. These optimized values are computed by the software connected to the Malvern Mastersizer 3000 and used for recalculating the initial obtained results. This is only an approximation based on the measured data, the exact values for the refractive and absorption index should be determined with suitable equipment. There is no data on SG 1 since the grains are, even after more than 10 hours of ball milling, to coarse to be analysed with wet dispersion.

Table 4.5: Optimized indices laser diffraction spectrometry

	MK 1	**MK 2**	**MK 3**	**GGBFS 1**	**GGBFS 2**	**GGBFS 3**	**GGBFS 4**	**GGBFS 5**	**GGBFS 6**	**WWA 1**	**WWA 2**
n_d	1,53	1,54	1,54	1,60	1,58	1,61	1,58	1,61	1,62	1,78	1,78
k	0,005	0,005	0,005	0,001	0,002	0,001	0,002	0,001	0,001	0,010	0,010

The analysis of the particle size distribution of the precursors is shown in Table 4.6 and graphically presented in Figure 4.4. The measured data is an average of at least 17 measurements to minimize the potential for errors. In Appendix J the measured data and individual particle size distribution reports are presented for the different resources. It should be noted that there is a large deviation between the TDS data and the measured data, most likely due to the approximation of the absorption index and the refractive index.

Table 4.6: Average results particle size distribution with laser diffraction method [µm]

Precursor ID	D(10)	D(50)	D(90)
MK 1	2,1 ± 0,1	13,9 ± 0,5	53,5 ± 1,0
MK 2	2,2 ± 0,1	13,7 ± 0,6	49,8 ± 1,2
MK 3	2,2 ± 0,1	14,1 ± 0,8	53,7 ± 1,4
MK_{TDS}	∼ 2,0	∼ 5,0	∼ 25,0
GGBFS 1	3,6 ± 0,1	14,3 ± 0,1	35,6 ± 0,2
GGBFS 2	3,5 ± 0,1	14,1 ± 0,1	34,9 ± 0,3
GGBFS 3	3,7 ± 0,1	13,8 ± 0,1	34,0 ± 0,1
GGBFS 4	3,6 ± 0,1	14,1 ± 0,1	34,9 ± 0,1
GGBFS 5	3,7 ± 0,1	13,2 ± 0,1	31,5 ± 0,1
GGBFS 6	3,5 ± 0,1	14,2 ± 0,1	37,6 ± 0,1
$GGBFS_{TDS}$ 1 - 5	-	11,0	-
WWA 1	4,9 ± 0,1	21,2 ± 0,1	94,7 ± 1,8
WWA 2	7,6 ± 2,2	49,2 ± 2,8	346,0 ± 6,6

Figure 4.4 shows the different groups of sources, with a significant deviation between WWA 1 and 2, which could be explained by various milling times. Where the WWA 1 had a milling time of 4 hours and WWA 2 had a milling time of 2 hours. MK 1-3 and GGBFS 1-5 are each produced by the same producer and followed the same production process, whereas GGBFS 6, produced by a different producer, showed a slightly different size distribution. This difference is shown in Appendix J.2.

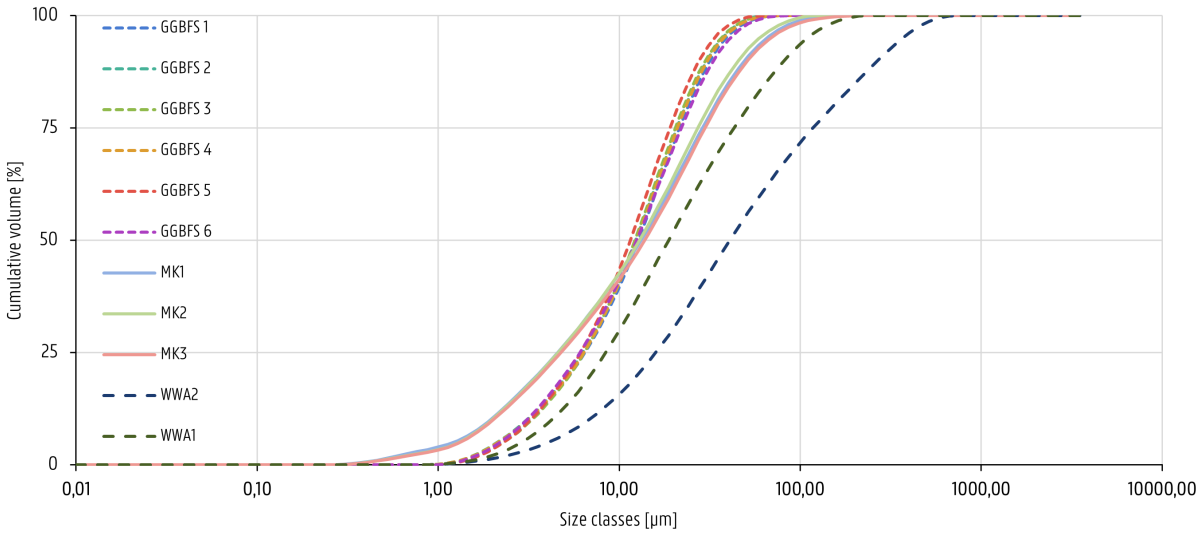

Figure 4.4: Comparison average results particle size distribution of the precursors

Sieving analysis

The analysis of the grain size distribution of the aggregates are shown in Figure 4.5. It compares the results from the unwashed 0/2 sand, standard distributed sand (CEN sand) practically determined and the technical data from the producer [218]. This graph indicates that the 0/2 sand has a higher mass percentage of fine particles, compared to the CEN sand. To minimise the potential for errors, an average of 7 sieving analyses for the 0/2 sand were performed. While the result of the CEN sand is based on the average of 4 sieving analysis. The detailed sieving analysis can be found in Appendix G.

The analysis is limited by sample size and measurement techniques. More sieving analyses were performed for the 0/2 sand, which could reduce potential errors. Fewer sieving analyses were performed for the CEN sand, which is a well-known sand with regulated grain size distribution specifics.

The difference in grain size distribution between the aggregates could impact the properties and performance of the final concrete. The presence of the fine particles in the 0/2 sand could lead to a denser mixture which could improve the final strength and durability of the concrete. On the other hand, the presence of the bigger particles in the CEN sand could improve the workability and flow of the mixture. This might lead to a more easy casting of the concrete [196].

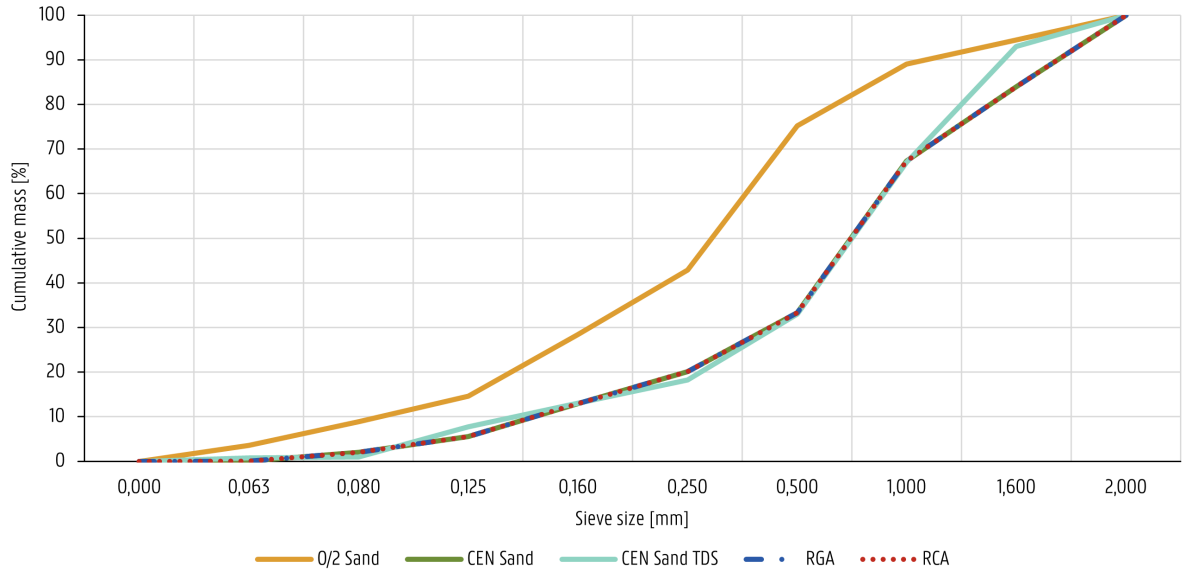

Figure 4.5: Grain size distribution of the used aggregates

5

Reference mix

The purpose of this chapter is to discuss the issues and challenges, other than those of a logistical nature, that were encountered during the development of the reference mix. It outlines the mixing procedure, curing conditions and mix proportions. By presenting this information, it is possible to reproduce the mixtures under identical conditions.

5.1 Geopolymer mix procedure

As mentioned earlier in Section 2.6, the mixing procedure is critical to manufacturing geopolymers. It is also completely different from conventional OPC-based concrete. According to the literature, several techniques are available with various mixing times, each with their advantages.

The mixing procedure applied in this research, schematically illustrated in Figure 5.1, is adapted from other research that focused on the experimental study of design parameters in AAMs, including the mixing procedure for geopolymers. It's partially based on the second method of RILEM and the mix procedure proposed by Zoi G. Ralli [219].

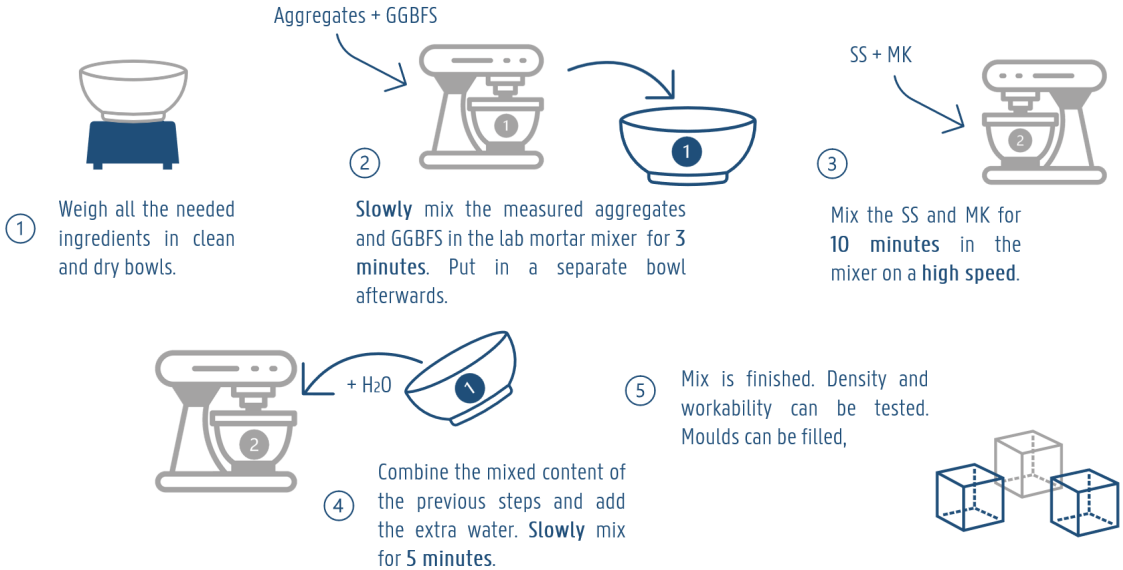

Figure 5.1: Applied mix procedure geopolymers

In the following paragraph Figure 5.1 is explained in further detail. When mixing, it is important to use clean and dry laboratory equipment. This will minimize unwanted early reactions and contaminations. The following steps provide more information about the followed mixing procedure. The mixing procedure to obtain a proper geopolymer concrete is carried out in the following way:

1. Weigh all needed ingredients. If the activator or silicate solution is prepared in-house, it should have stabilized for at least 24 hours. A pre-manufactured solution can be used immediately.
2. The sand and GGBFS are combined in the mixer. The materials are mixed at a low speed, approximately 140 rpm (rotations per minute), this gives mix 1.
3. SS and MK are added together and shortly mixed at 140 rpm to obtain a homogeneous mix and avoid excessive dust. Then mix at a high speed of approximately 350 rpm, resulting in mix 2.
4. Combine the extra water, mix 1 and mix 2 and mix at a low speed (140 rpm) for five minutes. This gives the final mix.
5. Fresh properties of the final mix can be measured according to the relevant standards. The final mix is poured into a mould used to make standard prisms, 40 mm x 40 mm x 160 mm according to EN 196-1. The mould is then vibrated for one minute to minimize the amount of air bubbles in the mixture. After creating an even prism surface with a metal ruler, the top of the moulds are covered. A good seal prevents evaporation of the water in the mix. It can be achieved by using a glass plate with compaction tape or by wrapping the mould with a plastic wrap.

5.2 Terminology for the mixes

Different batches of GPC were produced during the research. In order to keep track of which mixes were used and how they were cured, correct identification of these mixes was very important. With correct identification, the batch parameters could be read and understood at a glance. The various options for terminology of mixtures are summarized in Table 5.1, which can be combined if needed.

Table 5.1: Terminology mixes and curing conditions

DM - Mix ID		**Variations on mix X**	
DMX	Mix nr. X	DMX-AAA	Variation on ingredients coded "AAA"
DMXbis	Second version mix nr. X	DMX-RYY	Variation on reactivity R, R = YY%
DMXtris	Third version mix nr. X	DMX-D.M.TTT	Variation on curing conditions for D number of days
M - Curing preservation method		**TTT - Curing temperature**	
S	Mould or samples sealed	X°C	Oven-heated at X degrees Celsius
U	Mould or samples unsealed	AMB	Ambient temperature

For the purpose of clarification, the batches named DM8-1.S.70°C-27.S.AMB and DM8-RCA are discussed. The first batch of GPC is made according to mix number eight and is compared to the reference subjected to different curing conditions, the first day of sealed curing at 70°C followed by 27 days of sealed curing at ambient temperature. While DM8-RCA, with the use of recycled concrete aggregates (RCA), is a variation of the eighth mix of GPC.

5.3 Reference mix development

Establishing the reference mix was a long and challenging process. It required extensive experimentation and optimization. As shown in Table 5.4, numerous trials were investigated with different geopolymer mix designs, curing conditions and curing times. The main difficulties were related to the poor strength and workability of the geopolymer. A correct interpretation of the physical properties such as the specific surface area and water demand benefits the workability, but the poor performance is mainly due to the chemistry.

In this research, the mix designs and adjustments were provided by prof. dr. ir. Veerle Boel, who acted as supervisor from the Department of Structural Engineering and Building Materials at the Magnel-Vandepitte Laboratory of Ghent University, in collaboration with ing. Leo Van Cauter, who acted as a counsellor from Ghent University.

To exclude some parameters, the conditions were kept the same while changing the amount and type of ingredients.The chemical composition of the selected precursors used for reference mix development are shown in Table 5.2.

Table 5.2: Chemical composition of used precursors in trails [wt. -%]

Precursor ID	**SiO_2**	**Al_2O_3**	**Fe_2O_3**	**CaO**	**MgO**	**K_2O**
MK 2	53,09 $\pm$ 0,20	29,75 $\pm$ 0,28	4,80 $\pm$ 0,22	0,83 $\pm$ 0,01	-	0,75 $\pm$ 0,07
GGBFS 6	24,97 $\pm$ 0,04	6,65 $\pm$ 0,06	0,74 $\pm$ 0,02	48,02 $\pm$ 0,10	6,14 $\pm$ 0,15	1,13 $\pm$ 0,01

Finally, after mixing DM4 and DM5, it was concluded that there was a problem with the sodium silicate solution. The purchased sodium silicate solution had a molar ratio of SiO_2/Na_2O that was too high in the context of geopolymer concrete, which had a significant effect on the reactions and developed strength. According to Davidovits' Geopolymer Chemistry & Applications, it is recommended to use a SSS with a SiO_2/Na_2O molar ratio within the range of MR=1,7 to 1,9. This explains the poor strength of the initial mixes, as the purchased sodium silicate solution has an MR of approximately 3,4. A ready-to-use silicate solution can be purchased, but it must be manufactured and sold specifically for geopolymer applications.

Table 5.3 displays the characteristics of both the original and the adapted sodium silicate solution optimized for use in geopolymer applications. For further reference, the detailed calculations and procedures used in the adaptation process are available in Appendix E.

Table 5.3: Characteristics original and adjusted sodium silicate solution

	Quantity of Ingredients [% m]			**Ratio's**	
SSS	SiO_2	Na_2O	H_2O	WR_{SiO_2/Na_2O}	MR_{SiO_2/Na_2O}
Original	26,00	8,00	66,00	3,25	3,35
Adapted	23,70	14,13	62,17	1,68	1,73

After adjusting the molar ratio, new mixtures were tested. With good workability and reasonable strength, two promising mixes were found, DM8 and DM9. DM8 was chosen as the reference mix design not only because of its superior performance but also because of its high GGBFS content while requiring less SSS and MK. It is also the most economical, sustainable and environmentally friendly choice.

Table 5.4: Trial mixes towards reference mix

		Quantity of Ingredients [kg/m³]					Curing	Strength	Comments
Mix	Date	MK 2	GGBFS 6	SSS 3,4	CEN Sand[3]	Water	Curing conditions[4]	$\sigma_{c,avg}$ [MPa]	Workability
DM1	21/02/23	147,79	344,84	401,00	1325,00	10,00	1.S.60°C	< 3,0	Problematic
DM2	22/02/23	141,56	330,32	384,11	1325,00	30,00	1.S.70°C	< 3,0	Not great
	23/02/23						1.S.70°C	< 4,0	Better
							2.S.70°C	± 16	
							2.S.AMB	± 3	
DM2bis	25/02/23	128,89	300,00	404,44	1324,44	30,00	1.S.70°C	± 2,5	Ok
							2.S.70°C	± 16	
DM2tris	02/03/23	137,78	320,00	391,11	1324,44	30,00	1.S.70°C	± 1,5	Ok
							2.S.70°C	± 8,0	
							3.S.70°C	± 11,3	
	07/03/23	137,78	320,00	391,11	1324,44	30,00	1.S.70°C	± 2,1	Ok
							4.S.70°C	± 26,6	
DM3	25/02/23	208,89	88,89	501,11	1324,44	0,00	1.S.70°C	-	Ok
							2.S.70°C	± 2,5	
	02/03/23	208,89	88,89	501,11	1324,44	0,00	2.S.70°C	± 3,1	Ok
							3.S.70°C	± 7,6	
							4.S.70°C	± 13,8	
DM4	02/03/23	138,89	324,44[1]	387,78	1324,44	30,00	3.S.70°C	± 14,0	Ok
DM5	02/03/23	211,11	91,11[1]	498,89	1324,44	0,00	3.S.70°C	± 5,5	Ok
DM8	11/03/23	163,33	381,11	263,33[2]	1324,44	110,00	1.S.70°C	± 78,5	Good
DM9	11/03/23	333,33	143,33	447,78[2]	1324,44	0,00	1.S.70°C	± 43,1	Good

[1] GGBFS 1 was used instead of GGBFS 6

[2] SSS with MR = 1,7 was used instead of MR = 3,4

[3] Standard distributed sand according to EN 196-1

[4] Annotation according to Table 5.1

5.4 Final reference mix and curing conditions

The reference mix uses a blend of metakaolin and ground granulated blast-furnace slag with a sodium silicate solution. The chemical composition of the selected precursors used for reference mix are shown in Table 5.5. The elemental composition of the used precursors is provided by handheld-XRF measurements. Sodium oxide is not detected because, as mentioned before in Section 3.1.4, the handheld-XRF can only detect elements starting from magnesium and the atomic number of sodium is lower.

Table 5.5: Chemical composition of used precursors DM8 [wt. -%]

Precursor ID	SiO_2	Al_2O_3	Fe_2O_3	CaO	MgO	K_2O
MK 2	53,09 ± 0,20	29,75 ± 0,28	4,80 ± 0,22	0,83 ± 0,01	-	0,75 ± 0,07
GGBFS 6	24,97 ± 0,04	6,65 ± 0,06	0,74 ± 0,02	48,02 ± 0,10	6,14 ± 0,15	1,13 ± 0,01

After extensive trial-and-error, the mix had a desired workability and high strength. The proportions of the reference mix are displayed in Table 5.6. DM8 also serves as a reference for the curing conditions, in addition to mix design. The reference curing conditions and preservation method involve the first day of sealed curing at 70°C followed by 27 days of sealed curing at ambient temperature. The exact reference mix with respect to all the used ingredients, assumed reactivity and curing conditions, according to the appropriate terminology discussed in Table 5.1, is displayed in Table 5.6 but will be referred to as DM8-REF from now on.

Table 5.6: Mix proportions and used curing conditions DM8-REF

	Quantity of Ingredients [kg/m³]					**Curing**
Mix	MK 2	GGBFS 6	SSS 1,7	CEN Sand	Water	Curing Conditions[1]
DM8-REF	163,33	381,11	263,33	1324,44	110,00	1.S.70°C-27.S.AMB

DM8-REF
=
DM8-R50-MK2.GGBFS6.SSS1,7-1.S.70°C-27.S.AMB

[1] Annotation according to Table 5.1

All batches of geopolymer are prepared according to the discussed mixing procedure and the samples will be tested throughout the first 24 hours of curing at elevated temperature (70°C), to investigate development of mechanical and chemical properties. In order to serve as a reference to other research, the samples will also be tested at 28 days.

5.4.1 Alternative curing temperatures and conditions

As mentioned in Section 2.10, the curing time, temperature and conditions all play a significant role in the properties of the final hardened product. In order to evaluate the effect of the used curing conditions and preservation methods, others variations on DM8-REF are tested. The variations on DM8-REF with respect to the curing conditions are provided in Table 5.7.

Table 5.7: Variations on curing conditions and preservation methods compared to DM8-REF

	Quantity of Ingredients [kg/m³]					**Curing**
Mix	MK	GGBFS	SSS	CEN Sand	Water	Curing Conditions[1]
DM8-REF	163,33	381,11	263,33	1324,44	110,00	1.S.70°C-27.S.AMB
DM8-1.S-70°C-27.U.AMB	163,33	381,11	263,33	1324,44	110,00	1.S.70°C-27.U.AMB
DM8-28.S-70°C	163,33	381,11	263,33	1324,44	110,00	28.S.70°C
DM8-28.S-AMB	163,33	381,11	263,33	1324,44	110,00	28.S.AMB

[1] Annotation according to Table 5.1

5.4.2 Assuming different slag reactivity

In order to design a geopolymer mix, several assumptions must be made. Among these is determining the amount of some specific oxides from the precursors that can actively take participate in the geopolymerization, which is referred to as reactivity. The availability of Al_2O_3 is one of the most important oxides in defining the structure. The reference mix includes MK and GGBFS. While it is possible to make a valid assumption about the active Al_2O_3 in MK, there is a considerable amount of uncertainty about the reactivity of GGBFS. Different mix designs are made based on different assumptions about the active Al_2O_3 in GGBFS. Table 5.8 shows the different mix designs for a reactivity of 30, 40, 50 and 70%. For DM8-REF, the reactivity of Al_2O_3 is assumed to be 50%. It can be seen that the assumed reactivity directly correlates to the amount of metakaolin and ground granulated blast-furnace slag in the mix proportions.

Table 5.8: Mix proportions and used curing conditions DM8-R

	Quantity of Ingredients [kg/m³]					**Curing**
Mix	MK	GGBFS	SSS	CEN Sand	Water	Curing Conditions[1]
DM8-R30	165,56	385,56	244,44	1324,44	120,00	1.S.70°C-27.S.AMB
DM8-R40	164,44	383,33	254,44	1324,44	115,56	1.S.70°C-27.S.AMB
DM8-REF	163,33	381,11	263,33	1324,44	110,00	1.S.70°C-27.S.AMB
DM8-R70	161,11	375,56	281,11	1324,44	100,00	1.S.70°C-27.S.AMB

[1] Annotation according to Table 5.1

5.4.3 Implementing non-standard distributed sand

Standard distributed sand is often used for mortars and concrete in a laboratory environment. DM8-REF uses CEN sand according to EN 196-1. The use of CEN sand in OPC-based or geopolymer concrete applications helps to ensure consistent performance and quality of the finished product across different batches, while also being easier to compare with other research due to its consistent distribution. It ensures consistency in properties such as the particle size distribution and shape, which can affect the strength, durability and workability of the concrete [220, 221, 222].

CEN sand is often readily available in most countries, making it a practical choice for research purposes. However, there is no natural sand available that meets the distribution requirements of EN 196-1 [222]. As a result, the CEN sand is an artificial product consisting of several different sand types and fractions. Sand selection, sieving and blending are the most time-consuming processes, making it a less financially attractive choice for large-scale geopolymer concrete projects. A variation on the DM8-REF will investigate the effect of using non-standard distributed sand on early-age properties and the evolution of mineralogy and microstructure. The non-standard distributed sand was produced by sieving 0/8 natural aggregates from Beisfjord (Norway), supplied by HGB Betong, to 0/2 by using a 2 mm sieve. In the following chapters, this sand will be referred to as 0/2 sand. A sieve analysis was performed in Chapter 4, the grain size distribution the 0/2 Sand is displayed in Figure 5.2.

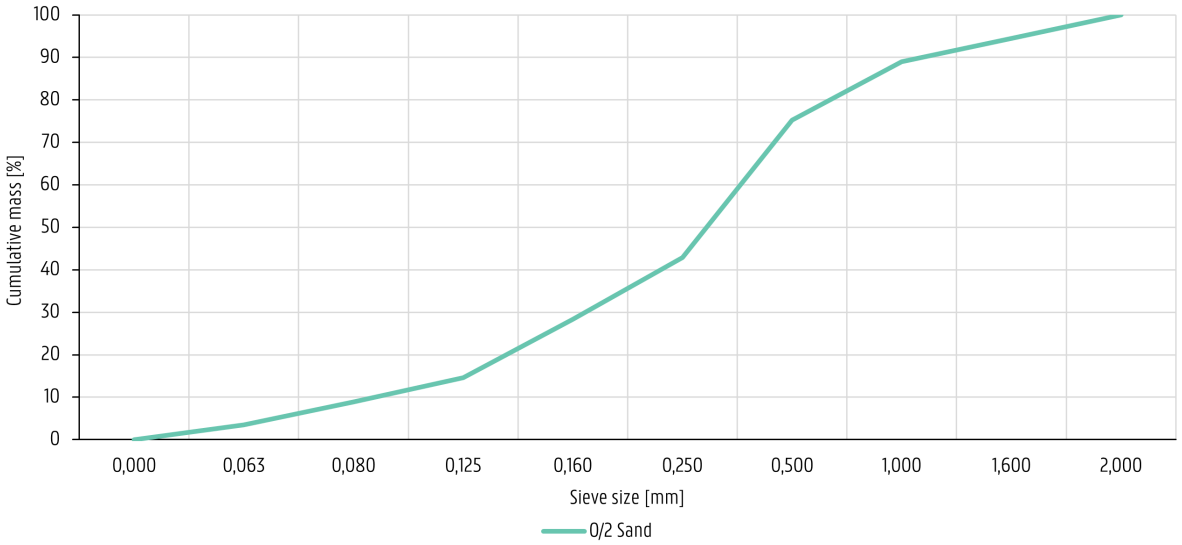

Figure 5.2: Grain size distribution of 0/2 Sand

Table 5.9 shows the mixing proportions and curing conditions for DM8-0/2. The only difference between this mix and the reference mix is the use of the 0/2 Sand, which allows for the analysis of non-standard distributed sand on the fresh and hardened properties of the geopolymer concrete.

Table 5.9: Mix proportions and used curing conditions DM8-0/2

	Quantity of Ingredients [kg/m³]						**Curing**
Mix	MK	GGBFS	SSS	CEN Sand	0/2 Sand	Water	Curing Conditions[1]
DM8-REF	163,33	381,11	263,33	1324,44	-	110,00	1.S.70°C-27.S.AMB
DM8-0/2	163,33	381,11	263,33	-	1324,44	110,00	1.S.70°C-27.S.AMB

[1] Annotation according to Table 5.1

6

Influence of alternative waste materials

This chapter provides an overview of some alternative waste materials that have the potential to be used in geopolymer concrete. It includes some first trails and possible mix designs to analyze the influence of these alternative waste materials on the early-age properties.

6.1 Alternative precursors

The critical role of precursors, as the alumino-silicate source materials, in the development of GPC is discussed in Section 2.5.1. These precursors influence the properties of geopolymers in terms of strength, setting, microstructure, etc. However, with the increasing focus on sustainability and alternative sources, some precursors may become unavailable. As a result, there is an increased need for research and development of alternative precursors, which is also beneficial from a sustainability perspective.

6.1.1 Waste wood ash

The abundance and wide availability of WWA makes it a promising precursor for GPC production. As mentioned before in Section 2.5.1, the chemical composition of WWA can vary profoundly depending on the source and manufacuring process of the ashes. This can have a huge impact on the performance of the resulting GPC. In addition, WWA particles are typically angular shaped and have a higher specific surface area than other precursors, negatively impacting the workability of GPC. Despite these challenges, waste wood ash still remains a promising precursor for geopolymer concrete but further research is needed [115, 159, 162].

Table 6.1 shows the chemical composition of the investigated waste wood ashes. WWA 1 is produced by Bodø Energy and WWA 2 by Harstad Startkraft. The other resources used (MK, GGBFS, and SSS) are the same as those used in the reference mix DM8-REF.

Table 6.1: Chemical composition of WWA [wt. -%]

Precursor ID	SiO_2	Al_2O_3	Fe_2O_3	CaO	MgO	K_2O
WWA 1	3,86 $\pm$ 0,13	1,04 $\pm$ 0,08	6,66 $\pm$ 0,27	36,95 $\pm$ 0,49	2,13 $\pm$ 0,56	3,91 $\pm$ 0,03
WWA 2	3,79 $\pm$ 0,06	1,31 $\pm$ 0,04	2,30 $\pm$ 0,05	49,95 $\pm$ 0,34	3,51 $\pm$ 0,47	17,04 $\pm$ 0,12

Table 6.2 shows each of the mixes, with the objective of replacing 50% of the GGBFS with WWA. The first two mixes were made using WWA 1, while the last two mixes with WWA 2. A good level of workability was not achieved in any of the trial mixes. The high specific surface area of WWA 1 demands more water, resulting in an atypical high water-to-solid ratio and reduced final strength. While the batches containing WWA 2 performed better, the high alkalinity of WWA 2 resulted in flash setting and problematic workability.

Table 6.2: Trial mixes mix with WWA

		Quantity of Ingredients [kg/m³]						Curing	Strength	Comments
Mix	Date	MK	GGBFS	WWA	SSS	CEN Sand	Water	Curing conditions	$\sigma_{c,avg}$ [MPa]	Workability
DM8-REF	11/03/23	163,33	381,11	-	263,33	1324,44	110,0	1.S.70°C	± 78,5	Good
DM8-WWA1.1	23/03/23	175,95	205,28	205,28	283,68	1324,44	138,61	3.S.70°C	± 8,0	Bad
DM8-WWA1.2	24/03/23	124,44	145,56	145,56	183,33	1324,44	200,00	3.S.70°C	± 3,5	Bad
DM8-WWA2.1	22/04/23	163,33	191,11	191,11	242,22	1324,44	120,00	1.S.70°C	± 50,8	Problematic
DM8-WWA2.1	22/04/23	163,33	191,11	191,11	242,22	1324,44	120,00	1.S.AMB	± 12,0	Problematic

6.1.2 Steel grit

Steel grit (SG) is a locally available waste material in Fauske (Norway). It is primarily used in the sandblasting industry to remove rust and old paint from structures before new paint is applied. This sandy material with traces of old paint or rust could potentially serve as a sustainable precursor. The chemical composition of the available SG sample is displayed in Table 6.3. The other resources used in the trails are the same as those used in the reference mix DM8.

Table 6.3: Chemical composition of SG [wt. -%]

Precursor ID	SiO_2	Al_2O_3	Fe_2O_3	CaO	MgO	K_2O
SG 1	26,18 ± 0,99	2,51 ± 0,04	53,22 ± 1,64	3,92 ± 0,20	3,92 ± 0,20	1,03 ± 0,03

Table 6.4 shows the trial mixes containing SG as a potential precursor at various weight percentages. Specifically, three mixes were prepared with respectively 10, 20, and 30 wt.-% SG. The mixes were cured at 70°C for one day, followed by an additional six days of ambient curing. Based on the trials, it can be concluded that the samples made with SG as a precursor did not perform well. This could be related to the very high iron content. Therefore, no further research was done using this waste material. SG may potentially perform better in a different configuration, but this needs extra research.

Table 6.4: Trial mixes mix with SG

		Quantity of Ingredients [kg/m³]					Curing	Strength	Comments
Mix	Date	MK	SG	SSS	CEN Sand	Water	Curing conditions	$\sigma_{c,avg}$ [MPa]	Workability
DM8-REF	11/03/23	163,33	381,11	263,33	1324,44	110,0	1.S-70°C	± 78,5	Good
DM10-10	22/04/23	375,56	42,22	483,33	1324,44	0,00	1.S.70°C-6.S.AMB	± 6,9	Good
DM10-20	22/04/23	348,89	86,67	451,11	1324,44	23,33	1.S.70°C-6.S.AMB	< 3,0	Good
DM10-30	22/04/23	320,00	136,67	416,67	1324,44	47,78	1.S.70°C-6.S.AMB	< 1,5	Ok

6.2 Alternative aggregates

One of the key factors in the strength and cost-effectiveness of geopolymer concrete is the use of aggregates. Aggregates can be used up to 75% by volume, with various options available. The chemistry of geopolymer concrete encourages the use of partially reactive aggregates such as waste sands. More details on this matter can be found in Section 2.5.3. All alternative aggregates used in this part of the research are distributed according to the measured grain size distribution of the CEN Sand, these distributions are illustrated in Figure 6.1.

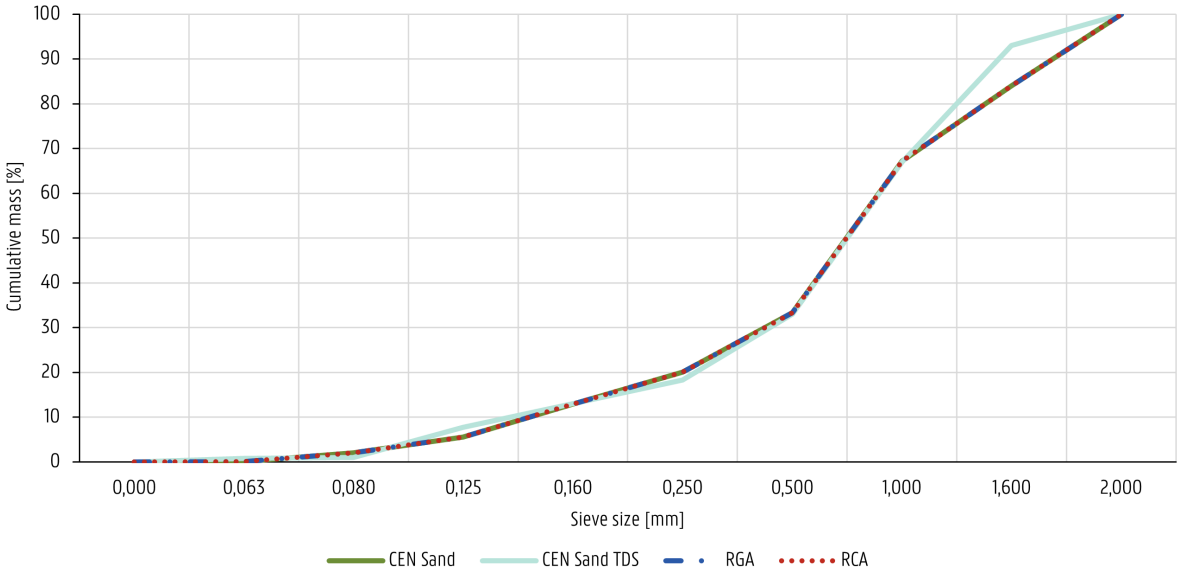

Figure 6.1: Grain size distribution of alternative aggregates

6.2.1 Recycled concrete aggregates

Replacing natural aggregates in GPC with recycled concrete aggregates (RCA) offers a sustainable solution to reduce the use of non-renewable resources. Coarse RCA mixed with natural sand is commonly used to replace natural aggregates. However, the use of the fine fraction RCA is often neglected due to its high water absorption coefficient, which negatively affects workability. Not using the fine fraction is counterproductive from both an environmental and economic point of view. Significant amounts of RCA are left unused in recycling platforms due to the crushing process of demolition waste. Therefore, the use of fine and coarse fractions of RCA either in combination or separately is highly beneficial for sustainable construction [223, 224].

The mixing proportions and curing conditions for DM8-RCA are shown in Table 6.5. Compared to the reference it contains a slightly increased water content to improve workability and aggregates made of RCA, which allows to analyze the effect the use of RCA on geopolymer concrete early-age properties. The RCA are originated from Nordland Betong (Norway) and distributed according to the EN 196-1 standard distribution.

Table 6.5: Mix proportions and used curing conditions DM8-RCA

	Quantity of Ingredients [kg/m³]						Curing
Mix	MK	GGBFS	SSS	CEN Sand	RCA	Water	Curing Conditions[1]
DM8-REF	163,33	381,11	263,33	1324,44	-	110,00	1.S.70°C-27.S.AMB
DM8-RCA	161,98	377,96	261,16	-	1313,51	127,61	1.S.70°C-27.S.AMB

[1] Annotation according to Table 5.1

6.2.2 Recycled geopolymer aggregates

As the use of geopolymer concrete to replace traditional concrete is widely promoted in the available literature, GPC waste is expected to increase rapidly in the future decades as the first generation of GPC structures near their end-of-life. Although the application of GPC in the construction industry is still in its early stages, special attention must be given to the understanding of the potential challenges of managing GPC waste. This information can be a big part in making decisions about the use of geopolymer concrete. This information can provide critical input into decision-making for the adoption of geopolymer concrete [225].

In Table 6.6, the mix proportions and curing conditions for DM8-RGA are displayed. As compared to the reference mix, it consists of recycled geopolymer aggregates (RGA) distributed according to the standard EN 196-1 and a slightly increased water content to improve workability. This makes it possible to study the influence of RGA, retrieved from previous trail batches, on the early-age properties of GPC.

Table 6.6: Mix proportions and used curing conditions DM8-RGA

	Quantity of Ingredients [kg/m³]						Curing
Mix	MK	GGBFS	SSS	CEN Sand	RGA	Water	Curing Conditions[1]
DM8-REF	163,33	381,11	263,33	1324,44	-	110,00	1.S.70°C-27.S.AMB
DM8-RGA	161,98	377,96	261,16	-	1313,51	127,61	1.S.70°C-27.S.AMB

[1] Annotation according to Table 5.1

6.3 Alternative for water

Water serves several functions in geopolymer concrete. As discussed in Sections 2.4 and 2.5.4, water is only required during the polymerization process. Hydrogen bonds create the 3D geopolymer network. When the process is complete, the water evaporates. Indicating that water only contributes to and can be used to improve the workability of the liquid concrete.

6.3.1 Seawater

With over 2 billion tons of freshwater used annually, concrete accounts for 9% of global industrial water demand. It is estimated that by 2050, 75% of this demand will come from regions already experiencing water shortages, exacerbating the problem of freshwater scarcity. In addition, desalination, a common solution to freshwater shortages, has harmful environmental consequences. As SW is an abundant and sustainable resource, it could reduce the strain on freshwater resources.

Researchers are proposing the use of SW as a substitute for fresh water in concrete production to address this issue. Due to the function of water in geopolymers, SW is expected to have less harmful consequences to geopolymers than OPC-based concrete [137, 226, 227].

The seawater used in this research was collected from Ornesvik beach in Narvik, Norway. Some initial properties were measured to gain some knowledge about the used SW, these are available in Chapter 4 and also shown in Figure 6.7. These properties are limited, extra research towards composition is recommended.

Table 6.7: Measured properties used SW

ID	ρ_{avg} [g/cm³]	$pH_{electrical}$
SW	1,02 ± 0,01	8,30 ± 0,02

Table 6.8 shows the mixing proportions and curing conditions for DM8-SW. The only difference between this mix and the reference mix is the use of SW, which allows for the analysis of its effect on the properties of GPC.

Table 6.8: Mix proportions and used curing conditions DM8-SW

	Quantity of Ingredients [kg/m³]						Curing
Mix	MK	GGBFS	SSS	CEN Sand	Water	SW	Curing Conditions[1]
DM8-REF	163,33	381,11	263,33	1324,44	110,00	-	1.S.70°C-27.S.AMB
DM8-SW	163,33	381,11	263,33	1324,44	-	110,00	1.S.70°C-27.S.AMB

[1] Annotation according to Table 5.1

6.4 Overview mixes with alternative waste materials

The following Table 6.9 gives an overview of the various mixes with alternative waste materials. It illustrates the composition of the mixes in comparison to the reference mix. Each one of them has one or more changed variables compared to the reference mix, allowing for the effect of that certain variable on the early-age properties to be studied.

Table 6.9: Composition various mixes with alternative waste materials

	Precursors				Aggregates			Activator	Extra water	
Mix	MK	GGBFS	WWA	SG	CEN Sand	RCA	RGA	SSS	Distilled	SW
DM8-REF	x	x			x			x	x	
DM8-WWA	x	x	x		x			x	x	
DM8-SG	x			x	x			x	x	
DM8-RCA	x	x				x		x	x	
DM8-RGA	x	x					x	x	x	
DM8-SW	x	x			x			x		x

Part III

Results and Discussion

7

Evolution early-age properties reference mix

This chapter analyses the evolution of early-age properties of the reference mix. An overview of the development of the mechanical properties are provided along with the evolution of mineralogy and microstructure. Connecting them will explain the strength development of GPC. Some variables of the mix are changed and the effect on the evolution is studied.

7.1 Characteristics of reference mix

In Table 7.1 all the info and fresh properties of the reference mix are combined. For every DM8-REF batch, the batch number, amount and date are being tracked. If there are unusual results, they can be investigated. Furthermore the density and workability for the fresh concrete of the batches are shown. In Appendix K.1 the details towards the values are presented.

Table 7.1: Fresh properties of DM8-REF batches

			Density of mix		**Workability**[1]	
	Batch nr.	Date	ρ [kg/m³]	S.G. [-]	D_{avg} [cm]	F_{avg} [-]
DM8-REF	2	20/03/23	2 196,75	2,20	23,38	133,75
	3	20/03/23	2 157,28	2,16	24,38	143,75
	4	20/03/23	2 195,99	2,20	24,50	145,00
	5	20/03/23	2 153,17	2,15	22,75	127,50
	6	20/03/23	2 146,75	2,15	24,75	147,50
	7	20/03/23	2 163,43	2,16	23,88	138,75
	8	20/03/23	2 104,44	2,10	25,13	151,25
	9	22/03/23	2 166,52	2,17	23,88	123,75
	10	22/03/23	2 157,71	2,16	23,13	131,25
	11	22/03/23	2 155,41	2,16	22,25	122,50
	12	23/03/23	2 186,09	2,19	23,25	132,50
	13	24/03/23	2 152,89	2,15	22,63	126,25
	15	24/03/23	2 158,21	2,16	22,50	125,00
	21	25/03/23	2 196,55	2,20	22,88	128,75
	28	27/03/23	2 162,68	2,16	23,00	130,00
	30	28/03/23	2 165,31	2,17	21,88	118,75
	31	24/04/23	2 193,16	2,19	21,88	128,75
	Average		**2 170**	**2,17**	**23,35**	**133,53**

[1] Tested with Hägermann flow table according to EN 1015-3

Figure 7.1: Greening effect on freshly demoulded DM8-REF samples

As shown in Figure 7.1, freshly removed samples from sealed moulds often display a temporary green-blue color. According to the literature, this greening effect is caused by the formation of ferrous sulfate ($FeSO_4$), a greenish crystalline salt, caused by the chemistry of the used precursors. However, when exposed to air, $FeSO_4$ quickly oxidizes and the samples gradually lose their green-blue color and turn grey [228, 229, 230].

7.2 Evolution of mechanical properties

In Table 7.2 the measured mechanical properties are shown at different curing times. First the absolute values followed by the values relative to 28 days. A detailed overview of the individual samples and tests are available in Appendix K.1. Outliers are treated according to EN 196-1 and ISO 5725-2 (Grubb's test for outliers) for compressive and flexural strengths, respectively. Figure 7.2 shows the development of compressive strength as a function of the age, whereas Figure 7.3 presents the flexural strength in function of the age.

Table 7.2: Early-age mechanical properties of DM8-REF mixtures

		Absolute values			**Relative values to 28 days**			**Sample info**	
	Age	$\sigma_{c,avg}$ [MPa]	$\sigma_{f,avg}$ [MPa]	S.G. [-]	$\sigma_{c,avg}$ [%]	$\sigma_{f,avg}$ [%]	S.G. [%]	Batch nr.[1]	# Samples $_{c\,;\,f}$
DM8-REF	0 h	-	-	2,17 ± 0,02	-	-	100,0 ± 2,6	-	-
	1 h	6,6 ± 0,2	0,6 ± 0,1	2,18 ± 0,01	9,3 ± 0,4	10,4 ± 0,5	100,5 ± 2,4	10	6 ; 3
	2 h	14,3 ± 0,5	1,3 ± 0,1	2,14± 0,02	19,9 ± 0,8	23,1 ± 0,9	98,6 ± 2,5	4	6 ; 3
	3 h	36,6 ± 1,3	2,1 ± 0,4	2,18 ± 0,02	51,1 ± 2,2	35,7 ± 7,3	100,5 ± 2,6	10	6 ; 3
	4 h	41,9 ± 1,7	2,6 ± 0,1	2,15 ± 0,01	58,6 ± 2,7	44,3 ± 1,0	99,1 ± 2,3	4	6 ; 3
	5 h	49,1 ± 0,6	2,9 ± 0,1	2,16 ± 0,01	68,7 ± 1,8	49,4 ± 0,9	99,5 ± 2,3	11	6 ; 3
	6 h	49,3 ± 1,3	3,5 ± 0,3	2,16 ± 0,03	68,9 ± 2,4	60,2 ± 5,3	99,5 ± 2,6	3	6 ; 3
	7 h	57,1 ± 1,6	2,5 ± 1,3	2,16 ± 0,02	79,8 ± 2,9	42,6 ± 23,1	99,5 ± 2,5	9 ; 12	11 ; 6
	8 h	60,7 ± 2,7	3,6 ± 0,2	2,17 ± 0,03	84,9 ± 4,3	62,0 ± 3,1	100,0 ± 2,7	3	6 ; 3
	9 h	61,9 ± 3,6	3,4 ± 0,6	2,17 ± 0,04	86,5 ± 5,4	59,1 ± 9,8	100,0 ± 2,9	9 ; 12	12 ; 6
	10 h	69,8 ± 2,5	5,2 ± 0,4	2,20 ± 0,01	97,5 ± 4,1	89,6 ± 7,3	101,4 ± 2,3	2	6 ; 3
	12 h	67,9 ± 2,0	5,7 ± 1,0	2,15 ± 0,02	94,8 ± 3,6	97,2 ± 16,9	99,1 ± 2,4	2	6 ; 3
	14 h	63,4 ± 2,8	5,0 ± 0,5	2,16 ± 0,04	88,6 ± 4,5	85,6 ± 8,9	99,5 ± 2,9	7	6 ; 3
	16 h	72,6 ± 1,6	5,4 ± 1,0	2,16 ± 0,02	101,5 ± 3,2	93,2± 16,8	99,5 ± 2,5	11	6 ; 3
	18 h	65,1 ± 4,4	5,1 ± 1,0	2,14 ± 0,03	91,0 ± 6,5	88,4± 17,9	98,6 ± 2,7	6	6 ; 3
	20 h	65,0 ± 3,6	4,3 ± 0,4	2,12 ± 0,01	90,8 ± 5,5	73,6 ± 7,1	97,7 ± 2,3	7	5 ; 3
	22 h	73,7 ± 3,2	4,9 ± 0,9	2,15 ± 0,02	103,0 ± 5,1	84,9 ± 15,8	99,1 ± 2,4	6	6 ; 3
	24 h	72,4 ± 3,9	4,7 ± 1,1	2,17 ± 0,01	101,2 ± 6,0	81,6 ± 19,0	100,0 ± 2,4	5	6 ; 3
	28 d	71,6 ± 1,7	5,8 ± 0,1	2,17 ± 0,01	100,0 ± 3,3	100,0 ± 1,7	100,0 ± 2,3	28	6 ; 3

[1] Batch numbers associated to Table 7.1

Since there is no further strength development within the margin of error, it can be concluded that the strength of the reference mix is fully developed after one day of curing at an elevated temperature of 70°C. As mentioned in Section 2.10.7, it is not uncommon for GPC to exhibit a rapid increase in strength at high temperatures, which is also visible here. The most rapid increase in strength, both compressive and flexural, happen within the first 4 hours of elevated curing. The development continues slowly until 10 hours after which more than 90% of full strength is reached. Further increases in strength after this are minimal, as these measured strengths fall within the margin of error of the 24-hour cured samples. Something unconventional happens to the measured flexural strength at 7 and 9 hours of curing. Because of this sudden loss in strength, additional samples were made to ensure that these values are representative.

In general, the margins of error are small. They are almost always smaller for the compressive strength because it is based on twice as many samples as the flexural strength. The measured values for flexural strength are much lower compared to the compressive strength values, which explains why the impact of a small error is proportionally greater.

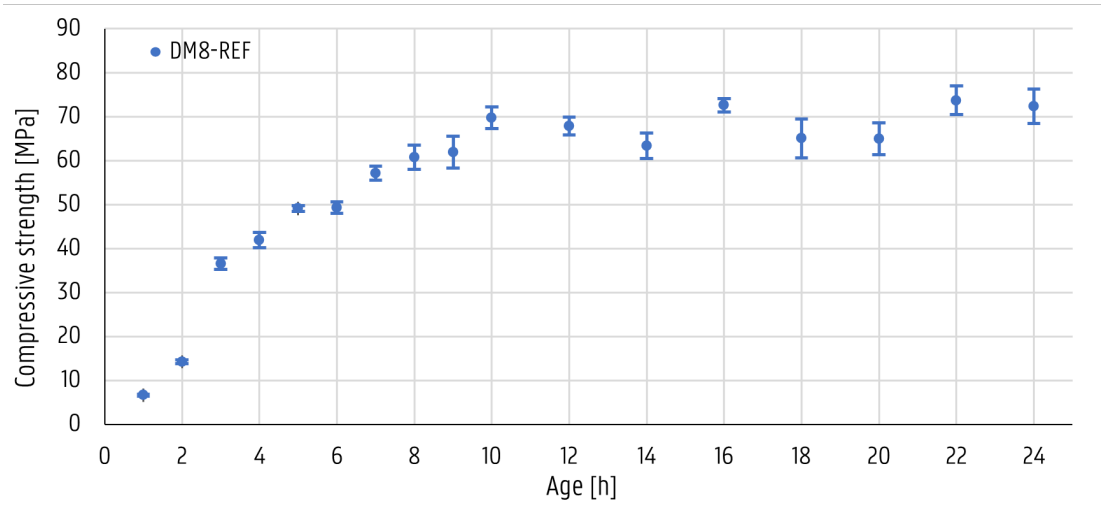

Figure 7.2: Development compressive strength DM8-REF

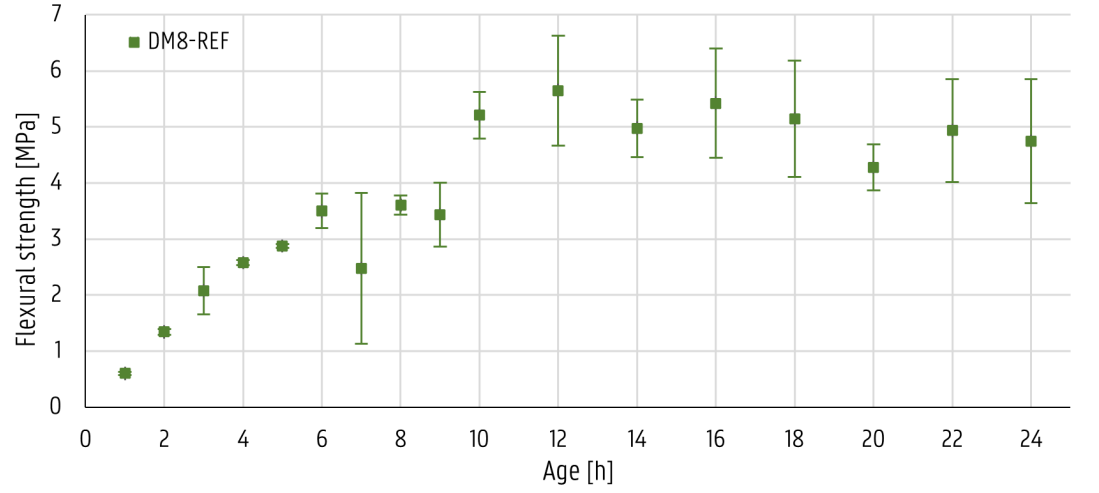

Figure 7.3: Development flexural strength DM8-REF

Figure 7.4 shows the compressive to flexural strength ratio as a function of curing time for DM8-REF. The graph illustrates that this ratio has remained relatively constant over time, with an average value of 15. The constant ratio indicates that the compressive and flexural strength properties of the reference mix are well balanced and that the performance is consistent over time. The only odd ones out are the values at 1, 2 and 7 hours. For these values a more intensive study with more samples, especially for the flexural strength is necessary.

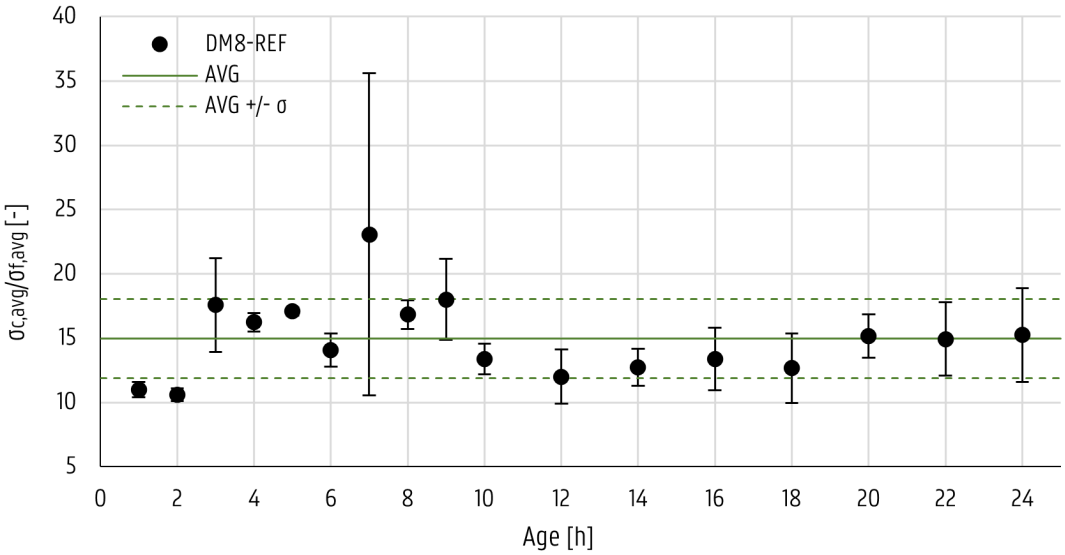

Figure 7.4: Ratio compressive and flexural strength DM8-REF

Figure 7.5 displays the relative strength development of the reference mix in terms of compressive and flexural strength as a percentage of the strength at 28 days of curing. The graph shows that both curves follow a similar curing pattern, with both strengths increasing rapidly during the first four hours of curing and then increasing at a slower rate.

The flexural and compressive strengths after 4 hours of curing have already reached nearly 45 and 60% of their total strength, respectively. After 6 hours of curing the flexural and the compressive strengths are even exceed 60% and 68% of their total strength at 28 days. The relative compressive and flexural strengths continue to increase until they reach almost full strength after 10 hours of curing. After this, the strength is more or less the same than at 28 days (1.S.70°C-27.S.AMB) curing. This observation suggests that the reference mix behaves similarly in terms of compressive and flexural strength development over time. However, the flexural strength lags slightly behind the compressive strength. There is no significant deviation in the trend between the two strength properties.

Figure 7.6 analyses the first 10 hours of curing and presents the curing time on a logarithmic scale. This shows that strength development can be approached as a logarithmic correlation until the maximum strength is reached. Various parameters influence the angle at which the curves are plotted and also the curing time after which the line becomes horizontal. The elevated temperature at which the samples are being cured is also one of these parameters.

Different temperatures have been found to have a significant impact on the curing time of the material. A higher temperature, for example, may accelerate the curing process, resulting in a shorter overall curing time. A lower temperature, on the other hand, may slow down the curing process. The effect of this is being further discussed in Section 7.4.1.

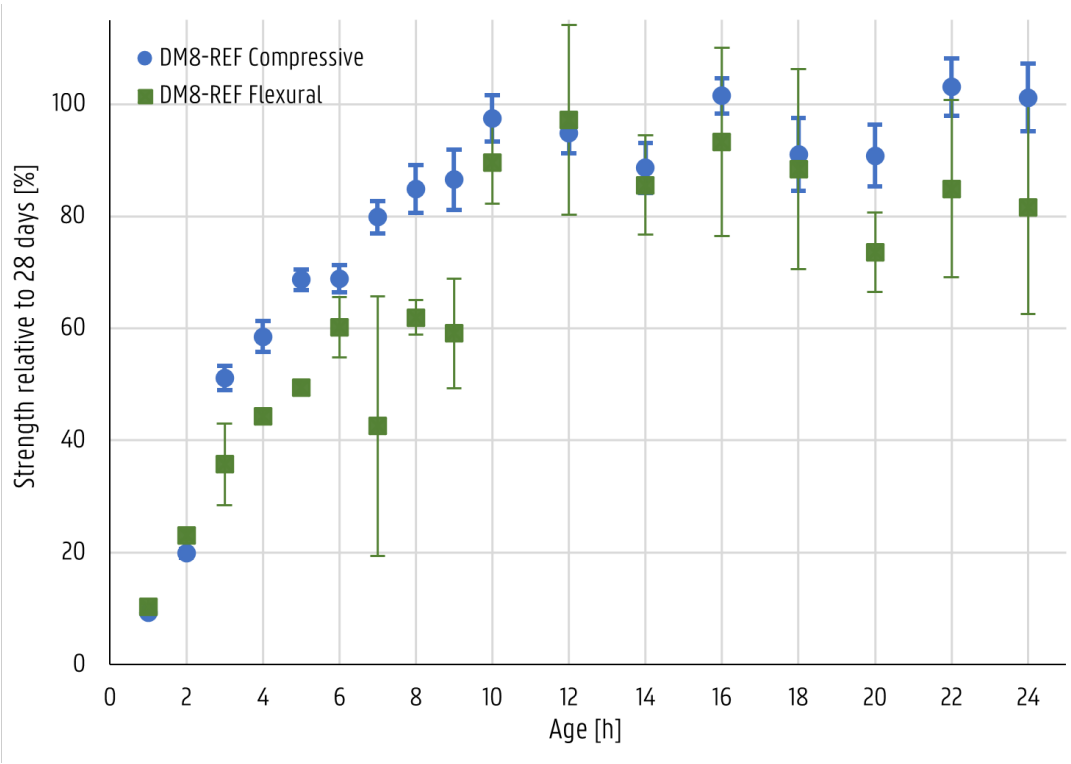

Figure 7.5: Relative strength development DM8-REF until 24 hours

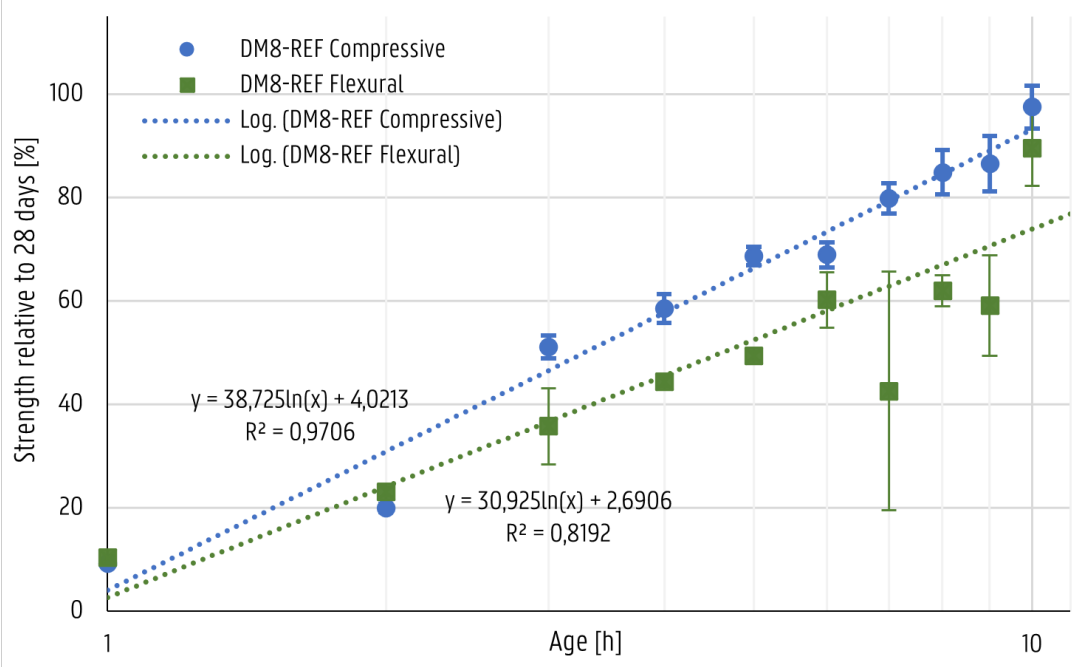

Figure 7.6: Relative strength development DM8-REF until 10 hours (log. scale)

7.3 Evolution of mineralogy and microstructure

As mentioned in Section 3.2.4, XRD is a powerful tool to obtain information about the composition and properties of the samples. The XRD patterns shown in Figures 7.7 and 7.8 were obtained from scanned powders prepared by milling samples previously tested for mechanical properties. These powders were analysed simultaneously with these properties to gain knowledge into the evolution of mineralogy, microstructure and how this relates to changes in mechanical properties over time.

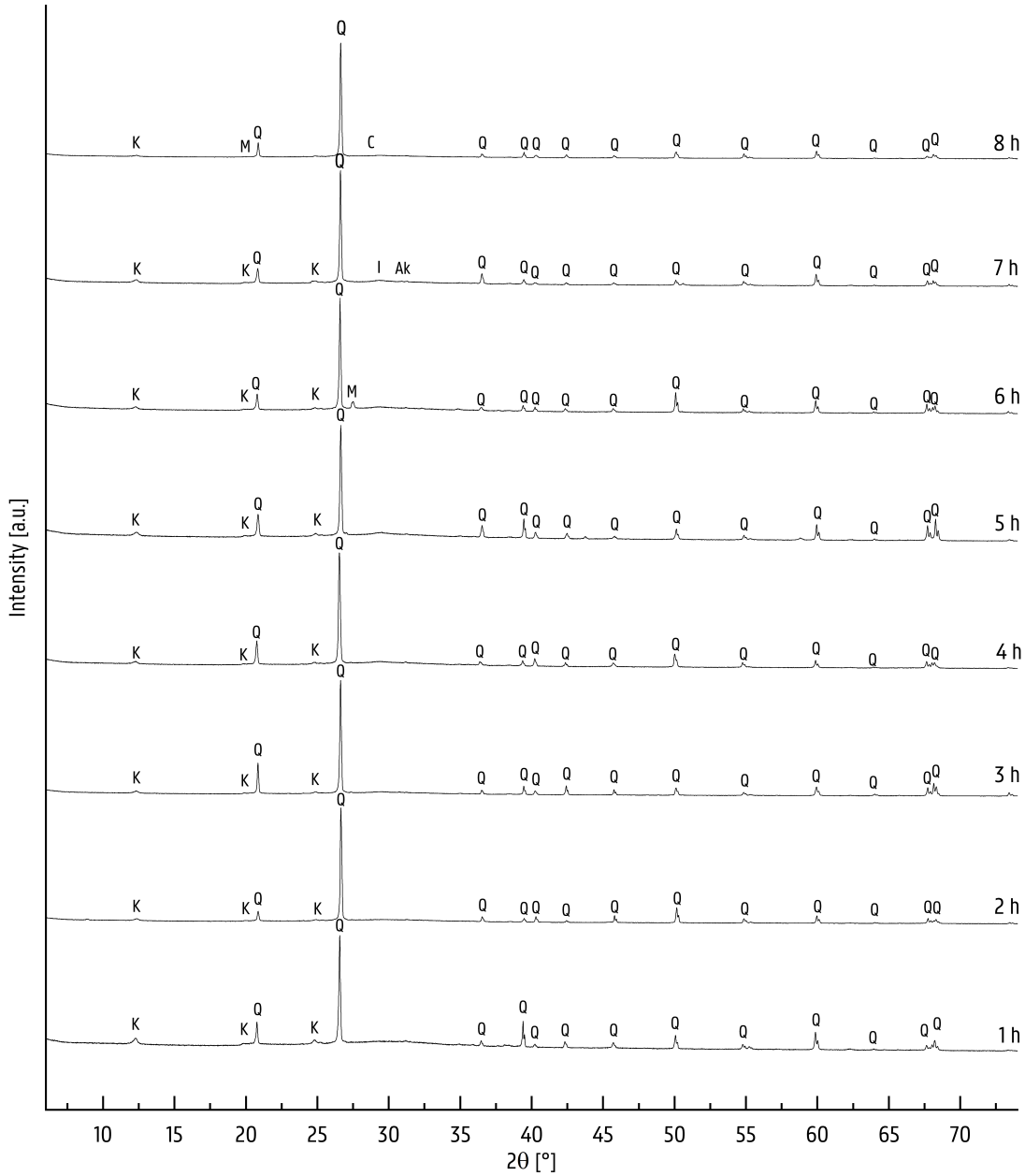

K: Kaolinite; M: Microcline; I: Illite; Q: Quartz; C: Calcite; Ak: Akermanite

Figure 7.7: XRD patterns DM8-REF 1 to 8 hours

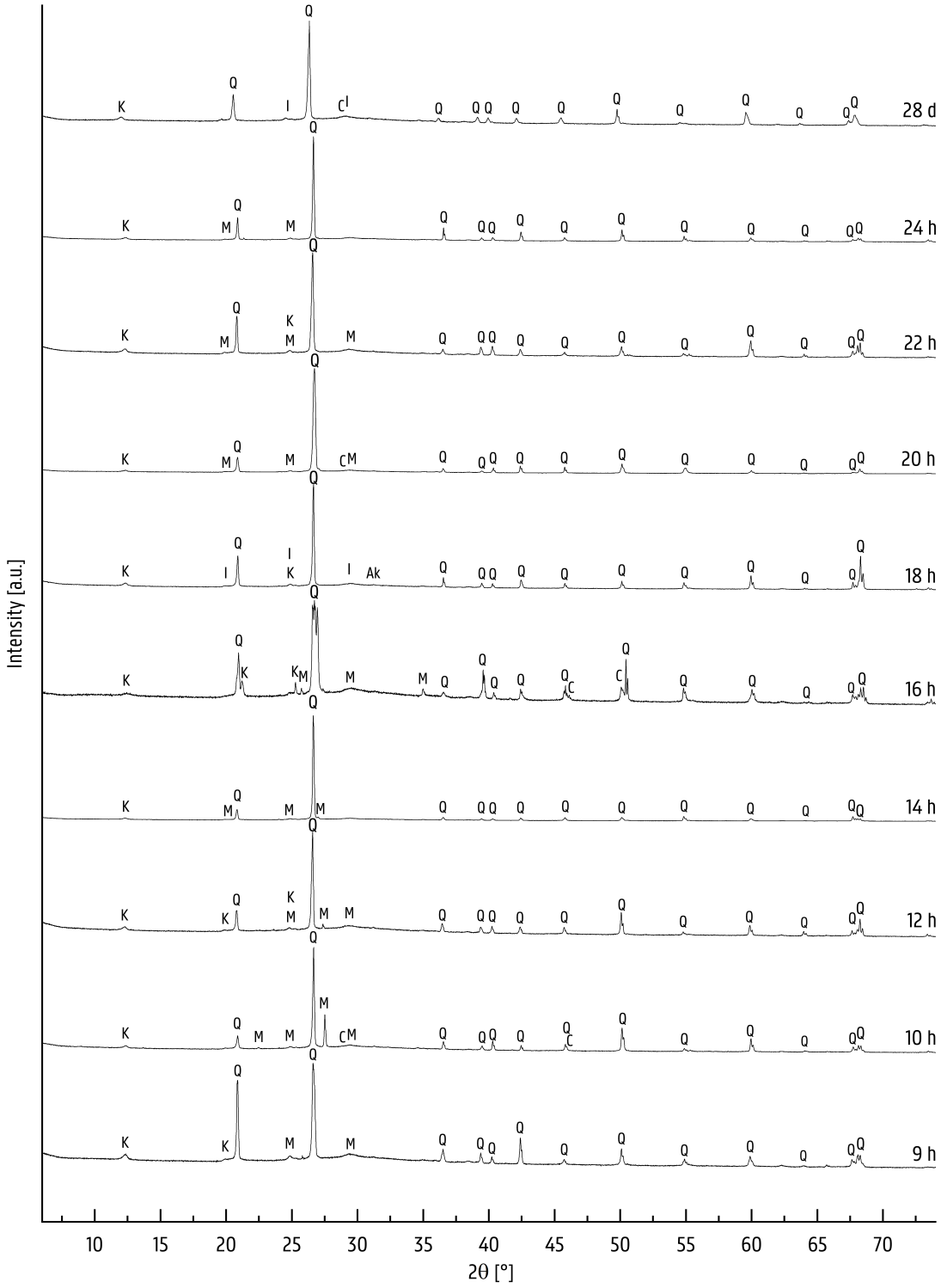

K: Kaolinite; M: Microcline; I: Illite; Q: Quartz; C: Calcite; Ak: Akermanite

Figure 7.8: XRD patterns DM8-REF 9 hours to 28 days

As shown in Figure 7.7, there are no significant changes in mineralogy during the first five hours of elevated curing. The majority of the phases detected in all patterns are quartz (SiO_2) and some additional traces of kaolinite ($(Al_2Si_2O_5(OH)_4)$) have been identified around 12°, 20° and 25° 2θ. This is most likely originating from metakaolin, since it is one of its main phases. The presence of an amorphous phase seems to increase on the patterns in the range 27,5 - 32,5° 2θ. This range is also the common angular band of the amorphous phases in both MK and GGBFS. The presence and increase of these amorphous phases indicates the formation of sodium alumino silicate hydrate (N-A-S-H) gel, which is amorphous in nature and structured as a 3D network [231]. It can be noted that approximately 70% and 50% of the compressive and flexural strength, respectively, have been developed by this time. Thus, the initial strength development could be related to the increase of the amorphous content, the N-A-S-H gel to be more specific.

The observed XRD patterns between six and ten hours occasionally identity other phases, while the amorphous phase shows a slight increase. The additional detected phases, mainly the clay mineral illite ($(K,H_3O)(Al,Mg,Fe)_2(Si,Al)_4O_{10}[(OH)_2,(H_2O)]$) and feldspar microcline ($KAlSi_3O_8$), tend to be identified in the 20 and 25° 2θ angles, where kaolinite was previously detected. In addition, at eight hours small peaks of calcite ($CaCO_3$) are detected in the amorphous region and a peak of akermanite ($Ca_2Mg(Si_2O_7)$ is detected in the scanned sample that was cured for seven hours at an elevated temperature. The effect of the presence of akermanite is unclear, but it is worth noting that at this point, the average flexural strength is greatly reduced at this time.

Figure 7.8 also displays the diffraction patterns from ten hours up to 28 days of curing, with the first 24 hours of elevated curing and the remaining 27 days at ambient temperature. The patterns do not detect any significant changes after ten hours of elevated curing and are mainly composed of quartz with some additional traces of kaolinite, illite and microcline identified. Starting from the samples of nine hours of elevated curing, it is observed that the presence of illite or microcline at 30° 2θ is detected in most of the patterns. Typically, but depending on the sample, the original peaks of kaolinite at 20 and 25° 2θ are replaced by either illite or microcline. It is possible that both phases coexist. However, due to the sensitivity of the software and the minimal difference in 2θ angle between the two, only one is detected. Some irregularities are present in the 14 and 16 hour samples, but this could be sample specific, as the same phases are detected but the peaks are just slightly different compared to the rest. In addition, some of the patterns only show the clay mineral illite, while others only show the feldspar microcline, suggesting that both may be present in the fully developed sample. Since the reference mix reaches more than 90% of full strength at approximately 10 hours, the presence and interaction of microcline and/or illite with the amorphous N-A-S-H gel may contribute to the overall strength of the material.

The results presented in this section provides an initial indication of a potential correlation between the early-age properties and the mineralogy and microstructure of the geopolymer concrete. However, the evolution of the N-A-S-H (and C-A-S-H) gel and its interaction with the clay and feldspar minerals must be researched to gain a more thorough knowledge of this correlation. While XRD is not ideal for detecting the amorphous gels, techniques such as solid-state nuclear magnetic resonance (NMR) spectroscopy and Fourier transform infrared (FTIR) spectroscopy can be used to identify and quantify the C-A-S-H and N-A-S-H gels in geopolymer concrete. These techniques have been used in previous studies to successfully characterize these amorphous phases [232, 233]. A more complete understanding of the development of early age properties can potentially be achieved by further investigation of both minerals and geopolymer gels.

The following paragraph summarises the previously mentioned observed changes in mineralogy and microstructure based on Figure 7.9. The main phases detected by XRD in the sample after one hour of elevated curing are quartz and some additional traces of kaolinite have been identified. This is most likely to be of metakaolin origin, as it is one of its main phases. After six hours, the presence and increasing amorphous content at 30° 2θ indicates the formation of sodium alumino silicate hydrate gel, which is amorphous and structured as a 3D network [231]. Approximately 70% of the final compressive strength has been developed by this time. The increase in amorphous content may be responsible for this initial strength development. Some small traces of microcline can also be detected from six hours onwards. The observed XRD patterns from six hours onwards occasionally identify other phases, while the amorphous phase shows a slight increase. The additional phases detected, mainly the clay mineral illite and feldspar microcline, tend to be identified at angles 20 and 25° 2θ where kaolinite was previously detected. The XRD patterns from ten hours up to 28 days of curing. The patterns do not show any significant changes after ten hours of elevated curing and are mainly composed of quartz with some additional traces of kaolinite, illite, and microcline identified by XRD. The presence of illite or microcline at 30° 2θ is observed in most of the samples from the nine hours of elevated curing samples. Typically, but depending on the sample, the original peaks of kaolinite at 20 and 25° 2θ are replaced by either illite or microcline.

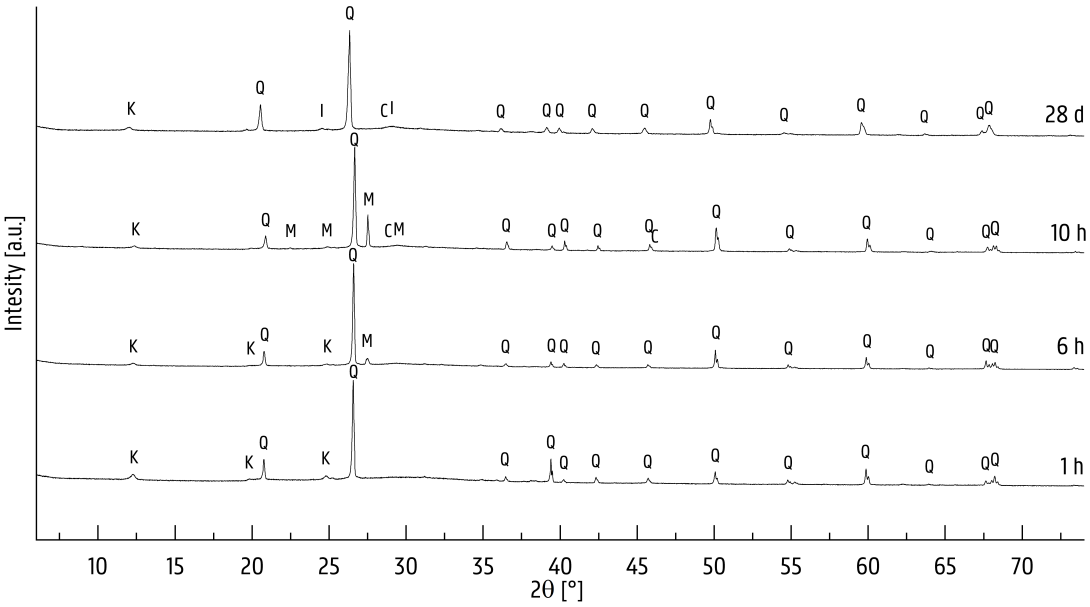

Figure 7.9: XRD patterns DM8-REF at 1, 6, 10 hours and 28 days

7.4 Variations on reference mix

Several factors can influence the final product, as discussed in Section 2.10. These variables include interactions between the source materials, the source materials themselves, and the conditions under which the samples are cured. In the following sections, some of these will be altered to analyze their influence on the early-age properties relative to DM8-REF.

7.4.1 Impact of ambient curing

Table 7.3 shows the results of the early-age properties of the samples subjected to ambient curing. Figures 7.10a and 7.10b compare the compressive and flexural strength, with the reference, which is cured first at elevated temperature of 70°C for 24 hours and then for the additional 27 days at ambient temperature.

It is important to mention that all of the DM8-28.S.AMB samples were only cured at ambient temperature. A significant disadvantage of ambient curing is that it takes longer to reach the final strength of the samples compared to other curing methods. In spite of the longer curing time, the samples had fewer cracks when compared to oven-cured samples.

A possible explanation for the reduced number of observed cracks in ambient cured samples, compared to samples cured at elevated temperature, is the absence of thermal shock after removing them from the moulds. Such thermal shock can increase the likelihood of cracking and reduce the flexural strength of the samples. The lack of thermal cracks during ambient curing might also contribute to the lower overall smaller margins of error for these samples.

Table 7.3: Early-age mechanical properties of DM8-28.S.AMB mixtures

		Absolute values			Relative values to 28 days			Sample info	
	Age	$\sigma_{c,avg}$ [MPa]	$\sigma_{f,avg}$ [MPa]	S.G. [-]	$\sigma_{c,avg}$ [%]	$\sigma_{f,avg}$ [%]	S.G. [%]	Batch nr.[1]	# Samples $_{c;f}$
DM8-28.S.AMB	0 h	-	-	2,17 ± 0,02	-	-	99,1 ± 1,0	-	-
	2 h	2,2 ± 0,1	0,5 ± 0,1	2,08 ± 0,02	3,1 ± 0,2	7,1 ± 0,5	95,0 ±1,1	31	6 ; 3
	4 h	4,8 ± 0,2	0,7 ± 0,1	2,19 ± 0,03	6,7 ± 0,3	10,3 ± 0,8	100,0 ± 1,4	15	6 ; 3
	8 h	6,6 ± 0,2	0,9 ± 0,1	2,18 ± 0,01	9,2 ± 0,4	11,8 ± 1,3	99,5 ± 0,6	15	6 ; 3
	12 h	7,4 ± 0,4	0,9 ± 0,1	2,18 ± 0,01	10,4 ± 0,6	12,9 ± 1,1	99,5 ± 0,7	13 ; 31	12 ; 5
	24 h	13,3 ± 0,2	1,6 ± 0,1	2,17 ± 0,03	18,6 ± 0,5	21,9 ± 2,0	99,1 ± 1,5	13	6 ; 3
	28 d	71,2 ± 1,6	7,2 ± 0,4	2,19 ± 0,01	100,0 ± 3,2	100,0 ± 7,1	100,0 ± 0,6	21	5 ; 3

[1] Batch numbers associated to Table 7.1

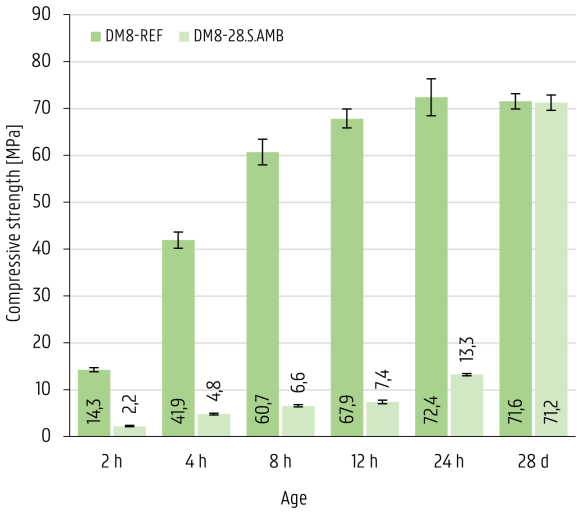

(a) Compressive strength DM8-REF & DM8-28.S.AMB

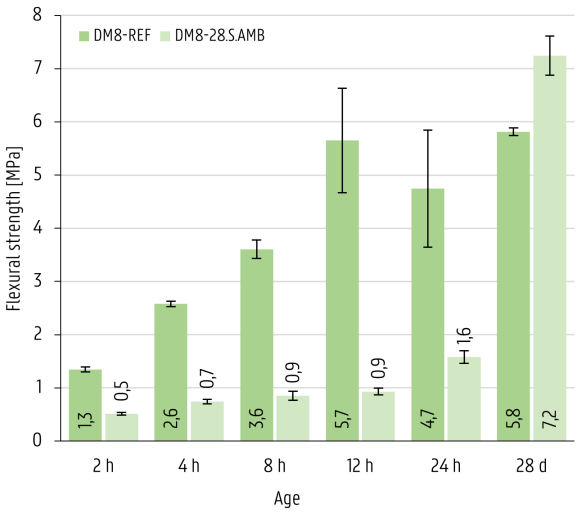

(b) Flexural strength DM8-REF & DM8-28.S.AMB

Figure 7.10: Results mix with ambient curing (DM8-28.S.AMB) cf. reference mix (DM8-REF)

To evaluate the effect of curing at an elevated temperature on the first day on the mineralogy, both curing temperatures were analysed by XRD. Figure 7.11 displays the XRD patterns of the analysed samples after 28 days of curing. The phases detected in both DM8-REF and DM8-28.S.AMB are mainly quartz with small traces of kaolinite, illite and calcite. No other or unexpected phases are identified. Some additional peaks of the mentioned phases are detected, but this could be specific to the sample, sample preparation and sensitivity of the analysis software. From this initial and limited analysis can be concluded that curing at 70°C for the first 24 hours does not significantly affect the mineralogy. However, further investigation is required to also examine the difference in amorphous content to fully confirm that curing at an elevated temperature during the first 24 hours does not affect the structure.

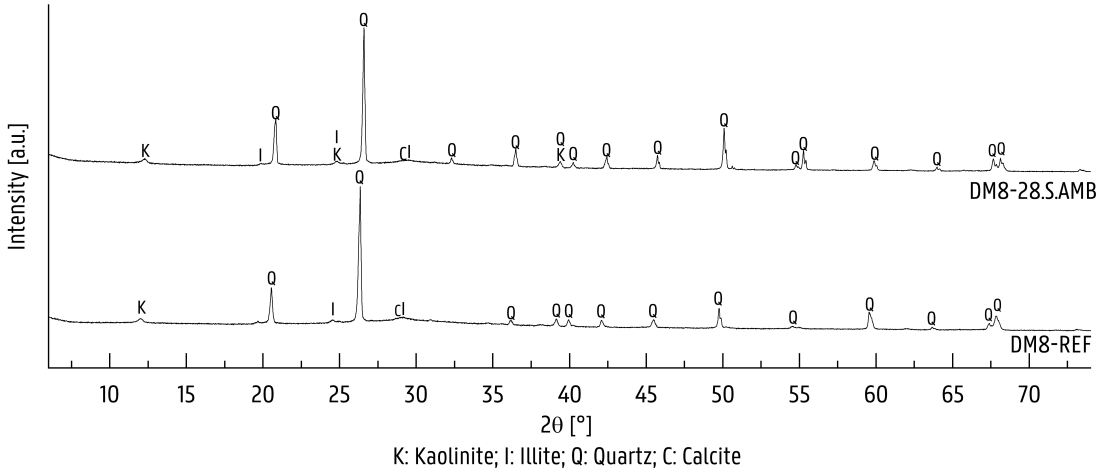

Figure 7.11: XRD patterns DM8-REF & DM8-28.S.AMB at 28 days

7.4.2 Impact of different long-term curing conditions

The mechanical properties of DM8 mixtures with various curing conditions are shown in Table 7.4. At 28 days, four different curing methods are observed. The first preservation method is the reference curing, in which the sample is cured for 24 hours at 70°C and then cured for another 27 days at ambient temperature. All the samples are always sealed to avoid premature water evaporation, unless mentioned otherwise. The second curing method is the same as the reference method, but the sample is unsealed after 24 hours and then cured for 27 days at ambient temperature ((RH $\simeq$ 50%). The third method includes curing the samples in elevated temperatures at 70°C for 28 days. The final preservation method is the curing for 28 days at ambient temperature, also referred to as ambient curing.

Table 7.4: Early-age mechanical properties of DM8 mixtures with different long term curing methods

		Absolute values			**Sample info**	
Curing method	Age	$\sigma_{c,avg}$ [MPa]	$\sigma_{f,avg}$ [MPa]	S.G. [-]	Batch nr.[1]	# Samples $_{c\,;\,f}$
DM8-REF	28 d	71,6 $\pm$ 1,7	5,8 $\pm$ 0,1	2,17 $\pm$ 0,01	28	6 ; 3
DM8-1.S-70°C-27.U.AMB	28 d	60,3 $\pm$ 3,3	2,9 $\pm$ 1,0	2,11 $\pm$ 0,01	21	6 ; 3
DM8-28.S.70°C	28 d	55,6 $\pm$ 2,2	5,1 $\pm$ 0,2	2,09 $\pm$ 0,03	30	6 ; 3
DM8-28.S.AMB	28 d	71,2 $\pm$ 1,6	7,2 $\pm$ 0,4	2,19 $\pm$ 0,01	21	6 ; 3

[1] Batch numbers associated to Table 7.1

Figures 7.12a and 7.12b illustrate the effect of various long-term curing methods on the final strength. When cured for 28 days at 70°C, the compressive strength is the lowest (55,6 MPa), followed by the second method (60,3 MPa). The reference and ambient curing are the strongest. The second method achieves the lowest flexural strength values (2,9 MPa), followed by 28 days at 70°C cured samples and reference mix. Overall, the ambient cured samples perform the best. The absence of thermal cracks is most likely to be responsible for the higher performance of these ambient cured samples. Furthermore, when the samples are unsealed, the water evaporates much faster, resulting in more shrinkage cracks. These cracks were also visible on these samples.

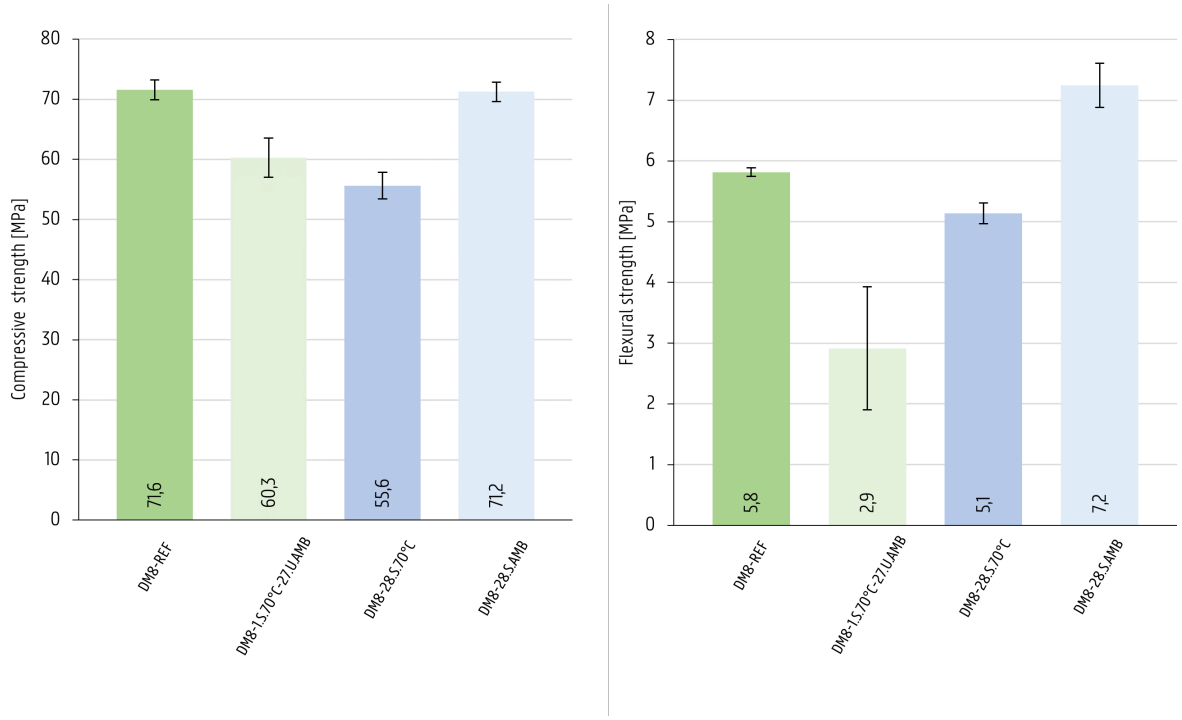

(a) Compressive strength various long-term curing methods

(b) Flexural strength various long-term curing methods

Figure 7.12: Results mix with different long term curing methods at 28 days

Figure 7.13 shows the effect of different long-term curing conditions on the mineralogy. Based on the samples, the analyses show that there are no other phases identified when the samples are, for example, cured at 70°C for 28 days. However, it can be visually observed for DM8-1.S.70°C that these peaks are more flattened out and its seems that the amorphous content is less present compared to the other long-term conditions. Some peaks show different phases within the feldspar group, but these observations are not irregular with the previous XRD patterns in Section 7.3. Further research is required to fully understand the effect of different long-term curing conditions on the mineralogy and microstructure. As DM8-28.S.70°C showed the poorest performance, there may be some defects or irregularities in the structure. In order to investigate the effect of different curing methods on the detected phases and amorphous content, extra research is required. It is recommended to extend the range of samples and to include other techniques.

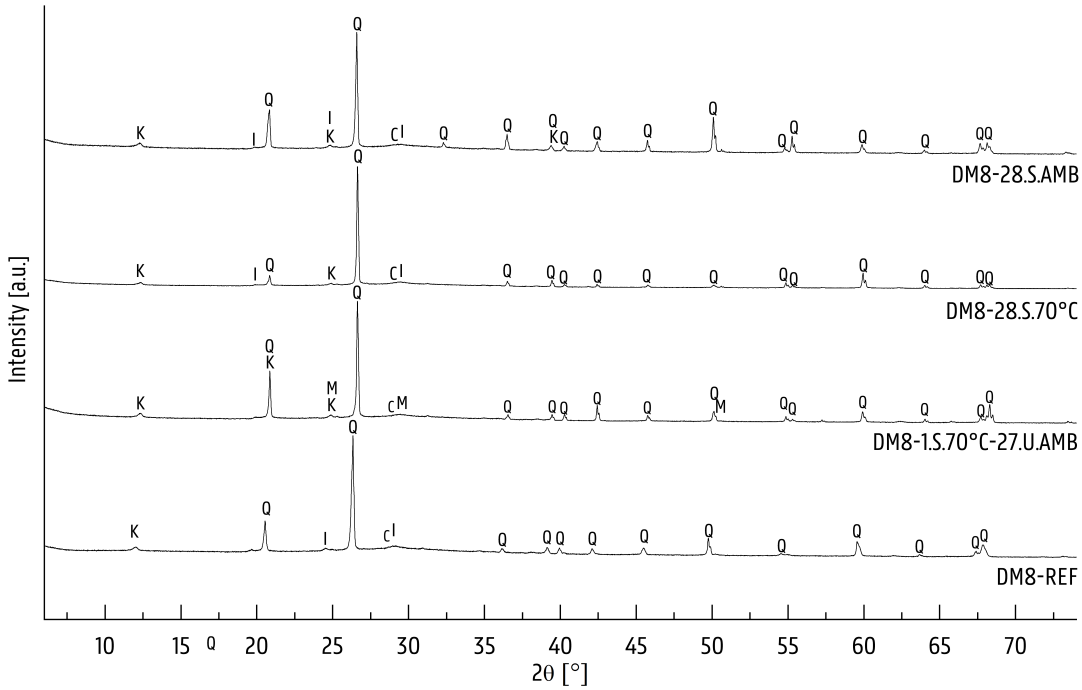

K: Kaolinite; I: Illite; Q: Quartz M: Microcline; C: Calcite

Figure 7.13: XRD patterns DM8 with different long term curing conditions

7.4.3 Impact of assumed slag reactivity

Different mix designs are made based on different assumptions about the active Al_2O_3 in GGBFS. Table 7.5 shows that the assumed reactivity affects the density and workability of the batches, as the mix design is adjusted according to the reactivity. More batches are needed to draw conclusions about the actual effect on workability and density.

Table 7.5: Fresh properties of DM8-R batches

			Density of mix		**Workability**[1]	
	Mix	Date	ρ [kg/m³]	S.G. [-]	D_{avg} [cm]	F_{avg} [-]
DM8-R	R30	23/04/23	2 220	2,20	23,00	130,00
	R40	23/04/23	2 170	2,17	23,75	137,50
	R70	23/04/23	2 190	2,19	23,38	133,75

[1] Tested with Hägermann flow table according to EN 1015-3

Table 7.6 shows the measured properties of the mixes with various assumed reactivity of Al_2O_3 in GGBFS. After four hours and 24 hours of elevated curing, the mixes are tested, which corresponds to the midpoint of the rapid strength increase and when the strength of DM8-REF is fully developed. These values are shown in Figure 7.14a and compared to the DM8-REF results. The assumed reactivity influences strength development, which is already noticeable in the early stages and increases with time. Based on the results, the mix with an assumed reactivity of 40% showed the best performance of compressive strength with 88,7 MPa after 24 hours, but the mix with 30% reactivity performed the best in terms flexural strength with a value of 7,1 MPa. The reference mix, which assumed a reactivity of 50%, performed the worst compared to the other mixes.

These results indicate that an accurate assumption of the active Al_2O_3 in the GGBFS used is a critical factor that significantly impacts the final result. Although the differences in mix proportions are minimal, a few grams per cubic meter, the final results vary considerably, highlighting the sensitivity of geopolymer chemistry and the importance of accurate resource quantification.

Table 7.6: Early-age mechanical properties of DM8-R mixtures

			Absolute values			Sample info	
	Age	Reactivity Al_2O_3	$\sigma_{c,avg}$ [MPa]	$\sigma_{f,avg}$ [MPa]	S.G. [-]	Mix[1]	# Samples $_{c\,;\,f}$
DM8-R	4 h	30	42,2 ± 0,8	2,7 ± 0,2	2,15 ± 0,01	R30	6 ; 3
	24 h	30	78,1 ± 2,7	6,7 ± 0,3	2,15 ± 0,01	R30	6 ; 3
	4 h	40	45,6 ± 1,1	2,5 ± 0,1	2,21 ± 0,03	R40	6 ; 3
	24 h	40	88,1 ± 4,2	6,3 ± 0,3	2,18 ± 0,02	R40	6 ; 3
	4 h	70	45,7 ± 1,2	2,3 ± 0,6	2,20 ± 0,01	R70	6 ; 3
	24 h	70	80,3 ± 2,2	6,2 ± 0,2	2,16 ± 0,02	R70	6 ; 3

[1] Mixes associated to Table 7.5

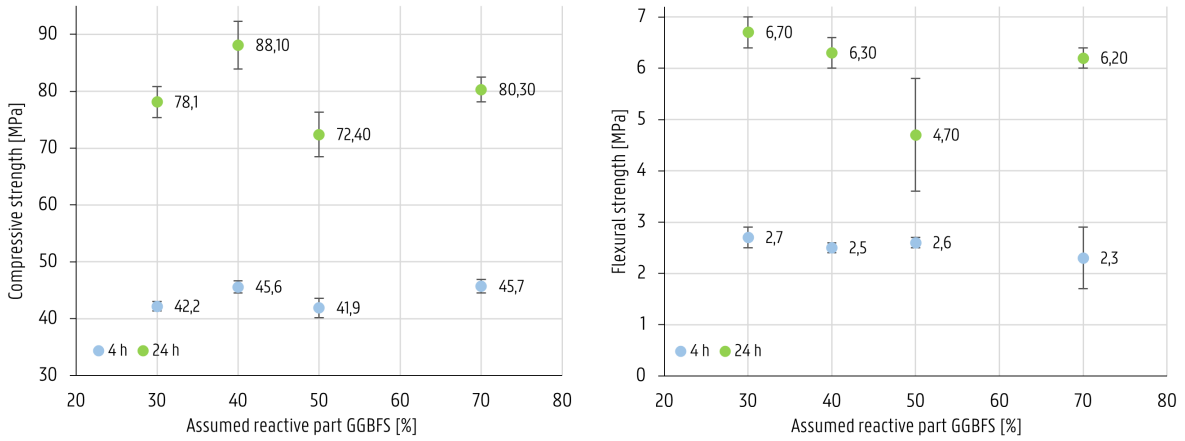

(a) Compressive strength DM8-R

(b) Flexural strength DM8-R

Figure 7.14: Results mix with different assumed reactivity of GGBFS

7.4.4 Impact of non-standard distributed sand

Table 7.7 shows the effect of replacing the CEN sand by the 0/2 sand on the measured density and workability. When compared to the reference mix in Table 7.1, it is clear that it has a slight effect on the fresh properties of DM8-0/2. DM8-0/2 has a fresh S.G. of 2,12, while the reference mix has a higher S.G. of 2,17. It is also noted that the mix with the 0/2 sand has a lower workability than the reference mix.

The difference in workability can be explained by the presence of more fine particles compared to the CEN sand, as concluded by the sieving analysis in Section 4.3.3. This can also be visually interpreted from the images of both types of sand shown in Figures 7.15a and 7.15b.This grain size has a large influence on the water demand, which also contributes to the lower workability. The lower density of DM8-0/2 is most likely explained by the lower density of the 0/2 sand itself.

Table 7.7: Fresh properties of DM8-0/2 batches

	Batch nr.	Date	Density of mix		Workability[1]	
			ρ [kg/m³]	S.G. [-]	D_{avg} [cm]	F_{avg} [-]
DM8-0/2	14	24/03/23	2 118,15	2,12	20,50	105,00
	16	24/03/23	2 113,69	2,11	20,75	107,50
	22	26/03/23	2 122,79	2,12	19,75	97,50
	Average		**2 120**	**2,12**	**20,33**	**103,33**

[1] Tested with Hägermann flow table according to EN 1015-3

(a) Microscopical image CEN sand

(b) Microscopical image 0/2 sand

Figure 7.15: Visual difference between CEN and 0/2 sand captured by digital microscope

The effect of replacing the CEN sand with 0/2 sand is not only seen in the fresh properties, but also in the hardened properties of the mix. The measured mechanical properties of these samples are displayed in Table 7.8. The results of the DM8-0/2 samples are compared to the reference mix in Figures 7.16a and 7.16b. Based on the comparison is concluded that the DM8-0/2 samples outperform the CEN sand samples. The improved strength is not significant at the early ages, but it is when final strengths are considered. This can be explained by the presence of a higher percentage of fine particles in the 0/2 sand. More fine grains in the grain size distribution equals to a higher contact area within the mix, this contributes to the high strength as in high strength concrete [234].

Table 7.8: Early-age mechanical properties of DM8-0/2 mixtures

	Age	Absolute values			Relative values to 28 days			Sample info	
		$\sigma_{c,avg}$ [MPa]	$\sigma_{f,avg}$ [MPa]	S.G. [-]	$\sigma_{c,avg}$ [%]	$\sigma_{f,avg}$ [%]	S.G. [%]	Batch nr.[1]	# Samples $_{c;f}$
DM8-0/2	0 h	-	-	2,12 ± 0,01	-	-	98,5 ± 1,2	-	-
	2 h	20,8 ± 0,2	1,3 ± 0,1	2,14 ± 0,02	25,3 ± 0,8	18,3 ± 2,7	99,5 ± 1,6	22	6 ; 3
	4 h	46,7 ± 1,3	2,8 ± 0,1	2,17 ± 0,05	57,0 ± 2,3	38,9 ± 5,5	100,9 ± 2,7	16	6 ; 3
	8 h	61,4 ± 2,2	4,8 ± 1,0	2,14 ± 0,02	74,8 ± 3,4	65,2 ± 16,0	99,5 ± 1,4	16	6 ; 3
	12 h	70,4 ± 1,8	5,4 ± 0,7	2,11 ± 0,01	85,8 ± 3,3	73,5 ± 13,6	98,1 ± 1,3	14	5 ; 3
	24 h	83,1 ± 3,5	7,8 ± 1,0	2,14 ± 0,04	101,3 ± 5,2	106,9 ± 20,0	98,6 ± 2,0	14	6 ; 3
	28 d	82,1 ± 2,4	7,3 ± 1,0	2,15 ± 0,03	100,0 ± 4,1	100,0 ± 19,1	100,0 ± 1,7	22	6 ; 3

[1] Batch numbers associated to Table 7.7

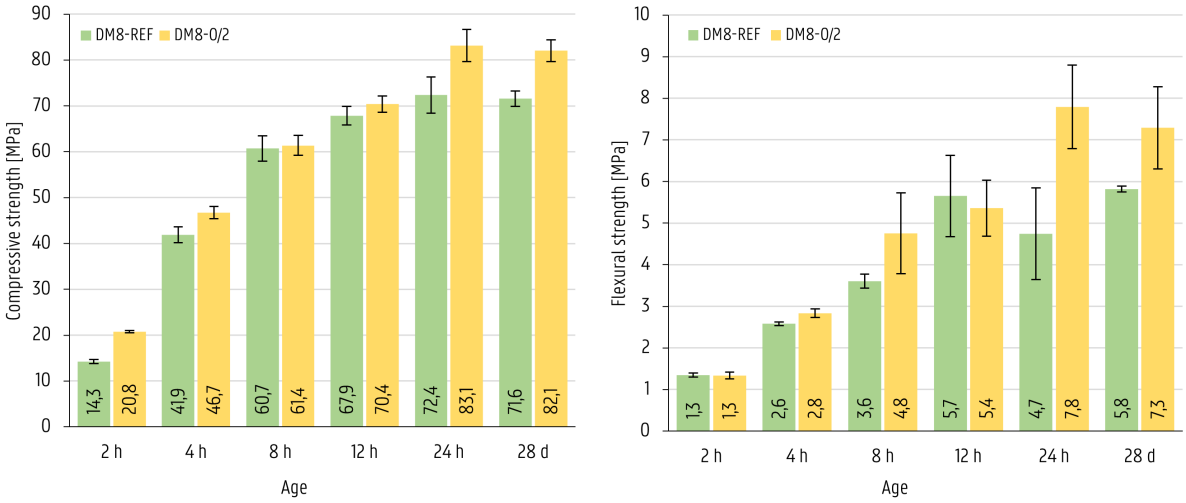

(a) Compressive strength DM8-REF & DM8-0/2

(b) Flexural strength DM8-REF & DM8-0/2

Figure 7.16: Results mix with non-standard distributed sand (DM8-0/2) cf. reference mix (DM8-REF)

Figure 7.17 displays the XRD pattern of DM8-0/2 and shows some additional peaks compared to the reference. As mentioned before, the analysis is very specific to the sample, the sample preparation and the analysis itself. The majority of the identified phases still remain quartz with some traces of kaolinite and the usual feldspar minerals (illite and microcline). However, compared to the reference, albite has been identified instead of calcite. Albite ($NaAlSi_3O_8$) is another type of feldspar and is not unexpected since is commonly found in Scandinavian soils and sediments. Other research concluded that concrete with albite rocks showed the highest mechanical properties [235, 236]. In addition to the smaller grains, the increased mechanical properties may also be due to the presence of albite in the 0/2 sand, but further research is required to confirm this hypothesis and the long term effect of its presence.

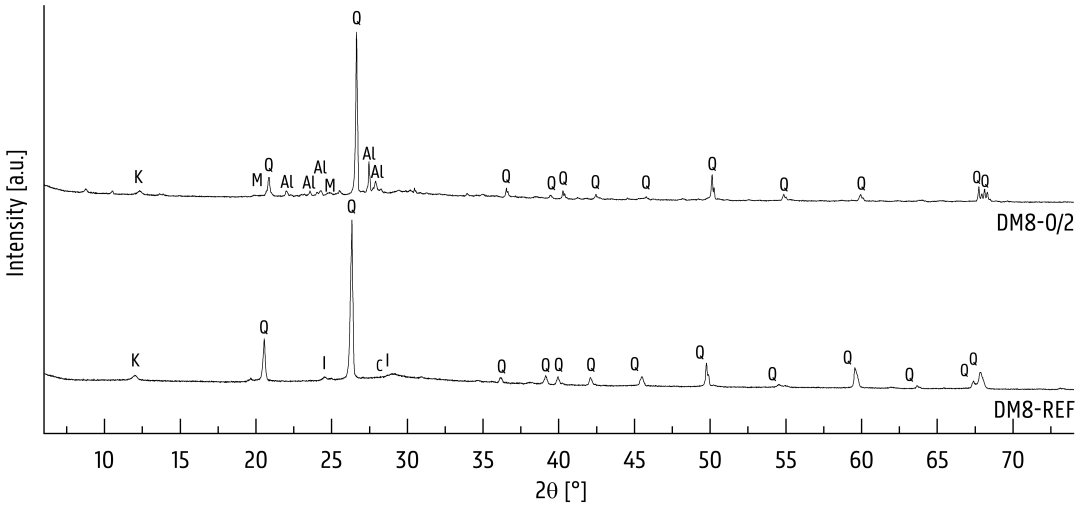

K: Kaolinite; M: Microline; Al: Albite; I Illite

Figure 7.17: XRD patterns DM8-REF & DM8-0/2 at 28 days

8

Influence of using alternative waste materials

In this chapter, an initial analysis is made to evaluate the influence of several alternative waste materials on the development of early-age properties, compared to the reference mix, and their potential as resources for geopolymers. The analysis is carried out by examining the final strengths, its development over time and any changes in mineralogy. This provides a first attempt in understanding how these alternative waste materials affect the mechanism of geopolymerization.

8.1 Influence of waste wood ash as precursor

As mentioned in Section 6.1.1, waste wood ash has great potential as a precursor due to its abundance and wide availability. An attempt was made to develop a geopolymer by replacing 50% of the ground granulated blast-furnace slag with waste wood ash. Of the ashes measured, WWA 2 showed the most favorable physical properties, with a specific surface area similar to that of GGBFS, which initially indicated a comparable water requirement and workability. However, due to the high pH level, which averaged 13,48 as measured by a pH electrode, the mix exhibited flash setting and caused difficulties in terms of workability and filling the moulds. No further testing was performed with WWA 1, its high water demand and poor chemical composition was not beneficial for the mixes.

Table 8.1 shows the measured results of the attempts of partially replacing GGBFS by WWA. After 24 hours of elevated curing a compressive and flexural strengths of 50,8 MPa and 4,8 MPa, respectively, were measured. Additional information on the tested prisms and corresponding measured strengths, including the other ones discussed in this chapter, can be found in Appendix K.2. Figure 8.1 visualizes the effect of using WWA by comparing the measured strengths with the reference mix for elevated and ambient curing. A lower compressive strength can initially be explained by the voids in the prisms as a result of poor workability and flash setting. The prisms were not compacted as much as they should have because the initial setting time didn't allow it. The measured compressive strength after ambient curing is proportional to that of the reference mix. The flexural strengths, both for elevated and ambient curing, showed proportionally comparable results.

Table 8.1: Early-age mechanical properties of DM8-WWA mixtures with different curing methods

			Absolute values			**Sample info**	
	Mix nr.[1]	Age	$\sigma_{c,avg}$ [MPa]	$\sigma_{f,avg}$ [MPa]	S.G. [-]	Curing	# Samples $_{c\,;\,f}$
DM8-WWA	WWA2.1	24 h	50,8 $\pm$ 1,4	4,9 $\pm$ 0,1	2,14 $\pm$ 0,01	1.S.70°C	6 ; 3
	WWA2.2	24 h	12,0 $\pm$ 0,9	1,9 $\pm$ 0,1	2,15 $\pm$ 0,02	1.S.AMB	6 ; 3

[1] Mix numbers associated to Table 6.2

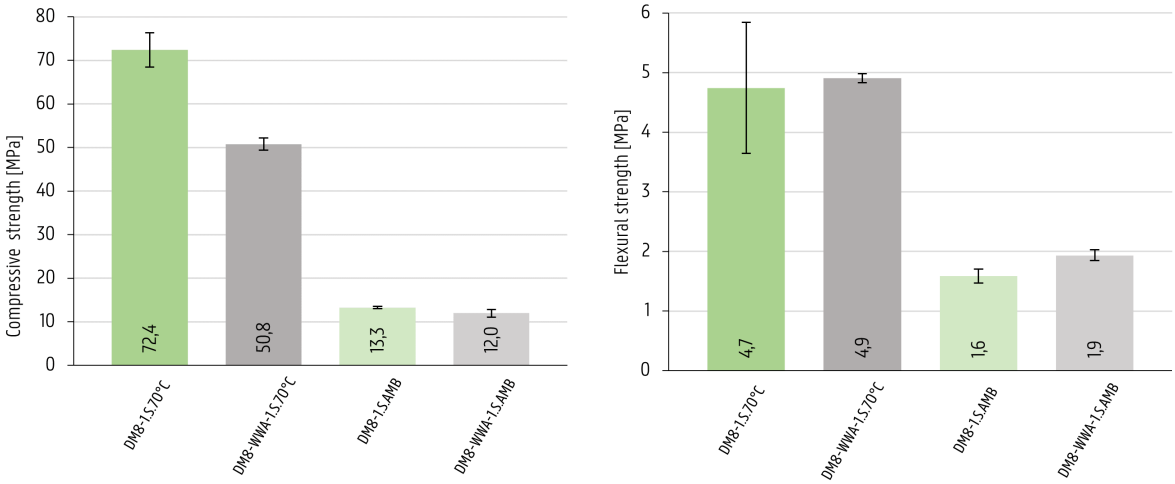

(a) Compressive strength DM8-REF & DM8-WWA

(b) Flexural strength DM8-REF & DM8-WWA

Figure 8.1: Results mixes with waste wood ash as precursor (DM8-WWA) cf. reference mix (DM8-REF) at 24 hours

In Figure 8.2, the XRD pattern of the mix with WWA is compared to the reference after 24 hours of elevated curing. The majority of phases detected in DM8-WWA is also quartz, but compared to DM8-REF there are also minor traces of arcanite identified instead of the feldspar mineral microcline. According to literature, arcanite (K_2SO_4) is commonly found in organic or wood ashes and is not unexpected due to the high potassium and sulfur detected in WWA 2 [237, 238].

This analysis indicates that there is potential in integrating waste wood ash as a precursor, but further research is needed to resolve the flash setting. The effect on mineralogy, absence of detected microcline and additional arcanite requires further evaluation. If the WWA should contain heavy metals, then long-term evaluation is also needed to determine the potential environmental impact of them leaching from the GPC into water or soil.

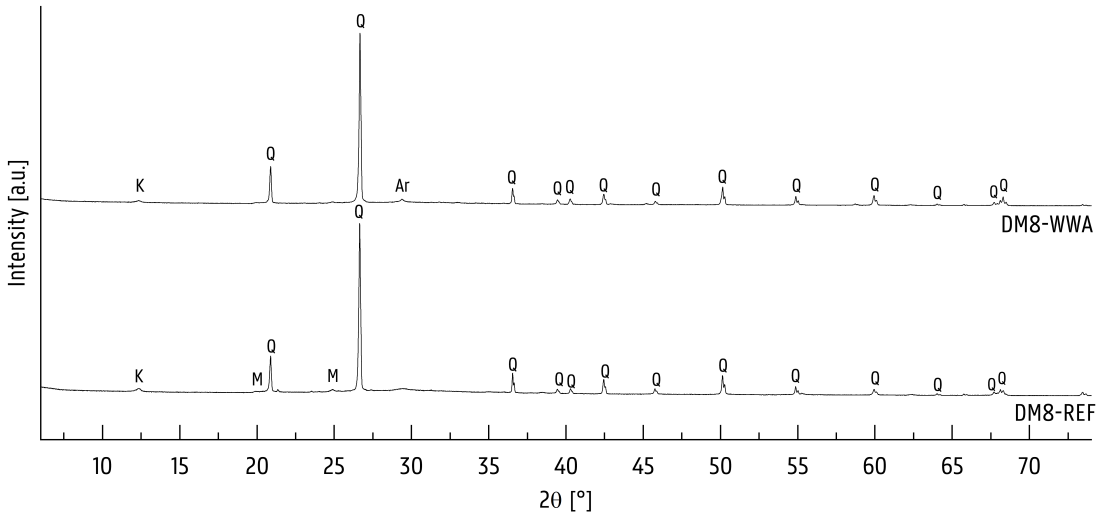

K: Kaolinite; M: Microcline; Q: Quartz; Ar: Arcanite

Figure 8.2: XRD patterns DM8-REF & DM8-WWA at 24 hours

8.2 Influence of recycled aggregates

The effect of the recycled aggregates (RA) can have a significant impact on the fresh properties of the mix as well as the mechanical properties of the hardened samples. To determine the effect, two different types of recycled aggregates, RCA and RGA, are used. They are distributed according to the EN 196-1 standard grain distribution, this in order to minimize the variables compared to the reference mix. In addition these mixes are also cured under reference curing conditions. The origin of the aggregates and some extra additional water to improve workability are the only variables. Tables 8.2 and 8.3 show the effect of RA on the measured density and workability. Both of the mixes are lighter compared to the reference mix, but DM8-RGA is the lightest because RGA fines are initially lighter than RCA fines.

Table 8.2: Fresh properties of DM8-RCA batches

			Density of mix		**Workability**[1]	
	Batch nr.	Date	ρ [kg/m³]	S.G. [-]	D_{avg} [cm]	F_{avg} [-]
DM8-RCA	18	25/03/23	2 154,92	2,15	13,88	38,75
	20	25/03/23	2 133,09	2,13	14,00	40,00
	29	28/03/23	2 129,61	2,13	17,00	70,00
Average			**2 140**	**2,14**	**14,96**	**49,58**

[1] Tested with Hägermann flow table according to EN 1015-3

Table 8.3: Fresh properties of DM8-RGA batches

			Density of mix		**Workability**[1]	
	Batch nr.	Date	ρ [kg/m³]	S.G. [-]	D_{avg} [cm]	F_{avg} [-]
DM8-RGA	17	25/03/23	2 031,25	2,03	18,63	86,25
	19	25/03/23	2 042,01	2,04	19,75	97,50
	23	26/03/23	2 036,64	2,04	18,63	86,25
Average			**2 040**	**2,04**	**19,00**	**90,00**

[1] Tested with Hägermann flow table according to EN 1015-3

Both the DM8-RCA and DM8-RGA mixes have a lower workability than the reference mix, which is not uncommon according to the literature [223, 224]. This results from a higher water demand of the recycled fines and the different grain shapes compared to natural aggregates. This is the main reason why the fine fraction of RCA are rarely used as aggregates in concrete, while coarse recycled aggregates are already used in combination with natural aggregates to some extent [223, 224]. The difference between the used recycled aggregates and the CEN Sand (natural aggregates) can be seen in Figure 8.3a. Both the recycled aggregates are more angular, and the difference in shape between RCA and RGA may be due to a different crushing method. In addition to the grain shape, there is less binder paste attached to the original sand of the RGA grains (Figure 8.3) compared to the RCA grains shown in Figure 8.3b. The presence of this paste on the aggregates can have a beneficial effect in the interfacial transition zone, where the geopolymer paste bonds with the aggregates, and can even lead to higher strengths.

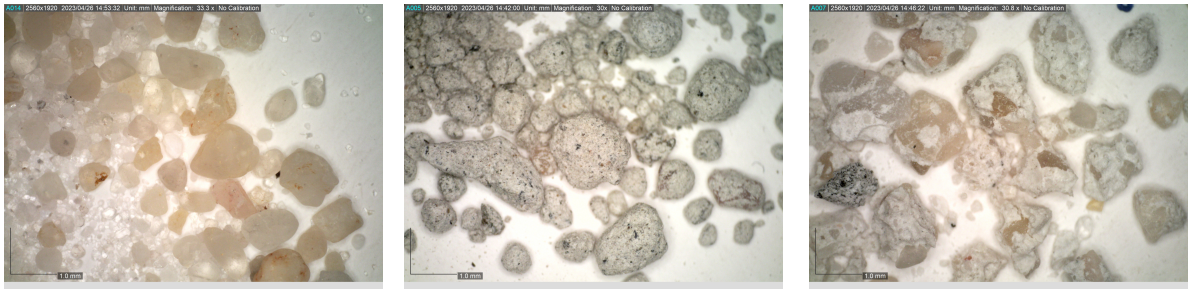

(a) Grain shape CEN Sand (b) Grain shape RCA (c) Grain shape RGA

Figure 8.3: Visual difference of grain shape CEN sand, RCA and RGA

Tables 8.4 and 8.5 show the early-age mechanical properties of the RCA and RGA mixes respectively. The use of recycled aggregates and the addition of water to improve workability has a direct effect on the achieved compressive strength but not on the flexural strength. Even with a higher W/S ratio, DM8-RCA performs almost as well as the reference mix.

Figure 8.4 compares the development and final strength of the mixes containing RA with the reference mix. While the strength development is slower in both cases, the development of DM8-RGA appears to be even slower than the others. This may be due to some residual chemical components in the RGA that slow down the reaction rate, but this needs to be confirmed by further research. The mixes containing recycled aggregates show improved flexural strength due to the angular shape of the grains. The angular shape allows for better interlocking and therefore stronger bonds compared to a mix with rounded grains.

Table 8.4: Early-age mechanical properties of DM8-RCA mixtures

		Absolute values			Relative values to 28 days			Sample info	
	Age	$\sigma_{c,avg}$ [MPa]	$\sigma_{f,avg}$ [MPa]	S.G. [-]	$\sigma_{c,avg}$ [%]	$\sigma_{f,avg}$ [%]	S.G. [%]	Batch nr.[1]	# Samples $_{c\,;\,f}$
DM8-RCA	0 h	-	-	2,14 ± 0,01	-	-	100,4 ± 0,7	-	-
	2 h	10,7 ± 0,1	1,8 ± 0,2	2,10 ± 0,02	16,3 ± 0,3	19,8 ± 2,3	98,6 ± 1,0	29	6 ; 3
	4 h	16,7 ± 0,3	2,5 ± 0,2	2,13 ± 0,01	25,4 ± 0,6	29,2 ± 2,8	100,0 ± 0,4	20	6 ; 3
	8 h	45,5 ± 1,4	3,6 ± 0,5	2,14 ± 0,01	69,3 ± 2,3	39,8 ± 6,2	100,5 ± 0,6	20	6 ; 3
	12 h	53,4 ± 2,3	5,4 ± 0,7	2,13 ± 0,01	81,4 ± 3,7	60,0 ± 8,5	100,0 ± 0,6	18	6 ; 3
	24 h	60,9 ± 1,7	7,2 ± 0,5	2,15 ± 0,01	92,9 ± 2,9	79,5 ± 7,1	100,9 ± 0,6	18	6 ; 3
	28 d	65,6 ± 0,9	9,0 ± 0,5	2,13 ± 0,01	100,0 ± 2,0	100,0 ± 8,4	100,0 ± 0,6	29	6 ; 3

[1] Batch numbers associated to Table 8.2

Table 8.5: Early-age mechanical properties of DM8-RGA mixtures

		Absolute values			Relative values to 28 days			Sample info	
	Age	$\sigma_{c,avg}$ [MPa]	$\sigma_{f,avg}$ [MPa]	S.G. [-]	$\sigma_{c,avg}$ [%]	$\sigma_{f,avg}$ [%]	S.G. [%]	Batch nr.[1]	# Samples $_{c\,;\,f}$
DM8-RGA	0 h	-	-	2,04 ± 0,01	-	-	98,9 ± 1,1	-	-
	2 h	6,6 ± 0,2	1,3 ± 0,1	2,02 ± 0,02	11,6 ± 0,5	16,6 ± 0,9	98,1 ± 1,4	23	6 ; 3
	4 h	23,3 ± 0,4	2,9 ± 0,1	2,04 ± 0,02	41,1 ± 1,1	37,5 ± 2,0	99,0 ± 1,6	19	6 ; 3
	8 h	48,5 ± 1,4	3,2 ± 0,2	2,04± 0,01	85,6 ± 3,0	42,1 ± 2,5	99,0 ± 1,2	19	6 ; 3
	12 h	50,8 ± 1,9	4,1 ± 0,2	2,05 ± 0,02	89,7 ± 3,9	53,6 ± 2,9	99,5 ± 1,5	17	6 ; 3
	24 h	56,9 ± 1,1	5,6 ± 0,5	2,03 ± 0,01	100,4 ± 2,9	73,9 ± 7,2	98,5 ± 1,1	17	6 ; 3
	28 d	56,7 ± 1,5	7,6 ± 0,3	2,06 ± 0,02	100,0 ± 3,4	100,0 ± 4,9	100,0 ± 1,5	23	5 ; 3

[1] Batch numbers associated to Table 8.3

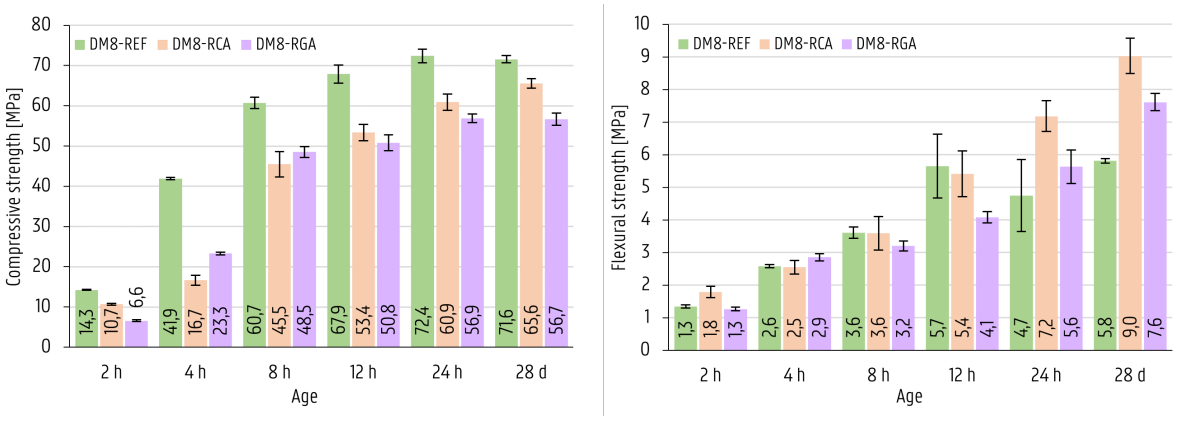

(a) Compressive strength DM8-REF, DM8-RCA & DM8-RGA

(b) Flexural strength DM8-REF, DM8-RCA & DM8-RGA

Figure 8.4: Results mixes with recycled aggregates (DM8-RCA, DM8-RGA) cf. reference mix (DM8-REF)

The XRD patterns of the mixes with different RA, as shown in Figure 8.5, indicate that the majority of the phases detected in the samples are quartz, even when RA are used. In particular, the DM8-RGA pattern has no new peaks and contains additional traces of kaolinite and illite, which are also present in DM8-REF. Analysis of DM8-RCA reveals the presence of new peaks, identified as anorthite ($CaAl_2Si_2O_8$), phlogopite ($KMg_3AlSi_3O_{10}F$) and calcium-silicate-hydrate (CSH), which are not detected in other mix. The improved performance of DM8-RCA compared to DM8-RGA may be explained by the presence of these phases which, given the composition, are likely to be present in the grains of RCA. The increased performance of DM8-RGA might be due to the presence of CSH in the geopolymer. Further research is required to confirm whether these additional phases are only present due to the RCA or whether they are also being formed in the during the geopolymerization process and how these phases influence the mechanical properties of GPC.

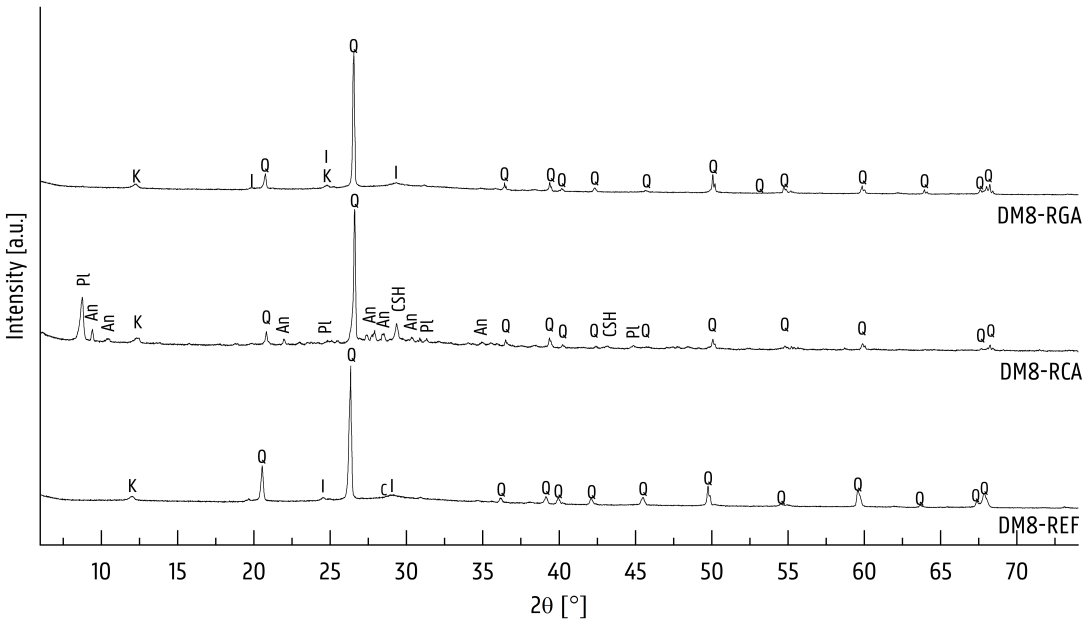

K: Kaolinite; I: Illite; Q: Quartz; An: Anorthite; Pl: Plogopite C: Calcite; CSH: Calcium-Silicate-Hydrate

Figure 8.5: XRD patterns DM8-REF & DM8-RCA, DM8-RGA at 28 days

8.3 Influence of seawater

Table 8.6 shows the measured characteristics of the mixes in which seawater was used instead of additional water. The density of DM8-SW is equal to that of the reference since the specific gravity of seawater is only slightly higher than that of distilled water and the additional water present in the sample is minimal. The literature and measurements confirm, that the presence of salt in the seawater affects the fresh properties, which explains the slightly reduced workability [137, 226, 227].

Table 8.6: Fresh properties of DM8-SW batches

			Density of mix		**Workability**[1]	
	Batch nr.	Date	ρ [kg/m³]	S.G. [-]	D_{avg} [cm]	F_{avg} [-]
DM8-SW	24	26/03/23	2 155,52	2,16	23,38	133,75
	25	26/03/23	2 166,08	2,17	23,13	131,25
	26	27/03/23	2 192,08	2,19	22,50	125,00
	27	27/03/23	2 153,03	2,15	22,25	122,50
Average			**2 170**	**2,17**	**22,81**	**128,13**

[1] Tested with Hägermann flow table according to EN 1015-3

The early-age mechanical properties of DM8-SW are summarized in Table 8.6. The results indicate that the final strength is not significantly affected by replacing the additional water with seawater while curing under reference curing conditions. A comparison with the reference mix is shown in Figure 8.6. It shows that the mix with seawater as additional water has a slightly faster strength development, but reaches a similar strength after full development. This effect could be related to the sodium in seawater, which can affect the SiO_2/Na_2O molar ratio of the activator and thereby increasing reactivity. Thus, the seawater would act as an accelerator to speed up the geopolymerization process. The successful use of seawater and sea sand in GPC has also been successfully demonstrated in previous studies conducted in China. Seawater was even used to produce the SSS, which resulted in slightly reduced workability but had little effect on compressive strength [239].

In addition, the XRD pattern in Figure 8.7 shows no significant changes in mineralogy compared to DM8-REF due to the use of seawater. The illite and microcline phases in DM8-SW have also been detected in other patterns of the reference, as can be seen in Section 7.3. However, additional research is needed to fully understand the impact of seawater on the geopolymerization process, mineralogy and its long-term effects.

Table 8.7: Early-age mechanical properties of DM8-SW mixtures

		Absolute values			**Relative values to 28 days**			**Sample info**	
	Age	$\sigma_{c,avg}$ [MPa]	$\sigma_{f,avg}$ [MPa]	S.G. [-]	$\sigma_{c,avg}$ [%]	$\sigma_{f,avg}$ [%]	S.G. [%]	Batch nr.[1]	# Samples $_{c\,;\,f}$
DM8-SW	0 h	-	-	2,17 ± 0,02	-	-	100,9 ± 1,4	-	-
	2 h	15,3 ± 0,2	1,2 ± 0,1	2,14 ± 0,02	21,7 ± 0,5	21,5 ± 2,5	100,0 ± 1,4	24	6 ; 3
	4 h	48,5 ± 1,2	2,2 ± 0,3	2,16 ± 0,03	69,0 ± 2,1	38,7 ± 5,0	100,9 ± 1,9	24 ; 27	6 ; 5
	8 h	61,8 ± 3,1	3,8 ± 0,2	2,16 ± 0,02	87,9 ± 4,7	66,4 ± 3,7	100,9 ± 1,3	26	6 ; 3
	12 h	71,1 ± 2,0	5,5 ± 0,7	2,21 ± 0,02	101,1 ± 3,3	94,8 ± 13,2	103,3 ± 1,8	26	6 ; 3
	24 h	74,7 ± 2,0	6,3 ± 0,3	2,17 ± 0,02	106,4 ± 3,4	109,8 ± 6,1	101,4 ± 1,4	25	6 ; 3
	28 d	70,3 ± 1,2	5,8 ± 0,2	2,14 ± 0,02	100,0 ± 2,4	100,0 ± 5,2	100,0 ± 1,6	25	6 ; 3

[1] Batch numbers associated to Table 8.6

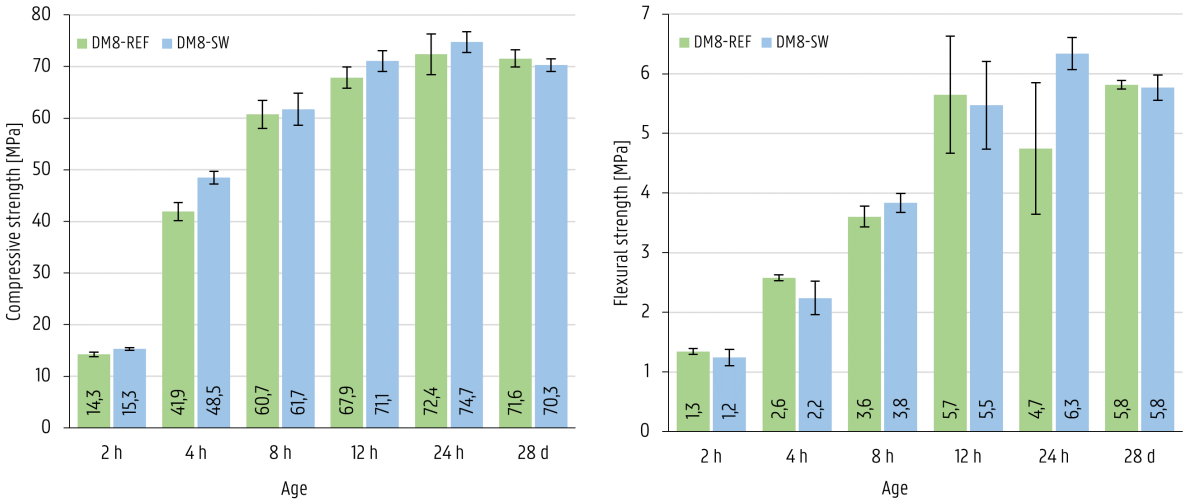

(a) Compressive strength DM8-REF & DM8-SW

(b) Flexural strength DM8-REF & DM8-SW

Figure 8.6: Results mix with seawater (DM8-SW) cf. reference mix (DM8-REF)

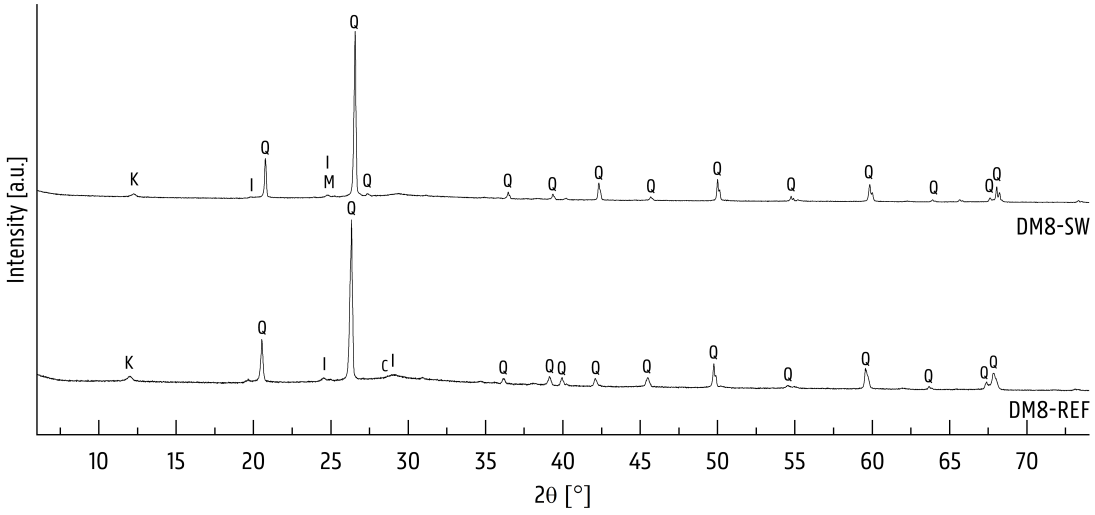

K: Kaolinite; I: Illite; Q: Quartz; M: Microcline; C: Calcite

Figure 8.7: XRD patterns DM8-REF & DM8-SW at 28 days

8.4 Comparative overview impact different waste materials

In this section the impact of various waste materials on each other and on the reference mix are compared. The comparison will be based on two important factors: early-age strength properties and environmental impact. The evaluation of early-age strength properties will provide insight into the beneficial effects of these waste materials in improving the overall strength of the mix. The analysis of their environmental impact, on the other hand, will provide insights into their sustainability and environmental impact.

8.4.1 Effect of using alternative waste materials on early-age properties

The compressive and flexural strengths in Figures 8.8 and 8.9 compare the impact of the various waste streams on the early-age strength development. The strengths are displayed in relation to their strength after 28 days. The use of various alternative waste materials does not only influences the final achieved strength but also the development. It is essential to keep in mind that not all waste materials affect the growth of sample strength in the same way. In this study, the DM8-REF and DM8-SW mixes cure at a faster rate, followed by the RCA and RGA mixes. This initial study shows that the use of alternative waste materials has an effect on the early-age properties of geopolymers.

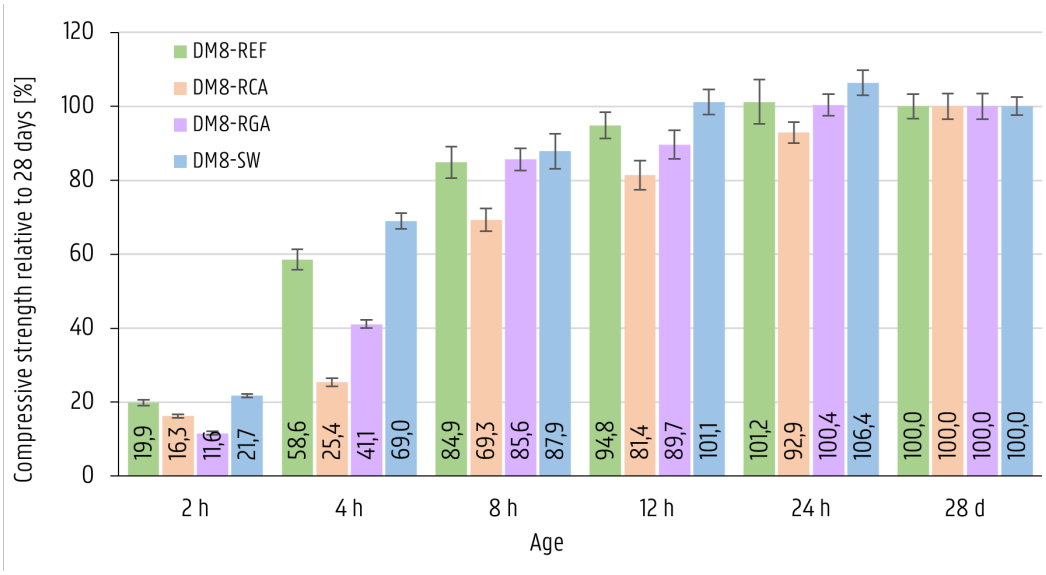

Figure 8.8: Influence of waste streams on the compressive strength

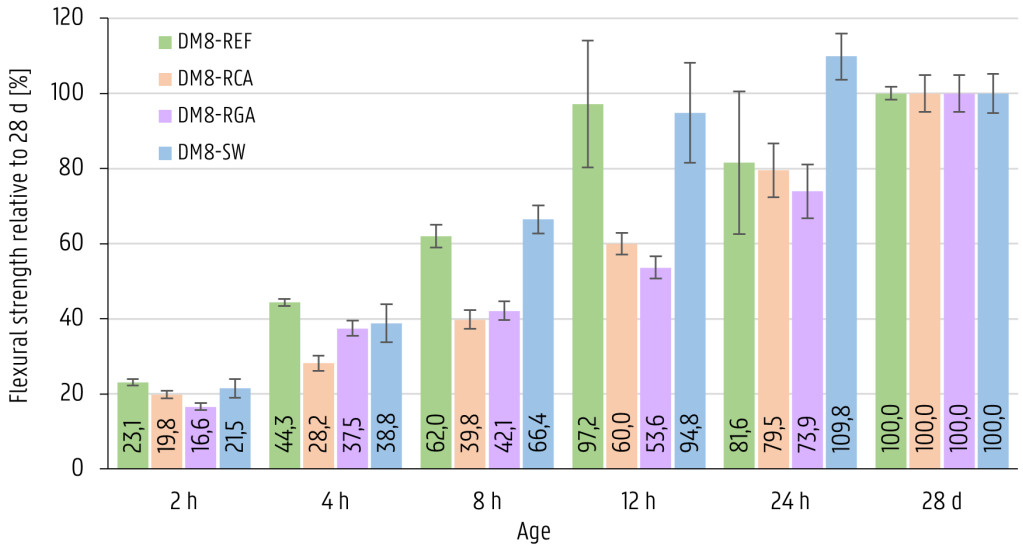

Figure 8.9: Influence of waste streams on the flexural strength

8.4.2 Ecological and environmental effect of using alternative waste materials

In general, it is preferable to be one step ahead of a product's end of life. It is only a win-win situation if waste streams can be used to create new products. Figure 8.10 demonstrates the potential amount of waste materials that can be used in a new GPC mixture. The first is the reference mix, which includes GGBFS and MK, these already account for 24,3 % of waste or industrial by-products. When seawater is added to the mixture as a water replacement or to make the SSS, the amount of waste in the mixture can reach up to 36,5%. When aggregates are replaced with recycled aggregates, the amount of waste increases significantly. When everything is added up, the total amount of waste in the GPC mix is nearly 94%. This shows the huge potential of incorporating waste materials into geopolymer concrete. Not only will this have significant environmental benefits by reducing landfill waste, conserving natural resources and saving energy, it will also significantly reduce the carbon footprint of the construction industry.

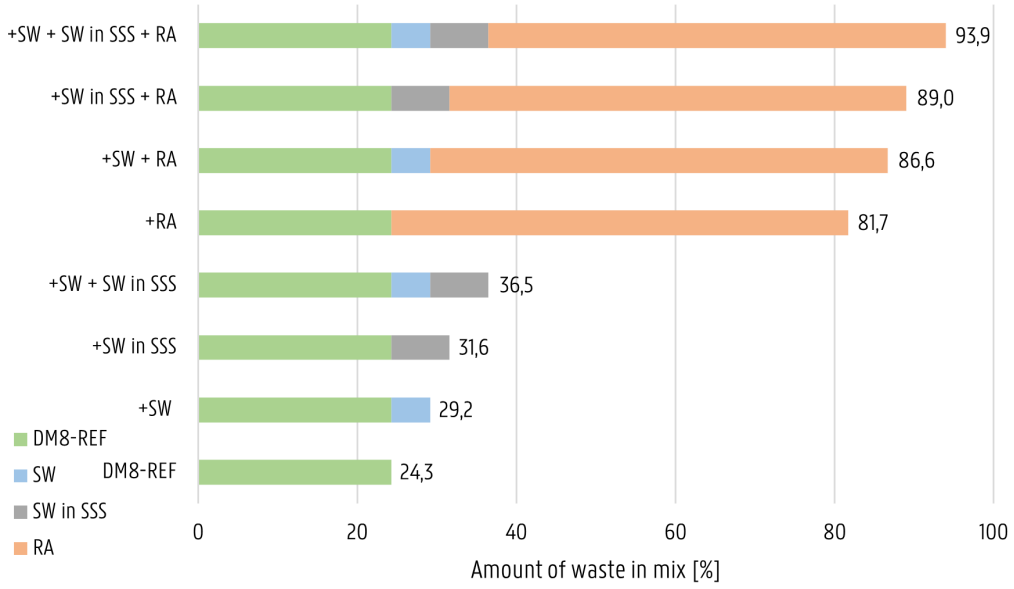

Figure 8.10: Potential amount of waste material in mix

Part IV

Conclusions and Future perspective

Conclusion

This master's thesis investigated the early-age development of geopolymer concrete (GPC) properties using a variety of raw materials or waste and industrial by-products. The main goal was to gain knowledge in the evolution of mineralogical and mechanical properties within the first 24 hours and assess locally available waste and their potential utilization in GPC.

Resource quantification is extremely important because the final product, GPC, is directly affected by the chemical, mineralogical and physical properties of the used resource materials. The chemical properties have a significant impact on the reaction and reaction rate. Analysis of the chemical composition of the used MK, using handheld XRF, demonstrated a dominant amount of SiO_2 and Al_2O_3 in quantities consistent with the literature. Similarly, the GGBFS was found to be mainly composed of CaO, SiO_2, Fe_2O_3 and Al_2O_3, with there sum being slightly lower than the values reported in the literature. XRD analysis detected crystalline and amorphous phases correlating well with the reviewed literature. The composition of steel grit (SG), waste from sandblasting, was mainly SiO_2 and Fe_2O_3. The 2 analysed types of waste wood ash (WWA) were found to be highly variable, mainly influenced by the type of waste wood burned, with a dominant presence of CaO. The results of the measurements with the pH electrode were more accurate and comparable to the literature than the pH strip measurements. The pH of the used MK was 5,1, the pH of the tested GGBFS ranged between pH 9,83 and pH 11,67, the SG had a pH of 9,7 and the pH of WWA was higher. WWA 1 had a pH of 11,1, where WWA 2 a pH had of 13,5, this increases the risk of flash setting.

The physical properties of the resources substantially influence the fresh and hardened properties of GPC. Analysis of the particle size distribution using LDM gave different results for all resources compared to the available TDS, even after optimizing the refractive and absorption indices using the manufacturer's software. The specific surface area affects the water demand of the particles and was determined using both the Blaine method and LDM. Only the results from the Blaine method were considered because they matched technical data sheets (TDS). The specific surface area of MK was 21710 cm^2/g, GGBFS ranges from 4400 to 4710 cm^2/g, WWA ranged from 3290 to 7530 cm^2/g, and SG was much coarser than the others, with 10 cm^2/g. For SG, the density of all materials used ranged between 2,45 and 3,45 g/cm^3. The molar ratio (MR) of the SSS for most of the majority mixes was 1,7%. Also for most of the mixes distilled water is used as additional water, except the mixes where seawater were used.

In this research, a GPC reference mix was developed using MK and GGBFS as precursors and a sodium silicate solution as the geopolymerization initiator. Reference curing was set at 70°C for the first 24 hours in sealed state and then stored at ambient temperature also sealed until the testing. Plastic foil was used to seal the samples at all times to prevent premature condensation. Samples of the GPC reference mix were examined for their mechanical properties and mineralogy in the early stages of curing every hour for 10 hours, followed by bihourly tests up to 24 hours. The results of this indicate that 45% (2,6 MPa) and 60% (41,9 MPa) of the flexural and compressive strength, respectively, is developed within the first 4 hours of elevated curing. After 10 hours of sealed curing at 70°C, the samples had achieved more than 90% of their final 28-day compressive and flexural strength (69,8 MPa and 5,2 MPa). When both flexural and compressive strengths are expressed relative to the values measured after 28 days of curing, they show that they could potentially follow the same curing pattern.

XRD is used to provide an initial understanding of the evolution of mineralogy in order to correlate it with the evolution of strength. The increasing presence of an amorphous phase in the range of 27,5 - 32,5° 2θ indicates, according to the literature, that a sodium alumino silicate hydrate gel is being formed in the first 6 hours. Later, as the amorphous content continues to increase, more clay and feldspar minerals, illite and microcline respectively, are being detected by XRD. After 10 hours, when

more then 90% of full strength is achieved, no significant changes are visible in the XRD patterns. The observed changes in mineralogy and microstructure indicate an initial correlation with the development of mechanical properties.

Preliminary studies on different curing conditions showed no significant effect on mineralogy and microstructure, but mainly on mechanical properties. Ambient curing showed a slower rate of strength development, 10,4% at 12 hours, but ultimately achieved a similar strength of 71,2 MPa after 28 days, while elevated curing for 28 days had a negative effect on mechanical properties, the 28 days compressive strength was lower by 22,3%. The assumptions made during the mix design process were found to have a significant impact on the performance of GPC. For example, the assumption of 40% active Al_2O_3 in GGBFS resulted in the best strength performance, up to 23,1% stronger than the reference mix. In addition, replacing the CEN Sand with 0/2 Sand containing more fines, resulted reduced workability but improved strength by 14,6% due to increased contact area in the microstructure.

An effect of various alternative waste sources on early-age properties was observed. Waste wood ash has great potential as a precursor due to its abundance and wide availability. An attempt was made to develop a geopolymer by replacing 50% of GGBFS with WWA. WWA 2 showed the most favourable physical properties, similar to GGBFS in terms of specific surface area, connected to water demand and therefore the same workability could be expected. However, the high pH level caused flash setting, which resulted in difficulties with workability and casting of samples. The effect on mineralogy, abscence of detected microcline and additional arcanite requires further evaluation. Long-term evaluation is also needed to determine the potential environmental impact, as WWA contain traces of heavy metals that may leach from GPC. Steel grit didn't show any promising results and its use in GPC in current configuration might be limited without treatment.

Recycled aggregates have a significant effect on the properties of the mix. Both DM8-RCA and DM8-RGA have lower workability, 35,9% and 18,6% lower compared to the reference mix with 23,35 cm flow, due to higher water demand and different grain shapes of RCA and RGA compared to CEN Sand. Strength development is slower in both cases, preciously 25,4% and 41,1% at 4 hours while the reference mix achieved 58,6%. Recycled aggregates improve early-age flexural strength due to their angular shape, providing better interlocking and stronger bonds. The use of RGA does not significantly change the mineralogy, while DM8-RCA shows new peaks identified as anorthite and calcium silicate hydrate. This could possibly explain the improved performance of DM8-RGA along with the improved mechanical bond and possibly also the reference mix if the same W/S factor is used.

Replacing the distilled water by seawater slightly reduced workability due to the salt content, as reported in the literature. However, the mechanical properties of the mix are not significantly affected by this substitution. The mix with seawater shows a slightly faster strength development compared to the reference mix 69,0% at 4 hours, but reaches a similar strength of 70,3 MPa after 28 days. This could possibly be due to the sodium content in seawater which affect the MR of the SSS. The XRD pattern shows no significant changes in mineralogy compared to the reference mix, but more research is needed to fully understand the effects of seawater on the geopolymerization process, mineralogy, and long-term durability.

Overall, the early-age development of the reference mix showed satisfactory results as the strength development correlated well with the mineralogical evolution. In addition, different curing conditions, different assumed reactivity of GGBFS and alternative aggregates showed promising results. Several waste or industrial by-products were tested as replacements for precursors, aggregates or additional water and showed significant potential to be used in GPC, replacing up to 93,9% of the reference input materials.

Future perspective

Accurate measurements are required to determine the exact properties and compositions of the resources. The particle shape and density can have a significant impact on the LDM results. If the particles are irregularly shaped or have a low density, they may scatter light differently than more regular or dense particles, leading to different results. Differences in refractive and absorption indices, on the other hand, can influence how light interacts with particles, introducing errors into the measurement process. Even when the refractive and absorption indices are optimised, the results deviate from the theoretical values. As a result, knowing these values is critical before beginning laser diffraction measurements. The handheld XRF machine provides a good indication of the elements present in the various resources. It is important to note that this handheld device cannot detect any elements lighter than magnesium. A desktop version is required to see the exact, more accurate, composition, including the light elements. This would avoid needing to convert them from elements to oxides and therefore avoid potential errors.

The results of this study are heavily influenced by the used resources (precursors, activators, aggregates, and water source), as well as the curing conditions. More research is required to make more general conclusions. Curing at various temperatures and the optimal duration time for elevated curing could be a subject of the further research. It may also be worthwhile to investigate the implementation of various aggregates.

Initial results of using WWA as a partial replacement for GGBFS show its potential as a precursor. However, the wide variation in its chemical and physical properties requires a screening system to assess its feasibility before using. This could prevent mixes with poor workability due to high water demand or flash setting. In cases where a high pH level cannot be avoided, further research should explore ways of treating the ashes to reduce the risk of flash setting. The use of other types of waste wood ash can also be investigated to determine the effect of different variables and to identify specific types of WWA that may be suitable as precursors.

It is important to note that the obtained results regarding mineralogy and microstructure are based on the specific samples and sample preparation methods used in this study. Therefore, further research is required to confirm these results, with a sufficient amount of data to support them. To gain a more accurate understanding of the amorphous content, additional techniques such as NMR and FTIR should be used, as XRD may not easily detect amorphous phases. By using these methods, researchers may be able to obtain a more complete picture of the geopolymerisation process, the resulting microstructure and how this relates to the development of the mechanical properties.

Sustainability review

Sustainability efforts in the research

Given the urgent need to adopt more sustainable practices and reduce CO_2 emissions, it is critical to consider not only carbon emissions but also waste production throughout a product's lifecycle. As part of this strategy, it is essential to plan for the disposal of product at the end of their use and thereby reduce the pressure on landfill. Given the decreased availability of many natural resources in modern society, it is also important to explore the use of renewable resources or replace those that are finite. These factors are critical in promoting sustainable practices and can be used to guide decision-making across industries and sectors.

The research looked at possible additions to make the GPC even more environmentally friendly. The reference mix already includes the use of 24,3% waste materials. The use of recycled aggregates is one of the improvements made in terms of sustainability. Not only are recycled GPC aggregates used, but recycled concrete aggregates as well. These used RCA consists of fine particles, that are rarely used in other applications due to their high water demand. This change will result in a nearly 58% increase in the amount of used waste. Aside from the use of RA, it has been implemented to replace the additional water in the mix with seawater. Whereas seawater is an infinite source, it is unsuitable for most applications and it reduces the pressure on freshwater sources.In addition to a more environmentally friendly concrete, seawater can be used to replace the water in the SSS. The replacement of all water with seawater can increase the total amount of used waste with 7,3%. When both SW and RA are used, the total amount of waste used in the mixture can reach to nearly 94%.

Many techniques were used throughout the research to reduce CO_2 emissions and landfill waste. To begin, used waste products were collected as close as possible to the lab in order to evaluate their potential to reduce both waste and transportation emissions. Secondly, small-scale tests were done to reduce the resource consumption and waste production. A series of different tests were performed on the individual samples. Besides this, the tested samples were repurposed to make new samples and even artwork. The small amount of concrete leftovers were reused to make doorstops and paper weights to be used in the lab.

Personal efforts towards sustainability

Where safety permitted, reusable personal protective equipment such as gloves and dust masks were used. All electricity used was entirely hydro powered, eliminating the use of non-renewable resources. In addition, although hydro power was used in this study, tests were also performed to cure at room temperature to assess the potential impact on the properties and inform future research.

These indicators show a comprehensive approach towards sustainability that can serve as a model for future research and practice in this field. Personal efforts were also made to reduce the impact as much as possible by doing all of the transportation in Narvik on foot. To reduce paper waste, this master's thesis is also submitted online.

Although much has been done to reduce environmental impact, there are a few things that can be improved to reduce the environmental impact of this research even further. A plastic wrapping foil was used to seal the samples. This can be replaced with a fireproof hermetic box or bag strong enough to hold the samples. A demoulding oil is used to improve the demoulding process. This oil could possible be replaced with a plant-based oil.

References

[1] A. Marker, "Risk assessment," Mar 2017. [Online]. Available: https://www.smartsheet.com/all-risk-assessment-matrix-templates-you-need

[2] L. Rodgers, "Climate change: The massive co2 emitter you may not know about," Dec 2018. [Online]. Available: https://www.bbc.com/news/science-environment-46455844?fbclid=IwAR3UdWPQ3F2jBqMHiARsbG4AWWaYCwFJgDQzRhi4NKCFeF3E5piJp8hgobY

[3] "Alkali activated materials : State-of-the-art report, rilem tc 224-aam," Dordrecht, 2014.

[4] F. Andrews-Phaedonos, "Geopolymer "green" concrete – reducing the carbon footprint – the vicroads experience," 2011.

[5] A. H. Mahmood, S. J. Foster, A. Castel, B. Modra, C. Heidrich, G. Tory, R. Genrich, and P. Engelen, "Development of high-density geopolymer concrete for breakwater armour units for port kembla harbour," *Concrete in Australia*, Jan 2018.

[6] J. Davidovits, "About geopolymerization," Apr 2006. [Online]. Available: https://www.geopolymer.org/science/about-geopolymerization/

[7] A. Nourredine and R. Jauberthie, "Calcium silicate materials: Substitution of hydrated lime by ground granulated blast furnace slag in autoclaving conditions," *Journal of Materials in Civil Engineering*, vol. 24, pp. 1230–1236, 09 2012.

[8] M. Torres-Carrasco and F. Puertas, "Alkaline activation of different aluminosilicates as an alternative to portland cement: alkali activated cements or geopolymers," Apr 2017.

[9] Upscstudysharing, "Earth's crust: Elements, minerals and rocks," Sep 2016. [Online]. Available: https://upscstudysharing.wordpress.com/2016/09/21/earths-crust-elements-minerals-and-rocks/

[10] M. Leute, "Geopolymer institute – promoting the geopolymer science since 1979," 2018. [Online]. Available: https://geopolymer.org/fichiers/gpcamp-2018/Leute%20-%20Woellner%20Geosil%20Alkaline%20solutions%20for%20Geopolymer.pdf

[11] Z. G. Ralli and S. J. Pantazopoulou, "State of the art on geopolymer concrete," *INTERNATIONAL JOURNAL OF STRUCTURAL INTEGRITY*, vol. 12, no. 4, pp. 511–533, AUG 9 2021.

[12] F. Okoye, J. Durgaprasad, and N. Singh, "Effect of silica fume on the mechanical properties of fly ash based-geopolymer concrete," *Ceramics International*, vol. 42, no. 2, Part B, pp. 3000–3006, 2016. [Online]. Available: https://www.sciencedirect.com/science/article/pii/S0272884215019860

[13] A. Zbiciak and T. Markiewicz, "A new extraordinary means of appeal in the polish criminal procedure: the basic principles of a fair trial and a complaint against a cassatory judgment," *Access to Justice in Eastern Europe*, vol. 6, no. 2, pp. 1–18, Mar. 2023.

[14] B. Walkley, R. San Nicolas, M.-A. Sani, G. J. Rees, J. V. Hanna, J. S. van Deventer, and J. L. Provis, "Phase evolution of c-(n)-a-s-h/n-a-s-h gel blends investigated via alkali-activation of synthetic calcium aluminosilicate precursors," *Cement and Concrete Research*, vol. 89, pp. 120–135, 2016. [Online]. Available: https://www.sciencedirect.com/science/article/pii/S0008884616302381

[15] J. Cameron, "Towards a future with geopolymer concrete," Sep 2021.

[16] D. Durrfeld, "Tiwanaku in bolivia, de pre-inca ruïnes in bolivia," Apr 2021. [Online]. Available: https://www.passporttheworld.com/nl/tiwanaku-bolivia-tiahuanacu/

[17] R. Figueira, R. Sousa, L. Coelho, M. Azenha, J. de Almeida, P. Jorge, and C. Silva, "Alkali-silica reaction in concrete: Mechanisms, mitigation and test methods," *Construction and Building Materials*, vol. 222, pp. 903–931, 2019. [Online]. Available: https://www.sciencedirect.com/science/article/pii/S0950061819318811

[18] B. Van Belleghem, "Schadediagnose en betonherstelling sanacon," Dec 2021.

[19] M. Cyr and A. Tagnit-Hamou, "Particle size distribution of fine powders by laser diffraction spectrometry. case of cementitious materials," *Materials and Structures*, vol. 34, pp. 342–350, 07 2001.

[20] Bruker. [Online]. Available: https://www.bruker.com/en/products-and-solutions/elemental-analyzers/xrf-spectrometers/how-does-xrf-work.html

[21] S. Kovac and P. Konopatzki, "Utilization of portable x-ray fluorescence-spectrometers for the registration of contaminated sites in vietnam," 01 2018.

[22] JoVE, "X-ray diffraction for determining atomic and molecular structure: Materials engineering," 2023. [Online]. Available: https://www.jove.com/v/10446/x-ray-diffraction

[23] K. K. Poloju, *Advanced materials and sustainability in civil engineering*, 1st ed. Singapore, Singapore: Springer, 2021.

[24] N. Shehata, O. A. Mohamed, E. T. Sayed, M. A. Abdelkareem, and A. G. Olabi, "Geopolymer concrete as green building materials: Recent applications, sustainable development and circular economy potentials," *SCIENCE OF THE TOTAL ENVIRONMENT*, vol. 836, AUG 25 2022.

[25] A. 2030, "Why the built environment?" 2022. [Online]. Available: https://architecture2030.org/why-the-building-sector/The%20built%20environment%20generates%2040,for%20an%20additional%2013%25%20annually

[26] S. Qaidi, H. Najm, S. Abed, H. Ahmed, H. Al Dughaishi, J. Al Lawati, M. Sabri, F. Alkhatib, and A. Milad, "Fly ash-based geopolymer composites: A review of the compressive strength and microstructure analysis," *Materials*, vol. 15, p. 7098, 10 2022.

[27] P. Neill, "Construction industry accounts for 38% of co2 emissions," Dec 2020. [Online]. Available: https://environmentjournal.online/articles/emissions-from-the-construction-industry-reach-highest-levels/?fbclid=IwAR3HYXqJ5QCbEzhtFAuM01FIICEdKUa_9eg-8TIu7TlXYsNcuL3AOVVedWI

[28] S. Luhar, D. Nicolaides, and I. Luhar, "Fire resistance behaviour of geopolymer concrete: An overview," *BUILDINGS*, vol. 11, no. 3, MAR 2021.

[29] P. SVOBODA, J. AL, Z. BITTNAR, L. Kopecky, and R. Šulc, "Geopolymer concrete - an ancient material too?" *Ceramics - Silikaty*, vol. 52, 01 2008.

[30] A. L. Almutairi, B. A. Tayeh, A. Adesina, H. F. Isleem, and A. M. Zeyad, "Potential applications of geopolymer concrete in construction: A review," *CASE STUDIES IN CONSTRUCTION MATERIALS*, vol. 15, DEC 2021.

[31] F. Andrews-Phaedonos, "Specification and use of geopolymer concrete," 2014. [Online]. Available: https://austroads.com.au/publications/bridges/abc-sas203-14

[32] Z. P. L. a. D. o. C. a. B. E. J S J van Deventer, "Geopolymer concrete - a commercial reality," Feb 2011. [Online]. Available: https://www.globalcement.com/magazine/articles/316-geopolymer-concrete-a-commercial-reality?fbclid=IwAR1lRO4oqWYZOo0aRqpi5wgHho4liOSEyTi6dntdGp2RGCRx_z3qHHC_YzU

[33] A. H. Mahmood, X. Shen, A. Parvez, J. Aldred, and S. Foster, "Performance of geopolymer concrete pavement at wyndham street for city of sydney: Update november 2020," in *Performance of Geopolymer Concrete Pavement at Wyndham Street for City of Sydney: Update November 2020*, 06 2021.

[34] R. Bligh and T. Glasby, "Development of geopolymer precast floor panels for the global change institute at university of queensland."

[35] K. H. Mo, U. J. Alengaram, and M. Z. Jumaat, "Structural performance of reinforced geopolymer concrete members: A review," *Construction and Building Materials*, vol. 120, pp. 251–264, 2016. [Online]. Available: https://www.sciencedirect.com/science/article/pii/S0950061816308121

[36] T. Glasby, J. Day, R. Genrich, and J. Aldred, "Efc geopolymer concrete aircraft pavements at brisbane west wellcamp airport," 2015.

[37] S. K. Rahman and R. Al-Ameri, "Marine geopolymer concrete-a hybrid curable self-compacting sustainable concrete for marine applications," *APPLIED SCIENCES-BASEL*, vol. 12, no. 6, MAR 2022.

[38] J. Royer and E. Allouche, "Laboratory testing and analysis of geopolymer pipe-lining technology for rehabilitation of sewer and stormwater conduits," in *North American Society for Trenchless Technology*, 04 2016.

[39] N. Dave, V. Sahu, and A. K. Misra, "Development of geopolymer cement concrete for highway infrastructure applications," *JOURNAL OF ENGINEERING DESIGN AND TECHNOLOGY*, vol. 18, no. 5, pp. 1321–1333, AUG 20 2020.

[40] A. Gholampour and T. Ozbakkaloglu, "8 - oven-cured alkali-activated concrete," in *Handbook of Advances in Alkali-Activated Concrete*, ser. Woodhead Publishing Series in Civil and Structural Engineering, F. Pacheco-Torgal, P. Chindaprasirt, and T. Ozbakkaloglu, Eds. Woodhead Publishing, 2022, pp. 157–186. [Online]. Available: https://www.sciencedirect.com/science/article/pii/B9780323854696000192

[41] D. Khale and R. Chaudhary, "Mechanism of geopolymerization and factors influencing its development: a review," *JOURNAL OF MATERIALS SCIENCE*, vol. 42, no. 3, pp. 729–746, FEB 2007.

[42] L. Yun-Ming, H. Cheng-Yong, M. M. Al Bakri, and K. Hussin, "Structure and properties of clay-based geopolymer cements: A review," *PROGRESS IN MATERIALS SCIENCE*, vol. 83, pp. 595–629, OCT 2016.

[43] M. Ghadban, "Amphoteric substances overview, properties, and amp; examples," Dec 2021. [Online]. Available: https://study.com/learn/lesson/amphoteric-substances-overview-properties-examples.html

[44] D. Dill, "Boston university - recipe for pi bonds in polyatomic molecules - notes on general chemistry," Dec 2007. [Online]. Available: https://www.bu.edu/quantum/notes/GeneralChemistry/RecipeForPiBondsInPolyatomicMolecules.pdf

[45] P. Duxson, "3 - geopolymer precursor design," in *Geopolymers*, ser. Woodhead Publishing Series in Civil and Structural Engineering, J. L. Provis and J. S. van Deventer, Eds. Woodhead Publishing, 2009, pp. 37–49. [Online]. Available: https://www.sciencedirect.com/science/article/pii/B9781845694494500035

[46] D. K. Panesar, "3 - supplementary cementing materials," in *Developments in the Formulation and Reinforcement of Concrete*, 2nd ed., ser. Woodhead Publishing Series in Civil and Structural Engineering, S. Mindess, Ed. Woodhead Publishing, 2019, pp. 55–85. [Online]. Available: https://www.sciencedirect.com/science/article/pii/B9780081026168000034

[47] J. M. Khatib, O. Baalbaki, and A. A. ElKordi, "15 - metakaolin," in *Waste and Supplementary Cementitious Materials in Concrete*, ser. Woodhead Publishing Series in Civil and Structural Engineering, R. Siddique and P. Cachim, Eds. Woodhead Publishing, 2018, pp. 493–511. [Online]. Available: https://www.sciencedirect.com/science/article/pii/B9780081021569000158

[48] K. Kim, H. M. Lim, S.-Y. Yoon, and H. Ko, "Fast-curing geopolymer foams with an enhanced pore homogeneity derived by hydrogen peroxide and sodium dodecyl sulfate surfactant," *Minerals*, vol. 12, p. 821, 06 2022.

[49] P. Keawpapasson, C. Tippayasam, S. Ruangjan, P. Thavorniti, T. Panyathanmaporn, A. Fontaine, C. Leonelli, and D. Chaysuwan, "Metakaolin-based porous geopolymer with aluminium powder," *Key Engineering Materials*, vol. 608, pp. 132–138, 04 2014.

[50] S. Scherb, M. Köberl, N. Beuntner, C. Thienel, and J. Neubauer, "Reactivity of metakaolin in alkaline environment: Correlation of results from dissolution experiments with xrd quantifications," *Materials*, vol. 13, p. 2214, 05 2020.

[51] N. Jaya, L. Ming, M. M. A. B. Abdullah, H. Yong, and H. Kamarudin, "Effect of sodium hydroxide molarity on physical, mechanical and thermal conductivity of metakaolin geopolymers," *IOP Conference Series: Materials Science and Engineering*, vol. 343, p. 012015, 03 2018.

[52] A. C. Trindade, H. Alcamand, P. Ribeiro Borges, and F. Silva, "On the durability behavior of natural fiber reinforced geopolymers," 09 2017.

[53] M. Lahoti, P. Narang, K.-H. Tan, and E.-H. Yang, "Mix design factors and strength prediction of metakaolin-based geopolymer," *Ceramics International*, vol. 43, 06 2017.

[54] Y.-C. Hsieh, W.-H. Lee, and P.-H. Liao, "Using geopolymer technology on synthesizing leucite ceramics," *Polymers*, vol. 13, p. 3621, 10 2021.

[55] S. Subagjo, E. Rahayu, T. Samadhi, and M. Gunawan, "Synthesis of nay zeolite using mixed calcined kaolins," *Journal of Engineering and Technological Sciences*, vol. 47, pp. 633–639, 12 2015.

[56] P.-I. Au and Y.-K. Leong, "Surface chemistry and rheology of slurries of kaolinite and montmorillonite from different sources," *KONA Powder and Particle Journal*, vol. 2016, 02 2016.

[57] H. Geng, W. Chen, Q. Li, Z. Shui, and B. Yuan, "Effect of pre-dispersing metakaolin in water on the properties, hydration, and metakaolin distribution in mortar," *Frontiers in Materials*, vol. 6, 2019. [Online]. Available: https://www.frontiersin.org/articles/10.3389/fmats.2019.00099

[58] Y. Shaheen, F. Eid, and E. Mahmoud, "Effect of aggregates with high gypsum content on the performance of concrete," *Challenge Journal of Concrete Research Letters*, vol. 8, p. 96, 12 2017.

[59] S. H. Mahure, V. M. Mohitkar, K. Ravi, and B. Naik, "Effect of metakaolin on fresh and hardened properties of self compacting concrete," 2014.

[60] H. Abdul Razak and H. S. Wong, "Re-evaluation of strength and stiffness relationship for high-strength concrete," *Asian J Civil Eng (Build Hous)*, vol. 5, 01 2004.

[61] M. Chandak and P. Pawade, "Influence of metakaolin in concrete mixture: A review," 05 2020.

[62] R. M. Sawant and Y. M. Ghugal, "Recent trend: Use of metakaolin as admixture: A review," 2015.

[63] L. Mlinárik and K. Kopecskó, "Impact of metakaolin-a new supplementary material-on the hydration mechanism of cements," 2013.

[64] M. Ogundiran and S. Ikpeni, "Metakaolin clay-derived geopolymer for recycling of waste cathode ray tube glass," *African Journal of Pure and Applied Chemistry*, vol. 12, pp. 42–49, 06 2018.

[65] A. Barboza Chavez, L. Gómez-Zamorano, and J. Acevedo, "Synthesis and characterization of a hybrid cement based on fly ash, metakaolin and portland cement clinker," *Materials*, vol. 13, p. 1084, 02 2020.

[66] J. Ahmad, K. J. Kontoleon, A. Majdi, M. T. Naqash, A. F. Deifalla, N. Ben Kahla, H. F. Isleem, and S. M. A. Qaidi, "A comprehensive review on the ground granulated blast furnace slag (ggbs) in concrete production," *Sustainability*, vol. 14, no. 14, 2022. [Online]. Available: https://www.mdpi.com/2071-1050/14/14/8783

[67] A. Nourredine and R. Jauberthie, "Calcium silicate materials: Substitution of hydrated lime by ground granulated blast furnace slag in autoclaving conditions," *Journal of Materials in Civil Engineering*, vol. 24, pp. 1230–1236, 09 2012.

[68] S. Blotevogel, A. Ehrenberg, L. Steger, L. Doussang, J. Kaknics, C. Patapy, and M. Cyr, "Ability of the r3 test to evaluate differences in early age reactivity of 16 industrial ground granulated blast furnace slags (ggbs)," *Cement and Concrete Research*, vol. 130, p. 105998, 2020. [Online]. Available: https://www.sciencedirect.com/science/article/pii/S0008884619311421

[69] A. Neto, M. Cincotto, and W. Repette, "Drying and autogenous shrinkage of pastes and mortars with activated slag cement," *Cement and Concrete Research*, vol. 38, pp. 565–574, 04 2008.

[70] M. Naveed, A. Metla, and R. U. Khan, "Activation of ground granulated blast furnace slag by alkalis in self-consolidating concrete," 2014.

[71] J. Wawrzeńczyk, A. Molendowska, and T. Juszczak, "Scaling resistance and air void characteristics in concrete containing ggbs," *Archives of Civil Engineering*, vol. 62, 04 2016.

[72] S. Astutiningsih and Y. Liu, "Geopolymerisation of australian slag with effective dissolution by the alkali," in *Geopolymer, Green Chemistry and Sustainable Development Solutions*, J. Davidovits, Ed., vol. 1. Institut Geopolymere, 2005, pp. 69–73, geopolymerisation of Australian slag with effective dissolution by the alkali ; Conference date: 01-01-2005.

[73] J. Davidovits, *Geopolymer Chemistry and Applications*. Geopolymer Institute, 2008. [Online]. Available: https://books.google.be/books?id=dliw_KTYq4oC

[74] D. Hardjito, "Studies on fly ash-based geopolymer concrete," Ph.D. dissertation, Curtin University of Technology, 2005.

[75] F. U. Rahman, "Fly ash - properties, types, mechanism and uses," Nov 2018. [Online]. Available: https://theconstructor.org/building/fly-ash-properties-types-mechanism/26654/

[76] X. Y. Zhuang, L. Chen, S. Komarneni, C. H. Zhou, D. S. Tong, H. M. Yang, W. H. Yu, and H. Wang, "Fly ash-based geopolymer: clean production, properties and applications," *Journal of Cleaner Production*, vol. 125, pp. 253–267, 2016. [Online]. Available: https://www.sciencedirect.com/science/article/pii/S0959652616300798

[77] A. Reddy and M. Thiruvadi, "An experimental investigation on mechanical behaviour of eco - friendly concrete," *IOP Conference Series: Materials Science and Engineering*, vol. 263, p. 032010, 11 2017.

[78] D. Law, A. Adam, T. Molyneaux, I. Patnaikuni, and A. Wardhono, "Long term durability properties of class f fly ash geopolymer concrete," *Materials and Structures*, vol. 48, 03 2014.

[79] J. Sadangi, S. D. Muduli, B. Nayak, and B. Mishra, "Effect of phosphate ions on preparation of fly ash based geopolymer," *International Journal of Applied Chemistry*, vol. 4, pp. 20–26, 06 2013.

[80] H. Nugteren, V. Butselaar-Orthlieb, M. Izquierdo, G.-J. Witkamp, and M. Kreutzer, "High strength geopolymers from fractionated and pulverized fly ash," *3rd World of Coal Ash, WOCA Conference - Proceedings*, 01 2009.

[81] A. Borsoi, S. Collepardi, C. Luigi, R. Troli, and M. Collepardi, "Effect of superplasticizer type on the performance of high-volume fly ash concrete," 01 2000.

[82] w. m. wan ibrahim, M. M. A. B. Abdullah, R. Ahmad, A. Naveed, C. Ruzaidi, and M. Ibrahim, "Effects of thermal resistance to fly ash-based lightweight geopolymer," *IOP Conference Series: Materials Science and Engineering*, vol. 551, p. 012082, 08 2019.

[83] N. Karthik, D. Kumar, and B. Mayuri, "Hazardous effect of coal ash b ." 2013.

[84] B. Nagaratnam, M. Rahman, and M. A. Mannan, "A study on hardened state properties of scc using fly ash and blended fine aggregate," *Advanced Materials Research*, vol. 622-623, 11 2012.

[85] G. Kisku and M. Tiwari, "Role of air pollutants emitted from coal power plant and meteorology in climate change," *Climate Change*, vol. 1, pp. 483–490, 01 2015.

[86] Q. Trinh, S. Nagy, and G. Mucsi, "Preliminary geopolymerization experiments of vietnamese fly ash and slag," 11 2019.

[87] R. Siddique, "Wear resistance of high-volume fly ash concrete," 12 2010.

[88] K. Ramamurthy, "Influence of fineness of fly ash on the aggregate pelletization process," pp. 456 – 464, 2007.

[89] Rachel, J., and Detwiler, "The role of fly ash composition in reducing alkali-silica reaction," 2002.

[90] M. Dahim, "Enhancement the performance of asphalt pavement using fly ash wastes in saudi arabia," *International Journal of Engineering and Technology(UAE)*, vol. 7, pp. 50–53, 01 2018.

[91] A. Mohajerani, D. Suter, T. Jeffrey-Bailey, T. Song, A. Arulrajah, and D. Law, "Recycling waste materials in geopolymer concrete," *Clean Technologies and Environmental Policy*, vol. 21, 04 2019.

[92] Antoni, J. G. Herianto, E. Anastasia, and D. Hardjito, "Effect of adding acid solution on setting time and compressive strength of high calcium fly ash based geopolymer," *AIP Conference Proceedings*, vol. 1887, no. 1, p. 020042, 2017. [Online]. Available: https://aip.scitation.org/doi/abs/10.1063/1.5003525

[93] M. Nodehi and V. Mohamad Taghvaee, "Alkali-activated materials and geopolymer: a review of common precursors and activators addressing circular economy," Jun 2021.

[94] C. Cheah and M. Ramli, "The implementation of wood waste ash:review paper," 04 2014.

[95] R. Siddique, "Utilization of industrial by-products in concrete," *Procedia Engineering*, vol. 95, 12 2014.

[96] "Mineral mondays: Silicates," Sep 2016. [Online]. Available: https://www.calacademy.org/explore-science/mineral-mondays-silicates#:~:text=Some%20silicates%20form%20deep%20beneath,then%20precipitate%20into%20mineral%20veins.

[97] G. W. Morey and P. Niggli, "The hydrothermal formation of silicates, a review," *Journal of the American Chemical Society*, vol. 35, no. 9, pp. 1086–1130, 1913. [Online]. Available: https://doi.org/10.1021/ja02198a600

[98] E. Schnebele, Jan 2018. [Online]. Available: https://www.earthmagazine.org/article/mineral-resource-month-silicon/

[99] "Chemical, toxicological, ecological and legal aspects of production ..." Mar 2019. [Online]. Available: https://www.cees-silicates.org/images/Publications/CEES1010c_-_Brochure.pdf

[100] S. Patankar, "Mix design of fly ash based geopolymer concrete," in */*, 12 2014.

[101] H. Dembicki, *Practical petroleum geochemistry for exploration and production*. Elsevier, 2017.

[102] G. De Schutter and P. Minne, *Chapter VII*, 2018th ed. Belgische Betongroepering, 2018, p. 325–392.

[103] M. Zuaiter, H. El-Hassan, T. El-Maaddawy, and B. El-Ariss, "Properties of slag-fly ash blended geopolymer concrete reinforced with hybrid glass fibers," *Buildings*, vol. 12, no. 8, 2022. [Online]. Available: https://www.mdpi.com/2075-5309/12/8/1114

[104] H. Khater, "Effect of silica fume on the characterization of the geopolymer materials," *International Journal of Advanced Structural Engineering (IJASE)*, vol. 5, 04 2013.

[105] U. Rattanasak, K. Pankhet, and P. Chindaprasirt, "Effect of chemical admixtures on properties of high-calcium fly ash geopolymer," *International Journal of Minerals, Metallurgy, and Materials*, vol. 18, pp. 364–369, 06 2011.

[106] A. H. Mahmood, S. J. Foster, and A. Castel, "Effects of mixing duration on engineering properties of geopolymer concrete," *Construction and Building Materials*, vol. 303, p. 124449, 2021. [Online]. Available: https://www.sciencedirect.com/science/article/pii/S0950061821022066

[107] A. Ashour, A. Ghallab, M. Khafaga, A. Ibraheem, and M. Kohail, "Using metakaolin and ground granulated blast furnace slag in production of geopolymer concrete," *Tianjin Daxue Xuebao (Ziran Kexue yu Gongcheng Jishu Ban)/Journal of Tianjin University Science and Technology*, vol. 54, pp. 84–112, 08 2021.

[108] A. Hasnaoui, E. Ghorbel, and G. Wardeh, "Optimization approach of granulated blast furnace slag and metakaolin based geopolymer mortars," *Construction and Building Materials*, vol. 198, pp. 10–26, 2019. [Online]. Available: https://www.sciencedirect.com/science/article/pii/S0950061818329441

[109] S. Ndaru Candra, P. Andry Agung, and A. Ufafa, "Optimization density of geopolymer concrete based on taguchi method," Aug 2018.

[110] K. Komnitsas and D. Zaharaki, "Geopolymerisation: A review and prospects for the minerals industry," *Minerals Engineering*, vol. 20, no. 14, pp. 1261–1277, 2007. [Online]. Available: https://www.sciencedirect.com/science/article/pii/S089268750700204X

[111] P. Duxson, A. Fernández-Jiménez, J. Provis, G. Lukey, A. Palomo, and J. Van Deventer, "Geopolymer technology: The current state of the art," *Journal of Materials Science*, vol. 42, pp. 2917–2933, 05 2007.

[112] J. Provis and S. Bernal, "Geopolymers and related alkali-activated materials," *Annual Review of Materials Research*, vol. 44, 07 2014.

[113] H. Alanazi, "Study of the interfacial transition zone characteristics of geopolymer and conventional concretes," *Gels*, vol. 8, no. 2, p. 105, Feb. 2022. [Online]. Available: https://doi.org/10.3390/gels8020105

[114] Z. Luo, W. Li, K. Wang, A. Castel, and S. P. Shah, "Comparison on the properties of itzs in fly ash-based geopolymer and portland cement concretes with equivalent flowability," *Cement and Concrete Research*, vol. 143, p. 106392, 2021. [Online]. Available: https://www.sciencedirect.com/science/article/pii/S0008884621000417

[115] N. N. M. Nikolić, A. B. Kandić, K. V. Trivunac, M. M. Mirković, I. S. Vukanac, S. S. Nenadović, and L. M. Kljajević, "Radiological and structural characterization of raw and alkali-activated wood ash and metakaolin blends," *Sustainability*, vol. 14, no. 20, p. 12960, Oct. 2022. [Online]. Available: https://doi.org/10.3390/su142012960

[116] X. Zhu, W. Li, Z. Du, S. Zhou, Y. Zhang, and F. Li, "Recycling and utilization assessment of steel slag in metakaolin based geopolymer from steel slag by-product to green geopolymer," *Construction and Building Materials*, vol. 305, p. 124654, 2021. [Online]. Available: https://www.sciencedirect.com/science/article/pii/S0950061821024090

[117] C. Ferone, F. Colangelo, G. Roviello, D. Asprone, C. Menna, A. Balsamo, A. Prota, R. Cioffi, and G. Manfredi, "Application-oriented chemical optimization of a metakaolin based geopolymer," *Materials*, vol. 6, no. 5, pp. 1920–1939, May 2013. [Online]. Available: https://doi.org/10.3390/ma6051920

[118] Z. Zidi, M. Ltifi, Z. B. Ayadi, and L. E. Mir, "Synthesis of nano-alumina and their effect on structure, mechanical and thermal properties of geopolymer," *Journal of Asian Ceramic Societies*, vol. 7, no. 4, pp. 524–535, Oct. 2019. [Online]. Available: https://doi.org/10.1080/21870764.2019.1676498

[119] D. Moro, R. Fabbri, J. Romano, G. Ulian, A. Calafato, A. Solouki, C. Sangiorgi, and G. Valdrè, "Thermal, x-ray diffraction and oedometric analyses of silt-waste/NaOH-activated metakaolin geopolymer composite," *Journal of Composites Science*, vol. 5, no. 10, p. 269, Oct. 2021. [Online]. Available: https://doi.org/10.3390/jcs5100269

[120] M. A. V. Caicedo and R. M. de Gutiérrez, "Synthesis of ternary geopolymers based on metakaolin, boiler slag and rice husk ash," *DYNA*, vol. 82, no. 194, pp. 104–110, Dec. 2015. [Online]. Available: https://doi.org/10.15446/dyna.v82n194.46352

[121] L. R. Caballero, M. das Dores Macedo Paiva, E. de Moraes Rego Fairbairn, and R. D. T. Filho, "Thermal, mechanical and microstructural analysis of metakaolin based geopolymers," *Materials Research*, vol. 22, no. 2, 2019. [Online]. Available: https://doi.org/10.1590/1980-5373-mr-2018-0716

[122] I. Sánchez, I. S. de Soto, M. Casas, R. V. de la Villa, and R. García-Giménez, "Evolution of metakaolin thermal and chemical activation from natural kaolin," *Minerals*, vol. 10, no. 6, p. 534, Jun. 2020. [Online]. Available: https://doi.org/10.3390/min10060534

[123] H. Kouamo, J. A. Mbey, A. Elimbi, B. Kenne Diffo, and D. Njopwouo, "Synthesis of volcanic ash-based geopolymer mortars by fusion method: Effects of adding metakaolin to fused volcanic ash," 03 2013.

[124] N. A. Jaya, Y. M. Liew, C. Y. Heah, and M. M. A. B. Abdullah, "Effect of solid-to-liquid ratios on metakaolin geopolymers," in *AIP Conference Proceedings*. Author(s), 2018. [Online]. Available: https://doi.org/10.1063/1.5080912

[125] K. Hemra and P. Aungkavattana, "Effect of cordierite addition on compressive strength and thermal stability of metakaolin based geopolymer," *Advanced Powder Technology*, vol. 27, no. 3, pp. 1021–1026, May 2016. [Online]. Available: https://doi.org/10.1016/j.apt.2016.04.019

[126] S. Adjei, S. Elkatatny, and K. Ayranci, "Effect of elevated temperature on the microstructure of metakaolin-based geopolymer," *ACS Omega*, vol. 7, no. 12, pp. 10 268–10 276, 2022. [Online]. Available: https://doi.org/10.1021/acsomega.1c06878

[127] S. Lee, B. Kim, J. Seo, and S. Cho, "Beneficial use of MIBC in metakaolin-based geopolymers to improve flowability and compressive strength," *Materials*, vol. 13, no. 17, p. 3663, Aug. 2020. [Online]. Available: https://doi.org/10.3390/ma13173663

[128] B. K. Diffo, A. Elimbi, M. Cyr, J. D. Manga, and H. T. Kouamo, "Effect of the rate of calcination of kaolin on the properties of metakaolin-based geopolymers," *Journal of Asian Ceramic Societies*, vol. 3, no. 1, pp. 130–138, Mar. 2015. [Online]. Available: https://doi.org/10.1016/j.jascer.2014.12.003

[129] G. Kakali, T. Perraki, S. Tsivilis, and E. Badogiannis, "Thermal treatment of kaolin: the effect of mineralogy on the pozzolanic activity," *Applied Clay Science*, vol. 20, no. 1-2, pp. 73–80, Sep. 2001. [Online]. Available: https://doi.org/10.1016/s0169-1317(01)00040-0

[130] J. Xing, Y. Zhao, J. Qiu, and X. Sun, "Microstructural and mechanical properties of alkali activated materials from two types of blast furnace slags," *Materials*, vol. 12, no. 13, p. 2089, Jun. 2019. [Online]. Available: https://doi.org/10.3390/ma12132089

[131] R. Serne and J. Westsik, "Data package for secondary waste form down-selectioncast stone," 04 2023.

[132] A. Allahverdi, E. Najafi, and M. Yazdanipour, "Effects of blast-furnace slag on natural pozzolan-based geopolymer cement," *Ceramics - Silikaty*, vol. 55, 03 2011.

[133] A. Hosan and F. U. A. Shaikh, "Compressive strength development and durability properties of high volume slag and slag-fly ash blended concretes containing nano-CaCO3," *Journal of Materials Research and Technology*, vol. 10, pp. 1310–1322, Jan. 2021. [Online]. Available: https://doi.org/10.1016/j.jmrt.2021.01.001

[134] T. J. Medina, S. P. Arredondo, R. Corral, A. Jacobo, R. A. Zárraga, C. A. Rosas, F. G. Cabrera, and J. M. Bernal, "Microstructure and pb2 adsorption properties of blast furnace slag and fly ash based geopolymers," *Minerals*, vol. 10, no. 9, p. 808, Sep. 2020. [Online]. Available: https://doi.org/10.3390/min10090808

[135] J. Li, L. Yang, F. Rao, W. Liu, H. Ma, X. Chi, and S. Zhong, "Influence of ca on the mechanical properties and microstructures of slag-fly ash geopolymers," *Minerals and Mineral Materials*, vol. 1, p. 2, 2022. [Online]. Available: https://doi.org/10.20517/mmm.2021.02

[136] I. Ismail, S. A. Bernal, J. L. Provis, R. S. Nicolas, S. Hamdan, and J. S. van Deventer, "Modification of phase evolution in alkali-activated blast furnace slag by the incorporation of fly ash," *Cement and Concrete Composites*, vol. 45, pp. 125–135, Jan. 2014. [Online]. Available: https://doi.org/10.1016/j.cemconcomp.2013.09.006

[137] Y. Jun, J. H. Kim, S. H. Han, and T. Kim, "Influence of seawater on alkali-activated slag concrete," *Materials and Structures*, vol. 54, no. 3, May 2021. [Online]. Available: https://doi.org/10.1617/s11527-021-01719-5

[138] H. Park, Y. Jeong, J.-H. Jeong, and J. Oh, "Strength development and hydration behavior of self-activation of commercial ground granulated blast-furnace slag mixed with purified water," *Materials*, vol. 9, no. 3, p. 185, Mar. 2016. [Online]. Available: https://doi.org/10.3390/ma9030185

[139] A. Hajimohammadi, T. Ngo, and J. Vongsvivut, "Interfacial chemistry of a fly ash geopolymer and aggregates," *Journal of Cleaner Production*, vol. 231, pp. 980–989, Sep. 2019. [Online]. Available: https://doi.org/10.1016/j.jclepro.2019.05.249

[140] Parveen, D. Singhal, M. T. Junaid, B. B. Jindal, and A. Mehta, "Mechanical and microstructural properties of fly ash based geopolymer concrete incorporating alccofine at ambient curing," *Construction and Building Materials*, vol. 180, pp. 298–307, Aug. 2018. [Online]. Available: https://doi.org/10.1016/j.conbuildmat.2018.05.286

[141] M. M. R. Taha, Ed., *International Congress on Polymers in Concrete (ICPIC 2018)*. Springer International Publishing, 2018. [Online]. Available: https://doi.org/10.1007/978-3-319-78175-4

[142] G. McCarthy, D. Johansen, S. Steinwand, and A. Thedchanamoorthy, "X-ray diffraction analysis of fly ASH," *Advances in X-ray Analysis*, vol. 31, pp. 331–342, 1987. [Online]. Available: https://doi.org/10.1154/s037603080002214x

[143] D. D. B. Nergis, M. M. A. B. Abdullah, A. V. Sandu, and P. Vizureanu, "XRD and TG-DTA study of new alkali activated materials based on fly ash with sand and glass powder," *Materials*, vol. 13, no. 2, p. 343, Jan. 2020. [Online]. Available: https://doi.org/10.3390/ma13020343

[144] P. Risdanareni, P. Puspitasari, and E. J. Jaya, "Chemical and physical characterization of fly ash as geopolymer material," *MATEC Web of Conferences*, vol. 97, p. 01031, 2017. [Online]. Available: https://doi.org/10.1051/matecconf/20179701031

[145] N. Ranjbar, M. Mehrali, A. Behnia, A. J. Pordsari, M. Mehrali, U. J. Alengaram, and M. Z. Jumaat, "A comprehensive study of the polypropylene fiber reinforced fly ash based geopolymer," *PLOS ONE*, vol. 11, no. 1, p. e0147546, Jan. 2016. [Online]. Available: https://doi.org/10.1371/journal.pone.0147546

[146] L. Coppola, D. Coffetti, and E. Crotti, "Plain and ultrafine fly ashes mortars for environmentally friendly construction materials," *Sustainability*, vol. 10, no. 3, p. 874, Mar. 2018. [Online]. Available: https://doi.org/10.3390/su10030874

[147] J. R, "Studies on physio chemical properties of fly ash for their effective alkali activation," *SOJ Materials Science and Engineering*, vol. 3, no. 3, pp. 1–6, Dec. 2015. [Online]. Available: https://doi.org/10.15226/sojmse.2015.00129

[148] G. Nagalia, Y. Park, A. Abolmaali, and P. Aswath, "Compressive strength and microstructural properties of fly ash–based geopolymer concrete," *Journal of Materials in Civil Engineering*, vol. 28, no. 12, Dec. 2016. [Online]. Available: https://doi.org/10.1061/(asce)mt.1943-5533.0001656

[149] K. Zhang, L. V. Dyk, D. He, J. Deng, S. Liu, and H. Zhao, "Synthesis of zeolite from fly ash and its adsorption of phosphorus in wastewater," *Green Processing and Synthesis*, vol. 10, no. 1, pp. 349–360, Jan. 2021. [Online]. Available: https://doi.org/10.1515/gps-2021-0032

[150] B. Bac, X.-N. Bui, D.-H. Vu, and N. Dung, "Characterization of a vietnamese coal fly ash and its possible utilizations," 08 2012.

[151] S. Bada and S. Potgieter-Vermaak, "Evaluation and treatment of coal fly ash for adsorption application." [Online]. Available: http://lejpt.academicdirect.org/A12/037_048.htm

[152] M. Mings, S. Schlorholtz, J. Pitt, and T. Demirel, "Characterization of fly ash by x-ray analysis methods," 1983.

[153] N. Lee, G. An, K. Koh, and G. Ryu, "Improved reactivity of fly ash-slag geopolymer by the addition of silica fume," *Advances in Materials Science and Engineering*, vol. 2016, pp. 1–11, 01 2016.

[154] L. S. Wong, "Durability performance of geopolymer concrete: A review," *Polymers*, vol. 14, no. 5, p. 868, Feb. 2022. [Online]. Available: https://doi.org/10.3390/polym14050868

[155] D. D. B. Nergis, M. M. A. B. Abdullah, A. V. Sandu, and P. Vizureanu, "XRD and TG-DTA study of new alkali activated materials based on fly ash with sand and glass powder," *Materials*, vol. 13, no. 2, p. 343, Jan. 2020. [Online]. Available: https://doi.org/10.3390/ma13020343

[156] M. Łach, K. Korniejenko, M. Hebdowska-Krupa, and J. Mikuła, "The effect of additives on the properties of metakaolin and fly ash based geopolymers," *MATEC Web of Conferences*, vol. 163, p. 06005, 01 2018.

[157] A. Hajimohammadi, T. Ngo, and J. Vongsvivut, "Interfacial chemistry of a fly ash geopolymer and aggregates," *Journal of Cleaner Production*, vol. 231, pp. 980–989, 2019. [Online]. Available: https://www.sciencedirect.com/science/article/pii/S0959652619317858

[158] Parveen, D. Singhal, M. T. Junaid, B. B. Jindal, and A. Mehta, "Mechanical and microstructural properties of fly ash based geopolymer concrete incorporating alccofine at ambient curing," *Construction and Building Materials*, vol. 180, pp. 298–307, Aug. 2018. [Online]. Available: https://doi.org/10.1016/j.conbuildmat.2018.05.286

[159] K. Arunkumar, M. Muthukannan, A. S. Kumar, A. C. Ganesh, and R. K. Devi, "Production of eco-friendly geopolymer concrete by using waste wood ash for a sustainable environment," *POLLUTION*, vol. 7, no. 4, pp. 993–1006, 2021.

[160] C. Ng, U. J. Alengaram, L. S. Wong, K. H. Mo, M. Z. Jumaat, and S. Ramesh, "A review on microstructural study and compressive strength of geopolymer mortar, paste and concrete," *Construction and Building Materials*, vol. 186, pp. 550–576, Oct. 2018. [Online]. Available: https://doi.org/10.1016/j.conbuildmat.2018.07.075

[161] Z. Cheng, R. Zhao, Y. Yuan, F. Li, A. Castel, and T. Xu, "Ageing coefficient for early age tensile creep of blended slag and low calcium fly ash geopolymer concrete," *Construction and Building Materials*, vol. 262, p. 119855, Nov. 2020. [Online]. Available: https://doi.org/10.1016/j.conbuildmat.2020.119855

[162] F. Ates, K. T. Park, K. W. Kim, B.-H. Woo, and H. G. Kim, "Effects of treated biomass wood fly ash as a partial substitute for fly ash in a geopolymer mortar system," *CONSTRUCTION AND BUILDING MATERIALS*, vol. 376, MAY 2 2023.

[163] J. Xing, Y. Zhao, J. Qiu, and X. Sun, "Microstructural and mechanical properties of alkali activated materials from two types of blast furnace slags," *Materials*, vol. 12, no. 13, p. 2089, Jun. 2019. [Online]. Available: https://doi.org/10.3390/ma12132089

[164] Z. Li, M. Nedeljković, B. Chen, and G. Ye, "Mitigating the autogenous shrinkage of alkali-activated slag by metakaolin," *Cement and Concrete Research*, vol. 122, pp. 30–41, Aug. 2019. [Online]. Available: https://doi.org/10.1016/j.cemconres.2019.04.016

[165] M. F. Zawrah, R. A. Gado, and R. M. Khattab, "Optimization of slag content and properties improvement of metakaolin-slag geopolymer mixes," *The Open Materials Science Journal*, vol. 12, no. 1, pp. 40–57, Jul. 2018. [Online]. Available: https://doi.org/10.2174/1874088x01812010040

[166] M. Łach, K. Korniejenko, M. Hebdowska-Krupa, and J. Mikuła, "The effect of additives on the properties of metakaolin and fly ash based geopolymers," *MATEC Web of Conferences*, vol. 163, p. 06005, 2018. [Online]. Available: https://doi.org/10.1051/matecconf/201816306005

[167] J. Davidovits, L. Huaman, and R. Davidovits, "Tiahuanaco monuments (tiwanaku / pumapunku) in bolivia are made of geopolymer artificial stones created 1400 years ago," 09 2019.

[168] T. Bakharev, "Resistance of geopolymer materials to acid attack," *Cement and Concrete Research*, vol. 35, no. 4, pp. 658–670, 2005. [Online]. Available: https://www.sciencedirect.com/science/article/pii/S0008884604002595

[169] B. Rangan, "11 - engineering properties of geopolymer concrete," in *Geopolymers*, ser. Woodhead Publishing Series in Civil and Structural Engineering, J. L. Provis and J. S. van Deventer, Eds. Woodhead Publishing, 2009, pp. 211–226. [Online]. Available: https://www.sciencedirect.com/science/article/pii/B9781845694494500114

[170] D. Annapurna and R. Kishore, "Influence of alkali–silica reaction on geopolymer concrete," in *Advances in Sustainable Construction Materials*, R. K. Pancharathi, B. Sangoju, and S. Chaudhary, Eds. Singapore: Springer Singapore, 2020, pp. 61–71.

[171] "Carbonation of concrete structures," May 2013. [Online]. Available: https://theconstructor.org/concrete/carbonation-of-concrete-structures/7791/

[172] Abhay, C. Litang, Jake, Kipler, Sharon, Thulasingam, and R. Cronk, "What is spalling of concrete - its causes and repair," Jan 2023. [Online]. Available: https://dailycivil.com/spalling-of-concrete-its-causes-and-repair/

[173] T. García-Mejía and M. Chávez-García, "Compressive strength of metakaolin-based geopolymers: Influence of koh concentration, temperature, time and relative humidity," *Materials Sciences and Applications*, vol. 07, pp. 772–791, 01 2016.

[174] M. Nurruddin, S. Haruna, B. Mohammed, and I. Shaaban, "Methods of curing geopolymer concrete: A review," *International Journal of ADVANCED AND APPLIED SCIENCES*, vol. 5, pp. 31–36, 01 2018.

[175] J. van Jaarsveld, J. van Deventer, and G. Lukey, "The effect of composition and temperature on the properties of fly ash- and kaolinite-based geopolymers," *Chemical Engineering Journal*, vol. 89, no. 1, pp. 63–73, 2002. [Online]. Available: https://www.sciencedirect.com/science/article/pii/S1385894702000256

[176] A. Horne and C. Goldman, *Limnology*, 2nd ed. McGraw-Hill, 1994.

[177] A. Malkawi, M. Nuruddin, A. Fauzi, H. Al-Mattarneh, and B. Mohammed, "Effects of alkaline solution on properties of the hcfa geopolymer mortars," *Procedia Engineering*, vol. 148, pp. 710–717, 12 2016.

[178] D. Feng, H. Tan, and J. S. J. van Deventer, "Ultrasound enhanced geopolymerisation," *Journal of Materials Science*, vol. 39, pp. 571–580, 2004.

[179] Bondar, Lynsdale, Milestone, Hassani, and Ramezanianpour, "Engineering properties of geopolymer concrete based on alkali activated ..." [Online]. Available: https://www.irbnet.de/daten/iconda/CIB13832.pdf

[180] P. Nuaklong, V. Sata, and P. Chindaprasirt, "Influence of recycled aggregate on fly ash geopolymer concrete properties," pp. 2300–2307, 2016. [Online]. Available: https://www.sciencedirect.com/science/article/pii/S0959652615015814

[181] P. Nath and P. K. Sarker, "Effect of ggbfs on setting, workability and early strength properties of fly ash geopolymer concrete cured in ambient condition," pp. 163–171, 2014. [Online]. Available: https://www.sciencedirect.com/science/article/pii/S0950061814005819

[182] A. Noushini, A. Castel, J. Aldred, and A. Rawal, "Chloride diffusion resistance and chloride binding capacity of fly ash-based geopolymer concrete," *Cement and Concrete Composites*, vol. 105, p. 103290, 2020. [Online]. Available: https://www.sciencedirect.com/science/article/pii/S0958946518305183

[183] N. A. Farhan, M. N. Sheikh, and M. N. Hadi, "Experimental investigation on the effect of corrosion on the bond between reinforcing steel bars and fibre reinforced geopolymer concrete," *Structures*, vol. 14, pp. 251–261, 2018. [Online]. Available: https://www.sciencedirect.com/science/article/pii/S2352012418300389

[184] M. Al-Azzawi, T. Yu, and M. N. Hadi, "Factors affecting the bond strength between the fly ash-based geopolymer concrete and steel reinforcement," *Structures*, vol. 14, pp. 262–272, 2018. [Online]. Available: https://www.sciencedirect.com/science/article/pii/S2352012418300353

[185] P. Nath and P. K. Sarker, "Use of opc to improve setting and early strength properties of low calcium fly ash geopolymer concrete cured at room temperature," *Cement and Concrete Composites*, vol. 55, pp. 205–214, 2015. [Online]. Available: https://www.sciencedirect.com/science/article/pii/S0958946514001681

[186] P. Nath, P. K. Sarker, and V. B. Rangan, "Early age properties of low-calcium fly ash geopolymer concrete suitable for ambient curing," *Procedia Engineering*, vol. 125, pp. 601–607, 2015, civil Engineering Innovation for a Sustainable. [Online]. Available: https://www.sciencedirect.com/science/article/pii/S1877705815033949

[187] A. Hassan, M. Arif, and M. Shariq, "Effect of curing condition on the mechanical properties of fly ash-based geopolymer concrete," *SN Applied Sciences*, vol. 1, no. 12, Nov. 2019. [Online]. Available: https://doi.org/10.1007/s42452-019-1774-8

[188] "International journal of civil engineering and construction." [Online]. Available: https://doi.org/10.22271/27078329

[189] M. M Katti, B. Jagadeesh, and N. Katti, "Experimental investigation of geopolymer concrete using fly ash and ggbs," pp. 404–410, 05 2016.

[190] ——, "Experimental investigation of geopolymer concrete using fly ash and ggbs," pp. 404–410, 05 2016.

[191] Z. Cheng, R. Zhao, Y. Yuan, F. Li, A. Castel, and T. Xu, "Ageing coefficient for early age tensile creep of blended slag and low calcium fly ash geopolymer concrete," *Construction and Building Materials*, vol. 262, p. 119855, 2020. [Online]. Available: https://www.sciencedirect.com/science/article/pii/S0950061820318602

[192] S. Divvala and S. R. M., "Early strength properties of geopolymer concrete composites: An experimental study," *Materials Today: Proceedings*, vol. 47, pp. 3770–3777, 2021, 3rd International Conference on Computational and Experimental Methods in Mechanical Engineering. [Online]. Available: https://www.sciencedirect.com/science/article/pii/S2214785321019337

[193] S. Vediyappan, P. K. Chinnaraj, B. B. Hanumantraya, and S. K. Subramanian, "An experimental investigation on geopolymer concrete utilising micronized biomass silica and GGBS," *KSCE Journal of Civil Engineering*, vol. 25, no. 6, pp. 2134–2142, Mar. 2021. [Online]. Available: https://doi.org/10.1007/s12205-021-1477-8

[194] M. Amin, Y. Elsakhawy, K. Abu el-hassan, and B. A. Abdelsalam, "Behavior evaluation of sustainable high strength geopolymer concrete based on fly ash, metakaolin, and slag," *Case Studies in Construction Materials*, vol. 16, p. e00976, 2022. [Online]. Available: https://www.sciencedirect.com/science/article/pii/S2214509522001085

[195] W. Liang and G. Zhang, "Effect of reduced graphene oxide on the early-age mechanical properties of geopolymer cement," *Materials Letters*, vol. 276, p. 128223, 2020. [Online]. Available: https://www.sciencedirect.com/science/article/pii/S0167577X20309289

[196] G. De Schutter and P. Minne, *Chapter II*, 2018th ed. Belgische Betongroepering, 2018, p. 29–190.

[197] E. Arvaniti, M. Juenge, S. Bernal, J. Duchesne, L. Courard, S. Leroy, J. Provis, A. Klemm, and N. De Belie, "Physical characterization methods for supplementary cementitious materials," *Materials and Structures*, vol. 48, 10 2014.

[198] G. Samson, M. Cyr, and X. X. Gao, "Formulation and characterization of blended alkali-activated materials based on flash-calcined metakaolin, fly ash and ggbs," *CONSTRUCTION AND BUILDING MATERIALS*, vol. 144, pp. 50–64, JUL 30 2017.

[199] R. Jewell and R. Rathbone, "Optical properties of coal combustion byproducts for particle-size analysis by laser diffraction," *Coal Combustion and Gasification Products*, vol. 1, pp. 1–6, 01 2009.

[200] S. Masahiro, "Synopsis: Refractive index and optical absorption coefficient of ..." 1992. [Online]. Available: https://www.pyrometallurgy.co.za/MoltenSlags1992/022-Susa.pdf

[201] Arvaniti, Eleni and Juenger, Maria and Bernal, Susan and Duchesne, Josee and Courard, Luc and Leroy, Sophie and Provis, John and Klemm, Agnieszka and De Belie, Nele, "Physical characterization methods for supplementary cementitious materials," *MATERIALS AND STRUCTURES*, vol. 48, no. 11, pp. 3675–3686, 2015. [Online]. Available: http://dx.doi.org/10.1617/s11527-014-0430-4

[202] J. G. C. Ball, B. E. Reed, R. G. Grainger, D. M. Peters, T. A. Mather, and D. M. Pyle, "Measurements of the complex refractive index of volcanic ash at 450, 546.7, and 650nm," *JOURNAL OF GEOPHYSICAL RESEARCH-ATMOSPHERES*, vol. 120, no. 15, pp. 7747–7757, AUG 16 2015.

[203] "Sodium silicate en solution aqueuse, technical." [Online]. Available: https://be.vwr.com/store/product?keyword=28079.363

[204] P. Pinet, *Oceanography*. Sudbury, MA: Jones and Bartlett, Jan. 1992.

[205] S. Karastogianni, S. Girousi, and S. Sotiropoulos, "ph: Principles and measurement," *Encyclopedia of Food and Health*, 12 2016.

[206] M. T. Tognonvi, S. Rossignol, and J.-P. Bonnet, "Physical-chemistry of sodium silicate gelation in an alkaline medium," *Journal of Sol-Gel Science and Technology*, vol. 58, no. 3, pp. 625–635, Mar. 2011. [Online]. Available: https://hal-unilim.archives-ouvertes.fr/hal-00632132

[207] Y. Zhang, B. Cetin, W. J. Likos, and T. B. Edil, "Impacts of ph on leaching potential of elements from msw incineration fly ash," *FUEL*, vol. 184, pp. 815–825, NOV 15 2016.

[208] E. Rehl, K. B. Reimer, and P. M. Rutherford, "ph-dependent release of elements from hardened and non-hardened wood ash," *WASTE MANAGEMENT*, vol. 138, pp. 140–147, FEB 1 2022.

[209] J. L. Provis and J. S. J. Van Deventer, *Geopolymers: structures, processing, properties and industrial applications*. Elsevier, 2009.

[210] A. Palomo, M. Grutzeck, and M. Blanco, "Alkali-activated fly ashes: A cement for the future," *Cement and Concrete Research*, vol. 29, no. 8, pp. 1323–1329, 1999. [Online]. Available: https://www.sciencedirect.com/science/article/pii/S0008884698002439

[211] A. A. S. Staff, "What is xrf (x-ray fluorescence) and how does it work?" Mar 2020. [Online]. Available: https://www.thermofisher.com/blog/ask-a-scientist/what-is-xrf-x-ray-fluorescence-and-how-does-it-work/

[212] Admin, "Oxide - meaning, types, trends in properties," Apr 2022. [Online]. Available: https://byjus.com/jee/oxide/

[213] By CCPS, John Wiley & Sons, Inc., Hoboken, NJ, 440 pages, $125.00, ISBN-13:978-0-470-76772-6. Reviewed by Stanley S. Grossel, Process Safety & Design Consultant, Clifton, NJ, "Guidelines for engineering design for process safety, 2nd edition (2012)," *Process Saf. Prog.*, vol. 31, no. 3, pp. 320–321, Sep. 2012.

[214] "What is x-ray diffraction analysis (xrd) and how does it work?" 2022. [Online]. Available: https://www.twi-global.com/technical-knowledge/faqs/x-ray-diffraction#:~:text=X%2Dray%20diffraction%20analysis%20(XRD)%20is%20a%20technique%20used,leave%20the%20material%20%5B1%5D.

[215] Libretexts, "X-ray diffraction (xrd) basics and application," Aug 2022. [Online]. Available: https://chem.libretexts.org/Courses/Franklin_and_Marshall_College/Introduction_to_Materials_Characterization_CHM_412_Collaborative_Text/Diffraction_Techniques/X-ray_diffraction_(XRD)_basics_and_application

[216] Admin, "Sample preparation – eas x-ray diffraction laboratory – university of alberta," 2023. [Online]. Available: https://cms.eas.ualberta.ca/xrd/sample-preparation/#:~:text=Usually%20powdered%20XRD%20samples%20are,agate%2C%20corundum%2C%20or%20mullite.

[217] D. Moro, R. Fabbri, J. Romano, G. Ulian, A. Calafato, A. Solouki, C. Sangiorgi, and G. Valdrè, "Thermal, x-ray diffraction and oedometric analyses of silt-waste/naoh-activated metakaolin geopolymer composite," 2021. [Online]. Available: https://www.mdpi.com/2504-477X/5/10/269

[218] "Cen standard sand according to en 196-1," 2023. [Online]. Available: https://www.normensand.de/en/products/cen-standard-sand-en-196-1/

[219] V. Boel, B. De Martelaere, G. De Schutter, and T. De Visscher, "Experimentele studie van ontwerpparameters bij alkali geactiveerde materialen," 2022. [Online]. Available: http://lib.ugent.be/catalog/rug01:003063295

[220] B. A. Tayeh, M. H. Akeed, S. Qaidi, and B. A. Bakar, "Influence of sand grain size distribution and supplementary cementitious materials on the compressive strength of ultrahigh-performance concrete," *Case Studies in Construction Materials*, vol. 17, p. e01495, 2022. [Online]. Available: https://www.sciencedirect.com/science/article/pii/S2214509522006271

[221] S. Alsadey and A. Omran, "Effect of the type of sand on the properties of concrete," p. 3, 01 2021.

[222] V. Deutscher Zementwerke, "Cen standard sand according to en 196-1," 2023. [Online]. Available: https://www.normensand.de/en/products/cen-standard-sand-en-196-1/

[223] P. Nuaklong, V. Sata, A. Wongsa, K. Srinavin, and P. Chindaprasirt, "Recycled aggregate high calcium fly ash geopolymer concrete with inclusion of OPC and nano-SiO2," *Construction and Building Materials*, vol. 174, pp. 244–252, Jun. 2018. [Online]. Available: https://doi.org/10.1016/j.conbuildmat.2018.04.123

[224] A. Hasnaoui, E. Ghorbel, and G. Wardeh, "Performance of metakaolin/slag-based geopolymer concrete made with recycled fine and coarse aggregates," *Journal of Building Engineering*, vol. 42, p. 102813, Oct. 2021. [Online]. Available: https://doi.org/10.1016/j.jobe.2021.102813

[225] S. Mesgari, A. Akbarnezhad, and J. Xiao, "Recycled geopolymer aggregates as coarse aggregates for portland cement concrete and geopolymer concrete: Effects on mechanical properties," *Construction and Building Materials*, vol. 236, p. 117571, Mar. 2020. [Online]. Available: https://doi.org/10.1016/j.conbuildmat.2019.117571

[226] A. Younis, U. Ebead, P. Suraneni, and A. Nanni, "Fresh and hardened properties of seawater-mixed concrete," *Construction and Building Materials*, vol. 190, pp. 276–286, 2018. [Online]. Available: https://www.sciencedirect.com/science/article/pii/S0950061818323055

[227] S. Luhar, , and I. L. and, "Application of seawater and sea sand to develop geopolymer composites," *International Journal of Recent Technology and Engineering (IJRTE)*, vol. 8, no. 5, pp. 5625–5633, Jan. 2020. [Online]. Available: https://doi.org/10.35940/ijrte.e5681.018520

[228] J. Couvidat, C. Diliberto, E. Meux, S. Cotelle, C. Bojic, L. Izoret, and A. Lecomte, "Greening effect of slag cement-based concrete: Environmental and ecotoxicological impact," *Environmental Technology and Innovation*, vol. 22, p. 101467, May 2021. [Online]. Available: https://doi.org/10.1016/j.eti.2021.101467

[229] F. Yuan, "Study on kinetics of fe (II) oxidized by air in FeSO4-h2so4 solutions," *Minerals Engineering*, vol. 121, pp. 164–168, Jun. 2018. [Online]. Available: https://doi.org/10.1016/j.mineng.2018.03.013

[230] "Ferrous sulfate," 2023. [Online]. Available: https://pubchem.ncbi.nlm.nih.gov/compound/24393

[231] M. Criado, W. Aperador, and I. Sobrados, "Microstructural and mechanical properties of alkali activated colombian raw materials," *Materials*, vol. 9, no. 3, p. 158, Mar. 2016. [Online]. Available: https://doi.org/10.3390/ma9030158

[232] J. L. Provis and S. A. Bernal, "Geopolymers and related alkali-activated materials," *Annual Review of Materials Research*, vol. 44, no. 1, pp. 299–327, Jul. 2014. [Online]. Available: https://doi.org/10.1146/annurev-matsci-070813-113515

[233] Z. Abdollahnejad, T. Luukkonen, M. Mastali, C. Giosue, O. Favoni, M. L. Ruello, P. Kinnunen, and M. Illikainen, "Microstructural analysis and strength development of one-part alkali-activated slag/ceramic binders under different curing regimes," *Waste and Biomass Valorization*, vol. 11, no. 6, pp. 3081–3096, Feb. 2019. [Online]. Available: https://doi.org/10.1007/s12649-019-00626-9

[234] B. Olawuyi, "Influence of particle size distribution on compressive strength and elastic modulus of high performance concrete." 01 2013.

[235] P. Petrounias, P. Giannakopoulou, A. Rogkala, P. Stamatis, P. Lampropoulou, B. Tsikouras, and K. Hatzipanagiotou, "The effect of petrographic characteristics and physico-mechanical properties of aggregates on the quality of concrete," *Minerals*, vol. 8, no. 12, p. 577, Dec. 2018. [Online]. Available: https://doi.org/10.3390/min8120577

[236] 2022. [Online]. Available: https://soilsfacstaff.cals.wisc.edu/facstaff/barak/virtual_museum/albite/albite_tx.html

[237] D. Smołka-Danielowska and M. Jabłońska, "Chemical and mineral composition of ashes from wood biomass combustion in domestic wood-fired furnaces," *International Journal of Environmental Science and Technology*, vol. 19, no. 6, pp. 5359–5372, Jul. 2021. [Online]. Available: https://doi.org/10.1007/s13762-021-03506-9

[238] H. Martinez Dyrzo, "Geochemical aspects of wood-derived ash as a fire proxy in archaeological contexts." 01 2018.

[239] X. Lyu, N. Robinson, M. Elchalakani, M. L. Johns, M. Dong, and S. Nie, "Sea sand seawater geopolymer concrete," *Journal of Building Engineering*, vol. 50, p. 104141, Jun. 2022. [Online]. Available: https://doi.org/10.1016/j.jobe.2022.104141

[240] M. Frías, M. Sánchez de Rojas, M. Luxán, and N. García, "Determination of specific surface area by the laser diffraction technique. comparison with the blaine permeability method," *Cement and Concrete Research*, vol. 21, no. 5, pp. 709–717, 1991. [Online]. Available: https://www.sciencedirect.com/science/article/pii/000888469190165E

Appendices

A Minutes of meetings

Analysis of early-age properties of geopolymers with various waste materials

2023

Meeting type:	Regular progress meeting for master thesis
Meeting leader:	Dario De Muynck and Marie-Laure Heyndrickx
Meeting participants:	Iveta Novakova
Optional participants:	Boy-Arne Buyle, Veerle Boel and Eirik Gjerlow

Meeting minutes 16/01/2023
Section 1 (What was planned for week 0)
1. Thesis contract
Section 2 (What was done in the week 0)
1. Signed contract
Section 3 (What is to be done for the weeks 1 and 2)
1. Read more 2. Introduction meeting thesis
Additional Information:

Meeting minutes 30/01/2023
Section 1 (What was planned for week 1 and 2)
1. Introduction meeting thesis 2. Test lab with Iveta 3. Ordering materials 4. Meeting Geosumat 5. Literature (curing conditions, mix design, XRD, etc…) 6. Test samples XRD
Section 2 (What was done in the week 1 and 2)
1. Introduction meeting thesis a. Discussed progress and gained knowledge first semester b. Focus on the curing of a couple of mixes with implementation of the WWA (1ref + 3) 2. Test lab with Iveta 3. Ordering materials a. Slags were ordered by BAB (would arrive this week?) b. Metaver K still no response? Should I remind her? (send slides, continue on MK potential) c. Activator could we use the same mix design as in Ghent if we have more or less the same materials? 4. Meeting Geosumat a. Not very response towards the questions? 5. Lab visit Norcem a. 6hrs of transport within same county (Narvik) 6. Literature (curing conditions, mix design, XRD, etc…) a. What materials? FA is also very interesting. Conditions 60°C and 90% RH b. Busy writing literature study, content is defined and distributed among the DDM & MLH 7. Test samples XRD (concrete from Martin) a. Trying different preparation methods and the influence b. Due to unexpected leave we were not able to do

Section 3 (What is to be done for the weeks 3 and 4)

1. Meeting Veerle Boel (DDM & MLH)
2. Literature study (writing)
3. Safety training (07/02)
4. Meeting with MLH, what should be her focus?
5. Test samples XRD
6. First trail mixes monitor at 24hrs to see the feasibility
7. Map the ref mix

Additional Information: Unexpected leave of DDM due to death in family

Meeting minutes 13/02/2023

Section 1 (What was planned for week 3 and 4)

1. Meeting Veerle Boel (DDM & MLH)
2. Literature study (writing)
3. Safety training (07/02)
4. Meeting with MLH, what should be her focus?
5. Test samples XRD
6. First trail mixes monitor at 24hrs to see the feasibility
7. Map the ref mix

Section 2 (What was done in the week 3 and 4)

1. Meeting Veerle Boel (DDM & MLH)
    a. Discussed scope thesis
    b. Once exact quantification of resources has been done, we need to send the %wt of materials and VB will calculate the mixes for us so it is almost the same as in Ghent (corrected amounts due to slight changes in materials). OK
    c. What paste amount do we need to work with? in Ghent they did 50% paste but she wanted to know what you would like to work with.
2. Literature study (writing)
    a. Ongoing, big part has been written and will be able for review soon
    b. Do we ask Ghent first to review and give feedback?
3. Safety training (07/02) **(Done)**
4. Meeting with MLH, what should be her focus?
    a. Should we split something to maximize efficiency?
    b. How do you see a thesis for 2 students?
5. XRD
    a. Eirik showed us how the machine and preparations work, 13/02 after lunch first samples to quantify the resources (MK, GGBFS).
6. First trail mixes monitor at 24hrs to see the feasibility
    a. Not all resources present and haven't been analysed yet.
7. Map the ref mix
    a. See 8.

Section 3 (What is to be done for the weeks 5 and 6)

1. Literature study wrapping up
2. pH tests of resources
3. Particle size analysis resources
4. XRD (resources) + analysis
5. Transfer analysis + technical sheets to VB for mix design
6. Metakaolin what do we do with it? (email Cesilie)
7. First trail mixes monitor at 24hrs to see the feasibility
   what curing conditions? 60°C?
   how frequent test until 24h ? 3d and 7d? How do we arrange it for XRD of samples?
8. Analyze WWA (PSA, XRD, pH)
9. Select ref. mix and map the evolution (xrd and destructive tests)

Additional Information:
Schedule for remainder of thesis

12/02-31/03: Mix design and labs
1/04-16/04: Easter break (focus on processing results and start discussing results, so if something is missing we can still intervene the week after so we don't lose track of the deadline.
17/04-1/05: Time for clean up (if extra tests are needed of expanding the research a little) and wrapping up writing.
02/05-15/05: Finish writing thesis, write abstract + buffer
Is it ok to spend easter break at home to process results and write about them?
10 pager of thesis??

Meeting minutes 23/02/2023

Section 1 (What was planned for week 5 and 6)

1. Literature study wrapping up
2. pH tests of resources
1. Particle size analysis resources
2. XRD (resources) + analysis
3. Transfer analysis + technical sheets to VB for mix design
4. Metakaolin what do we do with it? (email Cesilie)
5. First trail mixes monitor at 24hrs to see the feasibility
   what curing conditions? 60°C?
   how frequent test until 24h ? 3d and 7d? How do we arrange it for XRD of samples?
6. Analyze WWA (PSA, XRD, pH)
7. Select ref. mix and map the evolution (xrd and destructive tests)

Section 2 (What was done in the week 5 and 6)

1. Literature study wrapping up **(Done)**
2. pH tests of resources
   a. Finished partly, with electrode pH but we got an other method from Bobo
3. Particle size analysis resources **(Done)**
   a. But we have to redo with correct indices
4. XRD (resources) + analysis
   a. Finished, but no results due to difficult analysis
5. Transfer analysis + technical sheets to VB for mix design **(Done)**
6. Metakaolin what do we do with it? (e-mail Cesilie)
   a. No response, in need for a solution
7. First trail mixes monitor at 24hrs to see the feasibility
   a. No succes
8. what curing conditions? 60°C?
   a. 70°C, covered
9. how frequent test until 24h ? 3d and 7d? How do we arrange it for XRD of samples?
   a. We will have to see later
10. Analyze WWA (PSA, XRD, pH)
    a. XRF analysis done, PSA and pH need to be done again
11. Select ref. mix and map the evolution (xrd and destructive tests)
    a. No ref. mix found

Section 3 (What is to be done for the weeks 7 and 8)

1. Find/test reference mix
2. Blaine testing recourses
3. Sieving sands for test samples
4. Perform risk analysis
5. Methodology
6. Write "Methods of analysing"
7. Particle size analysis
8. PH methods
9. Solve resource issues

Additional Information: /

Meeting minutes 13/03/2023

Section 1 (What was planned for week 7 and 8)

1. Find/test reference mix
2. Blaine testing recourses
3. Sieving sands for test samples
4. Perform risk analysis
5. Methodology
6. Write "Methods of analysing"
7. Particle size analysis
8. PH methods
9. Solve resource issues

Section 2 (What was done in the week 7 and 8)

1. Find/test reference mix
    a. 16 different batches by now
    b. Overall bad performance with vwr activator, we even made the exact same mix (same resources besides the activator) from Ghent and still bad performance. Curing took a long time and only starting from 3d there is some strength.
    c. Figured out there was a problem with the activator (MR=3.4) while literature suggests it being somewhere between 1.7-1.9. Needed meeting with Jon to get approval.
    d. Activator was recalculated, for every 500 ml vwr activator, you need to add 65 gr of NaOH. See calculations. (2,5 l is made 12/03)
    e. Talked with Ashfaque about XRD, good updates.
    f. DM8 and DM9 are made with new activator, incredible results after 1d 70°C curing. DM8 (Flex. 5,871 MPa, Compr. 78,5 MPa) DM9 (Flex. 7,21 MPa, Compr. 42,5MPa). **Reference mix DM8 is found!**
2. XRF resources **(Done)**
    a. All recourses are quantified (10 x 1 min)
3. Blaine testing recourses **(Done)**
    a. Apparatus is being calibrated and K is determined.
    b. All recourses are tested 3 times.
4. Sieving sands for test samples
    a. Paste samples behave very different, a lot of shrinkage and cracks.
    b. Standard sand (grain distribution) is made from Aggregates (0/8) from HGB and used to have a better prediction of the behavior when in mortar.
5. Perform risk analysis
    a. Risk analysis performed and checked by Boy-Arne. Also checked by Jon Tellefsen when we needed clearance for the lab (mixing new activator)
6. Methodology
    a. Methodology is written and visualized in schemes
7. Write "Methods of analysing"
    a. Part resources almost finished (Reactivity and pH is left)
    b. Part GPC halfway
    What do we analysis from XRD so it qualifies to "mineralogy and microstructure"?
8. Particle size analysis
    a. Refractive index and absorption index is important to know.
    b. Ashfaque is asking around how to determine the RI from the laser diffraction data.
9. PH methods
    a. Found new methods and insights
10. Solve resource issues
    a. Activator from VWR is delivered

b. MK is sent from Ghent and should arrive in Kiruna 16/03/2023. Can we arrange transport (maybe with Klevis going with the pickup? Then we can start mixing in the weekend)
c. Do we have extra slags from Bremen? Bucket is halfway and I thought we had 100kg.

Section 3 (What is to be done for the weeks 9 and 10)

1. Particle size analysis
   a. Determine RI and absorption index
2. PH testing
3. Resources
   a. If delivered, get MK from Kiruna?
   b. Extra slags?
4. Mineralogy and microstructure.
   a. TEM? Or microstructure data from XRD
   b. What output from XRD towards mineralogy and microstructure?
5. Reference mix
   a. Start mapping reference mix (0-24h,7d)
   b. XRD scans
6. WWA mix
   a. Veerle will send us some trails to find a good mix at the end of week 9. Thinking about a mix were all the slags are changed by WWA and an optimum mix.
   b. Can Klevis remake his mix from last year but with the new modded. activator

Additional Information:

Deadline: When should we do the defense? We would like to know in advance to arrange the flights home and housing (before June so we don't need to pay for an extra month housing)
Ashes: Can the data be used for other research (PhD MLH) (yes, refer to Geosumat)
How many pages thesis?

Meeting minutes 27/03/2023

Section 1 (What was planned for week 9 and 10)

1. Particle size analysis
2. PH testing
3. Resources
4. Mineralogy and microstructure.
5. Reference mix
6. WWA mix

Section 2 (What was done in the week 9 and 10)

1. Particle size analysis
   a. MK 1-2, GGBFS 1-6, WWA 1
   b. Determine most accurate RI and absorption index
   c. Determine particle site distribution
2. PH testing
   a. MK 2 (used one), sodium silicate, WWA 1, GGBFS 6 (Bremen)
   b. 1 test takes 2,5 hours to do, so only the most necessary ones would be tested
3. Resources
   a. Activator modification works on larges scales.
   b. The MK 2 from Ghent and the remaining GGBFS arrived.
   c. Still no answers from Cecilily?
4. Mineralogy and microstructure.
   a. XRD for the reference mix done at all the different times.
5. Reference mix

a. Reference mix is mapped (1, 2, 3, 4, 5, 6, 7, 8, 9, 10, 12, 14, 16, 18, 20, 22, 24h) 6. WWA mix a. Searching for a good mix 7. Variations [4h, 8h, 12h, 24h] a. RCA fine --> Standard distribution b. Recycled grains from previous tested GPC --> Standard distribution c. HGB sand --> 0,8 to 0,2 d. Reference mix at room temp. (20°C) 8. Geosumat meetings and Betongfagdag a. Interesting insights and good discussions
Section 3 (What is to be done for the weeks 11 and 12)
1. Presentation 2. Processing data 3. Writing results 4. Reflecting on previous work
Additional Information: In week 12 there is easter break, we go home during this time, to spend some time together with family.

Meeting minutes 11/04/2023
Section 1 (What was planned for week 11 and 12)
1. Presentation 2. Processing data 3. Writing results 4. Reflecting on previous work
Section 2 (What was done in the week 11 and 12)
1. Presentation **(Done)** a. Overal feedback good? 2. Processing data a. PSA, optimized indices. Compared to blaine and TDS big deviations b. All test results processed (compressive + flexural) c. Evaluated for outliers, grubbs and 10% mean but what do we take ? depending on the sample series one is stricter d. XRD, no news from panalytical about student licence. 3. Writing results a. In progress, structure is taking good shape. b. New title is accepted by UGent, have to do the same for UiT 4. Reflecting on previous work a. In progress b. Adding some data to literature study to be able to reflect the results to the data the science community is having. Resources + geopolymer regarding properties, mineralogy and microstructure.
Section 3 (What is to be done for the weeks 13 and 14)
1. Reviewing and editing previous work 2. Testing 28d samples a. Different curing (1d 70°, 27d AMB sealed and unsealed/28d AMB /28d 70°) b. RCA fines c. RGA fines d. HGB sand (0/8 -> 0/2) e. SW 28d

f. XRD on al 28d see difference in mineralogy and microstructure 3. Ambient samples 2h + 12h 4. Processing data 5. Optical microscope other aggregates, precursors (grain size and shape) 6. pH 7. Writing results 8. Extra trails (WWA2, SG1, Reactivity)
Additional Information: In week 13 there is easter break, we go home during this time, to spend some time together with family. Paper, does I have the same first deadline as thesis? What about structure (A1?). How many pages can it be. (Between maximum 10 and 15 pages)

Meeting minutes 24/04/2023
Section 1 (What was planned for week 13 and 14)
1. Reviewing and editing previous work 2. Testing 28d samples 3. Ambient samples 2h + 12h 4. Processing data 5. Optical microscope other aggregates, precursors (grain size and shape) 6. pH 7. Writing results 8. Extra trails (WWA2, SG1, Reactivity)
Section 2 (What was done in the week 15 and 16)
1. Reviewing and editing previous work **(Done)** 2. Testing 28d samples a. Different curing (1d 70°, 27d AMB sealed and unsealed/28d AMB /28d 70°) b. RCA fines c. RGA fines d. HGB sand (0/8 -> 0/2) e. SW (1d 70°, 27d AMB /28d 70°) f. XRD on al 28d see difference in mineralogy and microstructure 3. Ambient samples 2h + 12h 4. Processing data a. In progress, XRD software is only on the lab computer available. Analyzing them takes a lot of time. List of possible minerals is made. 5. Optical microscope aggregates (grain size and shape) 6. PH **(Done)** a. All resources and activator(s), both pH-strips and electrical measurement are done 7. Writing results a. In progress 8. Extra trails (WWA2, SG1, Reactivity) a. WWA 2 at 24h [70°C: Flex.= 4,75 MPa; comp.= 50,78 MPa] & [AMB: Flex.=1,79 MPa; comp.=12,05 MPa] b. SG1 (3 variations) c. Reactivity trials (3 variations at 4h & 24h)
Section 3 (What is to be done for the weeks 15 and 16)
1. Testing 28d samples a. Different curing (1d 70°, 27d AMB sealed and unsealed) b. RCA fines c. SW (28d 70°) 2. Ambient samples 2h + 12h 3. Processing data

4. Optical microscope aggregates, precursors (grain size and shape)
5. Writing results
6. Extra trails
    a. Reactivity
7. Discussing paper subjects
8. Finish writing thesis
9. Presentation

Additional Information:

- PSA; What to do with the big deviation between Blaine/TDS and laser?
- Density

Meeting minutes 08/05/2023

Section 1 (What was planned for week 15 and 16)

1. Testing 28d samples
2. Ambient samples 2h + 12h
3. Processing data
4. Optical microscope aggregates, precursors (grain size and shape)
5. Writing results
6. Extra trails
7. Discussing paper subjects
8. Finish writing thesis
9. Presentation

Section 2 (What was done in the week 15 and 16)

1. Testing 28d samples **(Done)**
2. Ambient samples 2h + 12h **(Done)**
3. Processing data **(Done)**
4. Optical microscope aggregates, precursors (grain size and shape) **(Done)**
5. Writing results **(Done)**
6. Extra trails **(Done)**
7. Discussing paper subjects **(Done)**
8. Finish writing thesis **(Done)**
9. Presentation **(Done)**

Section 3 (What is to be done for the weeks 17 and 18)

1. Proofreading ourselves
2. Writing paper(s)
3. Making final presentation

Additional Information:

B Risk assessment

#	Risk	Description	Likelihood	Severity	Risk	Actions to minimize risk
		Used chemicals and materials				
1	Potassium chloride					
1.1	Inhalation	Inhalation of high concentrations may cause nasal or lung irritation.	2	2	4	Wearing a mouth mask.
1.2	Ingestion	Large quantities can produce gastrointestinal irritation and vomiting.	1	3	3	Wearing a mouth mask and gloves to avoid accidental ingestion after using.
1.3	Skin contact	Contact may cause irritation or rash, particulary with moist skin.	2	2	4	Wearing lab coat and proper gloves.
1.4	Eye contact	Moderate eye irritant. Redness, tearing, possible abrasion can occur.	2	2	4	Wash skin after handling, wear eye or face protection.
2	Calcium chloride hexahydrate					
2.1	Ingestion	Can lead to burns in the mouth and throat, excess thirst, vomiting, stomach pain, low blood pressure and other possible severe health effects.	1	4	4	Wash skin after handling. Wearing a mouth mask and gloves to avoid accidental ingestion after using.
2.2	Skin contact	Can cause excessive dryness or desiccating moist skin. In extreme cases it can cause skin burns.	2	2	4	Wearing lab coat and proper gloves.
2.3	Eye contact	Can cause serious eye irritation.	2	2	4	Wash skin after handling, wear eye or face protection.
3	Sodium oxide					
3.1	Physical hazards	May cause fire or explosion, it acts as a strong oxidiser.	2	5	10	Keep away from heat, hot surfaces, sparks, open flames and other ignition sources. No smoking.
3.2	Skin contact	Causes severe skin burns.	3	5	15	Wearing lab coat and proper gloves.
3.3	Eye contact	Causes serious eye damage.	2	5	10	Wash skin after handling, wear eye or face protection.
4	Portland cement					
4.1	Inhalation	May cause respiratory irritation	2	2	4	Avoid dust by proper ventilation, wearing a mouth mask.
4.2	Skin contact	Causes skin irritation, in serious cases it can even cause skin burns.	2	3	6	Wearing lab coat and proper gloves.
4.3	Eye contact	Can cause serious eye irritation.	2	3	6	Wash skin after handling, wear eye or face protection.
5	Aggregates					
5.1	Eye contact	Possible eye irritation due to dust while seeving of processing.	3	2	6	Avoid dust by proper ventilation, wearing goggles.
5.2	Inhalation	Inhalation of high concentations of dust while seeving or processing may cause lung irritation.	3	2	6	Avoid dust by proper ventilation, wearing a mouth mask.
6	Calcined clays (Metakaolin)					
6.1	Inhalation	Inhalation of high concentrations may cause nasal or lung irritation.	3	2	6	Wearing a mouth mask.
6.2	Skin contact	Prolonged or repeated exposure may cause skin irritation	2	1	2	Wearing lab coat and proper gloves.
6.3	Eye contact	Can cause eye irritation.	2	2	4	Wash skin after handling, wear eye or face protection.
7	Ground granulated blast furnace slags					
7.1	Inhalation	Inhalation causes respiratory irritation and may cause cancer.	3	5	15	Avoid dust by proper ventilation, wearing a mouth mask.
7.2	Skin contact	Excessive contact may cause irritation or rash.	3	2	6	Wearing lab coat and proper gloves.
7.3	Eye contact	Moderate eye damage.	2	2	4	Wash skin after handling, wear eye or face protection.

#	Risk	Description	Likelihood	Severity	Risk	Actions to minimize risk
7.4	Environmental hazards	Harmfull to the environment and aquatic life, even with long lasting effects.	2	5	10	Avoid contamination by proper housekeeping and waste control.
8	Waste wood ash					
8.1	Inhalation	Inhalation causes respiratory irritation and may have permanent effects due to heavy metals in ashes.	3	5	15	Avoid dust by proper ventilation, wearing a mouth mask.
8.2	Skin contact	Contact may cause irritation or rash.	3	2	6	Wearing lab coat and proper gloves.
8.3	Eye contact	Can cause serious eye irritation.	2	2	4	Wash skin after handling, wear eye or face protection.
8.4	Environmental hazards	Harmfull to the environment and aquatic life, even with long lasting effects due to the harmfull components and heavy metals in the ashes.	2	5	10	Avoid contamination by proper housekeeping and waste control.
9	Sodium silicate in aqueous solution (activator)					
9.1	Ingestion	Harmful if swallowed.	1	4	4	Wash skin after handling. Wearing a mouth mask and gloves to avoid accidental ingestion after using.
9.2	Skin contact	Corrosive, causes skin irritation.	3	3	9	Wearing lab coat and proper gloves.
9.3	Eye contact	Causes serious eye damage.	1	4	4	Wash skin after handling, wear eye or face protection.
9.5	Physical hazards	Dried material forms thin glass that can cut skin upon contact. Spilled material may cause a slipping hazard	2	2	4	Good housekeeping, proper safety equipment.
		Used devices and testing instruments				
10	Dry oven					
10.1	Physical hazards	Chance of burning the hands when handeling moulds in the oven, burning on the interior of the oven or the hot steel moulds.	4	3	12	Wearing proper heat-resistant gloves.
11	Samples					
11.1	Physical hazards	Samples could cause burn related injuries when demoulding from the steel moulds or heated samples.	3	3	9	Wearing proper heat-resistant gloves.
11.2	Physical hazards	Samples could possibly cause cut related injuries due to sharp edges or particles.	2	3	6	Wearing proper protective gloves.
12	Mixer					
12.1	Physical hazards	The rotation of the machine could grab onto loose hair or clothes, causing possible severe injuries.	1	5	5	Tie loose hair and avoid wearing loose clothing around rotating objects.
12.2	Inhalation	Produced dust during mixing can cause irritation of the respiratory system.	5	3	15	Avoid dust by proper ventilation, wearing a mouth mask.
12.3	Eye contact	Produced dust during mixing can cause eye irritation.	5	3	15	Wash skin after handling, wear eye or face protection.
12.4	Skin contact	During the mixing, some of the chemicals can splash outside the bowl, causing possible irritation depending on the content.	2	3	6	Wearing lab coat and proper gloves, wash skin after handling.
13	Electrical-pH meter					
13.1	Skin contact	When cleaning, some residue of possibly acidic or alkaline sample could splash on the skin.	1	3	3	Wearing proper protective lab clothing.

#	Risk	Description	Likelihood	Severity	Risk	Actions to minimize risk
14	Handheld XRF					
14.1	Inhalation	Produced dust during preparations of the samples for XRF can cause irritation of the respiratory system.	3	5	15	Avoid dust by proper ventilation, wearing a mouth mask.
14.2	Physical hazards	Excessive scanning without proper protection from the X-Rays could have serious health deficits.	2	5	10	Use proper protection from the X-Rays and avoid direct physical directed X-Rays.
15	XRD					
15.1	Inhalation	Produced dust during preparations of the samples for XRD can cause irritation of the respiratory system.	3	5	15	Avoid dust by proper ventilation, wearing a mouth mask.
15.2	Physical hazards	The robotic sample picking system could result in possible injuries (such as crushed fingers) when interfering with the movements.	1	5	5	Close the protective cover of the XRD machine and don't put things in the area of the robotic sample picking system.
16	Laser diffraction analysis					
16.1	Skin contact	During the analysis, some of the chemicals can splash causing possible irritation depending on the content.	1	1	1	Wearing lab coat and proper gloves, wash skin after handling.
16.2	Inhalation	Produced dust of the samples can cause irritation of the respiratory system.	1	5	5	Avoid dust by proper ventilation, wearing a mouth mask.
17	Blaine analysis					
17.1	Skin contact	During the analysis, some of the chemicals can splash causing possible irritation depending on the content.	3	3	9	Wearing lab coat and proper gloves, wash skin after handling.
17.2	Inhalation	Produced dust of the samples can cause irritation of the respiratory system.	2	5	10	Avoid dust by proper ventilation, wearing a mouth mask.
18	Jaw crusher					
18.1	Physical hazards	Crusher produces a loud noise, extensive use could result in hearing damage.	4	3	12	Wearing proper hearing protection.
18.2	Inhalation	Crushing produces a lot of dust that can cause irritation of the respiratory system.	2	5	10	Avoid dust by proper ventilation, wearing a mouth mask.

The 5x5 Risk Assessment matrix used to evaluate the risks. It is based on two parameters, likelihood and severity.
https://www.smartsheet.com/all-risk-assessment-matrix-templates-you-need

LIKELIHOOD ↓ / SEVERITY →	1	2	3	4	5
1	LOW 1	LOW 2	LOW 3	MEDIUM 4	MEDIUM 5
2	LOW 2	MEDIUM 4	MEDIUM 6	HIGH 8	HIGH 10
3	LOW 3	MEDIUM 6	HIGH 9	HIGH 12	EXTREME 15
4	MEDIUM 4	HIGH 8	HIGH 12	HIGH 16	EXTREME 20
5	MEDIUM 5	HIGH 10	EXTREME 15	EXTREME 20	EXTREME 25

C Technical data sheets

C.1 Sodium silicate in aqueous solution

Spécifications du produit

Produit	28079.363
Description du produit	Sodium silicate en solution aqueuse
Grade / qualité	TECHNICAL
Numéro CAS	1344-09-8
Formule moléculaire	Na2O. x SiO2.H2O (x = 3.4)

Analyses	Spécifications
Silicium dioxyde	25.6 - 27.6 %
Sodium oxyde	7.5 - 8.5 %

Signature

Nous certifions que ce lot est conforme aux spécifications listées ci-dessus.

Ce document a été produit électroniquement et est validé sans signature.

Isabelle Habay, Head of Laboratory - Briare
VWR International S.A.S.; Z.I. de Vaugereau; FR-45250 Briare; France

VWR International LLC, Radnor Corporate Center, Building One, Suite 200, 100 Matsonford Road, Radnor, PA 19087, USA
VWR International bv, Haasrode Research Park Zone 2020, Geldenaaksebaan 464, 3001 Leuven, Belgium

C.2 Powerpozz White

Product information

PowerPozz™ white

Thermal treated pure kaolin (metakaolin)
pozzolanic hardening admixture for cementitious building materials

Description

PowerPozz™ white is produced by calcination of purified kaolin and is a white, mostly amorphous alumosilicate reacting with Portlandite (calcium hydroxide) to build cementitious CSH-phases.

PowerPozz™ conforms to ASTM C-618 (Specifications for Natural and Calcined Pozzolans)

Chemical composition (M.-%)

SiO_2	54-56	CaO	< 0,1	SO_3	< 0,05
Al_2O_3	40-42	MgO	< 0,1	P_2O_5	< 0,2
Fe_2O_3	< 1,4	Na_2O	< 0,05		
TiO_2	< 3,0	K_2O	< 0,4	LOI	< 1,0

Physical characteristics

Specific density		2,6	g/cm³
Particle size distribution	D 10	~ 2	µm
	D 50	~ 5	µm
	D 90	~ 25	µm
Specific surface (Blaine)		ca. 26 000	cm²/g
Specific surface (BET)		ca. 20	m²/g
Colour		white	
Whiteness (Dr. Lange)		ca. 77	
Apparent density	freely settled	0,3 – 0,4	g/cm³
	tapped	ca. 0,5	g/cm³

Function

PowerPozz™ is mostly composed of the mineral Kaolinit – a layered silicate mineral with a distance of 7,2 Å between the layers. Between the layers of SiO_2 and Al_2O_3 in proportions of 1:2 water is imbedded in the layers that can be evaporated through heat treatment by calcination. The kaolin is then activated.

Portland cement develops 25 % calcium hydroxide (free lime) in its hydration. This alkaline by-product is very soluble and is primarily attacked and dissolved in the presence of acids or sulphates.

PowerPozz™ special feature is its capacity to bind large amount of free lime in the form of stable CSH-phases. Speed and amount of this reaction may be controlled through chemical and construction adequate methods

Felsenstrasse 12, CH-8808 Pfäffikon, Switzerland – www.newchem.info

In relation to its reactivity PowerPozz™ can be qualified as „rapid“. Together with lime and water the setting will occur in about 7 hours (method Newchem).

Application

PowerPozz™ is a pozzolanic mineral additive that may improve many performances of hydraulic cementitious mortars, concrete and analogous products.

PowerPozz™ is easily mixed in and gives a soft plastic consistence that is easy to work (buttery effect).

PowerPozz™ has shown its advantages in applications where strength, density and resistance are requested. Because of the finesse, high specific surface and reactivity it is well suited to replace silica fume.

In the following applications PowerPozz™ has been shown to be very useful:

Plasticity	shot-creet, repair mortars, coatings
Stability	self compacting mortar and concrete, selfleveling compounds
Strength	high performance concrete (HPC) or mortars (HPM)
Lime binding	tile adhesive, coating of water pipes, precast
Resistance	coatings of waste water or see water constructions
Pigmentation	better dispersion in precast or visible concrete
Efflorescence	roofing tiles, facade precast
Durability	improved alkali silicate reaction

Dosage 5 to 15 % replacement of cement by weight.

Stability unlimited in dry conditions.

Storage in protected and dry rooms.

Packaging in bags of 20 kg or in big bags of 1000 kg.

PInfo PPw 2007-07 – v5e

NEWCHEM AG **Felsenstrasse 12, CH-8808 Pfäffikon, Switzerland – www.newchem.info**

C.3 Slagg Ecocem

ecocem

GGBS
TECHNICAL DATA SHEET

Ecocem Ground Granulated Blastfurnace Slag is used in combination with Portland Cement to produce superior longer lasting concrete.

A replacement rate of up to 70% is permitted by the I.S EN 206-1. Ecocem GGBS replacement greater than 66% is classified as a sulfate resistant cement by EN 197 and can be used in aggressive ground conditions.

Ecocem GGBS is an industrial by-product that is diverted from landfill and upcycled into a commodity product. On exiting the iron processing system, molten blast furnace slag is rapidly quenched with water to form Granulated Blastfurnace Slag (GBS). The GBS is sourced from selected high quality suppliers in Europe. Ecocem GGBS is produced by drying and grinding the GBS at our milling plant in Dublin.

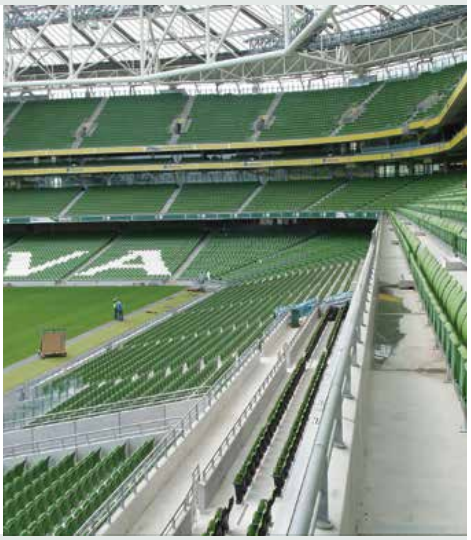

CHEMICAL COMPOSITION

The rate of vitrification means that the glass content of Ecocem GGBS is greater than 95%. (measured by X-ray diffraction) ensuring highly reactive material. The typical chemical composition of Ecocem GGBS is provided below:

SiO_2	Al_2O_3	Fe_2O_3	CaO	MgO	MnO	TiO_2	SO	Cl	S^{2-}	$Na_2O_{eqv.}$
36.5	10.4*	0.7	42.4	8.1	0.4	0.5	0.1	0.01	0.7	0.5

*Al_2O_3 content below 14% guarantees the durability performance of Ecocem

PHYSICAL CHARACTERISTICS

Standard Characteristics of Ecocem GGBS in combination with reference cement CEM I 42.5R:

COMBINATION		COMPREHENSIVE STRENGTH			ACTIVITY INDEX		INITIAL SETTING TIME
Ecocem GGBS	Cem I	7 Days	28 Days	56 Days	7 Days	28 Days	
0%	100%	45	58	61	-	-	120
50%	50%	35	59.5	65	78%	103%	170
70%	30%	27.5	54	58.5	61%	93%	200

Compressive strength reported in MPa measured by EN 196-1 mortar prisms.

Innovation Powering Sustainability

OTHER VALUES

BLAINE	450 ∓30m_2 /kg
D_{50}	11/µm
RELATIVE DENSITY	2.8 - 3g/cm^3
BULK DENSITY	0.9 - 1.2g/cm^3
ENVIRONMENTAL PRODUCT DECLARATION (EPD EN 15804)	42kg CO_2/tonne
L* (WHITNESS)	89
SOLAR REFLECTIVITY INDEX (SRI) OF CONCRETE	
50% GGBS	60
70% GGBS	74

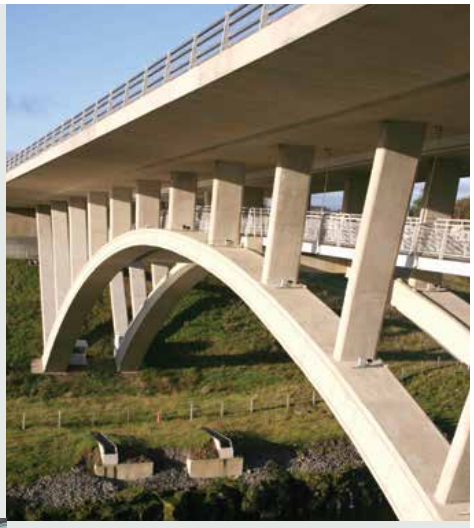

ENVIRONMENTAL CREDENTIALS

Ecocem Ireland Ltd. employs an ISO 14001 Environmental Management System and ISO Quality Management System to ensure we continuously improve our performance and decrease our impact on the environment. Ecocem GGBS has a Very Good rating certification for BES 6001 Responsible Sourcing of Construction Products from the BRE and a third party verified Environmental Product Declaration of 42kg CO2 per tonne. Replacing traditional Portland cement with Ecocem GGBS can help lower the overall embodied energy of your project and contribute to LEED and BREEAM green building rating systems.

CERTIFICATION

Ecocem GGBS has been rigorously tested in accordance with I.S. EN 15167 GGBS Standard. The product has been issued with an EC certificate of conformity to System +1 the NSAI and carries the CE mark 0050-CPR – 0074. A declaration of performance is available on request in accordance with the Construction Products Regulations.

CE 0050 - CPR - 0074

HEALTH & SAFETY OHSAS 18001:2007 NSAI Certified

CEMENT I.S. 197-1:2001 NSAI Certified

ENVIRONMENT I.S. EN ISO 14001:2015 NSAI Certified

QUALITY I.S. EN ISO 9001:2015 NSAI Certified

GROUND GRANULATED BLASTFURNACE SLAG I.S. EN 15167-1:2006 NSAI Certified

BES 6001 Responsible Sourcing www.greenbooklive.com

FSC

FEATURES

Ecocem GGBS is specified for its' technical, environmental and aesthetic qualities by engineers, architects and stakeholders. Using Ecocem GGBS in concrete can extend the lifespan, prevent cracking and lower the embodied energy of a project.

- **Increased durability against chemical and acid attack**
- **Increase long term strength**
- **Improved workability**
- **Lowers heat of hydration and reduces the risk of thermal cracking**
- **Sulfate and chloride resistant**
- **Whiter colour lowers pigment requirement**
- **Lower embodied energy**
- **Verified Environmental Product Declaration**
- **Contributes to credits under LEED and BREEAM building rating systems**

Version No: 181

Ecocem Ireland Ltd., Block F1, East Point Office Park, Dublin 3
T IRL +353 (0)1 678 1800 | UK +44 (0) 845 434 8191 E technical@ecocem.ie W www.ecocem.ie

C.4 Slagg Bremen

TEKNISK INFORMATION

Reviderad 2022-12-12OE. Gällande version kan laddas ner från www.thomasconcretegroup.com

Slagg Bremen

Mald granulerad masugnsslagg för användning i betong och bruk enligt SS 137003.

CE

0402

Thomas Cement AB, Box 5162, SE-402 26

2014

0402-CPR-SC0324

SS-EN 15167-1:2006

Mald granulerad masugnsslagg
för användning i betong, bruk och injekteringsbruk

GGBS – Slagg Bremen

Övriga specifikationer om produkten se aktuellt Produktdatablad (på www.thomasconcretegroup.com)

Slagg Bremen är ett mineraliskt tillsatsmaterial (typ II) med latent hydrauliska egenskaper, för användning som bindemedel i betong och bruk enligt SS 137003. Enligt standarden SS-EN 15167-1 benämns slagg som GGBS, vilket står för ”Ground Granulated Blast Furnace Slag” (mald granulerad masugnsslagg). Slagg Bremen kommer från järntillverkning i Tyskland och är ett kvalitetssäkrat och CE-märkt tillsatsmaterial som uppfyller kraven i SS-EN 15167-1 och -2. Användningen av Slagg Bremen som ett tillsatsmaterial/bindemedel erbjuder följande möjligheter:

- Minskad cementmängd (minskad CO_2 belastning)
- Förbättrad pump- och arbetbarhet samt minskat vattenbehov
- Minskad värmeutveckling och risk för temperatursprickor vid massiva konstruktioner
- Ökad beständighet (ökad sulfatbeständighet, ökat motstånd mot alkalikiselreaktioner, syra och kemiska angrepp, samt minskad inträngning och ökad bindning av klorider)
- Ljusare betong med högre ytfinish

Historik och ursprung

De latenta hydrauliska egenskaperna hos mald och granulerad masugnsslagg (GGBS) upptäcktes 1862 i Tyskland av Emil Langen, som visade att om man snabbt kylde (granulera) slaggsmältan från järnmasugnen och sedan malde denna samt blandade den med bränd kalk, kunde hög hållfasthet uppnås. Denna utveckling ledde till den första kommersiella produktionen av slagg-kalk-cement i Tyskland 1865. I Frankrike användes slaggcement år 1889 för att bygga Paris tunnelbana. Godhard Prüssig kombinerade GGBS och Portlandcement, vilket ledde till den första produktionen av Portland-slagg-cement i Tyskland år 1892. Sedan dess har användningen av GGBS varit omfattande, bl.a. i många europeiska länder, såsom Holland, Frankrike, Storbritannien och Tyskland, dels som råvara för tillverkning av cement, och dels som ett tillsatsmaterial i kombination med portlandcement, släckt kalk, naturlig gips, eller anhydrit. Det tillverkas idag årligen ca 100 miljoner ton GGBS i världen, men i Sverige är tillverkningen och användningen av GGBS begränsad.

Slagg Bremen tillverkas av Holcim AG i Bremen, Tyskland. Holcim är ett globalt företag med bas i Schweiz, med över 80 tusen anställda i drygt 70 länder. Holcim inledde produktion av cement år 1912 i Holderbank nära Zürich, och är idag den näst största cementtillverkaren i världen (efter Lafarge). Företaget levererar också fabriksbetong, ballast, asfalt och tillhörande byggtjänster. Slagg Bremen introducerades på den svenska marknaden av Thomas Cement AB under 2011, och distribueras från terminal i Landskrona, Oxelösund och Uddevalla.

Tillverkning

Masugnsslagg är en biprodukt vid tillverkning av råjärn i masugn. Järnmalm med järnoxid som huvudkomponent upphettas tillsammans med koks till över 1500°C, vilket gör att järnoxidens syre övergår till kolet i koksen under bildning av kolsyra, koldioxid och kolmonoxid. Järnet reduceras till metall, smälter och uppsamlas i flytande form i den nedre delen av masugnen. Men eftersom järnmalmen inte enbart består av järnoxid utan även av föroreningar s.k. gångart, gäller det att avskilja det metalliska järnet från denna. Gångarten, som huvudsakligen består av kiselsyra och aluminiumoxid, har en betydligt högre smältpunkt än järnet. Det skulle därför leda till stora svårigheter att avskilja järnet från gångarten så länge denna föreligger i fast form. Detta löses genom att man förutom järnmalm och koks även matar in så mycket kalk i masugnen att denna tillsammans med gångarten ger en förhållandevis lättsmält massa, så kallad masugnsslagg. Denna flyter på den tyngre jämsmältan och kan på samma sätt som järnet periodiskt tappas ut. Masugnsslagg är ett material som är nära släkt med portlandcementet. Dess huvudbeståndsdelar är kalk, kiselsyra och aluminiumoxid. Produktionen av järn och slagg sker kontinuerligt och oavbrutet under minst tre år, varför tillverkaren måste säkerställa ett lager av råmaterial av jämn kvalitet för en konstant matning. För varje ton producerat råjärn, genereras ca 300 kg slagg, och en masugn genererar upp till ca 1,0 miljoner ton slagg per år.

Men det är först efter att man genom snabb avkylning sörjt för att kristallisationen är minimal och den granulerade masugnsslaggen blir amorf (glasartad) i sin struktur, vilket resulterar i det latent hydrauliska reaktiva materialet som eftersträvas. Efter att slaggen tappats av sker avkylningen genom att spruta med stora mängder vatten (10-20 ggr slaggen), eller låta den smälta slaggen löpa ut i vatten, så den snabbt kommer ner i temperatur under 50°C. Den snabba avkylningen gör att ett hårt sintrat enskornigt (ca 5 mm stor) granulat med karaktär av sand erhålls. Därefter läggs den på hög och avvattnas, varefter den siktas och torkas. Vattenkyld granulerad masugnsslagg (GBS) kallas även för slaggsand eller hyttsand (från tyskans Hüttesand). Detta skall inte förväxlas med hyttsten, som är den mer kristallina luftkylda slaggen. GBS användas som vägmaterial och markstabilisering, eller av cementindustrin där den sam- eller separatmals för tillverkning av cement. GBS kan även separatmalas till ett fint pulver och man får tillsatsmaterialet ”mald granulerad masugnsslagg”, GGBS.

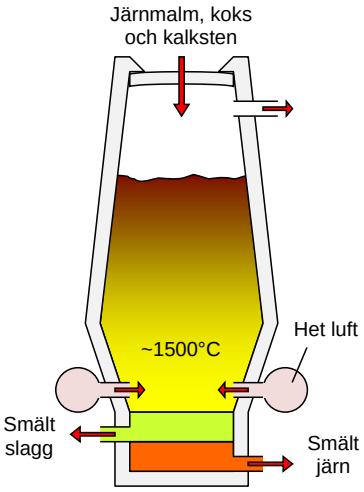

Kemisk sammansättning och reaktion/hydratation

GGBS är i princip sammansatt av samma oxider som Portlandscement, d.v.s. basiska oxider av kalcium (CaO), magnesium (MgO), och sura oxider av kisel (SiO_2) och aluminium (Al_2O_3). Avkylningen av den smälta slaggen är viktig för dess sammansättning. Sker denna långsamt genereras en samling av kristallina mineraler, men då den kyls snabbt skapas ett granulerat med ett glashaltigt (amorft) nätverk av de viktiga oxiderna (CaO, SiO_2, MgO och Al_2O_3) i oordnad kombination med syre. Mindre komponenter såsom natrium, kalium och titan förekommer också. Dessa alkaliska metalljoner förekommer som en integrerad del i den amorfa/glasiga strukturen, varför mängden vattenlösliga alkalier är låg hos GGBS. Glashalten skall vara minst 67% (SS-EN 15167-1), men bör vara över 90%. Utöver denna amorfa fas, beroende på slaggsammansättning och avkylningen, kan det förekomma små mängder av kristallina faser (bl.a. dikalciumsilikat, gehlenit, anortit, åkermanit och merwinit).

Förutom den kemiska sammansättningen av slaggen, är ugnens temperatur, resultatet av avkylningen och malningen viktiga egenskaper för att säkerställa en kvalitativ GGBS. Den kemiska sammansättningen kan variera något mellan olika järnverk, beroende på delmaterialens (malm, kalksten och koks) egenskaper och på masugnens funktion. Men från en och samma ugn är variationen generellt inte större än ±2% för CaO och SiO_2, samt ±1% för MgO och Al_2O_3.

Med enbart vatten reagerar GGBS så långsamt att den ej kan komma i betraktande som självständigt hydrauliskt bindemedel. För att hårdna/binda krävs det utöver vatten löslig kalkhydrat (kalciumhydroxid, $Ca(OH)_2$), eller annan stark bas såsom natrium- eller kaliumhydroxid (NaOH och KOH), vilka fungerar som alkalisk aktivator. $Ca(OH)_2$ bildas när portlandscement (PC) reagerar med vatten, och när väl reaktionerna satts igång finns det tillräckligt med CaO hos GGBS för att kalciumsilikathydrat (CSH) skall bildas. Dessa reaktioner är av samma art som de som sker under hårdnandet av PC, men sker i allmänhet något långsammare.

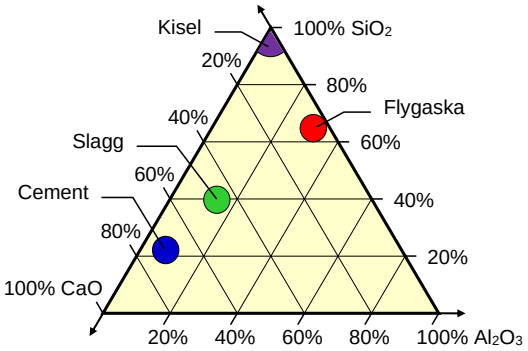

Man betecknar därför GGBS som ett "latent" hydrauliskt bindemedel, d.v.s. reaktionen med vatten är dold tills den framkallas av någon aktivator. Hos pozzolaner, exempelvis flygaska, är CaO-halten däremot otillräcklig. Reaktiviteten hos GGBS styrs främst av dess glashalt, finhet och andelen reaktiva oxider (CaO, SiO_2 och Al_2O_3). Den kemiska sammansättningen för Slagg Bremen redovisas i tabellen under ”Kemisk data”.

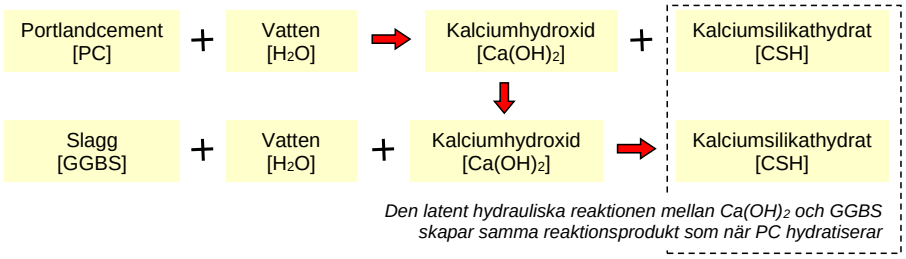

Den latent hydrauliska reaktionen mellan $Ca(OH)_2$ och GGBS skapar samma reaktionsprodukt som när PC hydratiserar

Finhet

Partikelstorleken och finheten styrs av malningen av den granulerade slaggen. Finheten (som specifik yta, uppmätt med Blaine) skall vara minst 275 m^2/kg (SS-EN 15167-1), men är generellt betydligt högre och ofta likvärdig med cement. Finheten styr till stor del reaktiviteten hos GGBS, samt dess vattenbehov. Granulerad slagg är ett mycket hårt material, varför malningen är energikrävande. Slagg Bremen har en finhet (Blaine) på 400-440 m^2/kg, vilket kan jämföras med Byggcementets ca 430 m^2/kg, men storleksfördelning (siktkurva) är något finare än Byggcement (se diagram).

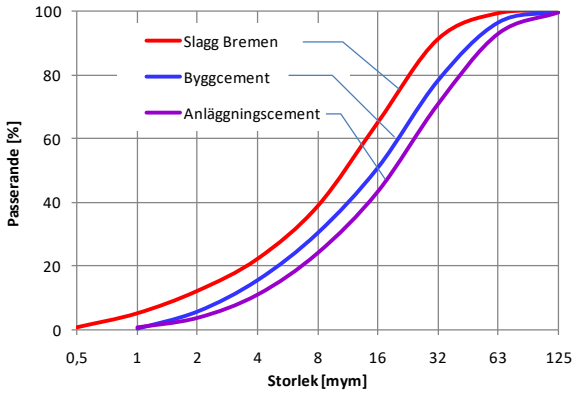

Densitet

Slagg Bremen har en kompaktdensitet på 2900 kg/m^3, vilket kan jämföras med cement som har ca 3100 kg/m^3, och skrymdensitet ca 1150 kg/m^3 (cement ca 1250 kg/m^3).

Exempel:	*För en betong med 400 kg cement och 160 liter vatten där 25% av cementmängden ersätts med lika vikt (k=1,0) GGBS ökar pastavolymen från* $V_p = C/\rho_c + GGBS/\rho_{GGBS} + V/\rho_v = 400/3{,}2+160/1{,}0 = 285$ *liter till* $300/3{,}2+100/2{,}9+160/1{,}0 = 288$ *liter*

Hårdnande och hållfasthetsutveckling

Hållfasthetsutvecklingen upp till ca 7 dygn går som regel långsammare när GGBS används som ersättning för en del av portlandcement i betong. Efter 7 dygn är utvecklingen den omvända, och vid 28 dygn är hållfastheten som regel likvärdig eller högre med GGBS, för att sedan fortsatt öka i högre utsträckning än vad som sker hos portlandcement. I vilken grad hållfastheten utvecklas är främst beroende på beroende på andel GGBS som ersätter cementen, men även på den initiala betongtemperaturen, vatten-cement-talet (*vct*), samt egenskaperna hos cement och GGBS. Även vilken effektivitetsfaktor (*k*) som ansätts har inverkan, där *k*=1,0 ger ett långsammare hårdnande än med *k*=0,6.

Med GGBS förlängs tidpunkten för betongens initiala tillstyvnande och vid höga doseringar kan den förlängas med upp till en timme vid 20°C, men liten eller ingen förändring sker vid temperaturer över 30°C. Vid låga temperaturer kan retardationen bli stor, varför extra isolering, tillskotsvärme eller acceleratorer kan behövas för att minimera denna effekt. Eftersom mängden av portlandcement i en blandning vanligtvis bestämmer tillstyvnandet, kan det vara aktuellt att minska doseringen GGBS i kallt väder, exempelvis max 25% (20% av bindemedel). Ett annat alternativt är att sänka effektivitetsfaktorn (*k*), om 1,0 ner till exempelvis 0,6. Vid högre temperaturer, exempelvis sommartid, eller tjockare konstruktioner, är en långsammare tillstyvnad däremot ofta önskvärd. Betong med höga doseringar GGBS är då ofta fördelaktigt.

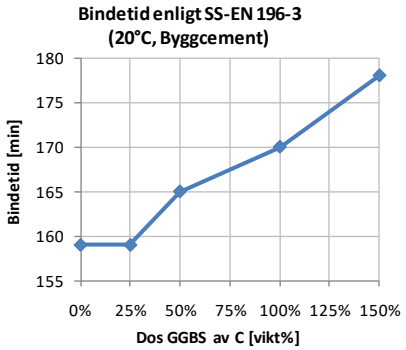

Eftersom hållfasthetsutvecklingen för betong med GGBS fortsätter i större utsträckning, kan en högre ålder än 28 dygn kan vara lämpligt som dimensionerande värde (exempelvis 56 eller 91 dygn).

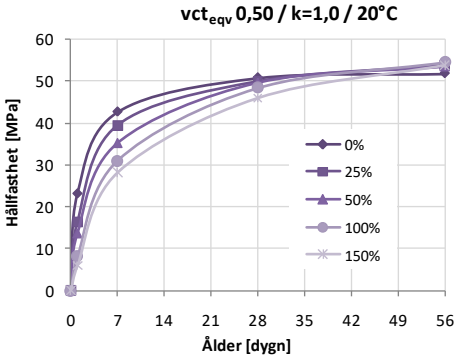

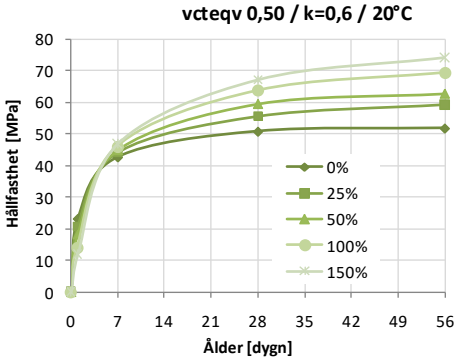

Temperaturutveckling

Vid betongtemperatur under 30°C blir temperaturutvecklingen både långsammare och lägre när en del av cement ersätts med GGBS (se diagram). Effekten ökar med ökad dos GGBS samt med minskad betongtemperatur. Även vilket värde på effektivitetsfaktorn (*k*) man ansätter påverkar temperaturutvecklingen, på samma sätt som den har på hållfasthetsutvecklingen (se diagram). Vid tillfällen då betongtemperaturen behöver begränsas, exempelvis under sommartid eller vid tjockare konstruktioner (exempelvis fundament), kan därför höga doser av GGBS vara gynnsamt.

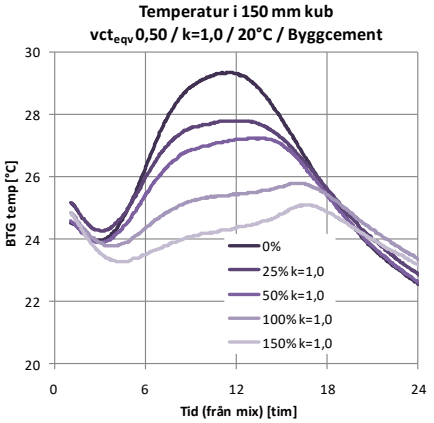

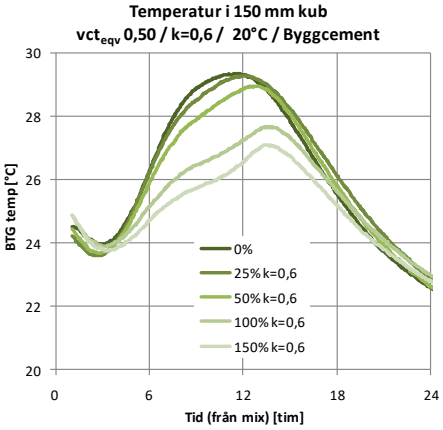

Dosering

Doseringen av slagg (GGBS) i betongen brukar anges som vikt% av bindemedelsmängden eller cementmängden. I senaste utgåvan av SS 137003 anges doseringen som vikt% på bindemedlet, medans i tidigare utgåvor var det på cementmängden. Exempelvis motsvarar 50% slagg av bindemedelsmängden 100% av cementmängden. På samma sett motsvarar 20% slagg av bindemedel 25% av cement. För att räkna om vikt% dosering slagg av bindemedelsmängden (XB_{GGBS}) till av cementmängden (XC_{GGBS}), och omvänt, görs det enligt:

$$XC_{GGBS} = \frac{XB_{GGBS}}{100\% - XB_{GGBS}} \qquad XB_{GGBS} = \frac{XC_{GGBS}}{100\% + XC_{GGBS}} \qquad [\%]$$

Se också under ”*k-faktor*”, ”*Maximal dosering*” och ”*Konsistens*”.

k-faktor

Effektivitetsfaktorn (*k*) gör det möjligt att tillgodoräkna sig slagg (och andra tillsatsmaterial av typ II), med hänsyn till betongens 28-dygnshållfasthet och beständighet. I stället för *vct* beräknas det ekvivalenta vatten-cement talet (vct_{eqv}) enligt:

$$\mathrm{vct}_{eqv} = \frac{V}{C + k \cdot GGBS} \qquad [-]$$

Alternativt kan cementmängden (*C*) för en given vattenmängd (*V*), dos slagg (av cementvikten, XC_{GGBS}) och vct_{eqv} beräknas enligt:

$$C = \frac{V}{\mathrm{vct}_{eqv} \cdot (1 + k \cdot XC_{GGBS})} \qquad [kg]$$

Vid beräkning vct_{eqv} med slagg som bindemedel gäller effektivitetsfaktorn *k*=0,7 (tidigare 0,6) enligt SS 137003, men en högre faktor (*k*=0,8 och 0,9) kan tillämpas med aktuellt cement om detta med slaggen har ett aktivitetsindex över 80% efter 28 dygn (provning och utvärdering enligt SS-EN 15167-1 och -2). Maximalt 50 vikt% av bindemedelsmängden får tillgodoräknas med k-faktor, enligt SS 137003. Vill man tillgodoräkna sig högre slagginblandning (motsvarande k=1,0), kan man tillämpa konceptet EPCC (Equal Performance Cement Combinations). Detta innebär att man själv sätter samman en bindemedelskombination (BK) av cement och slagg, motsvarande ett CEM II/A-S, II/B-S, III, eller kompositcement. Mer information om EPCC ges i SS 137003 (bilaga P).

Slagg Bremen är godkänd för k-faktor 0,9 med följande cement:

- Bygg (Skövde) CEM II/A-LL 42,5 R
- BAS (Slite) CEM II/A-LL 42,5 R
- ANL (Brevik) CEM I 42,5 N SR3/MH/LA
- ANL (Slite) CEM I 42,5 N SR3/MH/LA
- ANL FA (Slite) CEM II/A-V 42,5 N NSR/MH/LA
- Schwenk Komposit CEM II/A-M (S-LL) 52,5 N

I kombination med andra cement (exempelvis SH och Velox) gäller k=0,7.

Godkännandebevis från RISE för utökad k-faktor finns att hämtas på Thomas Cements hemsida (under www.thomasconcretegroup.com). För mer information om EPCC och BK, kontakta Thomas Cement.

Exempel:	*Med 160 liter vatten, 300 kg cement och 20% slagg* av B med k=0,9 blir slaggmängden 0,20/(1-0,20)·300= 0,25·300= 75 kg, vilket i sin tur ger* vct_{eqv} *= 160/(300+0,9·75) = 0,435*
Exempel:	*Med ett vattenbehov på 170 liter, ett krav på* vct_{eqv}*=0,50 och 20% slagg* av B med k=0,9 blir cementmängden C = 170/[0,50·(1+0,9·25%)] = 278 kg,* och slaggmängden GGBS = 278·25% = 70 kg

** 20% av bindemedelsmändel motsvarar 25% av cementmändel, se under "Dosering".*

Aktivitetsindex (28 dygn) med Slagg Bremen ligger på ca 90%-100%, beroende på vilket cement som används. Detta möjliggör den högre effektivitetsfaktorn *k*=0,9 förutsatt att detta har provats och utvärderats med aktuellt cement enligt standard. Dosering slagg upp till ca 50% (av B, eller 100% av C) har ingen större effekt på aktivitetsindex. *vct*

Användes den lägre effektivitetsfaktorn *k*=0,7 leder detta som regel till en överhållfasthet vid 28 dygn. För att reducera hållfastheten kan exempelvis luft tillsättas. För varje % luft sjunker betongens hållfasthet med ca 2,0-2,5 MPa (eller ca 5% av hållfastheten). Dessutom har luften en smörjande effekt, varför pastavolymen kan reduceras något (ca 0,5-0,7 liter vatten för varje % luft, eller 1,0-1,5 kg cement+slagg). Med ökad lufthalt ökar dock risken för delaminering vid glättade golv.

Hållfasthetsutvecklingen för betong med slagg fortsätter i större utsträckning (motsvarande *k*≈1,2 efter 91 dygn), se "*Hårdnande och hållfasthets-utveckling*".

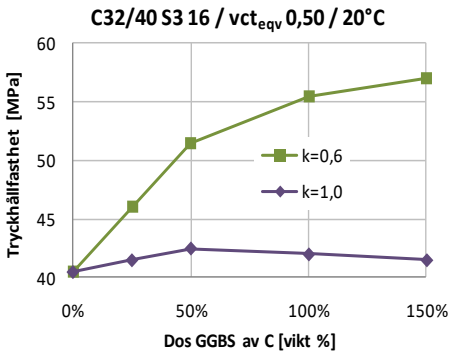

För betonger utan vct-krav, och slagg dos upp till 50%, kan en högre och mer realistisk faktor tillämpas, förslagsvis *k* ca 1,0 för Slagg Bremen (d.v.s. cement ersätts med ca lika vikt slagg, typ BK-konceptet). Dock kan högre doser (över ca 25%) slagg retardera betongen då cementmängden minskas, varför om tidig hållfasthet är ett krav kan en lägre faktor behöva tillämpas (alternativt accelerator, värme eller extra isolering). Med *k*=0,7 fås en likvärdig hållfasthet, som utan slagg, efter 4-6 dygn vid 20°C. Vid kallare klimat tenderar retardationen bli större med slagg, men vid högre temperaturer (över 30°C) är hållfasthetsutvecklingen minst likvärdig för slagg som cement.

Exempel:	*En betong med vct_{eqv} 0,50 och 33% Slagg Bremen (av B, eller 50% av C) och k=0,7 är sammansatt av 267 kg cement, 180 liter vatten och 134 kg slagg.* *En antagen överhållfasthet på 10 MPa reduceras genom att tillsätta luftporbildare så lufthalten blir L = Δf/2,0 = 10/2,0 = 5% luft.* *Luftens smörjande effekt gör att vattenmängden kan reduceras med 0,6 ·L = 0,6·5 = 3 liter.* *Sammansättningen blir i stället 180-3=177 liter vatten, cementmängden C = $V/[vct_{eqv}\cdot(1+k\cdot XC_{GGBS})]$ = 177/[0,50·(1+0,7·50%)] = 262 kg och mängden slagg S = $C\cdot XC_{GGBS}$ = 262·50% = 131 kg.*

Maximal dosering

Hur mycket slagg som kan tillsättas kan begränsas av *1)* hur mycket som får tillgodoräknas till vct_{ekv} och *2)* hur mycket som maximalt får tillsättas i respektive exponeringsklass.

För att tillgodoräkna sig effektivitetsfaktorn (k) i beräkningen av vct_{eqv} gäller generellt maximalt 50 vikt% av bindemedelsmängden, enligt SS 137003. Och har man ett cement som redan innehåller slagg skall även denna mängd räknas in, exempelvis med Komposit antaget innehållande 14% slagg (och 6% kalk) blir gränsen 41% av bindemedel (eller 70% av cement).

Största totala mängd slagg som får tillsättas i respektive exponeringsklass ges i SS-137003 (tabell 7-10), och anges som % andel (vikt) av bindemedel. Men eftersom man också skall förutsätta att cementet har en lägsta klinkerhalt (ges i SS-EN 197-1) blir det lägsta andel klinker för respektive exponeringsklass som gäller (i tabell 7-10, SS 137003). Det spelar således ingen roll vilken typ av tillsatsmaterial eller hur mycket som cementtillverkaren har tillsatt. Har man ett CEM II/A (Bygg, Bas, Komposit, mm) skall man anta att det innehåller 80% klinker och ett CEM I 95% klinker. Exempelvis för klass XC 1 gäller minsta andel klinker 35%, vilket ger maximal mängd slagg 100-35/0,95=63% för ANL (antaget 95% klinker) och 100-35/0,80=56% för Bygg (antaget 80% klinker).

Har man ett CEM II som innehåller slagg (exempelvis Schwenk Komposit, CEMII/A-M(S-LL)) skall detta medräknas in i den totala mängden slagg.

Enligt tabell 7-10 (SS 137003) blir maximal andel slagg som får tillsättas:

Exponeringsklass	CEM I + GGBS		CEM II/A** + GGBS	
	Högsta vct	vct -0,05***	Högsta vct	vct -0,05***
X 0	68%*		63%*	
XC1, XS1, XS2, XS3, XD1, XD2, XD3, XA1, XA2, XF1	63%*		56%*	
XC2, XC3, XC4	16%	63%*	0%	56%*
XF2, XF3	32%		19%	
XF4	16%	32%	0%	19%

** Maximal inblandning är högre än den som får tillgodoräknas vct_{ekv} med k-faktor (50%). Detta kan vara av mindre betydelse när man inte har vct-krav (ex. ofta i X 0 och XC 1) eller använder en betong med lägre vct än kravet för exponeringsklassen.*

*** Undantaget Schwenk Komposit vars innehåll (max) av slagg skall räknas samman med det som tillsätts.*

**** vct kan höjas med +0,05 enheter genom kvalifikationsprovning (fuktionsprovning)*

Exempel:	*För Byggcement (CEM II/A-LL), och exponeringsklass XS 1, är den maximala mängden slagg som få tillsättas 56% (eller 129% av cement). Av detta får enbart 50% tillgodoräknas till vct_{ekv}. Har man då vct 0,45 och 240 kg cement får 240·0,56/(1,0-0,56) = 305 kg slagg tillsättas men enbart 240·0,50/(1,0-0,50) = 240 kg tillgodoräknas. Med k=0,9 för slaggen ger det vattenmängden 0,45·(240+0,9·240) = 205 kg. Överskridande mängd 305-240 = 65 kg slagg räknas enbart som filler.*
Exempel:	*Med Komposit (CEM II/A-M S-LL) i ovan exempel blir den maximala mängden som får tillsättas densamma (56% eller 305 kg) eftersom det är klinkermängden i cementet som styr. Däremot minskar mängden slagg som får tillgodoräknas vct_{ekv} eftersom de 14% slagg som Komposit innehåller skall medräknas. Med 240 kg Komposit får 240·(0,50/(1,0-0,50)-0,14) = 206 kg av slaggen tillgodoräknas, och vattenmängden blir då 0,45·(240+0,9·206) = 191 kg.*

Konsistens

GGBS har slätare och tätare partikelyta än cement, vilket minskar betongens vattenbehov. Dessutom ökar pastavolymen då cement har en något högre densitet än GGBS. Den glasaktiga partikelytan har även en gynnsam effekt på konsistensförlusten.

Med Slagg Bremen och *k*=1,0 är andelen slagg som kan ersätta cement ca 50% av bindemedel (100% av C), med likvärdig konsistens. Denna konsistensfaktor (*a*) varierar med k-faktor, slaggdosering (av cementvikten, XC_{GGBS}) och till viss del cement typ samt vct_{eqv}. Mängden cement i betong med slagg (C_1) relativt utan (C_2) kan beräknas enligt:

$$C_2 = \frac{C_1}{1 + a \cdot XC_{GGBS}} \qquad [kg]$$

För *k*=0,7 är konsistensfaktorn (*a*) mer beroende av dosering (XC_{GGBS}) än vid *k*=1,0, se diagram. Överslagsmässigt kan man vid *k*=0,7 använda samma vattenmängd (*V*) med som utan Slagg Bremen.

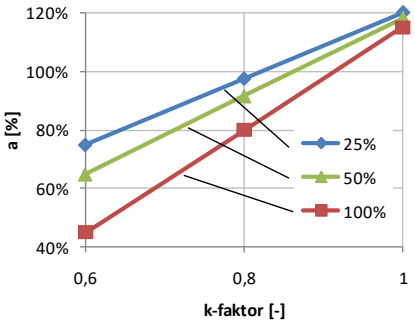

Exempel:	*En betong utan vct-krav med 360 kg cement (C_1) och 180 liter vatten (vct 0,50) har en given konsistens. Med k=1,0, a=115% och 25% Slagg Bremen av C blir den nya cementmängden C_2 = 360/(1+115%·25%)=280 kg och mängden slagg GGBS=280·25%=70 kg.* *Den nya vattenmängden blir $V_2=vct_{eqv}\cdot(C_2+k\cdot GGBS)$ = 0,50·(280+1,0·70)=175 liter*
Exempel:	*Samma betong, fast vct-krav, med k=0,7 och en överslagsmässigt lika vattenmängd på 180 liter ($V_1=V_2$).* *$vct_{eqv} = V_1/C_1 = V_2/(C_2+k\cdot GGBS) = V_2/[C_2\cdot(1+k\cdot XC_{GGBS})]$, vilket ger den nya cementmängden $C_2=C_1/(1+XC_{GGBS}\cdot k)$ = 360/(1+25%·0,7)= 306 kg, och slaggmängden GGBS=306·25%=77 kg*

SKB

Att göra självkompakterande betong (SKB) med GGBS skiljer sig inte från SKB utan. Proportionering och dosering m.a.p. hållfasthet, exponeringsklass, vct, tillsatsmedel, vattenbehov, konsistens, mm., är densamma som för vanlig betong (se tidigare avsnitt).

I vissa fall möjliggör SKB med GGBS att man kan minska fillern (ex. kalkfiller) något, då GGBS har lägre densitet än cement och genererar därför något större pastavolym. Och tillämpar man effektivitetsfaktorn k=0,9 (eller 0,7) kommer mängden finmaterial öka, varför fillermängden kan reduceras ytterligare.

För att illustrera hur en C30/37 vct 0,55 SKB kan vara sammansatt och hur receptet justeras med GGBS dos och olika k-faktor (k=0,95 för betong utan vct-krav), exempel enligt:

Id	**Ref**	**20% GGBS (av B)**			**33% GGBS (av B)**			**50% GGBS (av B)**		
k	-	*0,7*	*0,9*	*1,0*	*0,7*	*0,9*	*1,0*	*0,7*	*0,9*	*1,0*
Cement	**320**	272	255	244	237	214	201	188	163	147
Kalkfiller	**180**	150	165	170	120	145	155	90	115	145
GGBS	**0**	68	64	61	119	107	101	188	163	147
Vatten	**176**	176	172	168	176	171	166	176	170	162

Här hålls ballastfördelning, mängden (liter eller kg) flytmedel och luftporbildare oförändrad.

I de fall man inte har tillgång till kalkfiller (eller stenmjöl, osv) är proportionering av SKB med GGBS lite mer komplicerad. En SKB behöver en viss pastavolym (eller pastaöverskott) för att få rörlighet, en volym är större än för vanlig betong. Vidare behövs ett visst volymförhållande mellan vatten och pulver (finmaterial <0,125mm), för att skapa sammanhållning och robusthet så att betongen inte separerar. Detta volymförhållande bör ligga på vpt=1,0-1,1. Skulle man exempelvis skapa pastavolym genom att öka cement och vatten (konstant vct) kommer vpt bli för högt och betongen separationsbenägen. Ökar man däremot bara mängden cement blir betongen dyr och hållfastheten för hög, och genom att tillsätta GGBS som en ren filler effekten bli densamma.

För betong med lågt vct (<0,45) finns det som regel relativt mycket pasta och finmaterial, vilket gör det möjligt att göra en SKB utan filler. En viss justering i ballastsammansättningen kan behövas (ökad andel grus och sand). Använder man slagg med k-faktor blir mängden finmaterial och pastavolym högre, och därför enklare att få till. Med 33% GGBS (eller 50% av cement) eller mer, och k=0,7-0,9 brukar man utan större problem göra en SKB utan filler med vct upp till ca 0,50.

Vid vct över ca 0,50 behöver en betong relativt mycket finmaterial för att inte separera, att helt bort exempelvis 150 kg kalstensfiller kan vara problematiskt. Detta kan man lösa genom att gå ner i vct (och öka pastavolymen) i kombination med luftporbildare för att kompensera för hållfasthetsökningen (se avsnitt ”k-faktor” för hur hållfastheten reduceras med luft). Ett annat alternativ är att använda sig av stabilisator för att skapa sammanhållning.

Frostresistens

När betong med höga halter GGBS karbonatiserar kan detta på sikt ge en mer porös struktur, vilket resulterar i en minskad frostresistens. Vid saltfrost har det har visat sig att det funkar bra med upp till cirka 20-35% slagg av bindemedlesmängden (beroende på cement typ och vct), men vid högre doseringar kan avflagningen öka betydligt. Gränsvärden för maximal inblandning av slagg ges i SS 137003 tabell 9, där kravet på andel klinker styr maximal slagginblandning (likt de andra exponeringsklasserna). Förprov i XF4 med <80% klinker gäller provning på karbonatiserad yta förlängd till 112d och minst ”God” frostresistens.

Beständighet

Betong som innehåller GGBS har generellt en tätare porstruktur (mindre genomsläpplig). Detta ökar dess motståndskraft mot inträngande ämnen (sulfat- och kloridjoner, samt alkalier) som kan orsaka skadliga angrepp, såsom:

- Sönderfall på grund av sulfatangrepp
- Sprickor orsakade av alkali ballastreaktion
- Kloridrelaterade korrosion av armering

Sulfatbeständigheten förbättras även av att GGBS reagerar med kalciumhydroxid ($Ca(OH)_2$) som därför inte kan ingå i sulfatreaktioner senare, samt av att när cement ersätts med GGBS minskar mängden av

klinkermineralet trikalciumaluminat (C_3A), vilket är den primära källan till reaktivt aluminium vid skadliga sulfatreaktioner. När sulfatjonerna (SO_4^{2-}) reagerar med $Ca(OH)_2$ i betongens porvatten bildar svårlöslig gips ($CaSO_4^{2-}$), som i sin tur reagerar med C_3A. Detta bildar det expansiva mineralet ettringit som kan spränga sönder betongen. Innehåller betongen kalciumkarbonat (CO_3, t ex kalkfiller) kan denna på liknande sätt reagera med sulfatjonerna och bilda det expansiva mineralet thaumasit.

Enligt SS 137003 kan man genom att tillsätta 150-400% GGBS till ett icke sulfatresistent cement uppnå ett sulfatresistent bindemedel. Sulfater kan finnas i cement och ballast, men tillförs oftast utifrån (från mark, grund-/havs-/avloppsvatten, mm). Sulfathalten för Slagg Bremen är ca 0,01%, vilket kan jämföras med Byggcementets ca 3,5%.

Trots att alkaliteten (Na_2O_{ekv}) för Slagg Bremen är likvärdigt med Byggcement (ca 0,9-1,0%), har det visat sig att den effektiva alkaliteten blir lägre för betong GGBS. Med exempelvis 100% GGBS och Byggcement sjunker den effektiva alkaliteten från ca 1,0 till 0,5% (se diagram). För Anläggningscement är motsvarande effekt mindre (från ca 0,6 till 0,4%). Genom att reducera alkaliteten minskar risken för skadlig expansionen från alkali ballastreaktioner (alkalikiselsyra, alkalisilikat och alkalikarbonat). Potentiellt reaktiv ballast kan vara flinta och opalhaltig ballast (ex Skåne), kryptokristallin och deformerad kvarts (ex Stockholm), samt porfyrhaltig ballast (ex Dalarna).

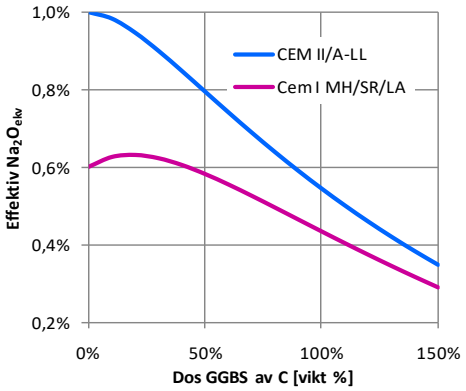

I Storbritannien finns riktlinjerna vid beräkning av alkaliteten (BRE Digest 330, 2004). Om mängden GGBS är ≥100% (av C) så behöver bidraget från GGBS ej medräknas, vid <25% så medräknas hela bidraget, och däremellan medräknas 50% av alkalibidraget från GGBS.

Den minskade effektiva alkaliteten har generellt ingen inverkan på armeringens korrosionsskydd. Det är först vid doser över ca 400% GGBS av cementvikten, som det alkaliska skyddet påverkas.

Inträngningen av kloridjoner (från tösalter, havsvatten, mm) minskar med den ökade tätheten GGBS ger betongen (minskad permeabilitet), på samma sätt som för sulfater och alkalier. Kloridinträngningen minskas även av att betong med GGBS har en ökad kloridbindning, p.g.a. ökad mängd fri aluminiumoxid samt av den lägre sulfathalten. Kloriderna har i sig ingen negativ inverkan på betongen, men för armerade konstruktioner kan de vara kritiska. Dessutom ger en ökade tätheten en ökad resistivitet, vilket i sin tur minskar förutsättningarna för armeringskorrosion. Utomlands är mycket höga doser av GGBS vanligt i exempelvis marina konstruktioner (kajer, fundament, mm).

Däremot kan frostbeständigheten försämras vid höga doser GGBS, på samma sätt som andra alternativa bindemedel (flygaska, silika/kisel), se under ”*Frostresistens*”.

Betongens syramotstånd ökar med ökad inblandning av GGBS. Detta förklaras av den ökade tätheten samt betongens minskade mängd fri kalk (GGBS reagerar med kalciumhydroxiden och bildar CSH). Syran löser upp $Ca(OH)_2$, som sedan lakas ur betongen. I andra länder rekommenderas normalt inblandning av GGBS vid konstruktioner exponerade för syror och sur miljö. Sura angrepp kan vara t ex kol-, svavel-, ättik- eller mjölksyra, där de organiska syrorna har visat sig vara mer aggressiva än de oorganiska. I miljöer som jordbruk och avloppshantering är därför höga doser av GGBS att rekommendera.

Lukt

GGBS innehåller generellt små mängder sulfider, främst kalciumsulfid, vilka oxiderar i luft och bildar vätesulfid viket gör att den färska betongen kan få en svag lukt av svavel vilket försvinner efter några dagar. Sulfiderna härstammar huvudsakligen från svavlet i koksen och järnverken eftersträvar att detta tas upp av slaggen istället för av järnet. Sulfiderna i GGBS har ingen negativ inverkan på betongen, och är begränsas till max 2% (SS-EN 15167-1).

Färg

GGBS är vit i färgen, vilket resulterar i att betongen blir ljusare. Skall betongen pigmenteras ger den ljusare tonen en bättre infärgning med klarare och djupare färg. Dessutom fås en mer homogen yta, då GGBS dispergeras bättre än cement och kalkutfällningen minskar. För betong med GGBS kan dosen pigment reduceras med ca 20% med bibehållen färg mätt med spektrofotometer.

Förutom en svag lukt av svavel kan sulfiderna i GGBS ge betongen en grönaktig nyans. Denna försvinner (oxiderar) ganska omgående för att sedan ge betongen dess karakteristiska ljusa yta.

Krympning

Det långsammare hårdnandet, när GGBS används som ersättning för cement, gör betongen mer känslig för tidiga sättsprickor och plastiska krympsprickor. Extra åtgärder kan behöva vidtas för att förhindra tidig vattenavgång och avkylning, förslagsvis genom tidig täckning med plast eller presenning.

Uttorkning

Betong med GGBS får en mer finporös struktur, vilket är gynnsamt för självuttorkningen. Men den ökade tätheten gör det också svårare för vatten att transporteras ur betongen, eller att omfördelas (ex. med vattenbaserat mattlim). Uttorkningen för betong med GGBS och *k*=1,0 (likvärdig hållfasthet) har visat sig vara motsvarande som betong utan GGBS. Och med lägre k-värde än detta går uttorkningen snabbare. Den ökade tätheten gör också att givaren vid fuktmätning kan behöva sitta längre än rekommenderad tid för att komma i jämvikt. Hur GGBS och andra alternativa bindemedel (flygaska och silika) påverkar mätmetoder och betongens uttorkning är ett område som kan behövas undersökas vidare.

Tillsatsmedel

Kompabiliteten och effekten av tillsatsmedel är densamma för betong med GGBS som utan. Eventuellt kan mängden luftporbildare behöva ökas något för given lufthalt. Om cementet ersätts med lika mängd slagg kommer vattenbehovet att minska, varför flytmedelsdosen generellt blir något lägre.

Miljöbelastning

GGBS är en biprodukt från tillverkning av järn. Utsläppen av växthusgaser för GGBS kommer främst vid malning och transport. Miljöbelastningen för Slagg Bremen, räknat som ekvivalent CO^2, är 62 kg/ton (45 kg/ton efter malning och torkning i Bremen samt 17 kg/ton för sjötransporten till Sverige). Detta kan jämföras med exempelvis Byggcement som har 759 kg/ton.

70-80% av betongens miljöbelastning kommer från cementtillverkningen. Genom att ersätta cement med GGBS kan belastningen minskas. Dessutom ger den förbättrade arbetbarheten av GGBS möjlighet till en reducerad pastavolym. Exempelvis med 100% Slagg Bremen (eller 50% av bindemedel) kan utsläppen för betongen reduceras med nästan 50% (se diagram).

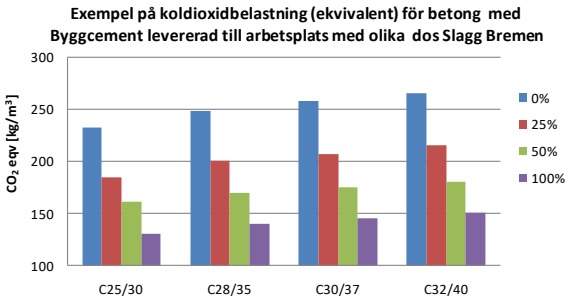

Standarder

De standarder som gäller för användningen av GGBS i betong som tillsatsmaterial är:

- SS-137003 som styr hur mycket slagg som får tillsättas (med effektivitetsfaktor och totalt), samt vilken effektivitetsfaktor (*k*) som gäller för beräkning av vct_{ekv}. Slaggen skall uppfylla kraven i SS-EN 15167-1 för att få användas som tillsatsmaterial typ II.
- SS-EN 15167-1 redovisar de krav på slaggens egenskaper som gäller, såsom aktivitetsindex, specifik yta, glashalt, alkalihalt, och kemisk sammansättning.
- SS-EN 15167-2 specificerar systemet för utvärdering av överensstämmelse, såsom regler för tillverkningskontroll, stickprov, åtgärder vid avvikelse, certifiering av och krav för distributionscentraler.
- SS-EN 206 tar inte upp användningen av slagg.

Slagg Bremen är ett mineraliskt tillsatsmaterial (typ II) med latent hydrauliska egenskaper, för användning som bindemedel i betong och bruk enligt SS 137003, och är kvalitetssäkrat och CE-märkt enligt kraven i SS-EN 15167-1 och -2.

Hantering

GGBS motsvarar cements egenskaper varför transport och förvaring bör ske på motsvarande sätt. Trots att GGBS är ett latent bindemedel, hårdnar den efter en tid i kontakt med fukt/vatten, varför lagringen skall ske i torrt klimat. GGBS kan vid kontakt verka irriterande på hud, andningsorgan och ögon, och kan vara skadligt att förtära. För fullständig information rörande hantering se separat Säkerhetsdatablad.

Fysikalisk data

Egenskap	Riktvärde	Variation	Enhet	Krav enligt SS-EN 15167-1	Standard
Specifik yta (Blaine)	420	±20	m^2/kg	≥ 275	SS-EN 196-6
Kompaktdensitet	2900	±50	kg/m^3	-	SS-EN 196-6
Skrymdensitet	1150	±200	kg/m^3	-	
Aktivitetsindex* 7/28/91d	≥ 55/75/100		%	≥ 45/70/-	SS-EN 15167-1
Bindetid*	≤ 1,3		-	≤ 2,0	SS-EN 196-3

** Standard bruk med 50% OPC (Cem I 42,5 eller 52,5) och 50% GGBS, relativt 100% OPC.*

Kemisk data

Egenskap	Riktvärde	Variation	Enhet	Krav	Standard
Kalcium (CaO)	40	±5	vikt-%	-	
Kisel (SiO_2)	35	±5	vikt-%	-	
Aluminium (Al_2O_3)	12	±3	vikt-%	-	
Magnesium (MgO)	7	±3	vikt-%	≤ 18,0	SS-EN 196-2
Titan (TiO_2)	≤ 1,2		vikt-%		
Mangan (Mn_2O_3)	≤ 0,6		vikt-%		
Sulfat (SO_3)	≤ 0,2		vikt-%	≤ 2,5	SS-EN 196-2
Klorid (Cl^-)	≤ 0,02		vikt-%	≤ 0,10	SS-EN 196-2
Alkalitet (Na_2O_{eq})	≤ 1,2		vikt-%	-	SS-EN 196-2
Glödförlust	≤ 2,0		vikt-%	≤ 3,0	SS-EN 196-2
Glashalt	≥ 90		%	≥ 67	

Vid enstaka tillfällen kan värdena avvika från angivna gränser och spann. Om så sker utfärdas larm till berörda.

I nedanstående tabell redovisas tungmetallhalter för Slagg Bremen och typvärden för portlandcement redovisas också som jämförelse. Halterna kan variera något med ingående material och är inte exakta. Gränsvärde gäller Naturvårdsverkets generella riktvärden för förorenad mark med grundvattenskydd.

Metall	Slagg Bremen	Cement	Gränsvärde	Enhet
Arsenik (As)	< 5	5	15	mg/kg
Bly (Pb)	< 5	20	80	mg/kg
Kadmium (Cd)	< 1	0,2	0,4	mg/kg
Kobolt (Co)	< 5	15	30	mg/kg
Koppar (Cu)	< 5	20	100	mg/kg
Krom (Cr)	55	50	120	mg/kg
Krom VI (Cr^{6+})	<0,2	2	5	mg/kg
Kvicksilver (Hg)	< 0,005	< 0,05	1	mg/kg
Nickel (Ni)	< 5	50	35	mg/kg
Vanadin (V)	105	60	120	mg/kg
Zink (Zn)	5	300	350	mg/kg

I GGBS förekommer endast små mängder tungmetaller, och då som en integrerad del i den glasiga strukturen. I betong blir de hårt bundna och undersökningar visar att endast en liten del kan lakas ur (mindre än 1%).

Litteratur

ACI Committee 233 (2000): GGBS as a cementitious constituent i concrete, Report ACI 233R-95.

BRE Digest 330 (2004): Alkali–silica reaction in concrete.

Chen W (2006): Hydration of slag cement - Theory, modeling and application.

Chen W, Brouwers H (2011): A method for predicting the alkali concentrations in pore solution of hydrated slag cement paste.

Concrete Society (1991): The use of GGBS and PFA in concrete, Technical report No. 40.

Hewlett P C (2003): Lea's Chemistry of Cement and Concrete.

Irfan M (2011): Carbon footprint of ready mix concrete and the role of environmental classification.

Locher F W (2006): Cement principles of production and use.

Luo R, et al (2003): Study of chloride binding and diffusion in GGBS concrete.

Marion A M, et al (2005): Study of the leaching behaviour of paving concretes.

Naturvårdsverket (1997a): Generella riktvärden för förorenad mark, Rapport 4638.

Newman J (2003): Advanced concrete technology – Constituent materials.

Parrott (1991): Factors influencing relative humidity in concrete

Pavia S, Condren E (2008): Study of the durability of OPC versus GGBS concrete.

Svensk Byggtjänst (1997): Betonghandbok – Material.

SS 137003 (2008): Betong - Användning av EN 206-1 i Sverige.

SS-EN 15167-1 (2006): Mald granulerad masugnsslagg - Definitioner, specifikationer och kriterier för överensstämmelse.

SS-EN 15167-2 (2006): Mald granulerad masugnsslagg - Utvärdering av överensstämmelse.

Taylor H F W (1997): Cement chemistry.

D Specific surface area, using Laser diffraction method

Table 8 shows the average results of the LDM for determining the specific area of the precursors as well as TDS values. The detailed results of at least 17 measurements for every precursor can be found in Appendix J. There are only TDS values available for MK, and the practical determined results deviate significantly from the TDS values. The differences in the particle size distribution of the precursors could explain the large deviation. The particle size distribution has a significant impact on the determination of specific surface area because it affects the number and size of particles in the sample. As a result, variations in particle size distribution may have resulted in variations in the specific surface area values obtained from LDM measurements.

Table 8: Results specific surface area laser diffraction method [cm²/g]

Precursor ID	S_{Laser}	$S_{Laser,TDS}$
MK 1	11 870 ± 301	20 000
MK 2	11 440 ± 282	20 000
MK 3	11 470 ± 421	20 000
GGBFS 1	7 167 ± 52	-
GGBFS 2	7 240 ± 22	-
GGBFS 3	7 055 ± 26	-
GGBFS 4	7 200 ± 10	-
GGBFS 5	7 230 ± 16	-
GGBFS 6	7 211 ± 22	-
SG 1	-	-
WWA 1	5 132 ± 32	-
WWA 2	3 190 ± 48	-

Blaine vs. laser diffraction method

In Table 9 the values of the specific surface area from Table 8 and Table 4.4 are compared to each other. Both the S_{Blaine} and the S_{Laser} vary. The size, pore shape and distribution directly influence the calculation of the specific surface area, using the Blaine method. Where the laser diffraction method may prove to be better for this type of determination in materials of very different origins when the exact refractive and absorption index is known. As a result, depending on the nature of the material being analysed, the results from these two methods may differ [240].

Table 9: Comparison results specific surface area [cm²/g]

Precursor ID	S_{Blaine}	$S_{Blaine,TDS}$	S_{Laser}	$S_{Laser,TDS}$
MK 1	20 920	26 000	11 870 ± 301	20 000
MK 2	21 710	26 000	11 440 ± 282	20 000
MK 3	21 700	26 000	11 470 ± 421	20 000
GGBFS 1	4 560	4 400 ± 200	7 167 ± 52	-
GGBFS 2	4 520	4 400 ± 200	7 240 ± 22	-
GGBFS 3	4 560	4 400 ± 200	7 055 ± 26	-
GGBFS 4	4 550	4 400 ± 200	7 200 ± 10	-
GGBFS 5	4 550	4 400 ± 200	7 230 ± 16	-
GGBFS 6	4 380	4 200 ± 200	7 211 ± 22	-
SG 1	10	-	-	-
WWA 1	7 530	-	5 132 ± 32	-
WWA 2	3 290	-	3 190 ± 48	-

E Modification VWR activator

E.1 Calculation new MR

Sodium silicate in aqueous solution, general chemical formula is stated below.

$$Na_2O.xSiO_2.H_2O \tag{1}$$

In the technical data sheet (Appendix C.1) of the purchased activator from VWR it is given that the molar ratio (MR) is equal to 3,4. This can be confirmed by calculating the MR based on the chemical composition of the activator:

SiO_2	25,6 - 27,6 %m	$\longrightarrow \pm$ 26 %m
Na_2O	7,5 - 8,5 %m	$\longrightarrow \pm$ 8 %m
H_2O	63,9 - 66,9 %m	

MR can be calculated out of the weight ratio (WR) of SiO_2 and Na_2O. A conversion is known between the two ratios, for sodium silicate MR = 1,032 x WR. The molar ratio is calculated below:

$$MR = \frac{SiO_2}{Na_2O} = 1,032.\frac{26\%m}{8\%m} = 3,35 \simeq 3,40 \tag{2}$$

A MR of 3,40 in the activator gives an almost neutral Na-glass, so it can not be expected to have a decent reaction. The following information, gathered from the book "Geopolymer chemistry and its applications" written by Joseph Davidovits:

> *The following alkali concentrations should be applied in the geopolymer formula: a potassium silicate with a molar ratio SiO_2:K_2O between MR=1,5 and 1,7 or a sodium silicate with a molar ratio SiO_2:Na_2O between MR=1,7 and 1,9. Researchers shall avoid manufacturing the silicate in-house and purchase instead the K-silicate solution and Na-silicate which have a molar ratio MR=1,7 that are specifically manufactured and commercialized for geopolymer applications. Other silicates with different ratios are not specifically made for geopolymers.*

This shows the need to adjust the bought sodium silicate activator so it has a MR close to 1.7 so it would be performing as it should in a geopolymer environment. The expressions below show how much %m of Na_2O (sodiumoxide) there needs to be (also telling how much there needs to be added since it is known how much there is currently) in the activator to have a suitable MR.

$$MR = \frac{SiO_2}{Na_2O} = 1,032.\frac{26\%m}{x} \simeq 1,7 \tag{3}$$

$$x = 1,032.\frac{26\%m}{1,7} \simeq 15,5\%m \simeq 8 + 7,5\%m \tag{4}$$

To be able to achieve a MR=1,7, the activator needs an extra 7,5%m of Na_2O in the solution. This can be achieved by adding a certain amount of NaOH (safer, cheaper and available in the lab), in the next calculations it is determined how much:

$$2NaOH \longrightarrow Na_2O + H_2O \tag{5}$$

$$80grams.NaOH \longrightarrow 62grams.Na_2O + 18grams.H_2O \tag{6}$$

So for every 80g of NaOH (sodiumhydroxide) added to the activator, there will be an increase of 62g of Na_2O and 18g of H_2O. Meaning that the reaction has a yield of 77,5% for this application and that there is a NaOH need of 1,29 times the wanted amount of Na_2O. Wanting to increase the mass percentage of Na_2O by 7,5% means that there needs to be 9,7 %m of NaOH added to the solution. Adding the extra Na_2O through reaction of NaOH means that the chemical composition of the sodium silicate activator will change. Calculations below show the calculations and the new chemical composition.

For 100g of activator:

SiO_2	26 %m		26 g
Na_2O	8 %m	=	8 g
H_2O	66 %m		66 g

Adding 9,7 grams of NaOH increases Na_2O by 7,5 grams and 2,2 grams of H_2O.

SiO_2	26 g		26 g
Na_2O	8 + 7,5 g	=	15,5 g
H_2O	66 + 2,2 g		68,2 g

The new sum of the components in the activator is 109,7 g. Dividing the new masses by this sum gives the new mass percent chemical composition of the adapted activator.

SiO_2	26/109,7 g		23,70 %m
Na_2O	15,5/109,7 g	=	14,13 %m
H_2O	68,2/109,7 g		62,17 %m

Based on this new chemical composition, the MR can be calculated as a check:

$$MR = \frac{SiO_2}{Na_2O} = 1,032.\frac{23,70\%m}{14,13\%m} = 1,73 \simeq 1,7 \tag{7}$$

The desired MR is achieved by thorough calculation of the extra needed sodium in the mix. A higher MR can also be used, but then the calculations would have to be adapted to that desired MR. The same method can be used for a potassium silicate activator but keep in mind that the relationship between MR and WR changes; MR = 1,566 x WR, with desired MR somewhere between 1,4 and 1,7.

E.2 Density of the modified activator

Adding extra material to the sodium silicate activator has without a doubt an effect on the density of the activator. The specific gravity of the original activator was 1,34. To determine the density of the modified activator, the procedure with the pycnometer from Section 3.1.2 is followed. The measured data and results are gathered in the table below.

Value		Pycnometer 1	Pycnometer 2	Pycnometer 3
m_0	[g]	29,407	28,483	26,239
m_1	[g]	102,220	100,952	98,714
m_2	[g]	79,279	78,127	75,872
ρ_a	[g/cm³]	0,0012	0,0012	0,0012
ρ_e	[g/cm³]	0,9964	0,9964	0,9964
ρ	[g/cm³]	1,4559	1,4557	1,4562

Adding the NaOH increases the density an unneglectable amount when designing something as delicate as geopolymer concrete. An average density of 1,456 g/cm³ for the modified sodium silicate activator is calculated, an increase of almost 10%.

E.3 Guideline mixprocedure new activator

The following guideline briefly describes the process of making the modified VWR activator (MR from 3,4 to 1,7). It is important to take enough precautions when handling the chemicals since they can cause serious burn wounds on the skin and heavy irritation and wounds in the eyes, so protective gear is advised. It is also advised to ask for supervision from someone in the chemical department. Chemical engineer Aritro Banerjee provided us the necessary assistance and insight into the risks of the chemicals and reactions that are happening. If needed there will also be an HSE meeting about this including a risk assessment. Besides the heavy burn wounds and regular wounds due to the chemicals, there is also a high heat development when the reaction is happening (Na2O and NaOH are highly oxidizing), so it is obligated to avoid the risks to a minimum. Some preventive actions that were taken to minimize heat development: do the mixing of the activator and NaOH under a decent working fume hood, use a basin with cool water, the bigger the better and enough water, to put the beaker in to cool down the new mixture and use sufficient supervision in the beginning and when in doubt.

Following table gives a quick overview of the dosages for some common amounts of desired modified activator, keep in mind that the developed heat increases with the amount of material. It is discouraged to fabricate more than 2500ml of modified activator at once since the heat is becoming almost to much and the handling becomes slightly awkward.

Volume [ml]	Mass activator [g]	Mass NaOH [g]
74,6	100,0	9,7
100,0	134,0	13,0
500,0	670,0	65,0
1000,0	1340,0	130,0
2500,0	3350,0	325,0

Example step-by-step guideline for making 0,5L of modified activator.

1. Provide the necessary safety related equipment: lab coat, suitable protective gloves, glasses, etc. Check if the fume hood is working as it should.
2. Gather all needed equipment for the mixing: suitable beaker(s), some spoon or something to use when weighing the NaOH, something suitable to stir with, measuring cylinder, basin with cool water, silicate activator and NaOH.
3. Weigh 65,0 g of NaOH and put somewhere safely.
4. Measure 500 ml of activator in a measuring cylinder, it is more accurate then a scale and some scales have a weight limit below 670,0 g. Once measured pour the activator in a beaker that is at least 1000ml to have enough buffer against splashing when stirring.
5. Close of the chemicals and store them to avoid any accidents.
6. Prepare the water basin with cool water under the fume hood. Avoid putting to much water inside so the buoyancy force could become greater then the weight of the beaker and the activator and risk it tipping over in the water basin.
7. Put the beaker with activator in the water basin and gather the material to stir and the weighed amount of NaOH under the fume hood.
8. Carefully add small portions of NaOH to the activator and keep stirring. If it becomes to hot, just keep stirring but don't add any extra NaOH.
9. When all the NaOH is added, keep stirring for a while. The final product should not contain any visible NaOH and will look a little bit cloudy.
10. Close off the beaker or pour the modified activator in a bottle or jar that can close and is suitable for an alkaline environment. Leave the modified activator for 24 hours in the water basin to cool down and stabilize.
11. After 24 hours the modified activator should be less cloudy is ready to use. Shake briefly before use.
12. Store the activator in a dark and moist free environment and keep sure it is closed off.

F Calculations towards oxide composition resources

FROM XRF																	MK1 (27/02)		
Element	% cation										AVG		MM (g/mol)	Compound	MM (g/mol)	%Cation	%Oxygen	M,-%		
Si	24,68	24,99	25,19	25,00	24,99	25,05	24,92	24,94	24,94	24,89	24,96	0,12	28,086	SiO2	60,08	0,468	0,533	53,392	0,262	SiO2
Al	15,86	15,79	15,72	15,96	15,96	15,74	15,51	15,68	15,54	15,67	15,74	0,15	26,982	Al2O3	101,96	0,529	0,471	29,745	0,277	Al2O3
Fe	3,51	3,31	3,18	3,27	3,16	3,17	3,53	3,42	3,52	3,46	3,35	0,14	55,845	Fe2O3	159,69	0,699	0,301	4,794	0,207	Fe2O3
Ti	1,93	1,87	1,83	1,78	1,81	1,84	1,86	1,75	1,79	1,79	1,83	0,05	47,867	TiO2	79,87	0,599	0,401	3,045	0,083	TiO2
K	0,60	0,54	0,54	0,54	0,53	0,52	0,56	0,57	0,56	0,57	0,55	0,02	39,098	K2O	94,20	0,830	0,170	0,666	0,027	K2O
V	0,36	0,38	0,38	0,37	0,38	0,35	0,36	0,36	0,37	0,37	0,37	0,01								
Ca	0,55	0,58	0,58	0,54	0,58	0,78	0,82	0,82	0,80	0,78	0,68	0,12	40,078	CaO	56,08	0,715	0,285	0,956	0,166	CaO
Ba	0,12	0,09	0,08	0,07	0,09	0,09	0,09	0,07	0,10	0,10	0,09	0,01								
Zr	0,06	0,06	0,05	0,05	0,05	0,06	0,05	0,05	0,05	0,05	0,05	0,00								
P	0,19	0,16	0,15	0,16	0,15	0,15	0,16	0,16	0,16	0,16	0,16	0,01	30,974	P2O5	283,89	0,218	0,782	0,733	0,050	P2O5
Sr	0,06	0,05	0,05	0,05	0,05	0,05	0,05	0,05	0,05	0,05	0,05	0,00								
Cr	0,07	0,06	0,06	0,05	0,06	0,05	0,06	0,06	0,07	0,06	0,06	0,01								
	test 1	test 2	test 3	test 4	test 5	test 6	test 7	test 8	test 9	test 10										
sum	47,99	47,88	47,81	47,84	47,81	47,85	47,97	47,93	47,95	47,95								93,331		

FROM XRF																	MK2 (02/03)		
Element	% cation										AVG		MM (g/mol)	Compound	MM (g/mol)	%Cation	%Oxygen	M,-%		
Si	24,97	24,80	24,70	24,87	24,85	24,83	24,85	24,61	24,88	24,80	24,82	0,09	28,086	SiO2	60,08	0,468	0,000	53,086	0,203	SiO2
Al	16,46	15,79	15,68	15,66	15,71	15,75	15,81	15,76	15,77	15,82	15,82	0,22	26,982	Al2O3	101,96	0,529	0,000	29,893	0,413	Al2O3
Fe	2,90	3,41	3,37	3,43	3,43	3,43	3,35	3,46	3,38	3,39	3,36	0,15	55,845	Fe2O3	159,69	0,699	0,301	4,797	0,222	Fe2O3
Ti	1,58	1,81	1,77	1,84	1,82	1,76	1,76	1,77	1,79	1,80	1,77	0,07	47,867	TiO2	79,87	0,599	0,401	2,953	0,114	TiO2
K	0,46	0,64	0,64	0,65	0,64	0,66	0,64	0,62	0,66	0,64	0,63	0,06	39,098	K2O	94,20	0,830	0,170	0,753	0,068	K2O
V	0,35	0,43	0,43	0,44	0,43	0,45	0,43	0,43	0,40	0,45	0,42	0,03								
Ca	0,57	0,60	0,60	0,60	0,59	0,59	0,60	0,59	0,60	0,59	0,59	0,01	40,078	CaO	56,08	0,715	0,285	0,830	0,013	CaO
Ba	0,07	0,09	0,09	0,07	0,09	0,10	0,08	0,09	0,09	0,08	0,09	0,01								
Zr	0,05	0,05	0,05	0,05	0,05	0,05	0,05	0,05	0,05	0,05	0,05	0,00								
P	0,17	0,18	0,19	0,18	0,17	0,17	0,18	0,17	0,18	0,17	0,18	0,01	30,974	P2O5	283,89	0,218	0,782	0,807	0,030	P2O5
Sr	0,05	0,05	0,05	0,05	0,05	0,05	0,05	0,05	0,05	0,05	0,05	0,00								
Cr	0,06	0,06	0,06	0,07	0,07	0,07	0,06	0,06	0,08	0,05	0,06	0,01								
	test 1	test 2	test 3	test 4	test 5	test 6	test 7	test 8	test 9	test 10										
sum	47,69	47,91	47,63	47,91	47,9	47,91	47,86	47,66	47,93	47,89								93,118		

FROM XRF																	MK3 (02/03)		
Element	% cation										AVG		MM (g/mol)	Compound	MM (g/mol)	%Cation	%Oxygen	M,-%		
Si	24,77	24,64	24,73	24,72	24,65	24,66	24,78	24,71	24,76	24,79	24,72	0,05	28,086	SiO2	60,08	0,468	0,000	52,883	0,113	SiO2
Al	16,88	16,95	16,88	16,88	16,97	16,91	16,91	17,12	17,07	16,96	16,95	0,08	26,982	Al2O3	101,96	0,529	0,000	32,032	0,148	Al2O3
Fe	3,15	3,21	3,17	3,18	3,16	3,21	3,08	2,91	2,92	2,94	3,09	0,12	55,845	Fe2O3	159,69	0,699	0,301	4,422	0,166	Fe2O3
Ti	1,60	1,65	1,63	1,63	1,64	1,65	1,62	1,63	1,61	1,65	1,63	0,02	47,867	TiO2	79,87	0,599	0,401	2,721	0,027	TiO2
K	0,39	0,38	0,38	0,37	0,39	0,38	0,36	0,35	0,35	0,36	0,37	0,01	39,098	K2O	94,20	0,830	0,170	0,447	0,017	K2O
V	0,30	0,30	0,30	0,31	0,30	0,30	0,30	0,30	0,30	0,30	0,30	0,00								
Ca	0,27	0,26	0,27	0,27	0,27	0,26	0,27	0,26	0,26	0,27	0,27	0,00	40,078	CaO	56,08	0,715	0,285	0,372	0,007	CaO
Ba	0,08	0,07	0,07	0,07	0,07	0,08	0,07	0,08	0,07	0,08	0,07	0,00								
Zr	0,05	0,05	0,05	0,05	0,05	0,05	0,05	0,05	0,05	0,05	0,05	0,00								
P	0,15	0,15	0,15	0,16	0,15	0,16	0,15	0,15	0,15	0,16	0,15	0,00	30,974	P2O5	283,89	0,218	0,782	0,701	0,021	P2O5
Sr	0,05	0,05	0,05	0,05	0,05	0,05	0,05	0,05	0,05	0,05	0,05	0,00								
Cr	0,05	0,06	0,05	0,06	0,05	0,07	0,05	0,05	0,04	0,05	0,05	0,01								
	test 1	test 2	test 3	test 4	test 5	test 6	test 7	test 8	test 9	test 10										
sum	47,74	47,77	47,73	47,75	47,75	47,78	47,69	47,66	47,63	47,66								93,578		

FROM XRF																	BFS1 (27/02)		
Element	% cation										AVG		MM (g/mol)	Compound	MM (g/mol)	%Cation	%Oxygen	M,-%		
Ca	37,37	37,54	37,45	37,19	38,11	37,68	38,29	37,84	37,74	37,34	37,66	0,33	40,078	CaO	56,08	0,715	0,285	52,687	0,460	CaO
Ti	0,81	0,81	0,82	0,80	0,84	0,83	0,84	0,82	0,80	0,83	0,82	0,01	47,867	TiO2	79,87	0,599	0,401	1,368	0,020	TiO2
Si	11,75	11,57	11,60	11,54	11,53	11,45	11,45	11,55	11,45	11,59	11,55	0,09	28,086	SiO2	60,08	0,468	0,533	24,703	0,190	SiO2
Mn	0,30	0,36	0,35	0,34	0,36	0,34	0,37	0,35	0,36	0,32	0,35	0,02	54,938	Mn2O3	157,87	0,696	0,304	0,496	0,030	MnO
K	0,56	0,57	0,57	0,57	0,56	0,56	0,57	0,57	0,56	0,56	0,57	0,00	39,098	K20	94,20	0,830	0,170	0,681	0,010	K20
V	0,23	0,24	0,23	0,23	0,24	0,22	0,24	0,23	0,23	0,24	0,23	0,01	50,942	V2O5	181,88	0,560	0,440	0,416	0,010	V2O5
Fe	0,60	0,63	0,63	0,61	0,57	0,60	0,59	0,61	0,61	0,63	0,61	0,02	55,845	Fe2O3	159,69	0,699	0,301	0,869	0,030	Fe2O3
Mg	2,84	2,96	2,99	3,24	2,59	3,03	2,45	2,70	2,86	2,94	2,86	0,22	24,305	MgO	40,30	0,603	0,397	4,743	0,360	MgO
Al	3,16	3,08	3,10	3,16	3,01	3,06	3,08	3,09	3,11	3,18	3,10	0,05	26,982	Al2O3	101,96	0,529	0,471	5,863	0,090	Al2O3
Ba	0,09	0,10	0,11	0,11	0,13	0,11	0,11	0,11	0,13	0,11	0,11	0,01	137,327							
Sr	0,09	0,10	0,10	0,10	0,10	0,10	0,10	0,10	0,10	0,10	0,10	0,00	87,62	SrO	103,62	0,846	0,154	0,117	0,000	SrO
S	0,78	0,76	0,77	0,76	0,79	0,77	0,79	0,79	0,83	0,82	0,79	0,02	32,065	SO3	80,06	0,401	0,600	1,962	0,060	SO3
	Test 1	Test 2	Test 3	Test 4	Test 5	Test 6	Test 7	Test 8	Test 9	Test 10										
sum	58,58	58,72	58,72	58,65	58,83	58,75	58,88	58,76	58,78	58,66								93,905		

FROM XRF

Element	% cation										AVG		MM (g/mol)	Compound	MM (g/mol)	%Cation	%Oxygen	BFS2 (27/02) M,-%		
Ca	36,10	36,20	35,90	35,70	37,42	37,26	36,67	35,93	36,07	35,86	36,31	0,57	40,078	CaO	56,08	0,715	0,000	50,807	0,800	CaO
Ti	0,78	0,78	0,78	0,77	0,83	0,80	0,80	0,79	0,77	0,78	0,79	0,02	47,867	TiO2	79,87	0,599	0,000	1,315	0,030	TiO2
Si	11,76	11,90	11,92	12,07	11,56	11,65	11,84	11,98	12,00	12,12	11,88	0,17	28,086	SiO2	60,08	0,468	0,533	25,413	0,370	SiO2
Mn	0,32	0,35	0,34	0,33	0,38	0,34	0,33	0,33	0,37	0,34	0,34	0,02	54,938	Mn2O3	157,87	0,696	0,304	0,493	0,030	MnO
K	0,55	0,53	0,52	0,52	0,57	0,56	0,57	0,55	0,55	0,56	0,55	0,02	39,098	K20	94,20	0,830	0,170	0,660	0,020	K20
V	0,22	0,21	0,21	0,21	0,24	0,23	0,22	0,22	0,22	0,22	0,22	0,01	50,942	V2O5	181,88	0,560	0,440	0,393	0,020	V2O5
Fe	0,61	0,59	0,60	0,57	0,59	0,61	0,57	0,59	0,58	0,59	0,59	0,01	55,845	Fe2O3	159,69	0,699	0,301	0,844	0,020	Fe2O3
Mg	3,55	3,25	3,42	3,49	3,07	2,99	3,17	3,50	3,28	3,38	3,31	0,18	24,305	MgO	40,3	0,603	0,397	5,489	0,300	MgO
Al	3,37	3,46	3,48	3,48	3,08	3,22	3,32	3,45	3,48	3,44	3,38	0,13	26,982	Al2O3	101,96	0,529	0,471	6,383	0,240	Al2O3
Ba	0,11	0,11	0,11	0,11	0,11	0,10	0,10	0,10	0,11	0,10	0,11	0,00	137,327							
Sr	0,10	0,10	0,10	0,10	0,10	0,10	0,09	0,09	0,10	0,09	0,10	0,00	87,62	SrO	103,62	0,846	0,154	0,115	0,010	SrO
S	0,92	0,88	0,89	0,86	0,74	0,76	0,73	0,72	0,74	0,74	0,80	0,07	32,065	SO3	80,06	0,401	0,600	1,992	0,190	SO3
	Test 1	Test 2	Test 3	Test 4	Test 5	Test 6	Test 7	Test 8	Test 9	Test 10										
sum	58,39	58,36	58,27	58,21	58,69	58,62	58,41	58,25	58,27	58,22								93,903		

FROM XRF

Element	% cation										AVG		MM (g/mol)	Compound	MM (g/mol)	%Cation	%Oxygen	BFS3 (27/02) M,-%		
Ca	36,07	35,47	36,27	36,54	36,66	37,02	36,69	36,66	37,08	37,09	36,56	0,48	40,078	CaO	56,08	0,715	0,000	51,148	0,670	CaO
Ti	0,77	1,04	1,05	1,11	1,09	1,09	1,10	1,09	1,11	1,10	1,06	0,10	47,867	TiO2	79,87	0,599	0,000	1,760	0,160	TiO2
Si	12,00	11,46	11,29	10,98	11,07	10,96	11,02	10,78	10,79	10,77	11,11	0,36	28,086	SiO2	60,08	0,468	0,533	23,771	0,780	SiO2
Mn	0,37	0,37	0,42	0,44	0,40	0,41	0,41	0,40	0,46	0,41	0,41	0,03	54,938	Mn2O3	157,87	0,696	0,304	0,588	0,040	MnO
K	0,55	0,45	0,79	0,79	0,79	0,80	0,79	0,78	0,79	0,79	0,73	0,12	39,098	K20	94,20	0,830	0,170	0,882	0,140	K20
V	0,22	0,25	0,25	0,26	0,27	0,28	0,26	0,28	0,27	0,28	0,26	0,02	50,942	V2O5	181,88	0,560	0,440	0,468	0,030	V2O5
Fe	0,58	0,45	0,47	0,51	0,54	0,52	0,49	0,52	0,54	0,53	0,52	0,04	55,845	Fe2O3	159,69	0,699	0,301	0,736	0,050	Fe2O3
Mg	3,28	3,39	3,15	3,14	2,95	2,88	2,98	3,46	3,02	2,97	3,12	0,19	24,305	MgO	40,30	0,603	0,397	5,177	0,310	MgO
Al	3,48	3,76	3,51	3,56	3,54	3,44	3,44	3,45	3,40	3,50	3,51	0,10	26,982	Al2O3	101,96	0,529	0,471	6,628	0,180	Al2O3
Ba	0,11	0,17	0,16	0,17	0,16	0,17	0,17	0,17	0,17	0,19	0,16	0,02	137,327							
Sr	0,10	0,12	0,12	0,13	0,13	0,14	0,13	0,13	0,14	0,14	0,13	0,01	87,620	SrO	103,62	0,846	0,154	0,151	0,010	SrO
S	0,74	1,31	1,32	1,30	1,32	1,31	1,31	1,31	1,28	1,30	1,25	0,17	32,065	SO3	80,06	0,401	0,600	3,121	0,430	SO3
	Test 1	Test 2	Test 3	Test 4	Test 5	Test 6	Test 7	Test 8	Test 9	Test 10										
sum	58,27	58,24	58,8	58,93	58,92	59,02	58,79	59,03	59,05	59,07								94,43		

FROM XRF

Element	% cation										AVG		MM (g/mol)	Compound	MM (g/mol)	%Cation	%Oxygen	BFS4 (27/02) M,-%		
Ca	38,31	38,02	38,28	37,94	37,96	37,65	36,88	37,84	37,51	37,92	37,83	0,39	40,078	CaO	56,08	0,715	0,000	52,933	0,550	CaO
Ti	0,96	0,99	0,97	0,97	0,98	0,98	0,94	1,00	0,94	0,97	0,97	0,02	47,867	TiO2	79,87	0,599	0,000	1,618	0,030	TiO2
Si	10,50	10,52	10,51	10,71	10,61	10,72	10,86	10,71	10,85	10,71	10,67	0,13	28,086	SiO2	60,08	0,468	0,533	22,825	0,270	SiO2
Mn	0,49	0,45	0,47	0,43	0,46	0,46	0,41	0,47	0,42	0,47	0,45	0,02	54,938	Mn2O3	157,87	0,696	0,304	0,651	0,030	MnO
K	0,76	0,73	0,73	0,73	0,74	0,72	0,72	0,73	0,72	0,73	0,73	0,01	39,098	K20	94,20	0,830	0,170	0,881	0,010	K20
V	0,35	0,32	0,32	0,31	0,31	0,31	0,30	0,30	0,31	0,32	0,32	0,01	50,942	V2O5	181,88	0,560	0,440	0,562	0,020	V2O5
Fe	0,64	0,64	0,63	0,62	0,60	0,62	0,59	0,62	0,64	0,62	0,62	0,02	55,845	Fe2O3	159,69	0,699	0,301	0,889	0,020	Fe2O3
Mg	2,99	3,17	2,81	3,03	3,12	3,13	3,51	2,96	3,03	2,87	3,06	0,18	24,305	MgO	40,30	0,603	0,397	5,078	0,310	MgO
Al	2,98	3,08	3,17	3,07	3,11	3,18	3,37	3,20	3,27	3,21	3,16	0,10	26,982	Al2O3	101,96	0,529	0,471	5,978	0,200	Al2O3
Ba	0,18	0,17	0,19	0,18	0,17	0,15	0,17	0,17	0,16	0,17	0,17	0,01	137,327							
Sr	0,14	0,13	0,14	0,13	0,13	0,13	0,12	0,13	0,13	0,13	0,13	0,01	87,620	SrO	103,62	0,846	0,154	0,155	0,010	SrO
S	0,93	0,94	0,96	0,98	0,96	1,01	0,96	0,97	0,98	0,98	0,97	0,02	32,065	SO3	80,06	0,401	0,600	2,414	0,050	SO3
	Test 1	Test 2	Test 3	Test 4	Test 5	Test 6	Test 7	Test 8	Test 9	Test 10										
sum	59,23	59,16	59,18	59,1	59,15	59,06	58,83	59,1	58,96	59,1								93,985		

FROM XRF

Element	% cation										AVG		MM (g/mol)	Compound	MM (g/mol)	%Cation	%Oxygen	BFS5 (27/02) M,-%		
Ca	37,55	36,24	36,01	35,99	35,79	35,37	35,61	34,93	35,20	34,67	35,74	0,77	40,078	CaO	56,08	0,715	0,285	50,002	1,080	CaO
Ti	1,07	1,02	1,02	0,99	1,00	1,01	0,98	0,96	0,98	0,94	1,00	0,03	47,867	TiO2	79,87	0,599	0,401	1,663	0,060	TiO2
Si	10,71	11,12	11,16	11,18	11,21	11,12	11,26	11,31	11,36	11,42	11,19	0,19	28,086	SiO2	60,08	0,468	0,533	23,927	0,400	SiO2
Mn	0,39	0,39	0,42	0,41	0,36	0,40	0,41	0,36	0,39	0,38	0,39	0,02	54,938	Mn2O3	157,87	0,696	0,304	0,562	0,030	MnO
K	0,77	0,75	0,75	0,74	0,75	0,75	0,74	0,75	0,75	0,74	0,75	0,01	39,098	K20	94,20	0,830	0,170	0,902	0,010	K20
V	0,26	0,24	0,25	0,25	0,25	0,24	0,24	0,24	0,23	0,23	0,24	0,01	50,942	V2O5	181,88	0,560	0,440	0,434	0,020	V2O5
Fe	0,58	0,56	0,55	0,57	0,56	0,56	0,55	0,54	0,56	0,52	0,56	0,02	55,845	Fe2O3	159,69	0,699	0,301	0,794	0,020	Fe2O3
Mg	2,97	3,39	3,53	3,42	3,52	4,01	3,61	4,07	3,80	4,03	3,64	0,33	24,305	MgO	40,30	0,603	0,397	6,028	0,550	MgO
Al	3,41	3,66	3,66	3,78	3,86	3,78	3,84	3,94	3,85	4,06	3,78	0,17	26,982	Al2O3	101,96	0,529	0,471	7,150	0,320	Al2O3
Ba	0,15	0,15	0,14	0,14	0,14	0,14	0,15	0,14	0,15	0,14	0,14	0,00	137,327							
Sr	0,16	0,15	0,15	0,15	0,15	0,15	0,15	0,14	0,14	0,14	0,15	0,01	87,620	SrO	103,62	0,846	0,154	0,175	0,010	SrO
S	0,97	0,98	0,96	0,95	0,95	0,93	0,97	0,97	0,96	0,99	0,96	0,02	32,065	SO3	80,06	0,401	0,600	2,404	0,040	SO3
	Test 1	Test 2	Test 3	Test 4	Test 5	Test 6	Test 7	Test 8	Test 9	Test 10										
sum	58,99	58,65	58,6	58,57	58,54	58,46	58,51	58,35	58,37	58,26								94,041		

FROM XRF

Element	% cation										AVG		MM (g/mol)
Ca	34,3	34,4	34,3	34,4	34,2	34,5	34,4	34,3	34,2	34,4	34,32	0,07	40,078
Ti	1,4	1,4	1,4	1,4	1,4	1,4	1,4	1,4	1,4	1,4	1,41	0,02	47,867
Si	11,7	11,7	11,7	11,7	11,7	11,7	11,6	11,7	11,7	11,7	11,67	0,02	28,086
Mn	0,5	0,5	0,5	0,5	0,5	0,5	0,5	0,5	0,5	0,5	0,50	0,01	54,938
K	0,9	0,9	0,9	0,9	0,9	0,9	0,9	1,0	1,0	0,9	0,93	0,01	39,098
V	0,3	0,3	0,3	0,3	0,3	0,3	0,3	0,3	0,3	0,3	0,33	0,00	50,942
Fe	0,5	0,5	0,5	0,5	0,5	0,5	0,5	0,5	0,5	0,5	0,52	0,01	55,845
Mg	3,8	3,7	3,7	3,7	3,8	3,6	3,8	3,7	3,7	3,5	3,70	0,09	24,305
Al	3,5	3,6	3,6	3,5	3,5	3,5	3,5	3,5	3,5	3,6	3,52	0,03	26,982
Ba	0,1	0,1	0,1	0,1	0,1	0,1	0,1	0,1	0,1	0,1	0,13	0,01	137,327
Sr	0,1	0,1	0,1	0,1	0,1	0,1	0,1	0,1	0,1	0,1	0,10	0,00	87,620
S	1,2	1,2	1,2	1,2	1,2	1,2	1,2	1,2	1,2	1,2	1,18	0,01	32,065
	Test 1	Test 2	Test 3	Test 4	Test 5	Test 6	Test 7	Test 8	Test 9	Test 10			
sum	58,3	58,3	58,32	58,32	58,27	58,33	58,32	58,33	58,34	58,32			

Compound	MM (g/mol)
CaO	56,08
TiO2	79,87
SiO2	60,08
Mn2O3	157,87
K20	94,20
V2O5	181,88
Fe2O3	159,69
MgO	40,30
Al2O3	101,96
SrO	103,62
SO3	80,06

%Cation	%Oxygen
0,715	0,285
0,599	0,401
0,468	0,533
0,696	0,304
0,830	0,170
0,560	0,440
0,699	0,301
0,603	0,397
0,529	0,471
0,846	0,154
0,401	0,600

BFS6 (27/02)

M,-%		
48,025	0,100	CaO
2,359	0,030	TiO2
24,971	0,040	SiO2
0,713	0,020	MnO
1,125	0,010	K20
0,589	0,010	V2O5
0,739	0,020	Fe2O3
6,139	0,150	MgO
6,647	0,060	Al2O3
0,118	0,000	SrO
2,939	0,040	SO3
94,364		

FROM XRF

Element	% cation					AVG		MM (g/mol)
Ca	3,01	2,74	2,93	2,66	2,68	2,80	0,14	40,078
Ti	0,34	0,27	0,27	0,27	0,27	0,28	0,03	47,867
Si	13,13	12,14	11,8	12,02	12,09	12,24	0,46	28,086
Mn	0,16	0,16	0,16	0,16	0,17	0,16	0,00	54,938
K	0,91	0,85	0,84	0,85	0,83	0,86	0,03	39,098
V								50,942
Fe	34,95	37,65	37,92	37,58	38,01	37,22	1,15	55,845
Mg	2,95	2,57	2,93	2,94	2,49	2,78	0,20	24,305
Al	1,37	1,32	1,31	1,34	1,31	1,33	0,02	26,982
Ba	0,19	0,16	0,18	0,17	0,19	0,18	0,01	137,327
Sr								87,620
S								32,065
	Test 1	Test 2	Test 3	Test 4	Test 5			
sum	57,01	57,86	58,34	57,99	58,04			

Compound	MM (g/mol)
CaO	56,08
TiO2	79,87
SiO2	60,08
Mn2O3	157,87
K20	94,20
V2O5	181,88
Fe2O3	159,69
MgO	40,30
Al2O3	101,96
BaO	153,33
SrO	103,62
SO3	80,06

%Cation	%Oxygen
0,715	0,285
0,599	0,401
0,468	0,533
0,696	0,304
0,830	0,170
0,560	0,440
0,699	0,301
0,603	0,397
0,529	0,471
0,896	0,104
0,846	0,154
0,401	0,600

SG1 (20/02)

M,-%		
3,920	0,200	CaO
0,470	0,050	TiO2
26,180	0,990	SiO2
0,230	0,010	MnO
1,030	0,030	K20
		V2O5
53,220	1,640	Fe2O3
4,600	0,340	MgO
2,510	0,040	Al2O3
0,200	0,010	BaO
		SrO
		SO3
92,360		

Element	% cation										AVG		MM (g/mol)
Si	1,81	1,90	1,92	2,01	1,88	1,92	1,87	1,98	1,99	2,03	1,93	0,07	28,086
Ti	3,19	3,26	3,22	3,20	3,29	3,31	3,28	3,23	3,26	3,19	3,24	0,04	47,867
Al	0,56	0,49	0,54	0,54	0,57	0,53	0,53	0,58	0,52	0,66	0,55	0,04	26,981
Fe	4,60	4,63	4,40	4,49	4,67	4,81	4,82	4,69	5,05	4,44	4,66	0,19	55,845
Mn	0,49	0,54	0,55	0,54	0,48	0,54	0,52	0,50	0,56	0,53	0,53	0,03	54,938
Ca	26,57	26,60	26,21	25,94	26,38	26,53	26,94	26,72	26,50	25,71	26,41	0,35	40,078
Na													
K	3,20	3,23	3,24	3,26	3,27	3,28	3,27	3,25	3,21	3,22	3,24	0,03	39,098
P													
S	5,44	5,38	5,64	5,61	5,48	5,24	5,42	5,22	5,11	5,47	5,40	0,16	32,065
Mg	1,14	0,59	1,40	1,47	1,16	1,10	1,20	1,64	1,23	1,93	1,29	0,34	24,305
	Test 1	Test 2	Test 3	Test 4	Test 5	Test 6	Test 7	Test 8	Test 9	Test 10			

Compound	MM (g/mol)
SiO2	56,08
TiO2	79,87
Al2O3	101,96
Fe2O3	159,69
MnO	70,94
CaO	56,08
Na2O	61,98
K2O	94,20
P2O5	283,89
SO3	80,06
MgO	40,30

%Cation	%Oxygen
0,501	0,499
0,599	0,401
0,529	0,471
0,699	0,301
0,775	0,226
0,715	0,285
0,830	0,170
0,401	0,600
0,603	0,397

WWA1 (27/02)

M,-%		
3,856	0,133	SiO2
5,411	0,068	TiO2
1,043	0,082	Al2O3
6,663	0,268	Fe2O3
0,678	0,033	MnO
36,953	0,487	CaO
		Na2O
3,907	0,031	K2O
		P2O5
13,485	0,401	SO3
2,133	0,563	MgO

Possible heavy metals	% cation										AVG		
Zn		12,03	11,5	11,5	11,31	11,37	10,9	10,7	11,31	11,3	11,32	+-	0,35
Cl	10,04	10,33	10,27	10,21	10,35	10,07	9,96	9,92	9,76	10,1	10,1		0,18
As		0,41	0,4	0,39	0,39	0,39	0,37	0,38	0,38	0,38	0,39		0,01
Ba	0,35	0,35	0,31	0,32	0,35	0,34	0,37	0,37	0,35	0,32	0,34		0,02
V	0,23	0,21	0,21	0,22	0,21	0,23	0,23	0,23	0,24	0,23	0,22		0,01
Cr	0,14	0,15	0,15	0,15	0,16	0,14	0,15	0,14	0,15	0,16	0,15		0,01
Sr	0,12	0,12	0,12	0,11	0,11	0,12	0,12	0,11	0,12	0,11	0,12		0,00
Sb	0,07	0,06	0,06	0,06	0,06	0,06	0,06	0,06	0,07	0,06	0,06		0,00
Pb		0,7	0,64	0,65	0,63	0,65	0,64	0,63	0,68	0,63	0,65		0,02
Pd													
Cu		0,29	0,26	0,27	0,28	0,29	0,26	0,25	0,27	0,27	0,27		0,01
sum	47	46,62	47,12	47,06	47,18	47,26	47,85	47,81	47,43	47,18			71,995

Element	% cation										AVG		MM (g/mol)
Si	1,89	1,85	1,88	1,88	1,87	1,91	1,90	1,93	1,95	1,94	1,9	0,03	28,086
Ti													47,867
Al	0,65	0,68	0,71	0,70	0,68	0,69	0,73	0,72	0,69	0,67	0,69	0,02	26,981
Fe	1,66	1,58	1,57	1,60	1,65	1,61	1,61	1,56	1,61	1,64	1,61	0,03	55,845
Mn	4,89	5,17	5,04	5,05	5,23	5,19	5,06	5,05	5,13	5,06	5,09	0,09	54,938
Ca	36,04	35,83	35,44	35,94	36,00	35,68	35,67	35,23	35,63	35,53	35,7	0,25	40,078
Na													
K	14,29	14,17	14,09	14,25	14,27	14,13	14,13	13,98	14,09	14,04	14,14	0,10	39,098
P	1,32	1,28	1,32	1,31	1,30	1,30	1,31	1,33	1,32	1,32			
S	0,83	0,82	0,81	0,83	0,82	0,84	0,83	0,83	0,81	0,82	0,82	0,01	32,065
Mg	1,94	2,05	2,43	1,87	1,59	2,03	2,16	2,63	2,11	2,34	2,12	0,28	24,305
	Test 1	Test 2	Test 3	Test 4	Test 5	Test 6	Test 7	Test 8	Test 9	Test 10			

Compound	MM (g/mol)
SiO2	56,08
TiO2	79,87
Al2O3	101,96
Fe2O3	159,69
MnO	70,94
CaO	56,08
Na2O	61,98
K2O	94,20
P2O5	283,89
SO3	80,06
MgO	40,30

%Cation	%Oxygen
0,501	0,499
0,599	0,401
0,529	0,471
0,699	0,301
0,775	0,226
0,715	0,285
0,830	0,170
0,401	0,600
0,603	0,397

WWA2 (19/03)

M,-%		
3,794	0,061	SiO2
		TiO2
1,308	0,043	Al2O3
2,3	0,045	Fe2O3
6,568	0,119	MnO
49,95	0,344	CaO
		Na2O
17,039	0,116	K2O
		P2O5
2,057	0,023	SO3
3,507	0,468	MgO

Possible heavy metals	% cation										AVG		
Zn	0,26	0,27	0,26	0,26	0,27	0,26	0,26	0,26	0,27	0,27	0,26	+-	0,00
Ba	0,73	0,80	0,81	0,81	0,82	0,77	0,78	0,77	0,81	0,78	0,79		0,03
V	0,24	0,25	0,24	0,24	0,25	0,23	0,24	0,23	0,22	0,23	0,24		0,01
Sr	0,40		0,39	0,40	0,40	0,40	0,39	0,39	0,40	0,39	0,4		0,00
Cu	0,04	0,04	0,03	0,04	0,04	0,04	0,04	0,03	0,04	0,04	0,04		0,00
Sum	63,51	63,43	63,29	63,43	63,41	63,38	63,4	63,26	63,34	63,36			

G Sieving analysis

Date 24/04/2023

0/2 sand												
	1			2			3			4		
	M_1 =	1350,00		M_1 =	1350,00		M_1 =	1350,00		M_1 =	1530,00	
Sieve (mm)	(g)	% Mass In	Σ (%)	(g)	% Mass In	Σ (%)	(g)	% Mass In	Σ (%)	(g)	% Mass In	Σ (%)
2,00	0,00	0,00	100,00	0,00	0,00	100,00	0,00	0,00	100,00	0,00	0,00	100,00
1,000	165,87	12,29	87,71	165,03	12,22	87,78	158,42	11,73	88,27	148,88	9,73	90,27
0,500	190,96	14,15	73,57	196,48	14,55	73,22	191,50	14,19	74,08	200,88	13,13	77,14
0,250	390,77	28,95	44,62	462,12	34,23	38,99	429,52	31,82	42,26	569,61	37,23	39,91
0,125	397,33	29,43	15,19	331,57	24,56	14,43	378,65	28,05	14,22	376,01	24,58	15,33
0,063	159,05	11,78	3,41	136,99	10,15	4,28	143,53	10,63	3,58	169,15	11,06	4,28
Material in the pan	46,02	3,41		57,81	4,28		48,38	3,58		65,47	4,28	
	5			6			7			Avg		
	M_1 =	1350,00		M_1 =	1350,00		M_1 =	1230,00		$M_{1,avg}$ =	1358,57	
Sieve (mm)	(g)	% Mass In	Σ (%)	(g)	% Mass In	Σ (%)	(g)	% Mass In	Σ (%)	(g)	% Mass In	Σ (%)
2,00	0,00	0,00	100,00	0,00	0,00	100,00	0,00	0,00	100,00	0,00	0,00	100,00
1,000	134,97	10,00	90,00	129,17	9,57	90,43	136,62	11,11	88,89	148,42	10,92	89,08
0,500	183,36	13,58	76,42	184,25	13,65	76,78	167,25	13,60	75,30	187,81	13,82	75,25
0,250	513,75	38,06	38,36	365,65	27,09	49,70	358,27	29,13	46,17	441,38	32,49	42,76
0,125	336,04	24,89	13,47	468,96	34,74	14,96	388,04	31,55	14,62	382,37	28,15	14,62
0,063	134,97	10,00	3,47	166,75	12,35	2,61	141,42	11,50	3,12	150,27	11,06	3,56
Material in the pan	46,91	3,47		35,22	2,61		38,40	3,12		48,32	3,56	
Standard sand EN 196-1												
	1			2			3			Avg		
	M_1 =	1350,00		M_1 =	1350,00		M_1 =	1350,00		M_1 =	1350,00	
Sieve (mm)	(g)	% Mass In	Σ (%)	(g)	% Mass In	Σ (%)	(g)	% Mass In	Σ (%)	(g)	% Mass In	Σ (%)
2,00	0,00	0,00	100,00	0,00	0,00	100,00	0,00	0,00	100,00	0,00	0,00	100,00
1,000	424,72	31,46	68,54	433,19	32,09	67,91	438,20	32,46	67,54	432,04	32,00	68,00
0,500	474,65	35,16	33,38	460,50	34,11	33,80	449,56	33,30	34,24	461,57	34,19	33,81
0,250	164,17	12,16	21,22	177,40	13,14	20,66	174,02	12,89	21,35	171,86	12,73	21,08
0,125	206,64	15,31	5,91	203,25	15,06	5,60	213,66	15,83	5,52	207,85	15,40	5,68
0,063	78,13	5,79	0,13	74,83	5,54	0,06	73,46	5,44	0,08	75,47	5,59	0,09
Material in the pan	1,69	0,13		0,83	0,06		1,10	0,08		1,21	0,09	

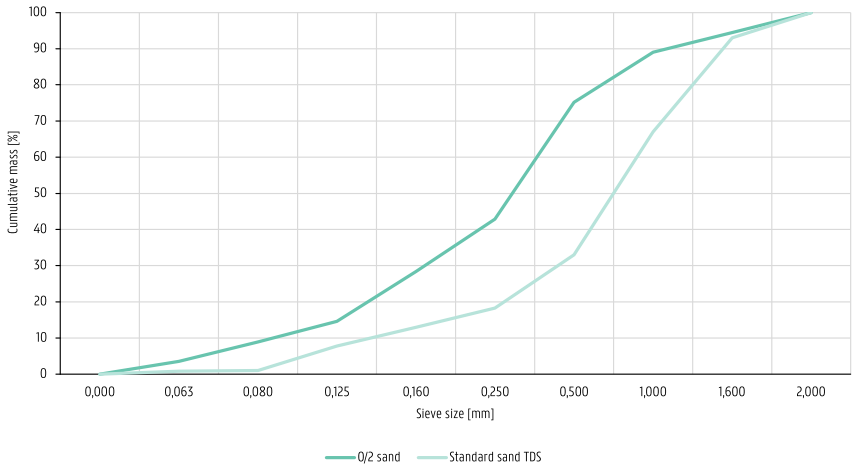

H Calculations towards density using a pycnometer

	1		2		3		[g/cm³]			[g/cm³]	
	$m_{1,1}$ [g]	m_P [g]	$m_{1,2}$	m_P [g]	$m_{1,3}$ [g]	m_P [g]	ρ_1	ρ_2	ρ_3	ρ_{avg}	
MK 1	670,80	39,12	680,99	41,45	675,02	35,21	2,65	2,71	2,62	2,66 +/-	0,04
MK 2	675,90	47,15	684,35	47,30	687,82	54,54	2,66	2,66	2,73	2,68 +/-	0,03
MK 3	668,66	35,51	680,38	41,32	675,02	34,35	2,67	2,62	2,73	2,67 +/-	0,05
GGBFS 1	670,74	36,78	666,91	18,91	681,13	42,89	2,94	2,76	2,86	2,85 +/-	0,07
GGBFS 2	680,28	52,91	690,93	55,14	689,99	55,24	2,77	2,89	2,98	2,88 +/-	0,09
GGBFS 3	674,97	43,39	683,47	45,05	678,16	38,07	2,92	2,74	2,89	2,85 +/-	0,08
GGBFS 4	669,58	35,14	681,09	40,61	678,02	37,99	2,92	2,83	2,87	2,87 +/-	0,04
GGBFS 5	667,35	32,51	675,14	32,12	674,22	32,00	2,80	2,72	2,90	2,80 +/-	0,08
GGBFS 6	694,80	73,07	709,77	85,45	697,78	67,92	2,95	2,80	2,90	2,89 +/-	0,06
SG 1	802,56	212,90	843,42	272,61	791,35	197,00	3,75	3,24	3,34	3,45 +/-	0,22
WWA1	663,34	28,32	671,24	28,88	669,85	27,15	2,48	2,31	2,57	2,45 +/-	0,11
WWA 2	681,64	54,58	690,15	53,35	687,42	52,25	2,81	2,96	2,89	2,89 +/-	0,06
SW	658,07		666,30		665,22		1,02	1,02	1,02	1,02 +/-	0,01
$SSS_{original}$	821,87		829,92		828,77		1,35	1,35	1,35	1,35 +/-	0,01
SSS	802,50		883,61		881,54		1,31	1,46	1,46	1,41 +/-	0,07
MK 2,2	675,90	47,15	684,35	47,30	687,82	54,54	2,66	2,66	2,73	2,68 +/-	0,03

ρ_a = 0,0012 g/cm³

ρ_e = 1,00 g/cm³

$m_{0,1}$= 148,73 g V_1 = 497,73 cm³

$m_{0,2}$= 157,15 g V_2 = 497,70 cm³

$m_{0,3}$= 156,08 g V_3 = 497,18 cm³

$$\rho_{liquid} = \frac{m_1 - m_0}{V} + \rho_a = \frac{(m_1 - m_0).(\rho_e - \rho_a)}{(m_2 - m_0)} + \rho_a$$

$$\rho_{powder} = \rho_e \frac{m_p}{m_p - (m_1 - m_2)}$$

I Calculations towards specific surface area using Blaine method

		specific surface area (Blaine method)										[cm²/g]	
		1			2			3			S_1	S_2	S_3
	ρ [g/cm³]	m_0 [g]	e [-]	t [s]	m_0 [g]	e [-]	t [s]	m_0 [g]	e [-]	t [s]			
MK 1	2,66	1,50	0,70	339,97	1,48	0,70	313,40	1,50	0,70	335,49	22084,61	21678,13	21938,62
MK 2	2,68	1,50	0,70	368,59	1,54	0,69	395,46	1,53	0,69	375,65	23196,52	23001,72	22662,94
MK 3	2,67	1,50	0,70	324,69	1,50	0,70	319,54	1,49	0,70	322,26	21707,87	21535,02	21865,92
GGBFS 1	2,85	2,55	0,53	94,95	2,60	0,52	103,59	2,32	0,57	65,20	4606,27	4594,77	4714,96
GGBFS 2	2,88	2,36	0,56	66,73	2,58	0,52	98,30	2,41	0,55	73,90	4594,77	4511,51	4573,12
GGBFS 3	2,85	2,22	0,59	51,22	2,41	0,55	74,52	2,24	0,58	55,50	4714,96	4646,15	4688,06
GGBFS 4	2,87	2,30	0,57	60,95	2,28	0,58	58,10	2,33	0,57	63,89	4609,67	4584,21	4591,13
GGBFS 5	2,80	2,45	0,55	76,10	2,29	0,58	60,83	2,28	0,58	59,43	4599,66	4763,48	4751,89
GGBFS 6	2,89	2,30	0,58	56,85	2,39	0,56	65,28	2,44	0,55	71,97	4433,84	4374,12	4386,74
SG 1	3,45	6,40	0,00	8,20	6,32	0,01	6,06	5,71	0,11	4,58	0,04	1,86	41,46
WWA1	2,45	1,49	0,66	47,50	1,51	0,66	52,23	1,51	0,66	51,82	7420,67	7599,31	7569,43
WWA 2	2,89	2,24	0,58	29,22	2,23	0,58	27,36	2,27	0,58	30,92	3315,84	3238,44	3317,51

S_0 = 3644 cm²/g

ρ_0 = 3,15 g/cm³

t_0 = 95,36 s

V = 1,86 cm³

K = 22,51

n = 0,00001834

$$m_i = (1 - e).\rho.V$$

$$K = S_0.\rho_0.\frac{(1-e)}{\sqrt{e^3}}.\frac{\sqrt{10.\eta_0}}{\sqrt{t_0}}$$

$$S_i = \frac{K}{\rho}.\frac{\sqrt{e^3}}{(1-e)}.\frac{\sqrt{t}}{\sqrt{10.\eta}}$$

$$S = \frac{S_1 + S_2 + S_3}{3}$$

J Reports laser diffraction method

J.1 Particle size analysis of MK

Analysis

Malvern Panalytical

Analysis

Particle Name	Metakaoline
Particle Refractive Index	1,530
Particle Absorption Index	0,005
Dispersant Name	Water
Dispersant Refractive Index	1,330
Scattering Model	Mie

Measurement Details

Sample Name	MK_1
Operator Name	mhe220
Analysis Date Time	4/04/2023 14:17:37
Measurement Date Time	28/03/2023 18:03:42

Average - Frequency (compatible) and Undersize

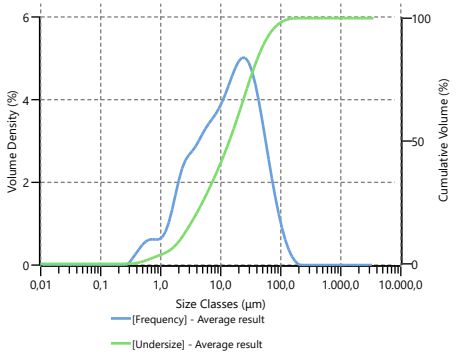

Trend

	Record Number	Sample Name	Dx (10) (µm)	Dx (50) (µm)	Dx (90) (µm)	Specific Surface Area (m^2/kg)
	21	MK_1	2,20	15,0	56,1	1132
	22	MK_1	2,18	14,6	54,3	1144
	23	MK_1	2,18	14,6	55,0	1146
	24	MK_1	2,17	14,4	54,1	1156
	25	MK_1	2,16	14,3	54,2	1162
	26	MK_1	2,16	14,2	54,2	1163
	27	MK_1	2,15	14,1	53,2	1173
	28	MK_1	2,15	14,1	54,1	1172
	29	MK_1	2,14	13,9	53,2	1179
	30	MK_1	2,14	13,8	52,8	1182
	31	MK_1	2,14	13,8	53,8	1182
	32	MK_1	2,12	13,7	52,9	1201
	33	MK_1	2,12	13,7	53,5	1206
	34	MK_1	2,11	13,5	52,5	1208
	35	MK_1	2,10	13,5	52,5	1223
	36	MK_1	2,11	13,5	52,9	1212
	37	MK_1	2,10	13,4	52,4	1224
	38	MK_1	2,10	13,4	52,8	1218
	39	MK_1	2,10	13,3	52,3	1225
	40	MK_1	2,10	13,3	52,6	1222
Mean			**2,14**	**13,9**	**53,5**	**1187**
1xStd Dev			**0,0321**	**0,492**	**0,991**	**30,07**
1xRSD (%)			**1,50**	**3,54**	**1,85**	**2,534**

Frequency (ISO) and Undersize

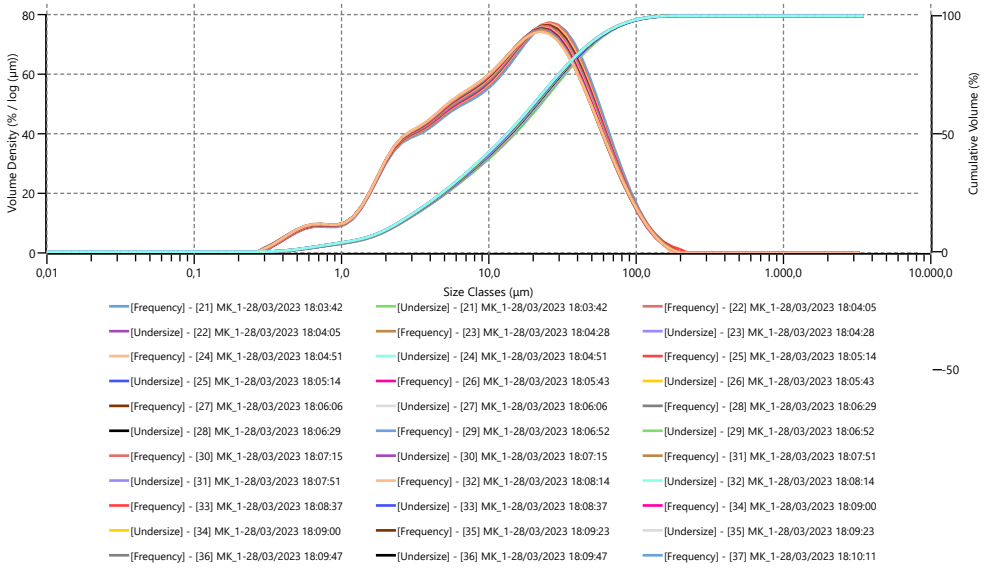

Malvern Panalytical
www.malvernpanalytical.com
C:\Users\marie\Downloads\MK_1.mmes

MK_1

Mastersizer - v3.88
Page 1 of 2

Instrument Serial No: MAL1271954
21CFR Mode: Inactive
Record Number: 21
Created: 28/03/2023 18:03
Printed: 5/04/2023 12:22

Analysis

Malvern Panalytical

Result

Size (µm)	% Volume In	Size (µm)	% Volume In	Size (µm)	% Volume In	Size (µm)	% Volume In	Size (µm)	% Volume In	Size (µm)	% Volume In
0,0100	0,00	0,0876	0,00	0,767	0,48	6,72	2,81	58,9	2,38	516	0,00
0,0114	0,00	0,0995	0,00	0,872	0,48	7,64	2,89	66,9	1,94	586	0,00
0,0129	0,00	0,113	0,00	0,991	0,52	8,68	3,00	76,0	1,52	666	0,00
0,0147	0,00	0,128	0,00	1,13	0,63	9,86	3,12	86,4	1,14	756	0,00
0,0167	0,00	0,146	0,00	1,28	0,82	11,2	3,29	98,1	0,81	859	0,00
0,0189	0,00	0,166	0,00	1,45	1,08	12,7	3,47	111	0,54	976	0,00
0,0215	0,00	0,188	0,00	1,65	1,38	14,5	3,68	127	0,33	1110	0,00
0,0244	0,00	0,214	0,00	1,88	1,67	16,4	3,88	144	0,18	1260	0,00
0,0278	0,00	0,243	0,00	2,13	1,90	18,7	4,07	163	0,09	1430	0,00
0,0315	0,00	0,276	0,00	2,42	2,05	21,2	4,20	186	0,00	1630	0,00
0,0358	0,00	0,314	0,12	2,75	2,14	24,1	4,27	211	0,00	1850	0,00
0,0407	0,00	0,357	0,20	3,12	2,20	27,4	4,25	240	0,00	2100	0,00
0,0463	0,00	0,405	0,29	3,55	2,29	31,1	4,14	272	0,00	2390	0,00
0,0526	0,00	0,460	0,38	4,03	2,40	35,3	3,93	310	0,00	2710	0,00
0,0597	0,00	0,523	0,45	4,58	2,52	40,1	3,62	352	0,00	3080	0,00
0,0679	0,00	0,594	0,48	5,21	2,63	45,6	3,25	400	0,00	3500	
0,0771	0,00	0,675	0,49	5,92	2,73	51,8	2,83	454	0,00		

Analysis

Malvern Panalytical

Analysis

Particle Name Metakaoline
Particle Refractive Index 1,540
Particle Absorption Index 0,005
Dispersant Name Water
Dispersant Refractive Index 1,330
Scattering Model Mie

Measurement Details

Sample Name MK_2
Operator Name mhe220
Analysis Date Time 5/04/2023 13:30:45
Measurement Date Time 28/03/2023 18:26:39

Average - Frequency (compatible) and Undersize

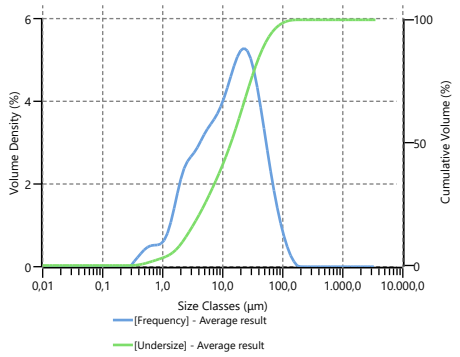

Trend

	Record Number	Sample Name	Dx (10) (µm)	Dx (50) (µm)	Dx (90) (µm)	Specific Surface Area (m^2/kg)
	36	MK_2	2,15	13,1	49,5	1181
	19	MK_2	2,25	14,7	51,8	1095
	20	MK_2	2,25	14,6	52,2	1091
	21	MK_2	2,23	14,4	51,2	1103
	22	MK_2	2,22	14,3	51,5	1111
	23	MK_2	2,22	14,2	50,9	1114
	24	MK_2	2,20	14,0	49,9	1125
	25	MK_2	2,18	13,9	50,0	1148
	26	MK_2	2,20	13,9	50,2	1133
	27	MK_2	2,18	13,7	49,8	1143
	28	MK_2	2,18	13,6	49,4	1144
	29	MK_2	2,17	13,5	49,5	1151
	30	MK_2	2,17	13,4	49,4	1153
	31	MK_2	2,16	13,3	48,9	1162
	32	MK_2	2,16	13,3	48,8	1161
	33	MK_2	2,16	13,2	48,8	1165
	34	MK_2	2,15	13,1	48,2	1171
	35	MK_2	2,16	13,1	48,8	1170
Mean			**2,19**	**13,7**	**49,9**	**1140**
1xStd Dev			**0,0329**	**0,540**	**1,17**	**27,59**
1xRSD (%)			**1,50**	**3,93**	**2,34**	**2,420**

Frequency (ISO) and Undersize

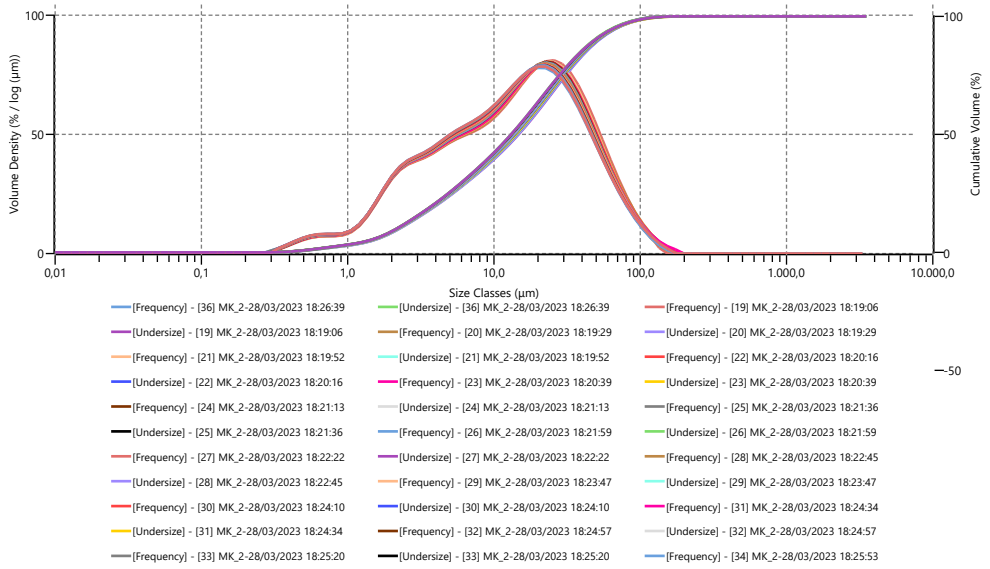

Analysis

Malvern Panalytical

Result

Size (µm)	% Volume In	Size (µm)	% Volume In	Size (µm)	% Volume In	Size (µm)	% Volume In	Size (µm)	% Volume In	Size (µm)	% Volume In
0,0100	0,00	0,0876	0,00	0,767	0,45	6,72	3,08	58,9	1,82	516	0,00
0,0114	0,00	0,0995	0,00	0,872	0,47	7,64	3,20	66,9	1,47	586	0,00
0,0129	0,00	0,113	0,00	0,991	0,53	8,68	3,34	76,0	1,17	666	0,00
0,0147	0,00	0,128	0,00	1,13	0,67	9,86	3,51	86,4	0,89	756	0,00
0,0167	0,00	0,146	0,00	1,28	0,90	11,2	3,71	98,1	0,65	859	0,00
0,0189	0,00	0,166	0,00	1,45	1,19	12,7	3,91	111	0,44	976	0,00
0,0215	0,00	0,188	0,00	1,65	1,50	14,5	4,10	127	0,27	1110	0,00
0,0244	0,00	0,214	0,00	1,88	1,79	16,4	4,24	144	0,14	1260	0,00
0,0278	0,00	0,243	0,00	2,13	2,02	18,7	4,32	163	0,00	1430	0,00
0,0315	0,00	0,276	0,06	2,42	2,16	21,2	4,31	186	0,00	1630	0,00
0,0358	0,00	0,314	0,12	2,75	2,26	24,1	4,21	211	0,00	1850	0,00
0,0407	0,00	0,357	0,20	3,12	2,35	27,4	4,02	240	0,00	2100	0,00
0,0463	0,00	0,405	0,29	3,55	2,46	31,1	3,73	272	0,00	2390	0,00
0,0526	0,00	0,460	0,36	4,03	2,60	35,3	3,39	310	0,00	2710	0,00
0,0597	0,00	0,523	0,42	4,58	2,74	40,1	3,00	352	0,00	3080	0,00
0,0679	0,00	0,594	0,45	5,21	2,87	45,6	2,60	400	0,00	3500	
0,0771	0,00	0,675	0,45	5,92	2,97	51,8	2,20	454	0,00		

Analysis

Malvern Panalytical

Analysis	
Particle Name	Metakaoline
Particle Refractive Index	1,540
Particle Absorption Index	0,005
Dispersant Name	Water
Dispersant Refractive Index	1,330
Scattering Model	Mie

Measurement Details	
Operator Name	mhe220
Sample Name	MK_3
Analysis Date Time	4/04/2023 14:00:55
Measurement Date Time	28/03/2023 18:33:32

Average - Frequency (ISO) and Undersize

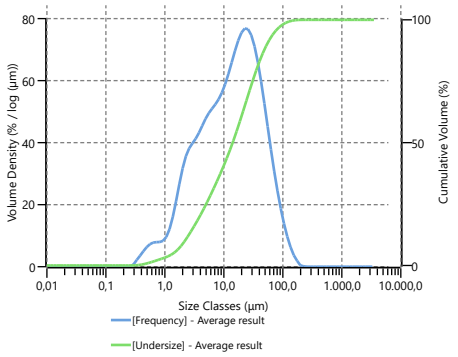

Trend

	Record Number	Sample Name	Dx (10) (µm)	Dx (50) (µm)	Dx (90) (µm)	Specific Surface Area (m^2/kg)
	21	MK_3	2,29	15,7	58,2	1062
	22	MK_3	2,25	15,2	56,0	1084
	23	MK_3	2,24	15,1	55,0	1092
	24	MK_3	2,22	14,9	54,2	1103
	25	MK_3	2,21	14,6	53,4	1111
	26	MK_3	2,20	14,5	53,5	1121
	27	MK_3	2,20	14,5	54,2	1122
	28	MK_3	2,19	14,3	53,5	1131
	29	MK_3	2,18	14,2	53,4	1147
	30	MK_3	2,17	14,1	53,3	1154
	31	MK_3	2,16	13,9	53,1	1161
	32	MK_3	2,17	14,0	54,2	1160
	33	MK_3	2,15	13,8	53,0	1169
	34	MK_3	2,15	13,6	52,6	1174
	35	MK_3	2,15	13,7	53,4	1170
	36	MK_3	2,14	13,3	53,1	1187
	37	MK_3	2,13	13,2	52,4	1196
	38	MK_3	2,12	13,1	51,9	1200
	39	MK_3	2,12	13,2	52,8	1199
	40	MK_3	2,12	13,1	52,3	1202
Mean			**2,18**	**14,1**	**53,7**	**1147**
1xStd Dev			**0,0472**	**0,746**	**1,42**	**42,12**
1xRSD (%)			**2,17**	**5,29**	**2,65**	**3,671**

Frequency (ISO) and Undersize

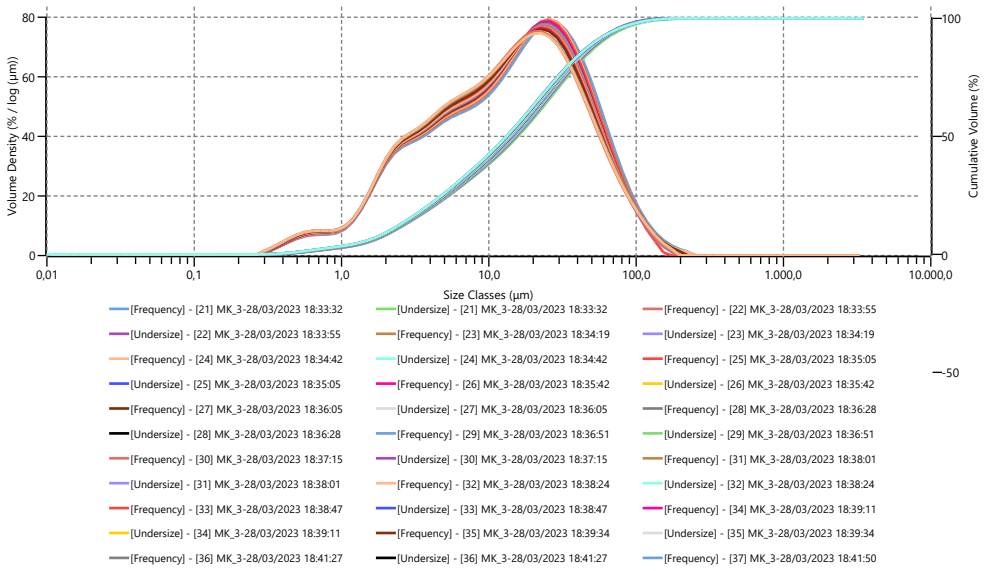

Analysis

Malvern Panalytical

Result

Size (µm)	% Volume In	Size (µm)	% Volume In	Size (µm)	% Volume In	Size (µm)	% Volume In	Size (µm)	% Volume In	Size (µm)	% Volume In
0,0100	0,00	0,0876	0,00	0,767	0,39	6,72	2,71	58,9	2,42	516	0,00
0,0114	0,00	0,0995	0,00	0,872	0,42	7,64	2,79	66,9	1,97	586	0,00
0,0129	0,00	0,113	0,00	0,991	0,49	8,68	2,90	76,0	1,56	666	0,00
0,0147	0,00	0,128	0,00	1,13	0,63	9,86	3,05	86,4	1,19	756	0,00
0,0167	0,00	0,146	0,00	1,28	0,85	11,2	3,23	98,1	0,87	859	0,00
0,0189	0,00	0,166	0,00	1,45	1,13	12,7	3,45	111	0,62	976	0,00
0,0215	0,00	0,188	0,00	1,65	1,42	14,5	3,68	127	0,43	1110	0,00
0,0244	0,00	0,214	0,00	1,88	1,69	16,4	3,91	144	0,29	1260	0,00
0,0278	0,00	0,243	0,00	2,13	1,89	18,7	4,11	163	0,19	1430	0,00
0,0315	0,00	0,276	0,00	2,42	2,02	21,2	4,26	186	0,12	1630	0,00
0,0358	0,00	0,314	0,10	2,75	2,09	24,1	4,34	211	0,07	1850	0,00
0,0407	0,00	0,357	0,17	3,12	2,16	27,4	4,32	240	0,00	2100	0,00
0,0463	0,00	0,405	0,24	3,55	2,25	31,1	4,21	272	0,00	2390	0,00
0,0526	0,00	0,460	0,30	4,03	2,37	35,3	3,99	310	0,00	2710	0,00
0,0597	0,00	0,523	0,35	4,58	2,48	40,1	3,69	352	0,00	3080	0,00
0,0679	0,00	0,594	0,38	5,21	2,57	45,6	3,31	400	0,00	3500	
0,0771	0,00	0,675	0,39	5,92	2,64	51,8	2,88	454	0,00		

J.2 Particle size analysis of GGBFS

Analysis

Malvern Panalytical

Analysis

Particle Name	Blast furnace slags
Particle Refractive Index	1,600
Particle Absorption Index	0,001
Dispersant Name	Water
Dispersant Refractive Index	1,330
Scattering Model	Mie

Measurement Details

Sample Name	BFS_1
Operator Name	mhe220
Analysis Date Time	5/04/2023 13:18:48
Measurement Date Time	28/03/2023 17:46:46

Average - Frequency (compatible) and Undersize

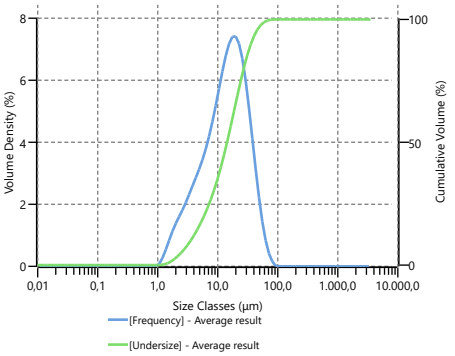

Trend

	Record Number	Sample Name	Dx (10) (µm)	Dx (50) (µm)	Dx (90) (µm)	Specific Surface Area (m^2/kg)
	36	BFS_1	3,52	14,2	35,5	721,2
	19	BFS_1	3,63	14,5	36,1	701,3
	20	BFS_1	3,59	14,4	35,9	708,0
	21	BFS_1	3,58	14,3	35,8	710,7
	22	BFS_1	3,56	14,3	35,6	715,7
	23	BFS_1	3,55	14,3	35,7	716,2
	24	BFS_1	3,55	14,3	35,7	716,2
	25	BFS_1	3,55	14,3	35,7	716,8
	26	BFS_1	3,54	14,3	35,6	717,6
	27	BFS_1	3,54	14,3	35,6	718,4
	28	BFS_1	3,53	14,3	35,5	719,3
	29	BFS_1	3,53	14,3	35,5	719,3
	30	BFS_1	3,53	14,2	35,5	719,6
	31	BFS_1	3,53	14,3	35,7	718,6
	32	BFS_1	3,52	14,2	35,4	721,4
	33	BFS_1	3,53	14,2	35,6	720,0
	34	BFS_1	3,53	14,2	35,6	720,4
	35	BFS_1	3,53	14,3	35,6	720,0
Mean			**3,55**	**14,3**	**35,6**	**716,7**
1xStd Dev			**0,0285**	**0,0690**	**0,167**	**5,192**
1xRSD (%)			**0,804**	**0,483**	**0,469**	**0,7244**

Frequency (ISO) and Undersize

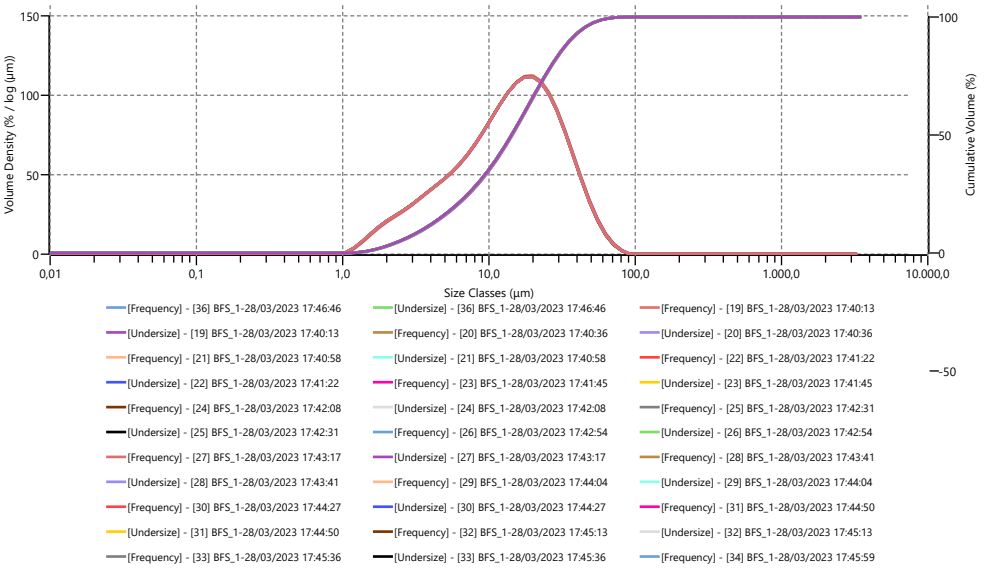

Analysis

Malvern Panalytical

Result

Size (µm)	% Volume In	Size (µm)	% Volume In	Size (µm)	% Volume In	Size (µm)	% Volume In	Size (µm)	% Volume In	Size (µm)	% Volume In
0,0100	0,00	0,0876	0,00	0,767	0,00	6,72	3,50	58,9	0,67	516	0,00
0,0114	0,00	0,0995	0,00	0,872	0,00	7,64	3,90	66,9	0,32	586	0,00
0,0129	0,00	0,113	0,00	0,991	0,07	8,68	4,34	76,0	0,12	666	0,00
0,0147	0,00	0,128	0,00	1,13	0,23	9,86	4,80	86,4	0,00	756	0,00
0,0167	0,00	0,146	0,00	1,28	0,46	11,2	5,26	98,1	0,00	859	0,00
0,0189	0,00	0,166	0,00	1,45	0,71	12,7	5,67	111	0,00	976	0,00
0,0215	0,00	0,188	0,00	1,65	0,96	14,5	6,00	127	0,00	1110	0,00
0,0244	0,00	0,214	0,00	1,88	1,17	16,4	6,18	144	0,00	1260	0,00
0,0278	0,00	0,243	0,00	2,13	1,34	18,7	6,19	163	0,00	1430	0,00
0,0315	0,00	0,276	0,00	2,42	1,52	21,2	5,99	186	0,00	1630	0,00
0,0358	0,00	0,314	0,00	2,75	1,72	24,1	5,58	211	0,00	1850	0,00
0,0407	0,00	0,357	0,00	3,12	1,93	27,4	4,98	240	0,00	2100	0,00
0,0463	0,00	0,405	0,00	3,55	2,16	31,1	4,23	272	0,00	2390	0,00
0,0526	0,00	0,460	0,00	4,03	2,38	35,3	3,41	310	0,00	2710	0,00
0,0597	0,00	0,523	0,00	4,58	2,61	40,1	2,58	352	0,00	3080	0,00
0,0679	0,00	0,594	0,00	5,21	2,87	45,6	1,82	400	0,00	3500	
0,0771	0,00	0,675	0,00	5,92	3,16	51,8	1,17	454	0,00		

Analysis

Malvern Panalytical

Analysis	
Particle Name	Blast furnace slags
Particle Refractive Index	1,580
Particle Absorption Index	0,002
Dispersant Name	Water
Dispersant Refractive Index	1,330
Scattering Model	Mie

Measurement Details	
Operator Name	mhe220
Sample Name	BFS_2
Analysis Date Time	3/04/2023 14:48:29
Measurement Date Time	28/03/2023 17:30:13

Average - Frequency (ISO) and Undersize

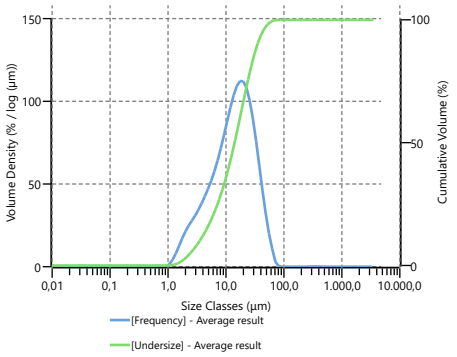

Trend

	Record Number	Sample Name	Dx (10) (µm)	Dx (50) (µm)	Dx (90) (µm)	Specific Surface Area (m^2/kg)
	36	BFS_2	3,52	14,0	34,7	725,6
	19	BFS_2	3,54	14,2	36,1	716,5
	20	BFS_2	3,52	14,1	35,1	722,4
	21	BFS_2	3,51	14,1	34,9	724,8
	22	BFS_2	3,51	14,1	34,8	724,6
	23	BFS_2	3,52	14,1	35,1	722,7
	24	BFS_2	3,51	14,1	34,8	724,7
	25	BFS_2	3,52	14,1	35,1	723,1
	26	BFS_2	3,52	14,1	35,1	722,8
	27	BFS_2	3,51	14,1	34,8	725,2
	28	BFS_2	3,52	14,1	34,9	724,7
	29	BFS_2	3,52	14,1	34,7	725,0
	30	BFS_2	3,52	14,1	34,8	724,5
	31	BFS_2	3,51	14,0	34,7	726,1
	32	BFS_2	3,51	14,0	34,6	726,3
	33	BFS_2	3,53	14,1	34,9	723,8
	34	BFS_2	3,53	14,1	34,9	723,9
	35	BFS_2	3,52	14,0	34,7	725,3
Mean			**3,52**	**14,1**	**34,9**	**724,0**
1xStd Dev			**0,00647**	**0,0513**	**0,332**	**2,187**
1xRSD (%)			**0,184**	**0,365**	**0,952**	**0,3020**

Frequency (ISO) and Undersize

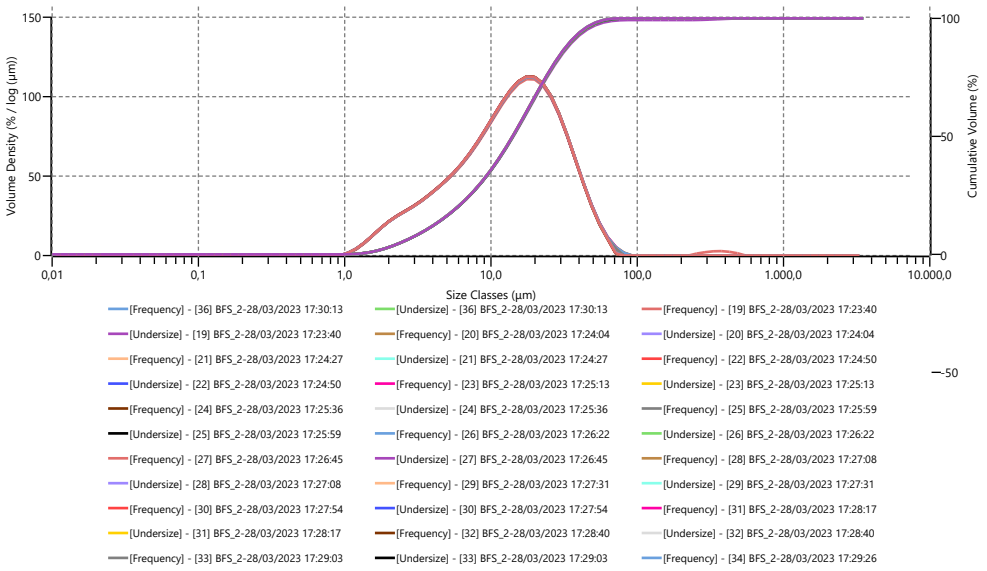

Analysis

Malvern Panalytical

Result

Size (µm)	% Volume In	Size (µm)	% Volume In	Size (µm)	% Volume In	Size (µm)	% Volume In	Size (µm)	% Volume In	Size (µm)	% Volume In
0,0100	0,00	0,0876	0,00	0,767	0,00	6,72	3,58	58,9	0,59	516	0,00
0,0114	0,00	0,0995	0,00	0,872	0,00	7,64	3,99	66,9	0,09	586	0,00
0,0129	0,00	0,113	0,00	0,991	0,10	8,68	4,44	76,0	0,00	666	0,00
0,0147	0,00	0,128	0,00	1,13	0,24	9,86	4,91	86,4	0,00	756	0,00
0,0167	0,00	0,146	0,00	1,28	0,45	11,2	5,36	98,1	0,00	859	0,00
0,0189	0,00	0,166	0,00	1,45	0,70	12,7	5,77	111	0,00	976	0,00
0,0215	0,00	0,188	0,00	1,65	0,95	14,5	6,07	127	0,00	1110	0,00
0,0244	0,00	0,214	0,00	1,88	1,18	16,4	6,24	144	0,00	1260	0,00
0,0278	0,00	0,243	0,00	2,13	1,37	18,7	6,22	163	0,00	1430	0,00
0,0315	0,00	0,276	0,00	2,42	1,53	21,2	5,99	186	0,00	1630	0,00
0,0358	0,00	0,314	0,00	2,75	1,70	24,1	5,56	211	0,00	1850	0,00
0,0407	0,00	0,357	0,00	3,12	1,90	27,4	4,94	240	0,00	2100	0,00
0,0463	0,00	0,405	0,00	3,55	2,12	31,1	4,19	272	0,00	2390	0,00
0,0526	0,00	0,460	0,00	4,03	2,35	35,3	3,36	310	0,00	2710	0,00
0,0597	0,00	0,523	0,00	4,58	2,61	40,1	2,53	352	0,00	3080	0,00
0,0679	0,00	0,594	0,00	5,21	2,89	45,6	1,76	400	0,00	3500	
0,0771	0,00	0,675	0,00	5,92	3,21	51,8	1,10	454	0,00		

Analysis

Malvern Panalytical

Analysis

Particle Name Blast furnace slags
Particle Refractive Index 1,610
Particle Absorption Index 0,001
Dispersant Name Water
Dispersant Refractive Index 1,330
Scattering Model Mie

Measurement Details

Sample Name BFS_3
Operator Name mhe220
Analysis Date Time 3/04/2023 15:37:31
Measurement Date Time 28/03/2023 16:44:46

Average - Frequency (compatible) and Undersize

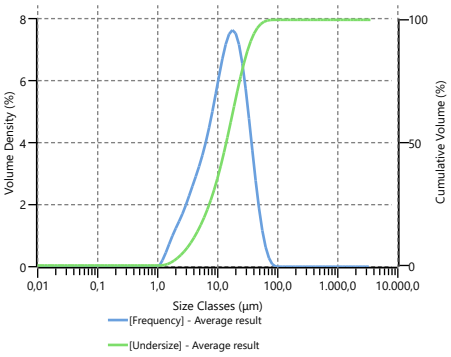

Trend

	Record Number	Sample Name	Dx (10) (µm)	Dx (50) (µm)	Dx (90) (µm)	Specific Surface Area (m^2/kg)
	19	BFS_3	3,74	13,9	34,1	701,0
	20	BFS_3	3,75	13,9	34,2	700,2
	21	BFS_3	3,74	13,9	34,0	703,1
	22	BFS_3	3,74	13,9	34,1	702,8
	23	BFS_3	3,73	13,9	34,1	703,4
	24	BFS_3	3,73	13,8	34,0	704,3
	25	BFS_3	3,73	13,9	34,0	704,1
	26	BFS_3	3,72	13,8	33,9	705,5
	27	BFS_3	3,72	13,8	33,9	706,1
	28	BFS_3	3,71	13,8	33,9	706,4
	29	BFS_3	3,71	13,8	34,0	706,4
	30	BFS_3	3,71	13,8	34,0	706,3
	31	BFS_3	3,71	13,8	34,0	706,6
	32	BFS_3	3,71	13,8	33,9	707,8
	33	BFS_3	3,70	13,8	33,8	708,5
	34	BFS_3	3,70	13,8	33,9	708,3
	35	BFS_3	3,70	13,8	33,9	708,6
	36	BFS_3	3,70	13,8	33,8	708,9
Mean			**3,72**	**13,8**	**34,0**	**705,5**
1xStd Dev			**0,0155**	**0,0434**	**0,0968**	**2,618**
1xRSD (%)			**0,416**	**0,314**	**0,285**	**0,3711**

Frequency (ISO) and Undersize

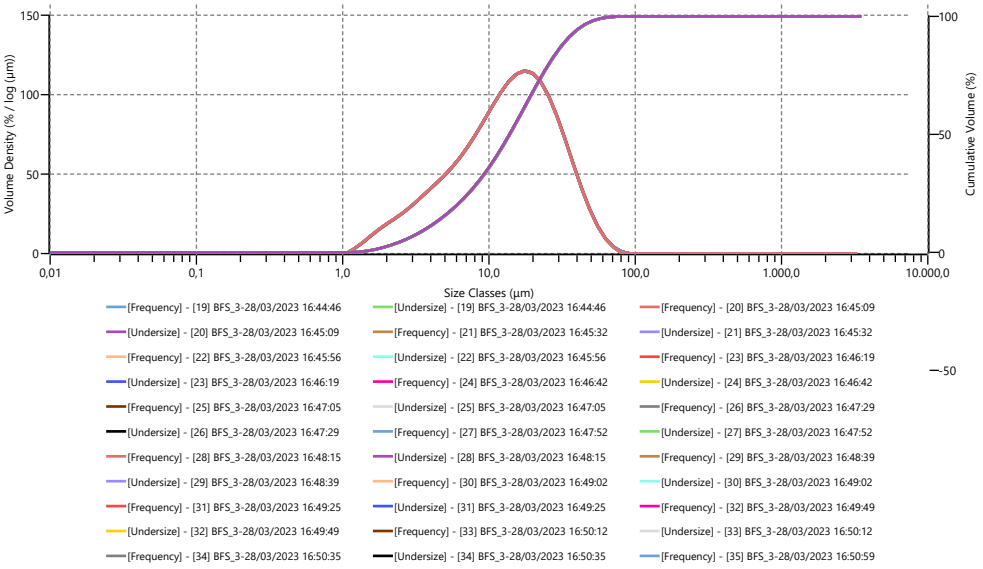

Analysis

Malvern Panalytical

Result

Size (µm)	% Volume In	Size (µm)	% Volume In	Size (µm)	% Volume In	Size (µm)	% Volume In	Size (µm)	% Volume In	Size (µm)	% Volume In
0,0100	0,00	0,0876	0,00	0,767	0,00	6,72	3,71	58,9	0,53	516	0,00
0,0114	0,00	0,0995	0,00	0,872	0,00	7,64	4,15	66,9	0,23	586	0,00
0,0129	0,00	0,113	0,00	0,991	0,00	8,68	4,63	76,0	0,07	666	0,00
0,0147	0,00	0,128	0,00	1,13	0,16	9,86	5,12	86,4	0,00	756	0,00
0,0167	0,00	0,146	0,00	1,28	0,36	11,2	5,58	98,1	0,00	859	0,00
0,0189	0,00	0,166	0,00	1,45	0,59	12,7	5,98	111	0,00	976	0,00
0,0215	0,00	0,188	0,00	1,65	0,82	14,5	6,26	127	0,00	1110	0,00
0,0244	0,00	0,214	0,00	1,88	1,02	16,4	6,38	144	0,00	1260	0,00
0,0278	0,00	0,243	0,00	2,13	1,21	18,7	6,30	163	0,00	1430	0,00
0,0315	0,00	0,276	0,00	2,42	1,41	21,2	6,01	186	0,00	1630	0,00
0,0358	0,00	0,314	0,00	2,75	1,64	24,1	5,50	211	0,00	1850	0,00
0,0407	0,00	0,357	0,00	3,12	1,90	27,4	4,82	240	0,00	2100	0,00
0,0463	0,00	0,405	0,00	3,55	2,16	31,1	4,01	272	0,00	2390	0,00
0,0526	0,00	0,460	0,00	4,03	2,41	35,3	3,16	310	0,00	2710	0,00
0,0597	0,00	0,523	0,00	4,58	2,68	40,1	2,33	352	0,00	3080	0,00
0,0679	0,00	0,594	0,00	5,21	2,98	45,6	1,59	400	0,00	3500	
0,0771	0,00	0,675	0,00	5,92	3,32	51,8	0,98	454	0,00		

Analysis

Malvern Panalytical

Analysis

Particle Name Blast furnace slags
Particle Refractive Index 1,580
Particle Absorption Index 0,002
Dispersant Name Water
Dispersant Refractive Index 1,330
Scattering Model Mie

Measurement Details

Sample Name BFS_4
Operator Name mhe220
Analysis Date Time 3/04/2023 15:44:26
Measurement Date Time 28/03/2023 16:27:16

Average - Frequency (compatible) and Undersize

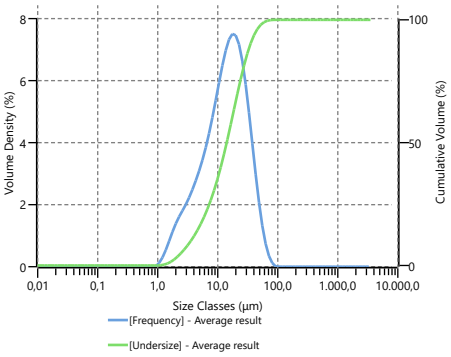

Trend

	Record Number	Sample Name	Dx (10) (µm)	Dx (50) (µm)	Dx (90) (µm)	Specific Surface Area (m^2/kg)
	19	BFS_4	3,57	14,1	35,0	717,9
	20	BFS_4	3,57	14,1	35,0	718,0
	21	BFS_4	3,56	14,1	34,9	720,2
	22	BFS_4	3,56	14,1	35,0	720,1
	23	BFS_4	3,56	14,1	34,9	720,4
	24	BFS_4	3,55	14,1	34,8	721,5
	25	BFS_4	3,56	14,1	34,9	720,4
	26	BFS_4	3,56	14,1	34,9	720,3
	27	BFS_4	3,56	14,1	34,9	720,8
	28	BFS_4	3,56	14,1	34,8	721,2
	29	BFS_4	3,56	14,1	34,9	720,2
	30	BFS_4	3,56	14,1	34,9	720,9
	31	BFS_4	3,56	14,1	34,8	721,4
	32	BFS_4	3,56	14,1	34,8	720,9
	33	BFS_4	3,56	14,1	34,8	721,2
	34	BFS_4	3,57	14,1	34,9	720,6
	35	BFS_4	3,56	14,1	34,8	720,9
	36	BFS_4	3,57	14,1	34,8	720,5
Mean			**3,56**	**14,1**	**34,9**	**720,4**
1xStd Dev			**0,00407**	**0,0271**	**0,0743**	**0,9940**
1xRSD (%)			**0,114**	**0,193**	**0,213**	**0,1380**

Frequency (ISO) and Undersize

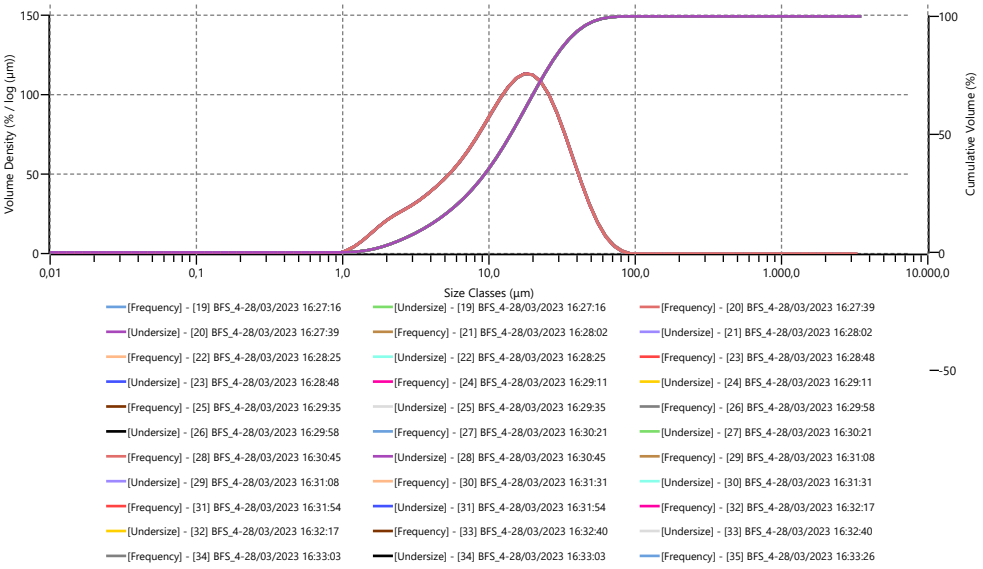

Analysis

Malvern Panalytical

Result

Size (µm)	% Volume In	Size (µm)	% Volume In	Size (µm)	% Volume In	Size (µm)	% Volume In	Size (µm)	% Volume In	Size (µm)	% Volume In
0,0100	0,00	0,0876	0,00	0,767	0,00	6,72	3,56	58,9	0,61	516	0,00
0,0114	0,00	0,0995	0,00	0,872	0,00	7,64	3,98	66,9	0,27	586	0,00
0,0129	0,00	0,113	0,00	0,991	0,09	8,68	4,44	76,0	0,08	666	0,00
0,0147	0,00	0,128	0,00	1,13	0,23	9,86	4,92	86,4	0,00	756	0,00
0,0167	0,00	0,146	0,00	1,28	0,44	11,2	5,38	98,1	0,00	859	0,00
0,0189	0,00	0,166	0,00	1,45	0,68	12,7	5,79	111	0,00	976	0,00
0,0215	0,00	0,188	0,00	1,65	0,93	14,5	6,10	127	0,00	1110	0,00
0,0244	0,00	0,214	0,00	1,88	1,16	16,4	6,27	144	0,00	1260	0,00
0,0278	0,00	0,243	0,00	2,13	1,35	18,7	6,24	163	0,00	1430	0,00
0,0315	0,00	0,276	0,00	2,42	1,51	21,2	6,01	186	0,00	1630	0,00
0,0358	0,00	0,314	0,00	2,75	1,67	24,1	5,57	211	0,00	1850	0,00
0,0407	0,00	0,357	0,00	3,12	1,86	27,4	4,94	240	0,00	2100	0,00
0,0463	0,00	0,405	0,00	3,55	2,08	31,1	4,18	272	0,00	2390	0,00
0,0526	0,00	0,460	0,00	4,03	2,31	35,3	3,35	310	0,00	2710	0,00
0,0597	0,00	0,523	0,00	4,58	2,57	40,1	2,52	352	0,00	3080	0,00
0,0679	0,00	0,594	0,00	5,21	2,85	45,6	1,75	400	0,00	3500	
0,0771	0,00	0,675	0,00	5,92	3,18	51,8	1,10	454	0,00		

Analysis

Malvern Panalytical

Analysis

Particle Name Blast furnace slags
Particle Refractive Index 1,610
Particle Absorption Index 0,001
Dispersant Name Water
Dispersant Refractive Index 1,330
Scattering Model Mie

Measurement Details

Sample Name BFS_5
Operator Name mhe220
Analysis Date Time 3/04/2023 17:08:33
Measurement Date Time 28/03/2023 15:57:02

Average - Frequency (compatible) and Undersize

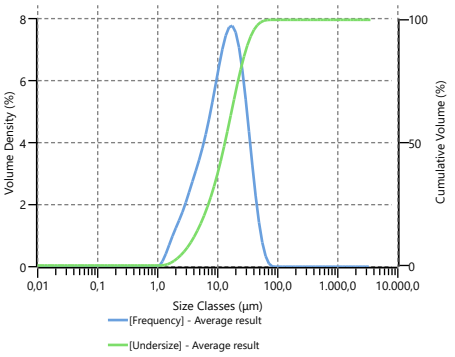

Trend

Record Number	Sample Name	Dx (10) (µm)	Dx (50) (µm)	Dx (90) (µm)	Specific Surface Area (m^2/kg)
19	BFS_5	3,68	13,1	31,5	723,6
20	BFS_5	3,67	13,1	31,5	724,5
21	BFS_5	3,67	13,1	31,5	725,1
22	BFS_5	3,67	13,1	31,4	725,4
23	BFS_5	3,67	13,1	31,5	724,7
24	BFS_5	3,67	13,1	31,5	724,8
25	BFS_5	3,67	13,1	31,5	724,2
26	BFS_5	3,68	13,2	31,6	723,0
27	BFS_5	3,68	13,2	31,5	723,4
28	BFS_5	3,68	13,2	31,6	722,5
29	BFS_5	3,68	13,2	31,6	722,6
30	BFS_5	3,68	13,2	31,6	721,9
31	BFS_5	3,68	13,2	31,6	721,9
32	BFS_5	3,68	13,2	31,6	722,6
33	BFS_5	3,69	13,2	31,7	721,1
34	BFS_5	3,69	13,2	31,6	720,7
35	BFS_5	3,69	13,2	31,6	721,1
36	BFS_5	3,70	13,2	31,6	720,5
Mean		**3,68**	**13,2**	**31,5**	**723,0**
1xStd Dev		**0,00829**	**0,0474**	**0,0824**	**1,575**
1xRSD (%)		**0,225**	**0,361**	**0,261**	**0,2178**

Frequency (ISO) and Undersize

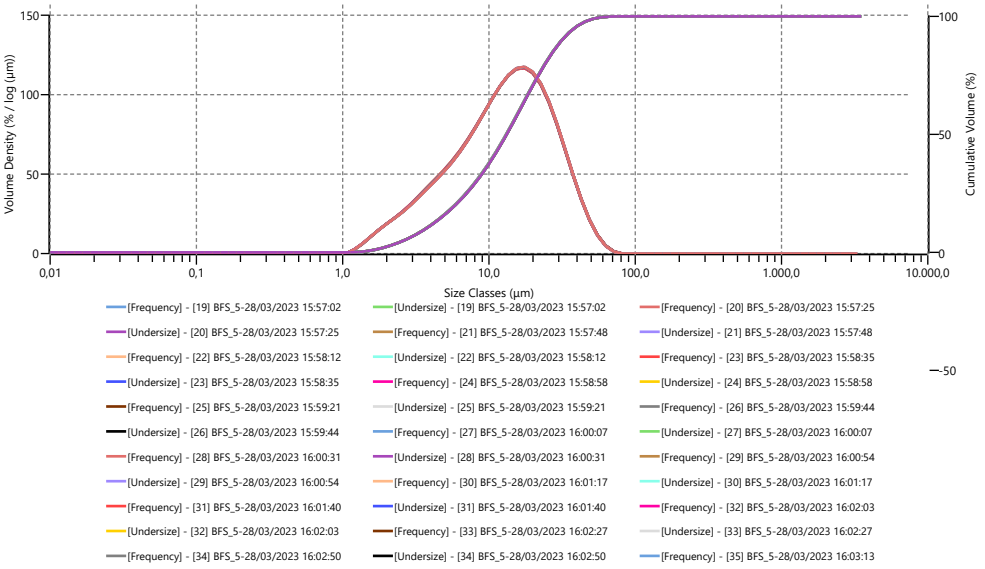

Analysis

Malvern Panalytical

Result

Size (µm)	% Volume In	Size (µm)	% Volume In	Size (µm)	% Volume In	Size (µm)	% Volume In	Size (µm)	% Volume In	Size (µm)	% Volume In
0,0100	0,00	0,0876	0,00	0,767	0,00	6,72	3,99	58,9	0,27	516	0,00
0,0114	0,00	0,0995	0,00	0,872	0,00	7,64	4,45	66,9	0,08	586	0,00
0,0129	0,00	0,113	0,00	0,991	0,00	8,68	4,93	76,0	0,00	666	0,00
0,0147	0,00	0,128	0,00	1,13	0,13	9,86	5,41	86,4	0,00	756	0,00
0,0167	0,00	0,146	0,00	1,28	0,33	11,2	5,85	98,1	0,00	859	0,00
0,0189	0,00	0,166	0,00	1,45	0,57	12,7	6,21	111	0,00	976	0,00
0,0215	0,00	0,188	0,00	1,65	0,81	14,5	6,44	127	0,00	1110	0,00
0,0244	0,00	0,214	0,00	1,88	1,03	16,4	6,48	144	0,00	1260	0,00
0,0278	0,00	0,243	0,00	2,13	1,24	18,7	6,30	163	0,00	1430	0,00
0,0315	0,00	0,276	0,00	2,42	1,47	21,2	5,89	186	0,00	1630	0,00
0,0358	0,00	0,314	0,00	2,75	1,74	24,1	5,27	211	0,00	1850	0,00
0,0407	0,00	0,357	0,00	3,12	2,03	27,4	4,48	240	0,00	2100	0,00
0,0463	0,00	0,405	0,00	3,55	2,32	31,1	3,60	272	0,00	2390	0,00
0,0526	0,00	0,460	0,00	4,03	2,61	35,3	2,70	310	0,00	2710	0,00
0,0597	0,00	0,523	0,00	4,58	2,90	40,1	1,87	352	0,00	3080	0,00
0,0679	0,00	0,594	0,00	5,21	3,22	45,6	1,17	400	0,00	3500	
0,0771	0,00	0,675	0,00	5,92	3,59	51,8	0,63	454	0,00		

Analysis

Malvern Panalytical

Analysis	
Particle Name	Blast furnace slags
Particle Refractive Index	1,620
Particle Absorption Index	0,001
Dispersant Name	Water
Dispersant Refractive Index	1,330
Scattering Model	Mie

Measurement Details	
Sample Name	BFS 6
Operator Name	mhe220
Analysis Date Time	3/04/2023 17:25:01
Measurement Date Time	28/03/2023 15:41:46

Average - Frequency (compatible) and Undersize

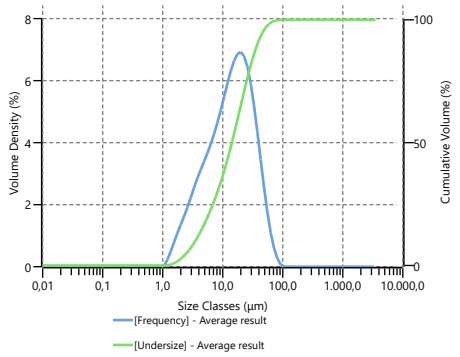

Trend

	Record Number	Sample Name	Dx (10) (µm)	Dx (50) (µm)	Dx (90) (µm)	Specific Surface Area (m^2/kg)
	19	BFS 6	3,47	14,2	37,5	723,9
	20	BFS 6	3,47	14,1	37,5	724,9
	21	BFS 6	3,48	14,2	37,7	723,2
	22	BFS 6	3,48	14,2	37,7	723,4
	23	BFS 6	3,48	14,2	37,6	723,1
	24	BFS 6	3,48	14,2	37,5	722,5
	25	BFS 6	3,49	14,2	37,7	721,9
	26	BFS 6	3,49	14,2	37,6	721,3
	27	BFS 6	3,49	14,2	37,7	721,2
	28	BFS 6	3,49	14,2	37,4	721,9
	29	BFS 6	3,50	14,2	37,6	720,2
	30	BFS 6	3,50	14,2	37,6	720,5
	31	BFS 6	3,51	14,2	37,8	718,9
	32	BFS 6	3,51	14,2	37,5	720,0
	33	BFS 6	3,51	14,2	37,7	718,8
	34	BFS 6	3,52	14,2	37,7	718,4
	35	BFS 6	3,52	14,2	37,6	718,4
	36	BFS 6	3,52	14,2	37,9	717,3
Mean			**3,49**	**14,2**	**37,6**	**721,1**
1xStd Dev			**0,0164**	**0,0193**	**0,125**	**2,184**
1xRSD (%)			**0,470**	**0,136**	**0,331**	**0,3029**

Frequency (ISO) and Undersize

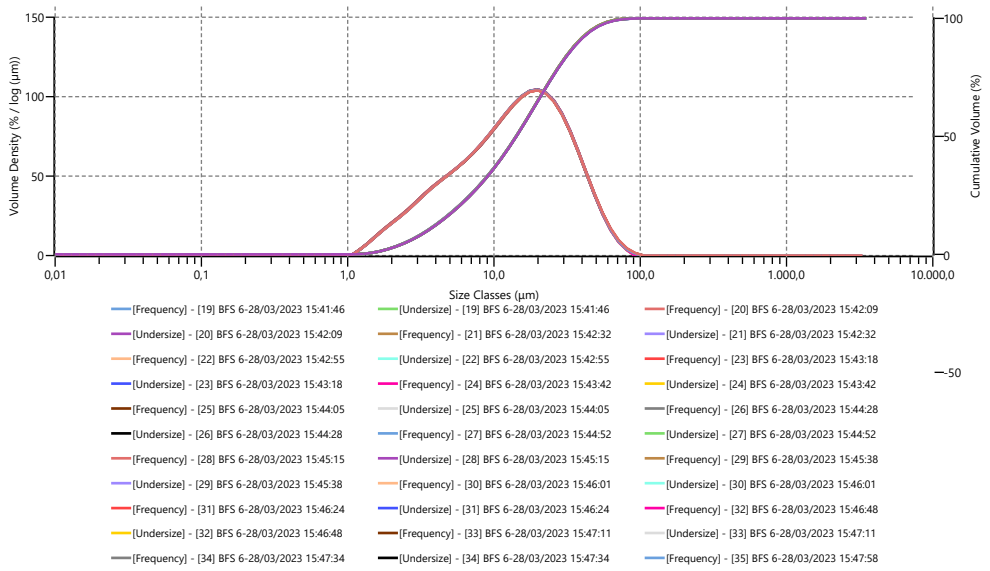

Analysis

Malvern Panalytical

Result

Size (µm)	% Volume In	Size (µm)	% Volume In	Size (µm)	% Volume In	Size (µm)	% Volume In	Size (µm)	% Volume In	Size (µm)	% Volume In
0,0100	0,00	0,0876	0,00	0,767	0,00	6,72	3,55	58,9	0,90	516	0,00
0,0114	0,00	0,0995	0,00	0,872	0,00	7,64	3,85	66,9	0,48	586	0,00
0,0129	0,00	0,113	0,00	0,991	0,00	8,68	4,18	76,0	0,20	666	0,00
0,0147	0,00	0,128	0,00	1,13	0,20	9,86	4,54	86,4	0,00	756	0,00
0,0167	0,00	0,146	0,00	1,28	0,42	11,2	4,90	98,1	0,00	859	0,00
0,0189	0,00	0,166	0,00	1,45	0,67	12,7	5,24	111	0,00	976	0,00
0,0215	0,00	0,188	0,00	1,65	0,92	14,5	5,53	127	0,00	1110	0,00
0,0244	0,00	0,214	0,00	1,88	1,15	16,4	5,72	144	0,00	1260	0,00
0,0278	0,00	0,243	0,00	2,13	1,37	18,7	5,79	163	0,00	1430	0,00
0,0315	0,00	0,276	0,00	2,42	1,61	21,2	5,69	186	0,00	1630	0,00
0,0358	0,00	0,314	0,00	2,75	1,88	24,1	5,42	211	0,00	1850	0,00
0,0407	0,00	0,357	0,00	3,12	2,15	27,4	4,96	240	0,00	2100	0,00
0,0463	0,00	0,405	0,00	3,55	2,40	31,1	4,36	272	0,00	2390	0,00
0,0526	0,00	0,460	0,00	4,03	2,62	35,3	3,65	310	0,00	2710	0,00
0,0597	0,00	0,523	0,00	4,58	2,83	40,1	2,89	352	0,00	3080	0,00
0,0679	0,00	0,594	0,00	5,21	3,05	45,6	2,14	400	0,00	3500	
0,0771	0,00	0,675	0,00	5,92	3,29	51,8	1,46	454	0,00		

J.3 Particle size analysis of WWA

Analysis

Malvern Panalytical

Analysis

Particle Name	WWA1
Particle Refractive Index	1,780
Particle Absorption Index	0,010
Dispersant Name	Water
Dispersant Refractive Index	1,330
Scattering Model	Mie

Measurement Details

Sample Name	WWA_1
Operator Name	mhe220
Analysis Date Time	4/05/2023 20:34:01
Measurement Date Time	28/03/2023 18:53:04

Average - Frequency (compatible) and Undersize

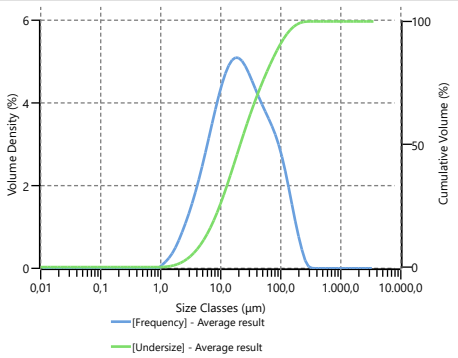

Trend

	Record Number	Sample Name	Dx (10) (µm)	Dx (50) (µm)	Dx (90) (µm)	Specific Surface Area (m^2/kg)
	37	WWA_1	4,83	21,3	93,0	515,5
	38	WWA_1	4,82	21,1	93,3	516,7
	39	WWA_1	4,84	21,3	95,6	514,5
	40	WWA_1	4,84	21,2	95,0	515,2
	41	WWA_1	4,83	21,1	94,4	515,7
	42	WWA_1	4,83	21,0	94,3	516,4
	43	WWA_1	4,83	20,9	91,5	517,6
	44	WWA_1	4,86	21,1	94,5	513,8
	45	WWA_1	4,86	21,1	95,0	514,2
	46	WWA_1	4,87	21,1	96,0	512,8
	47	WWA_1	4,87	21,1	93,8	513,4
	48	WWA_1	4,89	21,2	96,3	511,0
	49	WWA_1	4,88	21,1	94,0	512,8
	50	WWA_1	4,88	21,1	94,4	512,5
	51	WWA_1	4,90	21,1	94,4	511,0
	52	WWA_1	4,92	21,3	96,0	508,9
	53	WWA_1	4,95	21,6	99,7	504,2
	54	WWA_1	4,91	21,1	92,7	511,0
Mean			**4,87**	**21,2**	**94,7**	**513,2**
1xStd Dev			**0,0364**	**0,136**	**1,75**	**3,229**
1xRSD (%)			**0,747**	**0,644**	**1,85**	**0,6292**

Frequency (ISO) and Undersize

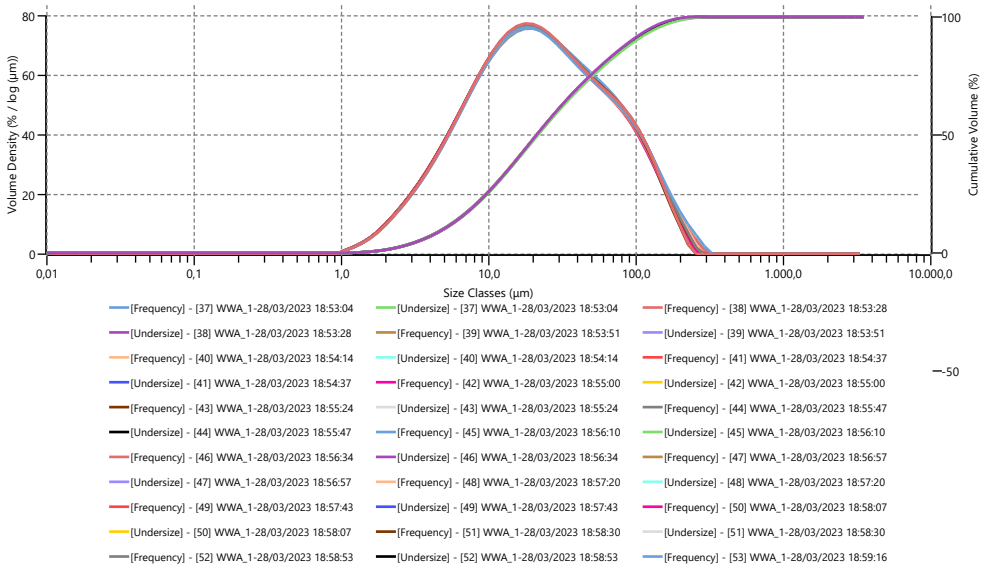

Analysis

Malvern Panalytical

Result

Size (µm)	% Volume In	Size (µm)	% Volume In	Size (µm)	% Volume In	Size (µm)	% Volume In	Size (µm)	% Volume In	Size (µm)	% Volume In
0,0100	0,00	0,0876	0,00	0,767	0,00	6,72	2,91	58,9	3,11	516	0,00
0,0114	0,00	0,0995	0,00	0,872	0,00	7,64	3,19	66,9	2,94	586	0,00
0,0129	0,00	0,113	0,00	0,991	0,08	8,68	3,45	76,0	2,75	666	0,00
0,0147	0,00	0,128	0,00	1,13	0,14	9,86	3,68	86,4	2,52	756	0,00
0,0167	0,00	0,146	0,00	1,28	0,21	11,2	3,87	98,1	2,25	859	0,00
0,0189	0,00	0,166	0,00	1,45	0,30	12,7	4,03	111	1,93	976	0,00
0,0215	0,00	0,188	0,00	1,65	0,42	14,5	4,14	127	1,58	1110	0,00
0,0244	0,00	0,214	0,00	1,88	0,57	16,4	4,19	144	1,22	1260	0,00
0,0278	0,00	0,243	0,00	2,13	0,73	18,7	4,20	163	0,88	1430	0,00
0,0315	0,00	0,276	0,00	2,42	0,92	21,2	4,15	186	0,58	1630	0,00
0,0358	0,00	0,314	0,00	2,75	1,11	24,1	4,07	211	0,34	1850	0,00
0,0407	0,00	0,357	0,00	3,12	1,32	27,4	3,96	240	0,16	2100	0,00
0,0463	0,00	0,405	0,00	3,55	1,56	31,1	3,82	272	0,00	2390	0,00
0,0526	0,00	0,460	0,00	4,03	1,81	35,3	3,68	310	0,00	2710	0,00
0,0597	0,00	0,523	0,00	4,58	2,07	40,1	3,54	352	0,00	3080	0,00
0,0679	0,00	0,594	0,00	5,21	2,35	45,6	3,40	400	0,00	3500	
0,0771	0,00	0,675	0,00	5,92	2,63	51,8	3,26	454	0,00		

Analysis

Malvern Panalytical

Analysis

Particle Name Waste wood ash
Particle Refractive Index 1,780
Particle Absorption Index 0,010
Dispersant Name Water
Dispersant Refractive Index 1,330
Scattering Model Mie

Measurement Details

Sample Name WWA_2
Operator Name mhe220
Analysis Date Time 5/04/2023 13:34:31
Measurement Date Time 28/03/2023 19:19:02

Average - Frequency (compatible) and Undersize

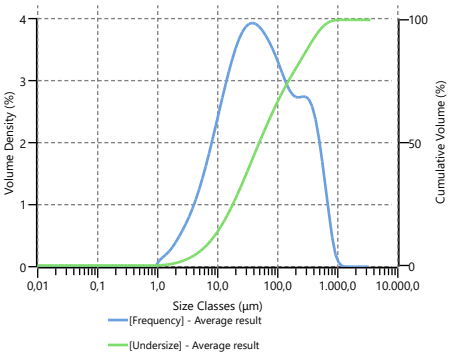

Trend

	Record Number	Sample Name	Dx (10) (µm)	Dx (50) (µm)	Dx (90) (µm)	Specific Surface Area (m²/kg)
	36	WWA_2	7,71	46,5	306	319,9
	35	WWA_2	7,84	48,9	350	312,6
	34	WWA_2	7,85	49,6	365	311,1
	33	WWA_2	7,68	47,6	310	319,5
	32	WWA_2	7,69	48,3	339	317,7
	29	WWA_2	7,70	50,2	358	314,5
	28	WWA_2	7,61	49,5	352	318,2
	27	WWA_2	7,54	49,0	358	320,3
	26	WWA_2	7,59	50,3	368	317,5
	25	WWA_2	7,50	49,3	355	321,2
	24	WWA_2	7,49	49,7	351	320,9
	22	WWA_2	7,61	52,6	392	313,9
	21	WWA_2	7,40	49,6	340	323,7
	20	WWA_2	7,29	48,1	320	328,9
	19	WWA_2	7,35	49,0	330	325,7
Mean			**7,59**	**49,2**	**346**	**319,0**
1xStd Dev			**0,166**	**1,37**	**22,9**	**4,840**
1xRSD (%)			**2,19**	**2,79**	**6,61**	**1,517**

Frequency (ISO) and Undersize

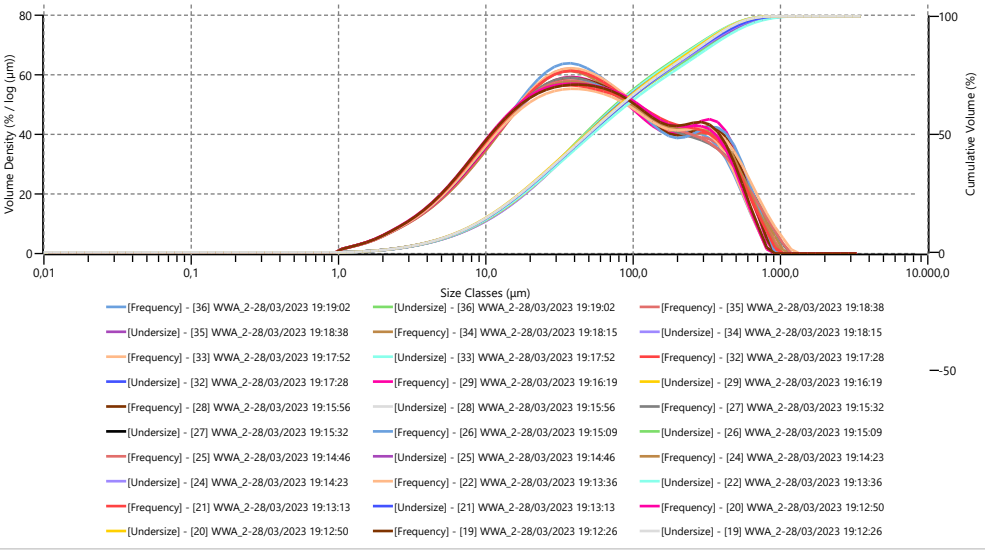

Analysis

Malvern Panalytical

Result

Size (µm)	% Volume In	Size (µm)	% Volume In	Size (µm)	% Volume In	Size (µm)	% Volume In	Size (µm)	% Volume In	Size (µm)	% Volume In
0,0100	0,00	0,0876	0,00	0,767	0,00	6,72	1,47	58,9	3,25	516	1,12
0,0114	0,00	0,0995	0,00	0,872	0,00	7,64	1,65	66,9	3,13	586	0,76
0,0129	0,00	0,113	0,00	0,991	0,09	8,68	1,85	76,0	3,01	666	0,43
0,0147	0,00	0,128	0,00	1,13	0,12	9,86	2,05	86,4	2,88	756	0,10
0,0167	0,00	0,146	0,00	1,28	0,16	11,2	2,26	98,1	2,75	859	0,00
0,0189	0,00	0,166	0,00	1,45	0,20	12,7	2,47	111	2,62	976	0,00
0,0215	0,00	0,188	0,00	1,65	0,26	14,5	2,68	127	2,51	1110	0,00
0,0244	0,00	0,214	0,00	1,88	0,33	16,4	2,88	144	2,41	1260	0,00
0,0278	0,00	0,243	0,00	2,13	0,40	18,7	3,07	163	2,34	1430	0,00
0,0315	0,00	0,276	0,00	2,42	0,48	21,2	3,24	186	2,30	1630	0,00
0,0358	0,00	0,314	0,00	2,75	0,57	24,1	3,38	211	2,28	1850	0,00
0,0407	0,00	0,357	0,00	3,12	0,66	27,4	3,48	240	2,26	2100	0,00
0,0463	0,00	0,405	0,00	3,55	0,77	31,1	3,53	272	2,23	2390	0,00
0,0526	0,00	0,460	0,00	4,03	0,88	35,3	3,54	310	2,14	2710	0,00
0,0597	0,00	0,523	0,00	4,58	1,01	40,1	3,51	352	1,99	3080	0,00
0,0679	0,00	0,594	0,00	5,21	1,15	45,6	3,45	400	1,77	3500	
0,0771	0,00	0,675	0,00	5,92	1,31	51,8	3,36	454	1,47		

K Measured mechanical properties mixes

K.1 Reference mix DM8

DM8 - 30%MK 70%GGBFS 70°C

Information about Batches

Batch nr.	amount	M.Date	Density m1 (g)	Density m2 (g)	Density V (l)	Density ρ (kg/m³)	S.G.	Workability Type test	Workability D1.1 (cm)	Workability D1.2 (cm)	Workability D1 (cm)	Workability F1	Workability D2.1 (cm)	Workability D2.2 (cm)	Workability D2 (cm)	Workability F2	Workability Davg	Workability Favg	Extra information batches
2	2x SS	20/mrt	2806,56	1159,00	0,75	2196,75	2,20	Flow	23,50	23,00	23,25	132,50	23,50	23,50	23,50	135	23,38	133,75	
3	2x SS	20/mrt	2776,96	1159,00	0,75	2157,28	2,16	Flow	24,00	24,00	24,00	140,00	24,50	25,00	24,75	148	24,38	143,75	
4	2x SS	20/mrt	2805,99	1159,00	0,75	2195,99	2,20	Flow	24,50	24,50	24,50	145,00	25,00	24,00	24,50	145	24,50	145,00	
5	2x SS	20/mrt	2773,88	1159,00	0,75	2153,17	2,15	Flow	22,00	22,00	22,00	120,00	24,00	23,00	23,50	135	22,75	127,50	
6	2x SS	20/mrt	2769,06	1159,00	0,75	2146,75	2,15	Flow	25,00	24,00	24,50	145,00	25,00	25,00	25,00	150	24,75	147,50	
7	2x SS	20/mrt	2781,57	1159,00	0,75	2163,43	2,16	Flow	23,50	24,00	23,75	137,50	23,00	25,00	24,00	140	23,88	138,75	
8	1xSS	20/mrt	2737,33	1159,00	0,75	2104,44	2,10	Flow	25,00	24,50	24,75	147,50	26,00	25,00	25,50	155	25,13	151,25	Samples had very low values compared to time frames around, something is wrong in the mix. Took XRD from sampl
9	2x SS	22/mrt	2763,89	1159,00	0,75	2166,52	2,17	Flow	23,00	23,50	23,25	132,50	23,00	26,00	24,50	145	23,88	138,75	Some material flew out during mixing, so it could be that some is missing
10	2x SS	22/mrt	2777,28	1159,00	0,75	2157,71	2,16	Flow	23,00	23,50	23,25	132,50	22,00	24,00	23,00	130	23,13	131,25	
11	2x SS	22/mrt	2775,56	1159,00	0,75	2155,41	2,16	Flow	22,00	22,50	22,25	122,50	22,50	22,00	22,25	123	22,25	122,50	
12	2x SS	23/mrt	2798,57	1159,00	0,75	2186,09	2,19	Flow	23,00	22,00	22,50	125,00	24,00	24,00	24,00	140	23,25	132,50	
13	2x SS	24/mrt	2773,67	1159,00	0,75	2152,89	2,15	Flow	22,50	23,00	22,75	127,50	22,50	22,50	22,50	125	22,63	126,25	standard DM8 mix, cured at room temp (12 and 24h)
15	2x SS	24/mrt	2777,66	1159,00	0,75	2158,21	2,16	Flow	22,50	22,50	22,50	125,00	22,00	23,00	22,50	125	22,50	125,00	standard DM8 mix, cured at room temp (4 and 8h)
21	2x SS	25/mrt	2805,69	1158,28	0,75	2196,55	2,20	Flow	22,50	23,00	22,75	127,50	23,00	23,00	23,00	130	22,88	128,75	One batch from the two used for ambient curing other one 28d
28	1xSS	27/mrt	2780,05	1158,04	0,75	2162,68	2,16	Flow	23,00	23,00	23,00	130,00	23,00	23,00	23,00	130	23,00	130,00	
30	1xSS	28/mrt	2781,66	1157,68	0,75	2165,31	2,17	Flow	21,50	22,00	21,75	117,50	22,00	22,00	22,00	120	21,88	118,75	
31	2x SS	24/apr	2804,12	1159,25	0,75	2193,16	2,19	Flow	22,50	23,00	22,75	127,50	24,00	22,00	23,00	130	22,88	128,75	
							0,02												
		AVG	2782,91			2170	2,17				23,15	131,47				135,59	23,35	133,53	

Information about prisms

Age (h)	Prism 1 l (mm)	Prism 1 b (mm)	Prism 1 h1 (mm)	Prism 1 h2 (mm)	Prism 1 h3 (mm)	Prism 1 h (mm)	Prism 1 m (g)	Prism 1 ρ (kg/m³)	Prism 1 S.G.	Prism 2 l (mm)	Prism 2 b (mm)	Prism 2 h1 (mm)	Prism 2 h2 (mm)	Prism 2 h3 (mm)	Prism 2 h (mm)	Prism 2 m (g)	Prism 2 ρ (kg/m³)	Prism 2 S.G.	Prism 3 l (mm)	Prism 3 b (mm)	Prism 3 h1 (mm)	Prism 3 h2 (mm)	Prism 3 h3 (mm)	Prism 3 h (mm)	Prism 3 m (g)	Prism 3 ρ (kg/m³)	Prism 3 S.G.	AVG ρ (kg/m³)	AVG STDEV	AVG S.G.	STDEV
1	159,93	39,97	40,54	40,09	40,31	40,31	561,18	2177,66	2,178	159,99	39,98	40,37	40,44	40,30	40,37	560,66	2171,23	2,171	160,37	39,72	40,97	40,00	40,23	40,40	563,12	2188,20	2,188	2180	8,57	2,18	0,009
2	160,00	39,89	40,75	41,23	40,45	40,81	563,82	2164,66	2,165	160,00	39,87	40,83	42,31	41,00	41,38	563,08	2133,11	2,133	160,00	40,14	40,27	41,40	40,85	40,84	556,32	2121,00	2,121	2140	22,54	2,14	0,023
3	160,16	39,81	40,61	40,58	39,90	40,36	566,85	2202,60	2,203	160,26	39,95	39,92	40,10	39,97	40,00	553,91	2163,08	2,163	160,32	39,71	41,10	40,59	40,32	40,67	559,47	2160,80	2,161	2180	23,50	2,18	0,023
4	160,00	40,08	41,00	42,05	40,68	41,24	572,18	2163,37	2,163	160,00	40,01	40,75	41,40	41,00	41,05	562,90	2142,05	2,142	160,00	40,10	40,46	40,62	40,57	40,55	560,00	2152,45	2,152	2150	10,66	2,15	0,011
5	160,21	39,86	40,18	40,91	39,70	40,26	557,33	2167,58	2,168	160,23	39,96	40,38	40,32	40,51	40,40	557,47	2154,94	2,155	160,29	39,85	40,44	40,91	40,30	40,55	556,87	2149,95	2,150	2160	9,09	2,16	0,009
6	160,00	40,23	40,58	42,18	40,88	41,21	566,72	2136,29	2,136	160,00	39,99	40,28	40,52	40,95	40,58	569,30	2192,41	2,192	160,00	40,01	41,40	41,09	40,98	41,16	568,55	2157,94	2,158	2160	28,30	2,16	0,028
7	160,17	39,85	41,22	40,16	40,36	40,58	568,33	2194,21	2,194	160,29	39,88	40,42	40,61	40,99	40,67	563,15	2165,97	2,166	160,51	39,80	40,76	40,31	40,49	40,52	564,19	2179,57	2,180	2160	21,35	2,16	0,021
7	159,77	39,86	41,30	40,54	41,11	40,98	562,56	2155,41	2,155	159,89	40,07	41,46	40,48	41,01	40,98	560,03	2132,87	2,133	159,50	39,88	41,05	41,05	40,72	40,94	561,26	2155,26	2,155	-	-	-	-
8	160,00	40,16	41,86	40,79	41,12	41,26	565,39	2132,75	2,133	160,00	40,00	41,32	40,30	40,34	40,65	567,48	2181,09	2,181	160,00	40,03	40,82	40,19	40,37	40,46	568,19	2192,61	2,193	2170	31,76	2,17	0,032
9	159,75	40,06	41,45	40,67	40,27	40,80	551,06	2110,68	2,111	159,79	39,89	41,37	41,76	40,33	41,15	558,11	2127,65	2,128	159,65	39,84	41,29	40,66	41,00	40,98	565,43	2169,12	2,169	2170	38,59	2,17	0,039
9	160,17	39,86	40,86	41,08	41,27	41,07	576,19	2197,47	2,197	160,10	39,98	40,89	40,33	40,55	40,59	570,86	2197,23	2,197	160,23	39,97	40,44	41,11	40,22	40,59	571,03	2196,66	2,197	-	-	-	-
10	160,00	40,02	40,76	40,68	40,32	40,59	572,10	2201,36	2,201	160,00	39,92	40,85	40,66	40,40	40,64	572,62	2206,16	2,206	160,00	40,05	40,65	40,92	40,60	40,72	573,59	2198,04	2,198	2200	4,08	2,20	0,004
12	160,00	40,09	41,05	40,82	41,04	40,97	569,37	2166,57	2,167	160,00	40,20	41,10	40,77	40,87	40,91	563,90	2142,85	2,143	160,00	40,17	40,64	40,39	40,64	40,56	555,22	2130,01	2,130	2150	18,55	2,15	0,019
14	160,47	39,76	39,75	39,73	39,83	39,77	545,59	2150,16	2,150	160,63	39,93	39,19	40,35	40,39	39,98	547,00	2133,31	2,133	160,47	39,77	39,44	40,02	38,75	39,40	554,11	2203,50	2,204	2160	36,64	2,16	0,037
16	160,29	39,92	39,65	40,80	39,30	39,98	558,11	2181,44	2,181	160,20	39,91	41,75	40,21	40,86	40,94	559,77	2178,54	2,179	160,51	40,12	39,92	40,56	40,72	40,40	560,15	2153,08	2,153	2160	21,82	2,16	0,022
18	159,78	39,76	40,61	40,35	40,57	40,51	548,09	2129,71	2,130	159,78	40,01	40,17	40,23	40,64	40,35	561,93	2178,63	2,179	159,86	40,01	40,21	40,22	40,32	40,32	547,10	2121,65	2,122	2140	30,84	2,14	0,031
20	159,96	39,94	40,14	40,74	40,69	40,52	549,93	2124,14	2,124	160,09	39,98	40,40	40,59	41,05	40,68	594,34	2129,06	2,129	160,14	40,00	40,24	41,20	41,70	41,05	555,07	2111,11	2,111	2120	9,28	2,12	0,009
22	159,78	40,15	40,91	40,42	40,87	40,73	560,12	2143,50	2,143	159,70	40,08	40,24	40,66	41,00	40,63	563,86	2167,98	2,168	159,92	40,25	41,48	41,29	41,49	41,42	570,76	2140,79	2,141	2150	14,98	2,15	0,015
24	160,19	39,90	39,93	40,27	39,83	40,01	552,53	2160,62	2,161	160,29	39,71	40,36	40,22	39,89	40,16	557,06	2179,41	2,179	160,18	39,89	40,47	40,34	39,90	40,24	561,49	2183,98	2,184	2170	12,38	2,17	0,012
284	159,94	40,03	41,00	41,06	41,44	41,17	570,80	2165,00	2,165	159,82	40,08	41,32	40,92	41,06	41,10	569,71	2165,00	2,165	159,71	40,16	40,89	41,04	40,68	40,87	569,46	2172,36	2,172	2170	4,25	2,17	0,004

DM8 - 30%MK 70%GGBFS 70°C

Information about Batches

Tensile strength (NBN EN 196 -1)

Age	Test 1 - Prism 1			Test 2 - Prism 2			Test 3 - Prism 3			AVG	
(h)	$2b^3/3l$ (mm²)	Fmax (kN)	σFlex (MPa)	$2b^3/3l$ (mm²)	Fmax (kN)	σFlex (MPa)	$2b^3/3l$ (mm²)	Fmax (kN)	σFlex (MPa)	σFlex (MPa)	STDEV
1	425,707	0,25	0,60	426,03	0,25	0,58	417,77	0,26	0,63	0,60	0,03
2	423,16	0,59	1,40	422,52	0,56	1,32	431,16	0,57	1,31	1,34	0,05
3	420,62	1,08	2,56	425,07	0,74	1,75	417,45	0,81	1,93	2,08	0,42
4	429,23	1,09	2,55	426,99	1,12	2,63	429,87	1,10	2,56	2,58	0,05
5	422,20	1,21	2,86	425,39	1,21	2,85	421,88	1,23	2,92	2,88	0,04
6	434,07	1,65	3,81	426,35	1,49	3,49	426,99	1,37	3,20	3,50	0,31
7	421,88	0,26	0,61	422,84	0,44	1,04	420,30	1,17	2,79	2,48	1,34
7	422,20	1,46	3,46	428,91	1,30	3,02	422,84	1,67	3,94	-	-
8	431,81	1,64	3,80	426,67	1,48	3,46	427,63	1,52	3,55	3,60	0,17
9	428,59	1,44	3,37	423,16	1,07	2,53	421,57	1,50	3,56	3,44	0,57
9	422,20	1,34	3,17	426,03	1,63	3,83	425,71	1,77	4,17	-	-
10	427,31	2,42	5,67	424,11	2,05	4,84	428,27	2,19	5,12	5,21	0,42
12	429,55	2,66	6,18	433,10	1,96	4,52	432,13	2,70	6,25	5,65	0,98
14	419,03	1,88	4,48	424,43	2,10	4,95	419,35	2,31	5,50	4,98	0,51
16	424,11	2,77	6,54	423,79	2,12	5,01	430,52	2,03	4,72	5,42	0,97
18	419,03	1,74	4,14	426,99	2,65	6,21	426,99	2,16	5,06	5,14	1,04
20	424,75	1,86	4,38	426,03	1,63	3,83	426,67	1,97	4,63	4,28	0,41
22	431,48	2,32	5,39	429,23	1,67	3,88	434,72	2,41	5,54	4,94	0,92
24	423,47	2,08	4,92	417,45	2,40	5,75	423,16	1,51	3,57	4,74	1,10
28d	**427,63**	**2,52**	**5,89**	**429,23**	**2,49**	**5,80**	**431,81**	**2,49**	**5,76**	**5,82**	**0,07**

Compressive strength (NBN EN 196 -1)

Age	Test 1 - Prism 1			Test 2 - Prism 1			Test 3 - Prism 2			Test 4 - Prism 2			Test 5 - Prism 3			Test 6 - Prism 3			AVG	
(h)	So (mm²)	Fmax (kN)	σc (MPa)	So (mm²)	Fmax (kN)	σc (MPa)	So (mm²)	Fmax (kN)	σc (MPa)	So (mm²)	Fmax (kN)	σc (MPa)	So (mm²)	Fmax (kN)	σc (MPa)	So (mm²)	Fmax (kN)	σc (MPa)	σc (MPa)	STDEV
1	1600	10,31	6,44	1600	10,67	6,67	1600	10,37	6,48	1600	10,46	6,54	1600	10,78	6,74	1600	11,16	6,98	**6,64**	**0,20**
2	1600	23,12	14,45	1600	23,87	14,92	1600	22,16	13,85	1600	22,09	13,81	1600	23,3	14,56	1600	22,32	13,95	**14,26**	**0,45**
3	1600	60,26	37,66	1600	61,27	38,29	1600	56,10	35,06	1600	56,99	35,62	1600	56,97	35,61	1600	59,42	37,14	**36,56**	**1,31**
4	1600	71,25	44,53	1600	68,43	42,77	1600	62,91	39,32	1600	66,42	41,51	1600	66,87	41,79	1600	66,38	41,49	**41,90**	**1,71**
5	1600	77,94	48,71	1600	79,37	49,61	1600	78,95	49,34	1600	78,95	49,34	1600	76,92	48,08	1600	79,61	49,76	**49,14**	**0,63**
6	1600	76,92	48,08	1600	77,47	48,42	1600	80,72	50,45	1600	80,58	50,36	1600	76,55	47,84	1600	81,06	50,66	**49,30**	**1,32**
7	1600	90,97	56,86	1600	92,62	57,89	1600	90,23	56,39	1600	92,08	57,55	1600	91,23	57,02	1600	80,78	**50,49**	**57,12**	**1,62**
7	1600	94,02	58,76	1600	94,66	59,16	1600	89,77	56,11	1600	85,02	**53,14**	1600	91,82	57,39	1600	92,93	58,08	-	-
8	1600	95,28	59,55	1600	98,10	61,31	1600	94,42	59,01	1600	91,21	57,01	1600	100,77	62,98	1600	103,19	64,49	**60,73**	**2,75**
9	1600	93,10	58,19	1600	91,05	56,91	1600	93,09	58,18	1600	97,83	61,14	1600	93,41	58,38	1600	95,68	59,80	**61,92**	**3,57**
9	1600	105,44	65,90	1600	106,71	66,69	1600	101,13	63,21	1600	106,04	66,28	1600	103,17	64,48	1600	102,28	63,93	-	-
10	1600	112,73	70,46	1600	111,52	69,70	1600	118,69	74,18	1600	110,78	69,24	1600	108,47	67,79	1600	107,51	67,19	**69,76**	**2,48**
12	1600	112,34	70,21	1600	111,95	69,97	1600	108,50	67,81	1600	108,67	67,92	1600	104,20	65,13	1600	105,76	66,10	**67,86**	**2,03**
14	1600	104,06	65,04	1600	99,31	62,07	1600	96,87	60,54	1600	99,22	62,01	1600	109,41	68,38	1600	99,73	62,33	**63,40**	**2,85**
16	1600	113,70	71,06	1600	115,29	72,06	1600	115,76	72,35	1600	119,72	74,83	1600	118,63	74,14	1600	113,85	71,16	**72,60**	**1,56**
18	1600	101,94	63,71	1600	98,18	61,36	1600	114,12	71,33	1600	111,87	69,92	1600	97,39	60,87	1600	101,65	63,53	**65,12**	**4,43**
20	1600	98,81	61,76	1600	100,70	62,94	1600	103,96	64,98	1600	102,42	64,01	1600	73,66	**46,04**	1600	113,77	71,11	**64,96**	**3,64**
22	1600	119,16	74,48	1600	111,24	69,53	1600	112,87	70,54	1600	119,40	74,63	1600	119,65	74,78	1600	125,43	78,39	**73,72**	**3,23**
24	1600	114,68	71,68	1600	105,32	65,83	1600	122,96	76,85	1600	114,23	71,39	1600	121,66	76,04	1600	116,16	72,60	**72,40**	**3,95**
28d	**1600**	**116,41**	**72,76**	**1600**	**118,27**	**73,92**	**1600**	**111,66**	**69,79**	**1600**	**112,80**	**70,50**	**1600**	**112,27**	**70,17**	**1600**	**115,55**	**72,22**	**71,56**	**1,65**

Analyses curing

Age	AVG		AVG (ref 24h)		AVG		AVG (ref 24h)		σc/σflex					AVG		AVG (ref 24h)	
(h)	σc (MPa)	STDEV	σc (%)	STDEV	σFlex (MPa)	STDEV	σFlex (%)	STDEV	(-)	STDEV	AVG	AVG-sig	AVG+sig	S.G. (-)	STDEV	S.G. (%)	STDEV
0	-	-	-	-	-	-	-	-	-	-	14,95	11,87	18,02	2,17	0,03	100,0	2,6
1	6,64	0,20	9,3	0,4	0,60	0,03	10,4	0,5	11,01	0,59	14,95	11,87	18,02	2,18	0,01	100,5	2,4
2	14,26	0,45	19,9	0,8	1,34	0,05	23,1	0,9	10,60	0,51	14,95	11,87	18,02	2,14	0,02	98,6	2,5
3	36,56	1,31	51,1	2,2	2,08	0,42	35,7	7,3	17,59	3,65	14,95	11,87	18,02	2,18	0,02	100,5	2,6
4	41,90	1,71	58,6	2,7	2,58	0,05	44,3	1,0	16,25	0,73	14,95	11,87	18,02	2,15	0,01	99,1	2,3
5	49,14	0,63	68,7	1,8	2,88	0,04	49,4	0,9	17,09	0,31	14,95	11,87	18,02	2,16	0,01	99,5	2,3
6	49,30	1,32	68,9	2,4	3,50	0,31	60,2	5,3	14,08	1,29	14,95	11,87	18,02	2,16	0,03	99,5	2,6
7	57,12	1,62	79,8	2,9	2,48	1,34	42,6	23,1	23,07	12,54	14,95	11,87	18,02	2,16	0,02	99,5	2,5
8	60,73	2,75	84,9	4,3	3,60	0,17	62,0	3,1	16,85	1,11	14,95	11,87	18,02	2,17	0,03	100,0	2,7
9	61,92	3,57	86,5	5,4	3,44	0,57	59,1	9,8	18,02	3,15	14,95	11,87	18,02	2,17	0,04	100,0	2,9
10	69,76	2,48	97,5	4,1	5,21	0,42	89,6	7,3	13,39	1,18	14,95	11,87	18,02	2,20	0,00	101,4	2,3
12	67,86	2,03	94,8	3,6	5,65	0,98	97,2	16,9	12,01	2,11	14,95	11,87	18,02	2,15	0,02	99,1	2,4
14	63,40	2,85	88,6	4,5	4,98	0,51	85,6	8,9	12,74	1,43	14,95	11,87	18,02	2,16	0,04	99,5	2,9
16	72,60	1,56	101,5	3,2	5,42	0,97	93,2	16,8	13,39	2,42	14,95	11,87	18,02	2,16	0,02	99,5	2,5
18	65,12	4,43	91,0	6,5	5,14	1,04	88,4	17,9	12,67	2,70	14,95	11,87	18,02	2,14	0,03	98,6	2,7
20	64,96	3,64	90,8	5,5	4,28	0,41	73,6	7,1	15,18	1,69	14,95	11,87	18,02	2,12	0,01	97,7	2,3
22	73,72	3,23	103,0	5,1	4,94	0,92	84,9	15,8	14,93	2,85	14,95	11,87	18,02	2,15	0,01	99,1	2,4
24	72,40	3,95	101,2	6,0	4,74	1,10	81,6	19,0	15,26	3,64	14,95	11,87	18,02	2,17	0,01	100,0	2,4
28d	**71,56**	**1,65**	100,0	3,3	**5,82**	**0,07**	100,0	1,7	12,30	0,32	14,95	11,87	18,02	2,17	0,00	100,0	2,3

K.2 Variations on DM8

DM8 - 30%MK 70%GGBFS - Variations

Information about Batches

Batch nr.	amount	M.Date	Density m1 (g)	Density m2 (g)	Density V (l)	Density ρ (kg/m³)	S.G.	Type test	Workability D1.1 (cm)	Workability D1.2 (cm)	Workability D1 (cm)	Workability F1 (cm)	Workability D2.1 (cm)	Workability D2.2 (cm)	Workability D2 (cm)	Workability F2 (cm)	Workability Davg (cm)	Workability Favg (cm)	Extra information batches
R30	2x5S	23/apr	2806,46	1159,25	0,75	2196,28	2,20	Flow	23,0	23,0	23,00	130,00	22,5	22,5	23,00	130,00	23,00	130,00	
R40	2x5S	23/apr	2788,02	1159,25	0,75	2171,69	2,17	Flow	23,5	23,5	23,50	135,00	24,0	24,0	24,00	140,00	23,75	137,50	
R70	2x5S	23/apr	2802,22	1159,25	0,75	2190,63	2,19	Flow	23,0	23,5	23,25	132,50	23,0	23,5	23,50	135,00	23,38	133,75	
REACT																			
14	2x0,9L	24/mrt	2747,61	1159,00	0,75	2118,15	2,12	Flow	20,0	20,0	20,00	100,00	21,5	20,5	21,00	110,00	20,50	105,00	Adapted DM8 mix, sieved sand from HGB 0/8 source (12 and 24h)
16	2x0,9L	24/mrt	2744,27	1159,00	0,75	2113,69	2,11	Flow	20,5	20,5	20,50	105,00	21,0	21,0	21,00	110,00	20,75	107,50	Adapted DM8 mix, sieved sand from HGB 0/8 source (4 and 8h)
22	2x0,9L	26/mrt	2751,09	1159,00	0,75	2122,79	2,12	Flow	19,0	20,0	19,50	95,00	20,0	20,0	20,00	100,00	19,75	97,50	Adapted DM8 mix, sieved sand from HGB 0/8 source (2h and 28d)
HGB	**AVG**		**2747,656667**			**2118,21**	**2,12**				**20,00**	**100,00**			**106,67**	**20,33**	**103,33**		
17	2x0,9L	25/mrt	2682,54	1159,10	0,75	2031,25	2,03	Flow	18,5	19,0	18,75	87,50	18,5	18,5	18,50	85,00	18,63	86,25	40g of water added in the mix to improve workability
19	2x0,9L	25/mrt	2690,36	1158,85	0,75	2042,01	2,04	Flow	20,0	19,0	19,50	95,00	19,0	21,0	20,00	100,00	19,75	97,50	40g of water added in the mix to improve workability
23	2x0,9L	26/mrt	2686,33	1158,85	0,75	2036,64	2,04	Flow	18,0	19,0	18,50	85,00	19,0	18,5	18,75	87,50	18,63	86,25	40g of water added in the mix to improve workability
GPC	**AVG**		**2686,41**			**2036,64**	**2,04**				**18,92**	**89,17**			**90,83**	**19,00**	**90,00**		
18	2x0,9L	25/mrt	2775,04	1158,85	0,75	2154,92	2,15	Flow	14,0	14,5	14,25	42,50	13,0	14,0	13,50	35,00	13,88	38,75	40g of water added in the mix to improve workability, still not good tho, Difficult to compact
20	2x0,9L	25/mrt	2758,10	1158,28	0,75	2133,09	2,13	Flow	14,0	14,0	14,00	40,00	13,5	14,5	14,00	40,00	14,00	40,00	40g of water added in the mix to improve workability, still not good tho, Difficult to compact
29	2x0,9L	28/mrt	2755,49	1158,28	0,75	2129,61	2,13	Flow	17,0	17,0	17,00	70,00	17,0	17,0	17,00	70,00	17,00	70,00	40g of water added in the mix to improve workability, still not good tho, Difficult to compact
RCA	**AVG**		**2762,878667**			**2139,21**	**2,14**				**15,08**	**50,83**			**48,33**	**14,96**	**49,58**		
24	2x5S	26/mrt	2775,64	1159,00	0,75	2155,52	2,16	Flow	23,0	23,5	23,25	132,50	23,5	23,5	23,50	135,00	23,38	133,75	water replaced by SW
25	2x5S	26/mrt	2783,56	1159,00	0,75	2166,08	2,17	Flow	22,5	22,5	22,50	125,00	23,5	24,0	23,75	137,50	23,13	131,25	water replaced by SW, cracked by demoulding low flexural
26	2x5S	27/mrt	2803,06	1159,00	0,75	2192,08	2,19	Flow	22,5	23,0	22,75	127,50	22,0	22,5	22,25	122,50	22,50	125,00	water replaced by SW
27	2x5S	27/mrt	2773,77	1159,00	0,75	2153,03	2,15	Flow	22,0	22,0	22,00	120,00	22,5	22,5	22,50	125,00	22,25	122,50	water replaced by SW
SW	**AVG**		**2784,0075**			**2170,00**	**2,17**				**22,63**	**126,25**			**130,00**	**22,81**	**128,13**		

Information about prisms DM8-R30

Tensile strength (NBN EN 196 -1)

Age (h)	Prism 1 l (mm)	Prism 1 b (mm)	Prism 1 h1 (mm)	Prism 1 h2 (mm)	Prism 1 h3 (mm)	Prism 1 h (mm)	Prism 1 m (g)	Prism 1 ρ (kg/m³)	Prism 1 S.G.	Prism 2 l (mm)	Prism 2 b (mm)	Prism 2 h1 (mm)	Prism 2 h2 (mm)	Prism 2 h3 (mm)	Prism 2 h (mm)	Prism 2 m (g)	Prism 2 ρ (kg/m³)	Prism 2 S.G.	Prism 3 l (mm)	Prism 3 b (mm)	Prism 3 h1 (mm)	Prism 3 h2 (mm)	Prism 3 h3 (mm)	Prism 3 h (mm)	Prism 3 m (g)	Prism 3 ρ (kg/m³)	Prism 3 S.G.	AVG ρ (kg/m³)	AVG ρ STDEV	AVG S.G (-)	STDEV
4	161,36	40,03	41,17	41,01	40,64	40,94	569,86	2153,07	2,153	161,45	39,91	40,88	40,87	40,45	40,73	563,86	2148,33	2,148	160,91	40,07	40,81	41,24	40,31	40,79	566,45	2155,98	2,154	2150	3,03	2,15	0,003
24	160,15	39,85	40,80	40,31	40,65	40,65	557,88	2150,25	2,150	160,12	40,01	40,35	40,55	40,32	40,41	561,34	2148,30	2,148	160,13	39,87	40,52	40,36	40,28	40,39	553,15	2145,29	2,145	2150	12,22	2,15	0,012

Compressive strength (NBN EN 196 -1)

Age (h)	Test 1 - Prism 1 2b²/3l (mm²)	Test 1 - Prism 1 Fmax (kN)	Test 1 - Prism 1 σflex (MPa)	Test 2 - Prism 2 2b²/3l (mm²)	Test 2 - Prism 2 Fmax (kN)	Test 2 - Prism 2 σflex (MPa)	Test 3 - Prism 3 2b²/3l (mm²)	Test 3 - Prism 3 Fmax (kN)	Test 3 - Prism 3 σflex (MPa)	AVG σflex (MPa)	STDEV	Test 1 - Prism 1 So (mm²)	Test 1 - Prism 1 Fmax (kN)	Test 1 - Prism 1 σC (MPa)	Test 2 - Prism 1 So (mm²)	Test 2 - Prism 1 Fmax (kN)	Test 2 - Prism 1 σC (MPa)	Test 3 - Prism 1 So (mm²)	Test 3 - Prism 1 Fmax (kN)	Test 3 - Prism 1 σC (MPa)	Test 4 - Prism 2 So (mm²)	Test 4 - Prism 2 Fmax (kN)	Test 4 - Prism 2 σC (MPa)	Test 5 - Prism 3 So (mm²)	Test 5 - Prism 3 Fmax (kN)	Test 5 - Prism 3 σC (MPa)	Test 6 - Prism 3 So (mm²)	Test 6 - Prism 3 Fmax (kN)	Test 6 - Prism 3 σC (MPa)	AVG σc (MPa)	STDEV
4	427,63	1,0739	2,5113	423,79	1,1876	2,8023	428,91	1,2574	2,9316	2,75	0,22	1600	67,98	42,49	1600	67,30	42,06	1600	68,79	42,99	1600	65,96	41,23	1600	69,74	43,59	1600	67,28	42,05	42,40	0,82
24	421,88	2,9259	6,9353	426,99	2,8976	6,7862	422,52	2,6586	6,2922	6,67	0,34	1600	122,31	76,44	1600	124,90	78,06	1600	126,86	79,29	1600	132,66	82,91	1600	120,70	75,44	1600	122,06	76,29	78,07	2,75

Analyses curing

Age (h)	AVG σc (MPa)	STDEV	AVG σflex (MPa)	STDEV	AVG S.G. (-)	STDEV
0	-	-	-	-		
4	42,4	0,8	2,7	0,2	2,15	0,00
24	78,1	2,7	6,7	0,3	2,15	0,01

DM8 - 30%MK 70%GGBFS - Variations

Information about prisms DM8-R40

Age	Prism 1									Prism 2										Prism 3										AVG			
	l	b	h1	h2	h3	h	m	ρ		l	b	h1	h2	h3	h	m	ρ			l	b	h1	h2	h3	h	m	ρ			ρ		S.G.	
(h)	(mm)	(mm)	(mm)	(mm)	(mm)	(mm)	(g)	(kg/m³)	S.G.	(mm)	(mm)	(mm)	(mm)	(mm)	(mm)	(g)	(kg/m³)	S.G.		(mm)	(mm)	(mm)	(mm)	(mm)	(mm)	(g)	(kg/m³)	S.G.		(kg/m³)	STDEV	(-)	STDEV
4	159,90	39,97	40,93	41,89	42,30	41,71	587,52	2204,12	2,204	159,83	39,90	41,72	41,50	40,89	41,37	578,02	2190,92	2,191		159,71	39,84	40,95	40,08	40,62	40,55	579,66	2246,63	2,247		2210	29,11	2,21	0,029
24	161,55	39,84	41,13	40,51	40,83	40,82	577,18	2196,73	2,197	161,70	39,79	41,83	40,91	42,47	41,74	581,71	2166,23	2,166		161,56	40,00	40,63	41,24	41,60	41,16	580,80	2183,70	2,184		2180	15,30	2,18	0,015

Tensile strength (NBN EN 196 -1)

Age	Test 1 - Prism 1			Test 2 - Prism 2			Test 3 - Prism 3			AVG		
	$2b^3/3l$	Fmax	σFlex	$2b^3/3l$	Fmax	σFlex	$2b^3/3l$	Fmax	σFlex	σFlex		
(h)	(mm²)	(kN)	(MPa)	(mm²)	(kN)	(MPa)	(mm²)	(kN)	(MPa)	(MPa)	STDEV	
4	425,71	1,14	2,68	423,47	1,05	2,49	421,57	1,03	2,44	2,53	0,13	
24	421,57	2,53	6,00	419,98	2,80	6,67	426,67	2,64	6,19	6,28	0,35	

Compressive strength (NBN EN 196 -1)

Age	Test 1 - Prism 1			Test 2 - Prism 1			Test 3 - Prism 2			Test 4 - Prism 2			Test 5 - Prism 3			Test 6 - Prism 3			AVG	
	So	Fmax	σc	So	Fmax	σc	So	Fmax	σc	So	Fmax	σc	So	Fmax	σc	So	Fmax	σc	σc (MPa)	
(h)	(mm²)	(kN)	(MPa)	(mm²)	(kN)	(MPa)	(mm²)	(kN)	(MPa)	(mm²)	(kN)	(MPa)	(mm²)	(kN)	(MPa)	(mm²)	(kN)	(MPa)	(MPa)	STDEV
4	1600	70,76	44,23	1600	75,04	46,90	1600	74,73	46,71	1600	72,73	45,46	1600	70,96	44,35	1600	73,40	45,88	45,59	1,14
24	1600	148,46	92,79	1600	145,52	90,95	1600	144,07	90,04	1600	141,92	88,70	1600	135,65	84,78	1600	130,40	81,50	88,13	4,21

Analyses curing

Age	AVG σc		AVG σFlex		AVG S.G.	
(h)	(MPa)	STDEV	(MPa)	STDEV	(-)	STDEV
0	-	-	-	-		
4	45,6	1,1	2,5	0,1	2,21	0,03
24	88,1	4,2	6,3	0,3	2,18	0,02

Information about prisms DM8-R70

Age	Prism 1									Prism 2										Prism 3										AVG			
	l	b	h1	h2	h3	h	m	ρ		l	b	h1	h2	h3	h	m	ρ			l	b	h1	h2	h3	h	m	ρ			ρ		S.G.	
(h)	(mm)	(mm)	(mm)	(mm)	(mm)	(mm)	(g)	(kg/m³)	S.G.	(mm)	(mm)	(mm)	(mm)	(mm)	(mm)	(g)	(kg/m³)	S.G.		(mm)	(mm)	(mm)	(mm)	(mm)	(mm)	(g)	(kg/m³)	S.G.		(kg/m³)	STDEV	(-)	STDEV
4	160,07	39,95	41,87	41,32	40,19	41,13	579,67	2204,10	2,204	160,14	39,79	40,75	41,51	41,50	41,25	576,85	2194,47	2,194		160,10	39,73	41,13	40,70	40,91	40,91	576,65	2215,84	2,216		2200	10,70	2,20	0,011
24	159,76	40,30	40,48	40,83	41,56	40,96	567,06	2150,46	2,150	159,78	40,07	40,45	40,83	41,51	40,93	565,53	2158,10	2,158		159,72	40,02	41,01	40,74	41,12	40,96	572,14	2185,45	2,185		2160	18,40	2,16	0,018

Tensile strength (NBN EN 196 -1)

Age	Test 1 - Prism 1			Test 2 - Prism 2			Test 3 - Prism 3			AVG		
	$2b^3/3l$	Fmax	σFlex	$2b^3/3l$	Fmax	σFlex	$2b^3/3l$	Fmax	σFlex	σFlex		
(h)	(mm²)	(kN)	(MPa)	(mm²)	(kN)	(MPa)	(mm²)	(kN)	(MPa)	(MPa)	STDEV	
4	425,07	1,2574	2,9581	419,98	0,8497	2,0232	418,08	0,8314	1,9886	2,32	0,55	
24	436,34	2,6104	5,9825	428,91	2,7534	6,4195	427,31	2,6412	6,1810	6,19	0,22	

Compressive strength (NBN EN 196 -1)

Age	Test 1 - Prism 1			Test 2 - Prism 1			Test 3 - Prism 2			Test 4 - Prism 2			Test 5 - Prism 3			Test 6 - Prism 3			AVG	
	So	Fmax	σc	So	Fmax	σc	So	Fmax	σc	So	Fmax	σc	So	Fmax	σc	So	Fmax	σc	σc (MPa)	
(h)	(mm²)	(kN)	(MPa)	(mm²)	(kN)	(MPa)	(mm²)	(kN)	(MPa)	(mm²)	(kN)	(MPa)	(mm²)	(kN)	(MPa)	(mm²)	(kN)	(MPa)	(MPa)	STDEV
4	1600	71,11	44,44	1600	73,02	45,64	1600	70,88	44,30	1600	74,46	46,54	1600	75,45	47,16	1600	74,08	46,30	45,73	1,16
24	1600	133,12	83,20	1600	128,45	80,28	1600	126,75	79,22	1600	122,68	76,68	1600	129,96	81,23	1600	129,88	81,18	80,30	2,21

Analyses curing

Age	AVG σc		AVG σFlex		AVG S.G.	
(h)	(MPa)	STDEV	(MPa)	STDEV	(-)	STDEV
0	-	-	-	-		
4	45,7	1,2	2,3	0,6	2,20	0,01
24	80,3	2,2	6,2	0,2	2,16	0,02

DM8 - 30%MK 70%GGBFS - Variations

Information about prisms cured at ambient temperature DM8-28.S-AMB

Age	Prism 1									Prism 2									Prism 3									AVG			
	l	b	h1	h2	h3	h	m	ρ		l	b	h1	h2	h3	h	m	ρ		l	b	h1	h2	h3	h	m	ρ		ρ		S.G.	
(h)	(mm)	(mm)	(mm)	(mm)	(mm)	(mm)	(g)	(kg/m³)	S.G.	(mm)	(mm)	(mm)	(mm)	(mm)	(mm)	(g)	(kg/m³)	S.G.	(mm)	(mm)	(mm)	(mm)	(mm)	(mm)	(g)	(kg/m³)	S.G.	(kg/m³)	STDEV	(-)	STDEV
2	159,74	40,21	41,58	40,17	42,75	41,50	556,71	2088,49	2,088	160,01	40,25	41,73	42,04	41,64	41,80	554,24	2058,61	2,059	159,85	40,03	41,30	41,30	41,64	41,41	557,42	2103,51	2,104	2080	22,86	2,08	0,023
4	159,61	39,93	40,04	40,07	40,40	40,17	556,12	2172,24	2,172	159,53	39,86	40,10	39,91	40,26	40,09	555,28	2178,19	2,178	159,72	39,76	40,50	39,56	39,40	39,82	562,49	2224,37	2,224	2190	28,54	2,19	0,029
8	160,16	39,88	40,25	40,40	40,22	40,29	560,68	2178,76	2,179	160,23	40,02	40,08	40,02	39,90	40,00	559,29	2180,50	2,181	160,09	39,94	40,40	40,13	40,42	40,32	564,92	2191,44	2,191	2180	6,88	2,18	0,007
12	160,22	39,78	40,24	40,38	40,23	40,28	557,87	2172,83	2,173	160,15	39,85	39,67	40,46	40,29	40,14	555,07	2166,78	2,167	160,36	39,79	39,97	40,51	40,61	40,36	563,46	2187,79	2,188	2180	10,70	2,18	0,011
	160,24	40,03	40,08	40,22	40,83	40,38	567,24	2190,18	2,190	160,16	40,01	39,64	40,98	40,13	40,25	559,58	2169,57	2,170	160,39	39,99	41,00	40,90	40,23	40,71	571,50	2188,70	2,189				
24	160,02	39,95	40,76	40,74	40,36	40,62	571,14	2199,44	2,199	159,82	39,92	40,78	40,28	41,08	40,71	565,79	2178,20	2,178	159,92	40,06	40,77	40,55	41,83	41,05	562,57	2139,19	2,139	2170	30,56	2,17	0,031
28d	159,36	39,80	40,47	40,14	40,78	40,46	564,55	2200,00	2,200	159,86	39,99	40,02	40,3	40,86	40,39	562,41	2180,00	2,180	159,25	39,75	39,95	40,99	40,07	40,34	559,62	2191,68	2,192	2190	10,05	2,19	0,010

Tensile strength (NBN EN 196 -1)

Age	Test 1 - Prism 1			Test 2 - Prism 2			Test 3 - Prism 3			AVG	
	$2b^3/3l$	F_{max}	σ_{Flex}	$2b^3/3l$	F_{max}	σ_{Flex}	$2b^3/3l$	F_{max}	σ_{Flex}	σ_{Flex}	
(h)	(mm^2)	(kN)	(MPa)	(mm^2)	(kN)	(MPa)	(mm^2)	(kN)	(MPa)	(MPa)	STDEV
2	433,42	0,2233	0,5152	434,72	0,2322	0,5341	427,63	0,2072	0,4845	0,51	0,03
4	424,43	0,3353	0,7900	422,20	0,3124	0,7399	419,03	0,2948	0,7035	0,74	0,04
8	422,84	0,3751	0,8871	427,31	0,3898	0,9122	424,75	0,3209	0,7555	0,85	0,08
12	419,67	0,3695	0,8805	421,88	0,4369	1,0356	419,98	-	-	0,93	0,06
12	427,63	0,3852	0,9008	426,99	0,4019	0,9412	426,35	0,3833	0,8990	-	-
24	425,07	0,6229	1,4654	424,11	0,7216	1,7014	428,59	0,6781	1,5822	1,58	0,12
28d	**420,30**	**3,17**	**7,55**	**426,35**	**2,92**	**6,84**	**418,72**	**3,08**	**7,35**	**7,24**	**0,37**

Compressive strength (NBN EN 196 -1)

Age	Test 1 - Prism 1			Test 2 - Prism 1			Test 3 - Prism 2			Test 4 - Prism 2			Test 5 - Prism 3			Test 6 - Prism 3			AVG	
	S_o	F_{max}	σ_C	S_o	F_{max}	σ_C	S_o	F_{max}	σ_C	S_o	F_{max}	σ_C	S_o	F_{max}	σ_C	S_o	F_{max}	σ_C	σ_C (MPa)	
(h)	(mm^2)	(kN)	(MPa)	(mm^2)	(kN)	(MPa)	(mm^2)	(kN)	(MPa)	(mm^2)	(kN)	(MPa)	(mm^2)	(kN)	(MPa)	(mm^2)	(kN)	(MPa)		STDEV
2	1600	3,28	2,05	1600	3,55	2,22	1600	3,51	2,19	1600	3,62	2,26	1600	3,75	2,34	1600	3,82	2,39	2,24	0,12
4	1600	7,59	4,74	1600	7,48	4,68	1600	7,47	4,67	1600	7,52	4,70	1600	7,93	4,96	1600	8,14	5,09	4,81	0,17
8	1600	10,35	6,47	1600	10,21	6,38	1600	10,03	6,27	1600	10,59	6,62	1600	10,63	6,64	1600	11,08	6,93	6,55	0,23
12	1600	11,36	7,10	1600	11,12	6,95	1600	11,26	7,04	1600	11,37	7,11	1600	11,39	7,12	1600	11,83	7,39	7,41	0,38
12	1600	12,28	7,68	1600	12,43	7,77	1600	11,74	7,34	1600	11,96	7,48	1600	12,56	7,85	1600	13,04	8,15		
24	1600	21,38	13,36	1600	21,92	13,70	1600	21,00	13,13	1600	21,19	13,24	1600	21,00	13,13	1600	20,86	13,04	13,27	0,24
28d	**1600**	**113,60**	**71,00**	**1600**	**114,79**	**71,74**	**1600**	**112,19**	**70,12**	**1600**	**117,97**	**73,73**	**1600**	**111,36**	**69,60**	**1600**	**93,83**	**58,64**	**71,24**	**1,62**

Analyses curing at ambient temperature

Age	AVG		AVG (ref 28d)		AVG		AVG (ref 28dh)		AVG		AVG (ref 28d)	
	σ_C		σ_C		σ_{Flex}		σ_{Flex}		S.G.		S.G.	
(h)	(MPa)	STDEV	(MPa)	STDEV	(MPa)	STDEV	(%)	STDEV	(-)	STDEV	(%)	STDEV
0	-	-	-	-	-	-	-	-	2,170	0,02	*99,1*	*1,0*
2	2,2	0,1	*3,1*	*0,2*	0,5	0,0	*7,1*	*0,5*	2,08	0,02	*95,0*	*1,1*
4	4,8	0,2	*6,7*	*0,3*	0,7	0,0	*10,3*	*0,8*	2,19	0,03	*100,0*	*1,4*
8	6,6	0,2	*9,2*	*0,4*	0,9	0,1	*11,8*	*1,3*	2,18	0,01	*99,5*	*0,6*
12	7,4	0,4	*10,4*	*0,6*	0,9	0,1	*12,9*	*1,1*	2,18	0,01	*99,5*	*0,7*
24	13,3	0,2	*18,6*	*0,5*	1,6	0,1	*21,9*	*2,0*	2,17	0,03	*99,1*	*1,5*
28d	71,2	1,6	*100,0*	*3,2*	7,2	0,4	*100,0*	*7,1*	2,19	0,01	*100,0*	*0,6*

DM8 - 30%MK 70%GGBFS - Variations

Information about prisms DM8-28.S-70°C

Age	Prism 1									Prism 2									Prism 3									AVG			
	l	b	h1	h2	h3	h	m	ρ		l	b	h1	h2	h3	h	m	ρ		l	b	h1	h2	h3	h	m	ρ		ρ		S.G.	
(h)	(mm)	(mm)	(mm)	(mm)	(mm)	(mm)	(g)	(kg/m³)	S.G.	(mm)	(mm)	(mm)	(mm)	(mm)	(mm)	(g)	(kg/m³)	S.G.	(mm)	(mm)	(mm)	(mm)	(mm)	(mm)	(g)	(kg/m³)	S.G.	(kg/m³)	STDEV	(-)	STDEV
28d	159,22	39,72	39,55	40,31	39,90	39,92	534,05	2115,00	2,115	159,19	39,89	39,89	39,95	40,33	40,06	535,91	2105	2,105	159,22	39,92	39,97	39,92	40,98	40,29	525,83	2053,34	2,053	2090	33,10	2,09	0,033

Tensile strength (NBN EN 196 -1)

Age	Test 1 - Prism 1			Test 2 - Prism 2			Test 3 - Prism 3			AVG	
	$2b^3/3l$	F_{max}	σ_{Flex}	$2b^3/3l$	F_{max}	σ_{Flex}	$2b^3/3l$	F_{max}	σ_{Flex}	σ_{Flex}	
(h)	(mm²)	(kN)	(MPa)	(mm²)	(kN)	(MPa)	(mm²)	(kN)	(MPa)	(MPa)	STDEV
28d	**417,77**	**2,1081**	**5,04609**	**423,16**	**2,2573**	**5,3344**	**424,11**	**2,1347**	**5,0333**	**5,14**	**0,17**

Compressive strength (NBN EN 196 -1)

Age	Test 1 - Prism 1			Test 2 - Prism 1			Test 3 - Prism 2			Test 4 - Prism 2			Test 5 - Prism 3			Test 6 - Prism 3			AVG	
	S_o	F_{max}	σ_C	S_o	F_{max}	σ_C	S_o	F_{max}	σ_C	S_o	F_{max}	σ_C	S_o	F_{max}	σ_C	S_o	F_{max}	σ_C	σ_C	
(h)	(mm²)	(kN)	(MPa)	(mm²)	(kN)	(MPa)	(mm²)	(kN)	(MPa)	(mm²)	(kN)	(MPa)	(mm²)	(kN)	(MPa)	(mm²)	(kN)	(MPa)	(MPa)	STDEV
28d	**1600**	**92,14**	**57,59**	**1600**	**89,79**	**56,12**	**1600**	**93,20**	**58,25**	**1600**	**89,29**	**55,81**	**1600**	**84,84**	**53,03**	**1600**	**84,92**	**53,08**	**55,64**	**2,20**

Analyses curing at 70°C, sieved HGB sand

Age	AVG		AVG		AVG	
	σ_C		σ_{Flex}		S.G.	
(h)	(MPa)	STDEV	(MPa)	STDEV	(-)	STDEV
28d	55,6	2,2	5,1	0,2	2,09	0,03

Information about prisms DM8-1.70°C-27.U-AMB

Age	Prism 1									Prism 2									Prism 3									AVG			
	l	b	h1	h2	h3	h	m	ρ		l	b	h1	h2	h3	h	m	ρ		l	b	h1	h2	h3	h	m	ρ		ρ		S.G.	
(h)	(mm)	(mm)	(mm)	(mm)	(mm)	(mm)	(g)	(kg/m³)	S.G.	(mm)	(mm)	(mm)	(mm)	(mm)	(mm)	(g)	(kg/m³)	S.G.	(mm)	(mm)	(mm)	(mm)	(mm)	(mm)	(g)	(kg/m³)	S.G.	(kg/m³)	STDEV	(-)	STDEV
28d	160,24	39,77	40,22	39,82	40,33	40,12	535,10	2095,00	2,095	160,11	39,78	40,63	40,11	40,39	40,38	543,08	2110	2,11	160,34	39,74	41,15	40,04	40,62	40,60	549,63	2124,41	2,124	2110	14,71	2,11	0,015

Tensile strength (NBN EN 196 -1)

Age	Test 1 - Prism 1			Test 2 - Prism 2			Test 3 - Prism 3			AVG	
	$2b^3/3l$	F_{max}	σ_{Flex}	$2b^3/3l$	F_{max}	σ_{Flex}	$2b^3/3l$	F_{max}	σ_{Flex}	σ_{Flex}	
(h)	(mm²)	(kN)	(MPa)	(mm²)	(kN)	(MPa)	(mm²)	(kN)	(MPa)	(MPa)	STDEV
28d	**419,35**	**1,04**	**2,48**	**419,67**	**0,92**	**2,18**	**418,40**	**1,7027**	**4,07**	**2,91**	**1,01**

Compressive strength (NBN EN 196 -1)

Age	Test 1 - Prism 1			Test 2 - Prism 1			Test 3 - Prism 2			Test 4 - Prism 2			Test 5 - Prism 3			Test 6 - Prism 3			AVG	
	S_o	F_{max}	σ_C	S_o	F_{max}	σ_C	S_o	F_{max}	σ_C	S_o	F_{max}	σ_C	S_o	F_{max}	σ_C	S_o	F_{max}	σ_C	σ_C	
(h)	(mm²)	(kN)	(MPa)	(mm²)	(kN)	(MPa)	(mm²)	(kN)	(MPa)	(mm²)	(kN)	(MPa)	(mm²)	(kN)	(MPa)	(mm²)	(kN)	(MPa)	(MPa)	STDEV
28d	**1600**	**90,91**	**56,82**	**1600**	**91,18**	**56,99**	**1600**	**93,86**	**58,66**	**1600**	**97,90**	**61,19**	**1600**	**103,12**	**64,45**	**1600**	**101,64**	**63,53**	**60,27**	**3,29**

Analyses curing at 70°C, sieved HGB sand

Age	AVG		AVG		AVG	
	σ_C		σ_{Flex}		S.G.	
(h)	(MPa)	STDEV	(MPa)	STDEV	(-)	STDEV
28d	60,3	3,3	2,9	1,0	2,11	0,01

DM8 - 30%MK 70%GGBFS - Variations

Information about prisms cured at 70°C, sieved sand from HGB 0/8 to 0/2 without specific distribution DM8-0/2

Age	Prism 1									Prism 2									Prism 3									AVG			
	l	b	h1	h2	h3	h	m	ρ		l	b	h1	h2	h3	h	m	ρ		l	b	h1	h2	h3	h	m	ρ		ρ		S.G.	
(h)	(mm)	(mm)	(mm)	(mm)	(mm)	(mm)	(g)	(kg/m³)	S.G.	(mm)	(mm)	(mm)	(mm)	(mm)	(mm)	(g)	(kg/m³)	S.G.	(mm)	(mm)	(mm)	(mm)	(mm)	(mm)	(g)	(kg/m³)	S.G.	(kg/m³)	STDEV	(-)	STDEV
2	162,52	39,95	40,64	40,64	40,67	40,65	568,46	2153,85	2,154	162,30	39,91	40,57	40,40	40,81	40,59	567,63	2158,79	2,159	162,48	40,06	40,19	40,37	40,86	40,47	557,66	2116,85	2,12	2140	22,92	2,14	0,023
4	160,10	39,82	40,60	41,03	40,62	40,75	564,91	2174,50	2,174	160,02	38,82	40,20	40,17	40,42	40,26	555,35	2220,38	2,220	160,18	39,72	40,84	41,04	39,81	40,56	545,84	2115,02	2,12	2170	52,83	2,17	0,053
8	160,14	39,61	39,91	39,81	39,77	39,83	539,58	2135,70	2,136	160,06	39,65	39,83	39,93	39,73	39,83	539,39	2133,86	2,134	159,90	39,76	40,02	39,86	39,77	39,88	548,71	2164,00	2,16	2140	16,89	2,14	0,017
12	159,80	39,92	40,24	40,64	40,63	40,50	542,82	2100,86	2,101	159,68	39,80	40,35	40,56	40,08	40,33	544,07	2122,72	2,123	159,95	39,95	40,44	40,52	40,53	40,50	547,00	2113,82	2,11	2110	10,99	2,11	0,011
24	162,03	39,88	40,41	40,72	41,16	40,76	560,36	2127,39	2,127	161,21	40,00	39,51	40,55	40,83	40,30	556,98	2143,48	2,143	162,33	40,00	40,81	40,36	41,07	40,75	549,34	2076,30	2,08	2120	35,07	2,12	0,035
28d	159,99	39,86	40,01	40,17	40,26	40,15	555,37	2170,00	2,17	159,92	39,85	39,91	39,99	39,92	39,94	551,22	2165,00	2,165	159,92	39,86	40,5	40,41	41,95	40,95	554,47	2123,97	2,12	2150	25,26	2,15	0,025

Tensile strength (NBN EN 196 -1)

Age	Test 1 - Prism 1			Test 2 - Prism 2			Test 3 - Prism 3			AVG	
	$2b^3/3l$	F_{max}	σ_{Flex}	$2b^3/3l$	F_{max}	σ_{Flex}	$2b^3/3l$	F_{max}	σ_{Flex}	σ_{Flex}	
(h)	(mm²)	(kN)	(MPa)	(mm²)	(kN)	(MPa)	(mm²)	(kN)	(MPa)	(MPa)	STDEV
2	425,07	0,5704	1,3418	423,79	0,5998	1,4153	428,59	0,5358	1,2501	1,34	0,08
4	420,93	1,1729	2,7864	390,01	1,1540	2,9589	417,77	1,1530	2,7599	2,84	0,11
8	414,31	1,9441	4,6924	415,56	1,5842	3,8122	419,03	2,4136	5,7599	4,75	0,98
12	424,11	2,5773	6,0769	420,30	2,2070	5,2510	425,07	2,0165	4,7439	5,36	0,67
24	422,84	3,7689	8,9133	426,67	3,1895	7,4754	426,67	2,9802	6,9848	7,79	1,00
28d	**422,20**	**3,3645**	**7,96893**	**421,88**	**3,2641**	**7,7369**	**422,20**	**2,5991**	**6,1561**	**7,29**	**0,99**

Compressive strength (NBN EN 196 -1)

Age	Test 1 - Prism 1			Test 2 - Prism 1			Test 3 - Prism 2			Test 4 - Prism 2			Test 5 - Prism 3			Test 6 - Prism 3			AVG	
	S_o	F_{max}	σ_C	S_o	F_{max}	σ_C	S_o	F_{max}	σ_C	S_o	F_{max}	σ_C	S_o	F_{max}	σ_C	S_o	F_{max}	σ_C	σ_C	
(h)	(mm²)	(kN)	(MPa)	(mm²)	(kN)	(MPa)	(mm²)	(kN)	(MPa)	(mm²)	(kN)	(MPa)	(mm²)	(kN)	(MPa)	(mm²)	(kN)	(MPa)	(MPa)	STDEV
2	1600	32,66	20,41	1600	33,25	20,78	1600	33,44	20,90	1600	33,69	21,06	1600	33,40	20,88	1600	32,85	20,53	20,76	0,24
4	1600	75,48	47,18	1600	74,76	46,73	1600	75,17	46,98	1600	77,33	48,33	1600	70,82	44,26	1600	75,19	46,99	46,74	1,34
8	1600	96,97	60,61	1600	98,00	61,25	1600	94,03	58,77	1600	95,47	59,67	1600	102,95	64,34	1600	101,77	63,61	61,37	2,20
12	1600	111,04	69,40	1600	114,65	71,66	1600	115,84	72,40	1600	112,97	70,61	1600	108,68	67,93	1600	99,17	**61,98**	70,40	1,79
24	1600	133,81	83,63	1600	140,92	88,08	1600	137,64	86,03	1600	131,15	81,97	1600	125,41	78,38	1600	129,30	80,81	83,15	3,53
28d	**1600**	**136,02**	**85,01**	**1600**	**127,91**	**79,94**	**1600**	**127,12**	**79,45**	**1600**	**128,93**	**80,58**	**1600**	**134,58**	**84,11**	**1600**	**133,24**	**83,28**	**82,06**	**2,36**

Analyses curing at 70°C, sieved HGB sand

Age	AVG		AVG (ref 28d)		AVG		AVG (ref 28dh)		AVG		AVG (ref 28d)	
	σ_C		σ_C		σ_{Flex}		σ_{Flex}		S.G.		S.G.	
(h)	(MPa)	STDEV	(MPa)	STDEV	(MPa)	STDEV	(%)	STDEV	(-)	STDEV	(%)	STDEV
0	-	-	-	-	-	-	-	-	2,12	0,005	98,5	1,2
2	20,8	0,2	25,3	0,8	1,3	0,1	18,3	2,7	2,14	0,02	99,5	1,6
4	46,7	1,3	57,0	2,3	2,8	0,1	38,9	5,5	2,17	0,05	100,9	2,7
8	61,4	2,2	74,8	3,4	4,8	1,0	65,2	16,0	2,14	0,02	99,5	1,4
12	70,4	1,8	85,8	3,3	5,4	0,7	73,5	13,6	2,11	0,01	98,1	1,3
24	83,1	3,5	101,3	5,2	7,8	1,0	106,9	20,0	2,12	0,04	98,6	2,0
28d	82,1	2,4	100,0	4,1	7,3	1,0	100,0	19,1	2,15	0,03	100,0	1,7

DM8 - 30%MK 70%GGBFS - Variations

Information about prisms cured at 70°C, RCA fines standard distribution DM8-RCA

Age	Prism 1									Prism 2									Prism 3									AVG			
	l	b	h1	h2	h3	h	m	ρ		l	b	h1	h2	h3	h	m	ρ		l	b	h1	h2	h3	h	m	ρ		ρ		S.G.	
(h)	(mm)	(mm)	(mm)	(mm)	(mm)	(mm)	(g)	(kg/m³)	S.G.	(mm)	(mm)	(mm)	(mm)	(mm)	(mm)	(g)	(kg/m³)	S.G.	(mm)	(mm)	(mm)	(mm)	(mm)	(mm)	(g)	(kg/m³)	S.G.	(kg/m³)	STDEV	(-)	STDEV
2	161,56	40,70	40,38	40,60	40,63	40,54	559,68	2099,73	2,100	161,50	40,00	40,47	40,52	40,29	40,43	554,09	2121,68	2,122	161,30	40,70	40,36	40,40	40,25	40,34	550,59	2079,22	2,079	2100	21,24	2,100	0,021
4	159,80	39,93	40,61	40,85	40,34	40,60	552,31	2131,97	2,132	159,89	40,01	40,86	40,21	41,41	40,83	553,95	2120,98	2,121	159,88	40,00	41,36	40,75	40,70	40,94	557,52	2129,58	2,130	2130	5,78	2,130	0,006
8	160,13	39,93	40,35	40,39	40,26	40,33	554,77	2151,18	2,151	160,19	40,00	40,43	40,20	40,43	40,35	554,77	2145,55	2,146	160,08	39,96	40,14	40,81	40,65	40,53	552,44	2130,64	2,131	2140	10,61	2,140	0,011
12	159,79	40,00	40,16	40,82	40,31	40,43	552,07	2136,39	2,136	159,65	39,98	39,55	40,56	40,23	40,11	546,49	2134,43	2,134	159,72	40,11	40,74	40,30	41,22	40,75	552,09	2114,63	2,115	2130	12,04	2,130	0,012
24	161,54	39,86	40,71	40,36	40,76	40,61	558,36	2135,32	2,135	160,41	39,90	40,44	40,23	40,24	40,30	555,26	2152,54	2,153	160,93	39,79	40,12	39,94	40,39	40,15	554,84	2158,10	2,158	2150	11,87	2,150	0,012
28d	159,87	39,80	40,22	40,45	40,33	40,33	546,28	2130,00	2,13	159,92	39,88	39,89	40,47	40,3	40,22	546,42	2130	2,13	159,81	39,67	40,41	40,68	40,23	40,44	543,65	2120,52	2,12	2130	5,47	2,130	0,005

Tensile strength (NBN EN 196 -1)

Age	Test 1 - Prism 1			Test 2 - Prism 2			Test 3 - Prism 3			AVG	
	$2b^3/3l$	F_{max}	σ_{Flex}	$2b^3/3l$	F_{max}	σ_{Flex}	$2b^3/3l$	F_{max}	σ_{Flex}	σ_{Flex}	
(h)	(mm²)	(kN)	(MPa)	(mm²)	(kN)	(MPa)	(mm³)	(kN)	(MPa)	(MPa)	STDEV
2	449,46	0,71	1,59	426,67	0,82	1,93	449,46	0,83	1,85	1,79	0,18
4	424,43	1,00	2,36	426,99	1,18	2,77	426,67	1,07	2,51	2,55	0,20
8	424,43	1,70	4,00	426,67	1,60	3,76	425,39	1,28	3,02	3,59	0,51
12	426,67	2,38	5,58	426,03	1,98	4,65	430,20	2,59	6,02	5,42	0,70
24	422,20	2,90	6,87	423,47	2,94	6,95	419,98	3,25	7,73	7,18	0,47
28d	**420,30**	**3,68**	**8,75**	**422,84**	**3,68**	**8,69**	**416,19**	**4,02**	**9,65**	**9,03**	**0,54**

Compressive strength (NBN EN 196 -1)

Age	Test 1 - Prism 1			Test 2 - Prism 1			Test 3 - Prism 2			Test 4 - Prism 2			Test 5 - Prism 3			Test 6 - Prism 3			AVG	
	S_o	F_{max}	σ_C	S_o	F_{max}	σ_C	S_o	F_{max}	σ_C	S_o	F_{max}	σ_C	S_o	F_{max}	σ_C	S_o	F_{max}	σ_C	σ_C	
(h)	(mm²)	(kN)	(MPa)	(mm²)	(kN)	(MPa)	(mm²)	(kN)	(MPa)	(mm²)	(kN)	(MPa)	(mm²)	(kN)	(MPa)	(mm²)	(kN)	(MPa)	(MPa)	STDEV
2	1600	16,84	10,53	1600	16,95	10,59	1600	17,20	10,75	1600	17,11	10,69	1600	17,18	10,74	1600	17,24	10,78	10,68	0,10
4	1600	25,89	16,18	1600	26,61	16,63	1600	27,30	17,06	1600	26,67	16,67	1600	26,80	16,75	1600	26,73	16,71	16,67	0,28
8	1600	72,06	45,04	1600	73,65	46,03	1600	71,32	44,58	1600	71,54	44,71	1600	71,01	44,38	1600	76,77	47,98	45,45	1,37
12	1600	82,80	51,75	1600	79,30	49,56	1600	87,79	54,87	1600	86,13	53,83	1600	89,26	55,79	1600	87,01	54,38	53,36	2,30
24	1600	96,45	60,28	1600	100,63	62,89	1600	94,63	59,14	1600	99,82	62,39	1600	98,93	61,83	1600	94,34	58,96	60,92	1,69
28d	**1600**	**104,98**	**65,61**	**1600**	**103,53**	**64,71**	**1600**	**103,53**	**64,71**	**1600**	**104,13**	**65,08**	**1600**	**107,30**	**67,06**	**1600**	**105,92**	**66,20**	**65,56**	**0,93**

Analyses curing at 70°C, RCA fines curved

Age	AVG		AVG (ref 28d)		AVG		AVG (ref 28dh)		AVG		AVG (ref 28d)	
	σ_C		σ_C		σ_{Flex}		σ_{Flex}		S.G.		S.G.	
(h)	(MPa)	STDEV	(MPa)	STDEV	(MPa)	STDEV	(%)	STDEV	(-)	STDEV	(%)	STDEV
0	-	-	-	-	-	-	-	-	2,14	0,01	100,4	0,7
2	10,7	0,1	16,3	0,3	1,8	0,2	19,8	2,3	2,10	0,02	98,6	1,0
4	16,7	0,3	25,4	0,6	2,5	0,2	28,2	2,8	2,13	0,01	100,0	0,4
8	45,5	1,4	69,3	2,3	3,6	0,5	39,8	6,2	2,14	0,01	100,5	0,6
12	53,4	2,3	81,4	3,7	5,4	0,7	60,0	8,5	2,13	0,01	100,0	0,6
24	60,9	1,7	92,9	2,9	7,2	0,5	79,5	7,1	2,15	0,01	100,9	0,6
28d	65,6	0,9	100,0	2,0	9,0	0,5	100,0	8,4	2,13	0,01	100,0	0,4

DM8 - 30%MK 70%GGBFS - Variations

Information about prisms cured at 70°C, GPC fines standard distribution DM8-RGA

Age	Prism 1									Prism 2									Prism 3									AVG			
	l	b	h1	h2	h3	h	m	ρ	S.G.	l	b	h1	h2	h3	h	m	ρ	S.G.	l	b	h1	h2	h3	h	m	ρ	S.G.	ρ		S.G.	
(h)	(mm)	(mm)	(mm)	(mm)	(mm)	(mm)	(g)	(kg/m³)		(mm)	(mm)	(mm)	(mm)	(mm)	(mm)	(g)	(kg/m³)		(mm)	(mm)	(mm)	(mm)	(mm)	(mm)	(g)	(kg/m³)		(kg/m³)	STDEV	(-)	STDEV
2	160,71	40,00	40,30	39,82	40,32	40,15	526,60	2040,46	2,040	160,62	39,91	40,32	40,71	40,16	40,40	522,84	2019,03	2,019	160,82	40,00	41,00	40,77	40,82	40,86	527,08	2005,13	2,01	2020	17,80	2,02	0,018
4	159,80	40,00	41,25	41,13	41,09	41,16	536,38	2038,90	2,039	160,02	39,89	40,04	40,37	40,48	40,30	531,80	2067,48	2,067	160,00	40,02	40,99	41,01	41,29	41,10	531,21	2018,66	2,02	2040	24,53	2,04	0,025
8	160,22	39,92	40,93	41,35	41,28	41,19	535,78	2033,87	2,034	160,14	39,82	41,18	40,65	41,71	41,18	536,15	2041,73	2,042	160,26	40,00	41,39	40,37	40,82	40,86	538,93	2057,54	2,06	2040	12,06	2,04	0,012
12	162,22	39,92	41,77	39,99	40,15	40,64	532,57	2023,78	2,024	161,91	39,71	40,08	39,94	40,28	40,10	529,60	2054,14	2,054	161,52	39,68	40,47	39,89	40,08	40,15	530,96	2063,55	2,06	2050	20,78	2,05	0,021
24	160,00	40,00	40,17	40,11	40,38	40,22	519,70	2018,97	2,019	160,00	40,02	40,13	40,30	40,01	40,15	520,94	2026,47	2,026	160,00	39,97	40,31	40,19	40,27	40,26	523,78	2034,50	2,03	2030	7,76	2,03	0,008
28d	159,50	40,00	40,93	41,04	40,45	40,81	535,49	2055,00	2,055	159,96	39,88	41,51	40,59	40,27	40,79	529,45	2035,00	2,035	159,55	40,04	40,02	40,19	40,21	40,14	533,26	2079,56	2,08	2060	22,32	2,06	0,022

Tensile strength (NBN EN 196 -1)

Age	Test 1 - Prism 1			Test 2 - Prism 2			Test 3 - Prism 3			AVG	
	$2b^3/3l$	F_{max}	σ_{Flex}	$2b^3/3l$	F_{max}	σ_{Flex}	$2b^3/3l$	F_{max}	σ_{Flex}	σ_{Flex}	
(h)	(mm²)	(kN)	(MPa)	(mm²)	(kN)	(MPa)	(mm³)	(kN)	(MPa)	(MPa)	STDEV
2	426,67	0,5543	1,2991	423,79	0,5074	1,1973	426,67	0,5522	1,2942	1,26	0,06
4	426,67	1,2705	2,9777	423,16	1,1962	2,8269	427,31	1,1751	2,7500	2,85	0,12
8	424,11	1,2846	3,0289	420,93	1,3921	3,3072	426,67	1,3984	3,2775	3,20	0,15
12	424,11	1,8166	4,2833	417,45	1,6569	3,9691	416,51	1,6655	3,9987	4,08	0,17
24	426,67	2,1673	5,0796	427,31	2,5996	6,0837	425,71	2,4363	5,7229	5,63	0,51
28d	**426,67**	**3,37**	**7,89**	**422,84**	**3,11**	**7,36**	**427,95**	**3,25**	**7,59**	**7,61**	**0,26**

Compressive strength (NBN EN 196 -1)

Age	Test 1 - Prism 1			Test 2 - Prism 1			Test 3 - Prism 2			Test 4 - Prism 2			Test 5 - Prism 3			Test 6 - Prism 3			AVG	
	S_o	F_{max}	σ_C	S_o	F_{max}	σ_C	S_o	F_{max}	σ_C	S_o	F_{max}	σ_C	S_o	F_{max}	σ_C	S_o	F_{max}	σ_C	σ_C	
(h)	(mm²)	(kN)	(MPa)	(mm²)	(kN)	(MPa)	(mm²)	(kN)	(MPa)	(mm²)	(kN)	(MPa)	(mm²)	(kN)	(MPa)	(mm²)	(kN)	(MPa)	(MPa)	STDEV
2	1600	10,86	6,79	1600	11,12	6,95	1600	10,18	6,36	1600	10,23	6,39	1600	10,33	6,46	1600	10,57	6,61	6,59	0,235
4	1600	37,36	23,35	1600	38,21	23,88	1600	36,61	22,88	1600	37,48	23,43	1600	36,66	22,91	1600	37,18	23,24	23,28	0,370
8	1600	76,16	47,60	1600	78,02	48,76	1600	75,55	47,22	1600	76,23	47,64	1600	81,51	50,94	1600	78,37	48,98	48,53	1,375
12	1600	81,51	50,94	1600	80,86	50,54	1600	76,16	47,60	1600	83,97	52,48	1600	84,93	53,08	1600	80,44	50,28	50,82	1,930
24	1600	88,80	55,50	1600	89,71	56,07	1600	89,83	56,14	1600	92,68	57,93	1600	92,48	57,80	1600	92,47	57,79	56,87	1,084
28d	**1600**	**92,72**	**57,95**	**1600**	**92,87**	**58,04**	**1600**	**61,34**	**38,34**	**1600**	**90,16**	**56,35**	**1600**	**90,68**	**56,68**	**1600**	**86,93**	**54,33**	**56,67**	**1,508**

Analyses curing at 70°C, GPC fines curved

Age	AVG		AVG (ref 28d)		AVG		AVG (ref 28dh)		AVG		AVG (ref 28d)	
	σ_C		σ_C		σ_{Flex}		σ_{Flex}		S.G.		S.G.	
(h)	(MPa)	STDEV	(MPa)	STDEV	(MPa)	STDEV	(%)	STDEV	(-)	STDEV	(%)	STDEV
0	-	-	-	-	-	-	-	-	2,04	0,01	98,9	1,1
2	6,6	0,2	11,6	0,5	1,3	0,1	16,6	0,9	2,02	0,02	98,1	1,4
4	23,3	0,4	41,1	1,1	2,9	0,1	37,5	2,0	2,04	0,02	99,0	1,6
8	48,5	1,4	85,6	3,0	3,2	0,2	42,1	2,5	2,04	0,01	99,0	1,2
12	50,8	1,9	89,7	3,9	4,1	0,2	53,6	2,9	2,05	0,02	99,5	1,5
24	56,9	1,1	100,4	2,9	5,6	0,5	73,9	7,2	2,03	0,01	98,5	1,1
28d	56,7	1,5	100,0	3,4	7,6	0,3	100,0	4,9	2,06	0,02	100,0	1,5

DM8 - 30%MK 70%GGBFS - Variations

Information about prisms cured at 70°C, added water replaced by seawater DM8-SW

	Prism 1									Prism 2									Prism 3									AVG			
Age	l	b	h1	h2	h3	h	m	ρ		l	b	h1	h2	h3	h	m	ρ		l	b	h1	h2	h3	h	m	ρ		ρ		S.G.	
(h)	(mm)	(mm)	(mm)	(mm)	(mm)	(mm)	(g)	(kg/m³)	S.G.	(mm)	(mm)	(mm)	(mm)	(mm)	(mm)	(g)	(kg/m³)	S.G.	(mm)	(mm)	(mm)	(mm)	(mm)	(mm)	(g)	(kg/m³)	S.G.	(kg/m³)	STDEV	(-)	STDEV
2	160,30	40,00	39,88	41,00	40,40	40,43	555,65	2143,58	2,144	160,28	39,96	40,21	41,19	40,52	40,64	561,44	2156,97	2,157	160,12	40,92	40,16	40,60	40,20	40,32	560,75	2122,60	2,123	2140	17,33	2,14	0,017
4	162,20	40,12	41,06	40,31	41,01	40,79	575,28	2167,10	2,167	162,44	39,80	40,68	40,55	40,25	40,49	572,41	2186,49	2,186	161,86	39,77	40,86	40,29	40,19	40,45	572,31	2198,13	2,198	2160	33,15	2,16	0,033
	159,91	40,03	40,66	40,63	40,20	40,50	552,32	2130,64	2,131	159,90	40,03	40,62	41,24	40,30	40,72	554,08	2125,84	2,126	160,10	40,07	40,88	40,90	40,83	40,87	556,51	2122,55	2,123				
8	160,15	40,14	40,05	40,17	41,30	40,51	566,56	2175,78	2,176	160,32	40,08	40,80	40,93	41,37	41,03	565,99	2146,63	2,147	160,22	39,97	41,89	40,85	40,52	41,09	566,44	2152,79	2,153	2160	15,36	2,16	0,015
12	160,85	39,86	40,63	41,31	40,47	40,80	569,16	2175,61	2,176	160,94	39,88	40,26	39,92	39,79	39,99	569,59	2219,18	2,219	161,02	40,04	40,38	40,12	38,14	39,55	569,64	2234,17	2,234	2210	30,42	2,21	0,030
24	161,09	39,83	40,85	41,23	40,01	40,70	570,95	2186,55	2,187	161,17	39,92	40,66	40,89	40,45	40,67	570,02	2178,60	2,179	161,65	40,00	40,66	40,40	40,58	40,55	563,83	2150,59	2,151	2170	18,89	2,17	0,019
28d	160,33	40,08	41,38	41,50	40,96	41,28	562,14	2120,00	2,12	160,54	39,88	41,4	40,98	41,12	41,17	565,71	2145,00	2,15	160	40,08	41,09	39,33	41,26	40,56	563,87	2167,87	2,168	2140	23,94	2,14	0,024

Tensile strength (NBN EN 196 -1)

	Test 1 - Prism 1			Test 2 - Prism 2			Test 3 - Prism 3			AVG	
Age	2b³/3l	Fmax	σFlex	2b³/3l	Fmax	σFlex	2b³/3l	Fmax	σFlex	σFlex	
(h)	(mm²)	(kN)	(MPa)	(mm²)	(kN)	(MPa)	(mm²)	(kN)	(MPa)	(MPa)	STDEV
2	426,67	0,48	1,12	425,39	0,52	1,22	456,79	0,63	1,39	1,24	0,14
4	430,52	0,97	2,25	420,30	0,79	1,89	419,35	0,19	**0,45**	2,24	0,28
	427,63	0,89	2,08	427,63	1,12	2,63	428,91	1,01	2,35		
8	431,16	1,72	3,99	429,23	1,65	3,84	425,71	1,56	3,67	3,83	0,16
12	422,20	2,33	5,52	422,84	1,99	4,71	427,95	2,64	6,18	5,47	0,74
24	421,25	2,58	6,13	424,11	2,82	6,64	426,67	2,66	6,24	6,34	0,27
28d	**429,23**	**2,44**	**5,68**	**422,84**	**2,38**	**5,62**	**429,23**	**2,58**	**6,01**	**5,77**	**0,21**

Compressive strength (NBN EN 196 -1)

	Test 1 - Prism 1			Test 2 - Prism 1			Test 3 - Prism 2			Test 4 - Prism 2			Test 5 - Prism 3			Test 6 - Prism 3			AVG	
Age	So	Fmax	σc	So	Fmax	σc	So	Fmax	σc	So	Fmax	σc	So	Fmax	σc	So	Fmax	σc	σc	
(h)	(mm²)	(kN)	(MPa)	(mm²)	(kN)	(MPa)	(mm²)	(kN)	(MPa)	(mm²)	(kN)	(MPa)	(mm²)	(kN)	(MPa)	(mm²)	(kN)	(MPa)	(MPa)	STDEV
2	1600	24,41	15,26	1600	24,16	15,10	1600	24,71	15,44	1600	24,90	15,56	1600	24,56	15,35	1600	23,95	14,97	15,3	0,2
4	1600	76,01	47,51	1600	74,56	46,60	1600	78,33	48,96	1600	80,24	50,15	1600	77,65	48,53	1600	78,39	48,99	48,5	1,2
	1600	63,83	**39,89**	1600	66,45	**41,53**	1600	62,18	**38,86**	1600	60,98	**38,11**	1600	64,99	**40,62**	1600	65,67	**41,04**		
8	1600	101,35	63,34	1600	91,29	57,06	1600	96,31	60,19375	1600	100,72	62,95	1600	97,27	60,79	1600	105,82	66,14	61,7	3,1
12	1600	113,11	70,69	1600	113,59	70,99	1600	111,22	69,51	1600	110,11	68,82	1600	115,11	71,94	1600	119,17	74,48	71,1	2,0
24	1600	118,38	73,99	1600	117,23	73,27	1600	121,09	75,68	1600	125,53	78,46	1600	117,35	73,34	1600	117,91	73,69	74,7	2,0
28d	**1600**	**111,35**	**69,59**	**1600**	**109,10**	**68,19**	**1600**	**114,55**	**71,59**	**1600**	**113,47**	**70,92**	**1600**	**112,85**	**70,53**	**1600**	**113,31**	**70,82**	**70,3**	**1,2**

Analyses curing at 70°C, seawater

	AVG		AVG (ref 28d)		AVG		AVG (ref 28dh)		AVG		AVG (ref 28d)	
Age	σc		σc		σFlex		σFlex		S.G.		S.G.	
(h)	(MPa)	STDEV	(MPa)	STDEV	(MPa)	STDEV	(%)	STDEV	(-)	STDEV	(%)	STDEV
0	-	-	-	-	-	-	-	-	2,17	0,02	100,9	1,4
2	15,3	0,2	21,7	0,5	1,2	0,1	21,5	2,5	2,14	0,02	100,0	1,4
4	48,5	1,2	69,0	2,1	2,2	0,3	38,8	5,0	2,16	0,03	100,9	1,9
8	61,7	3,1	87,9	4,7	3,8	0,2	66,4	3,7	2,16	0,02	100,9	1,3
12	71,1	2,0	101,1	3,3	5,5	0,7	94,8	13,2	2,21	0,03	103,3	1,8
24	74,7	2,0	106,4	3,4	6,3	0,3	109,8	6,1	2,17	0,02	101,4	1,4
28d	70,3	1,2	100,0	2,4	5,8	0,2	100,0	5,2	2,14	0,02	100,0	1,6

Information about prisms cured at 70°C, GGBFS 50% replaced by 50% DM8-WWA

	Prism 1									Prism 2									Prism 3									AVG			
Age	l	b	h1	h2	H3	h	m	ρ		l	b	h1	h2	H3	h	m	ρ		l	b	h1	h2	H3	h	m	ρ		ρ		S.G.	
(h)	(mm)	(mm)	(mm)	(mm)	(mm)	(mm)	(g)	(kg/m³)	S.G.	(mm)	(mm)	(mm)	(mm)	(mm)	(mm)	(g)	(kg/m³)	S.G.	(mm)	(mm)	(mm)	(mm)	(mm)	(mm)	(g)	(kg/m³)	S.G.	(kg/m³)	STDEV	(-)	STDEV
24	159,89	39,72	40,69	41,97	40,57	41,08	557,81	2138,26	2,138	160,00	39,77	41,25	41,41	41,21	41,29	563,52	2144,81	2,145	159,90	39,88	41,15	40,87	40,79	40,94	558,45	2139,28	2,139	2140	3,52	2,14	0,004

Tensile strength (NBN EN 196 -1)

	Test 1 - Prism 1			Test 2 - Prism 2			Test 3 - Prism 3			AVG	
Age	2b³/3l	Fmax	σFlex	2b³/3l	Fmax	σFlex	2b³/3l	Fmax	σFlex	σFlex	
(h)	(mm²)	(kN)	(MPa)	(mm²)	(kN)	(MPa)	(mm²)	(kN)	(MPa)	(MPa)	STDEV
24	417,77	2,06	4,94	419,35	2,02	4,82	422,84	2,10	4,96	4,91	0,07

Compressive strength (NBN EN 196 -1)

	Test 1 - Prism 1			Test 2 - Prism 1			Test 3 - Prism 2			Test 4 - Prism 2			Test 5 - Prism 3			Test 6 - Prism 3			AVG	
Age	So	Fmax	σc	So	Fmax	σc	So	Fmax	σc	So	Fmax	σc	So	Fmax	σc	So	Fmax	σc	σc	
(h)	(mm²)	(kN)	(MPa)	(mm²)	(kN)	(MPa)	(mm²)	(kN)	(MPa)	(mm²)	(kN)	(MPa)	(mm²)	(kN)	(MPa)	(mm²)	(kN)	(MPa)	(MPa)	STDEV
24	1600	80,25	50,16	1600	81,68	51,05	1600	79,34	49,59	1600	84,25	52,66	1600	83,43	52,14	1600	78,56	49,10	50,8	1,4

Analyses

	AVG		AVG (ref 28d)		AVG		AVG (ref 28dh)		AVG		AVG (ref 28d)	
Age	σc		σc		σFlex		σFlex		S.G.		S.G.	
(h)	(MPa)	STDEV	(MPa)	STDEV	(MPa)	STDEV	(%)	STDEV	(-)	STDEV	(%)	STDEV
24	50,8	1,4	72,3	2,4	4,9	0,1	85,0	3,4	2,14	0,00	100,0	1,1

DM8 - 30%MK 70%GGBFS - Variations

Information about prisms ambient curing, GGBFS 50% replaced by 50% DM8-WWA

	Prism 1									Prism 2									Prism 3									AVG			
Age	l	b	h1	h2	h3	h	m	ρ		l	b	h1	h2	h3	h	m	ρ		l	b	h1	h2	h3	h	m	ρ		ρ		S.G.	
(h)	(mm)	(mm)	(mm)	(mm)	(mm)	(mm)	(g)	(kg/m³)	S.G.	(mm)	(mm)	(mm)	(mm)	(mm)	(mm)	(g)	(kg/m³)	S.G.	(mm)	(mm)	(mm)	(mm)	(mm)	(mm)	(g)	(kg/m³)	S.G.	(kg/m³)	STDEV	(-)	STDEV
24	160,02	40,03	40,23	40,23	40,35	40,27	555,70	2154,26	2,15	159,64	39,92	40,63	40,25	40,28	40,39	555,07	2156,64	2,157	159,88	39,88	41,25	40,14	40,37	40,59	549,99	2125,31	2,125	2150	17,44	2,150	0,017

Tensile strength (NBN EN 196 -1)

	Test 1 - Prism 1			Test 2 - Prism 2			Test 3 - Prism 3			AVG	
Age	$2b^3/3l$	F_{max}	σ_{Flex}	$2b^3/3l$	F_{max}	σ_{Flex}	$2b^3/3l$	F_{max}	σ_{Flex}	σ_{Flex}	
(h)	(mm²)	(kN)	(MPa)	(mm²)	(kN)	(MPa)	(mm²)	(kN)	(MPa)	(MPa)	STDEV
24	427,63	0,79	1,85	424,11	0,86	2,03	422,84	0,81	1,92	1,93	0,09

Compressive strength (NBN EN 196 -1)

	Test 1 - Prism 1			Test 2 - Prism 1			Test 3 - Prism 2			Test 4 - Prism 2			Test 5 - Prism 3			Test 6 - Prism 3			AVG	
Age	S_o	F_{max}	σ_C	S_o	F_{max}	σ_C	S_o	F_{max}	σ_C	S_o	F_{max}	σ_C	S_o	F_{max}	σ_C	S_o	F_{max}	σ_C	σ_C	
(h)	(mm²)	(kN)	(MPa)	(mm²)	(kN)	(MPa)	(mm²)	(kN)	(MPa)	(mm²)	(kN)	(MPa)	(mm²)	(kN)	(MPa)	(mm²)	(kN)	(MPa)	(MPa)	STDEV
24	1600	20,89	13,06	1600	19,99	12,49	1600	17,37	10,86	1600	20,03	12,52	1600	18,44	11,53	1600	18,00	11,25	12,0	0,9

Analyses

	AVG		AVG (ref 28d)		AVG		AVG (ref 28dh)		AVG		AVG (ref 28d)	
Age	σ_c		σ_c		σ_{Flex}		σ_{Flex}		S.G.		S.G.	
(h)	(MPa)	STDEV	(MPa)	STDEV	(MPa)	STDEV	(%)	STDEV	(-)	STDEV	(%)	STDEV
24	12,0	0,9	17,0	1,3	1,9	0,1	33,5	2,0	2,15	0,02	100,5	1,4